

UNIVERSITY OF BIRMINGHAM

DEVELOPMENT OF IRINOTECAN HYDROCHLORIDE LOADED PLGA NANOPARTICLES FOR THE TREATMENT OF GLIOBLASTOMA

by

ALI HAMOD ALAMRI

A thesis submitted to the University of Birmingham for the degree of DOCTOR OF PHILOSOPHY

School of Pharmacy
College of Medical and Dental Sciences
University of Birmingham

April 2021

UNIVERSITY OF
BIRMINGHAM

University of Birmingham Research Archive

e-theses repository

This unpublished thesis/dissertation is copyright of the author and/or third parties. The intellectual property rights of the author or third parties in respect of this work are as defined by The Copyright Designs and Patents Act 1988 or as modified by any successor legislation.

Any use made of information contained in this thesis/dissertation must be in accordance with that legislation and must be properly acknowledged. Further distribution or reproduction in any format is prohibited without the permission of the copyright holder.

Abstract

Glioblastoma multiforme (GBM) is one of the most aggressive and deadliest types of tumours in both adults and children. The difficulty of delivering drugs to the brain is a major obstacle in the treatment of GBMs. Nanoparticles (NPs) are a promising strategy that can be designed to improve drug delivery to the brain. In this study, Irinotecan Hydrochloride (IRN)-loaded poly(lactide-co- glycolide) (PLGA) NPs and IRN and Pitavastatin (PTV) co-loaded PLGA NPs were developed to improve their delivery to the brain and increase their efficacy as a treatment for GBM.

The IRN-loaded PLGA NPs were developed using a Box-Behnken design (BBD) study to investigate the effect of formulation variables on their critical quality attributes and prepared by the single emulsion solvent evaporation method. The formulation variables of the amount of IRN and PLGA, as well as the percent of Poly (vinyl alcohol) (PVA), were investigated for their impact on the physical properties of the NPs. The cytotoxicity, cellular uptake, and apoptotic effect of the IRN-loaded PLGA NPs was evaluated using primary GBM cells. The ability of the NPs to cross the blood brain barrier (BBB) was investigated using a cerebral microvascular endothelial cell line D3 (hCMEC/D3) monolayer BBB model and hCMEC/D3 cells with astrocytes multilayer BBB model. The permeability of the BBB was determined using the transendothelial electrical resistance (TEER) value. TEER values in the monoculture BBB model were measured using EVOM2 and ECIS, while cellZscope was used to measure the TEER values with the co-culture BBB model. The optimised IRN-loaded PLGA NPs showed a nearly spherical shape with particle sizes ranging from 150 - 300 nm, a polydispersity index (PDIs) less than 0.3, zeta potentials of -10 to -30, and EEs ranging from 40.8 to 88.94 depending on the formulation and type of PLGA (5002 and 5004). PLGA 5002 had the highest EE due to it being acid terminated resulting in an electrostatic interaction with

the HCL group of the IRN. The in vitro drug release demonstrated a prolonged release over 9 days with a maximum of 40% released from the 5002 NPs, and 85% from the 5004 NPs. The lower level of IRN release from 5002 was due to the electrostatic interaction. The release of the IRN was much higher in acidic media compared to the normal pH. All of the optimised NPs were shown to have comparable cytotoxicity to the free IRN at 1 and 10 μM as well as reducing the TEER value of the mon- and co-culture BBB models, which suggests their ability to cross the BBB. The optimised NPs were able to internalize in the primary GBM cells and their cellular uptake was time and concentration dependent.

Three different formulations of the IRN and PTV co-loaded NPs (C1, C2, and C2) were developed and characterised for their size, zeta potential, PDI, EE, and drug release. The C2 NPs were chosen for evaluation of their cytotoxicity and cellular uptake using primary GBM cells as well as their ability to cross BBB models (mono- and co-culture BBB models). The size of the C2 NPs was 70 nm with a PDI of 0.21, while the EEs of the IRN and PTV were 44.56 and 18.50%, respectively. The C2 NPs were shown to be cytotoxic against primary GBM cells and were able to cross the mono- and co-culture BBB models. Overall, the results demonstrate that the IRN-loaded as well as the IRN and PTV co-loaded PLGA NPs have the potential to be an effective treatment for GBM.

Acknowledgments

First and foremost, I would like to thank my supervisor Dr. Christopher McConville for his continued advice and guidance throughout this project and over the years of my PhD study.

Also, I would like to thank my parents, Hamod and Zarah, for all their concern and encouragement and my wife, Asma, for her love, encouragement and support all the time.

My appreciation goes to Zaynah Maherally from Portsmouth University for helping me with the BBB model work in this project. I would also like to acknowledge King Khalid University for funding this project. I extend my gratitude to all my friends and lab mates in the pharmacy school for their kindness and support.

Publications

- Basant Salah Mahmoud, Ali Hamod AlAmri, Christopher McConville (2020): Polymeric nanoparticles for the treatment of malignant gliomas. Cancer 2020, 12, 75, doi:10.3390/cancers12010175; www.mdpi.com/journal/cancers. The paper has been accepted on 6th January 2020, and published on 10 January 2020.

- Alamri A, Huang Y, Zhang H. Liposomal Nanoformulation of Piperlongumine for Improved Aqueous Solubility and Enhanced Anti-tumour Activity In-vitro. Int J Pharm Pharmacol 2018; 2: 133. doi: 10.31531/2581-3080.1000133

- **In progress;** Ali Alamri, Zaynah Maherally, Christopher McConville (2021)**:** Development and in vitro evaluation of irinotecan-loaded PLGA nanoparticles for the treatment of glioblastoma: A Box-Behnken design of experiments approach. Submitted to the International Journal of Pharmaceutics

Presentation

- **In 2020,** I presented an abstract titled “Development Irinotecan Hydrochloride-loaded PLGA Nanoparticle Formulations for Treatment of Glioblastoma Multiforme” at the in International Conference on Nanopharmaceutical and drug delivery, and was awarded the best presentation at the conference.

Covid-19 impact statement

As I have completed my PhD lab work by the deadline of 06TH November 2020, there have been some impacts on my project as a result of the Covid-19 pandemic. The main impacts are listed below:

- I did not get to test the IRN-loaded PLGA NPs in animal study. The animal study has now started but the result won't be back in time for submission.
- The lockdown stopped me investigating targeted NPs. It was planned to modify the surface of IRN-loaded PLGA NPs with PEG and a monoclonal antibody.
- The lockdown also stopped me investigating the cytotoxicity effect and cellular uptake of the NPs against 3D cells. I have optimised and cultured 3D primary GBM cells but could not test the NPs in the 3D cells.
- I did not test all optimised NPs in the co-culture BBB model for the permeability study. This work has been done at the University of Portsmouth due to the lockdown restrictions we were only able to test two of the five NPs formulations.

Table of contents

Abstract ..... **ii**

Acknowledgments ..... **iv**

Publications ..... **v**

Covid-19 impact statement ..... **vi**

Table of contents ..... **vii**

List of tables ..... **xvi**

List of figures ..... **xvii**

List of abbreviation ..... **xxii**

Chapter 1: Introduction **1**

1.1 Gliomas 1

1.1.1 Circumscribed glioma (WHO grade I) 2

1.1.2 Diffuse gliomas (WHO grades II-III) 2

1.2 Glioblastoma Multiforme (GBM) (WHO Grade IV) 3

1.2.1 GBM classification 5

1.2.1.1 Primary and secondary GBMs 5

1.2.1.2 Molecular subtypes 7

1.2.2 Treatment of GBM 7

1.2.2.1 Surgical resection 8

1.2.2.2 Radiation therapy 9

1.2.2.3 Chemotherapy 10

1.2.2.3.1 Temozolomide 11

1.2.2.3.2 Gliadel wafer 12

1.2.2.3.3 Irinotecan Hydrochloride (IRN) 13
1.2.2.3.3.1 IRN properties and chemical structure 13
1.2.2.3.3.2 IRN as a treatment for GBM 14
1.3 Challenges of GBM treatment 15
1.3.1 Toxicity 15
1.3.2 Chemotherapy resistance in GBM 15
1.3.3 Blood brain barrier (BBB) 16
1.3.3.1 Function and structure of BBB 17
1.3.3.2 Status of the BBB in GBM 18
1.4 Drug delivery to the brain 19
1.4.1 Invasive strategies for drug delivery to the brain 19
1.4.1.1 Disruption of the BBB 19
1.4.1.2 Intraventricular/Intrathecal administration 19
1.4.1.3 Convection-enhanced delivery (CED) 20
1.4.2 Non-invasive strategies for drug delivery to the brain 20
1.4.2.1 Passive diffusion 20
1.4.2.2 Carrier-mediated transport (CMT) 21
1.4.2.3 Endocytotic transcytosis 21
1.4.2.3.1 Adsorptive mediated transcytosis (AMT) 22
1.4.2.3.2 Receptor mediated transcytosis (RMT) 22
1.5 Nanoparticles (NPs) in drug delivery system 23
1.6 Nanoparticles (NPs) for drug delivery to the brain 25
1.7 Polymeric Nanoparticles (NPs) for drug delivery to the brain 27
1.7.1 Targeted polymeric NPs for the Treatment of GBM 29

1.7.2 Application of targeted polymeric NPs in drug delivery to the brain 31
1.7.2.1 Ligand-polymeric NPs 31
1.7.2.2 Coated-polymeric NPs 33
1.8 Routes of Administration of NPs in the Treatment of Malignant Gliomas 34
1.8.1 Direct delivery 34
1.8.2 Direct systemic delivery 34
1.8.3 Indirect systemic delivery 35
1.9 Additional challenges to using NPs as in the treatment of GBMs 35
1.9.1 The reticuloendothelial system (RES) 35
1.9.2 The renal system 36
1.9.3 Pathophysiological barrier in tumours 36
1.10 Clinical Transition of Polymeric NPs 37
1.11 Poly(lactide-co-glycolide) (PLGA) in drug delivery 39
1.11.1 Physio-chemical properties of PLGA 39
1.11.1.1 Structure, synthesis, and general properties of PLGA 39
1.11.1.2 Degradation of PLGA 41
1.11.2 PLGA NPs preparation 42
1.11.2.1 Preparation of NPs by dispersion of pre-formed polymers. 42
1.11.2.2 Single emulsion technique 43
1.11.2.3 Double emulsion technique 44
1.11.3 PVA as a surfactant 45
1.12 Aims and objectives 45
Chapter 2: Development and characterisation of Irinotecan hydrochloride-loaded PLGA NPs 47

2.1 Introduction 47
2.2 Materials, Instruments and Methods 49
2.2.1 Materials 49
2.2.2 PLGA IRN-NPs preparation and characterisation 49
2.2.2.1 Preparation of blank and IRN-loaded PLGA NPs using the single emulsion solvent evaporation method 49
2.2.2.2 Pre-screen study for the IRN-loaded PLGA NPs 50
2.2.2.3 Design of Experiments (DoE) for the IRN-loaded PLGA NPs using a Box-Behnken design (BBD). 50
2.2.3 HPLC analysis 52
2.2.3.1 HPLC assay condition 52
2.2.3.2 Stock solution and calibration curve. 53
2.2.4 Size, PDI, zeta potential and EE of IRN-loaded PLGA NPs. 53
2.2.5 In vitro release 54
2.2.6 Transmission Electron Microscope (TEM) 54
2.2.7 Differential scanning calorimetry (DSC) 54
2.2.8 Powder X-ray diffraction (PXRD) 54
2.2.9 Statistical analysis 54
2.3 Results 55
2.3.1 Pre-screening of the key parameters involved in the development of IRN-loaded PLGA NPs using the single emulsion solvent evaporation technique 55
2.3.1.1 The amount of PLGA 55
2.3.1.2 Effect the molecular weight of PVA as surfactant 57
2.3.1.3 Percentage PVA 57
2.3.1.4 Influence of sonication time on the size and PDI of the NPs 60

2.3.1.5 Influence of freeze drying on the size of NPs 60
2.3.1.6 Effect the type of the PLGA on the EE of NPs 61
2.3.2 DoE process to determine the key quality parameters for the IRN-loaded PLGA NPs. 62
2.3.2.1 Effect of the independent variables on the particle size of IRN-loaded PLGA NPs. 62
2.3.2.2 Effect of the independent variables on the EE of the IRN-loaded PLGA NPs. 64
2.3.3 Zeta potential and PDI. 69
2.3.4 HPLC analysis for IRN 70
2.3.5 Optimization of the IRN-loaded PLGA NPs 71
2.3.6 Transmission Electron Microscopy (TEM). 71
2.3.7 Differential scanning calorimetry (DSC) 72
2.3.8 X-ray diffraction (XRD) 73
2.3.9 pH-dependent drug release 74
2.4 Discussion 75
2.5 Conclusion 79
Chapter 3: Evaluation of the cytotoxicity of the IRN-loaded PLGA NPs using primary High Grade Glioma cells. 80
3.1 Introduction 80
3.2 Materials and methods 82
3.2.1 Materials 82
3.2.2 Biopsy collection and dispersion 82
3.2.3 Cell viability (MTT assay) 83
3.2.4 Cellular uptake by flow cytometry 84

3.2.5 Confocal laser scanning microscopy 84
3.2.6 Apoptosis assay labelling with Alexa® Fluor 488 annexin V and PI 85
3.2.7 Statistical analysis..... 85
3.3 Results..... 86
3.3.1 Cytotoxicity of the IRN-loaded PLGA NPs against primary GBM cells..... 86
3.3.2 Cellular uptake ..... **Error! Bookmark not defined.**
3.3.3 Confocal laser scanning microscopy 93
3.3.4 Quantitative analysis of apoptosis using the Annexin V/PI double-staining assay and flow cytometry calculations..... 95
3.4 Discussion..... 97
3.5 Conclusion 99
Chapter 4: The ability of the IRN-loaded PLGA NPs to cross in vitro mono- and co-culture BBB models..... 100
4.1 Introduction..... 100
4.2 Materials and Methods 102
4.2.1 Materials..... 102
4.2.2 Monoculture of human BBB models using the hCMEC/D3 cells 102
4.2.3 Co-culture of the human BBB model using hCMEC/D3 cells and human astrocytes 103
4.2.4 EVOM2 method for TEER measurement of the monoculture BBB model (hCMEC/D3 cells)..... 103
4.2.5 ECIS method of TEER measurement on the mono-culture BBB model (hCMEC/D3 cells)..... 104

4.2.6 CellZscope method for TEER measurement of co-culture BBB model (hCMEC/D3 cells and astrocytes) 105
4.2.7 Statistical analysis 106
4.3 Results 106
4.3.1 Monitoring the change in resistance of the monoculture BBB model using EVOM2 106
4.3.2 Monitoring the change in resistance of the mono-culture BBB model using the ECIS system 109
4.3.3 Monitoring the change in resistance of the co-culture BBB model using the cellZscope system 110
4.4 Discussion 111
4.5 Conclusion 113
Chapter 5: Dual formulation of Irinotecan hydrochloride and Pitavastatin calcium into PLGA NPs 115
5.1 Introduction 115
5.2 Materials and Methods 117
5.2.1 Materials 117
5.2.2 Preparation of IRN and PTV-loaded PLGA NPs using single emulsion solvent evaporation method 117
5.2.3 HPLC analysis, size, zeta potential, EE, and in vitro release 117
5.2.4 Biopsy collection and dispersion, cell viability study, cellular uptake, and apoptosis assay labelling with Alexa® Fluor 488 annexin V and PI 117
5.2.5 Monoculture and coculture BBB models, EVOM2, ECIS, and cellZscope methods 118

5.2.6 Statistical analysis 118

5.3 Results 118

5.3.1 Preparation IRN and PTV co-loaded PLGA NPs by single emulsion solvent evaporation method 118

5.3.2 HPLC analysis for IRN and PTV 119

5.3.3 pH-dependent drug release 120

5.3.4 Cytotoxicity study using MTT assay for IRN and PTV co-loaded PLGA NPs against the primary GBM cells 121

5.3.5 Cellular uptake using flow cytometry 123

5.3.6 Quantitative analysis of apoptosis using the Annexin V/PI double-staining assay and flow cytometry calculations 125

5.3.7 Permeability of the IRN and PTV co-loaded PLGA NPs across in vitro monoculture and coculture BBB models 127

5.3.7.1 Monitoring the change in resistance of the monoculture BBB model using EVOM2 127

5.3.7.2 Monitoring the change in resistance of the mono-culture BBB model using ECIS system 128

5.3.7.3 Monitoring the change in resistance of the co-culture BBB model using cellZscope system 129

5.4 Discussion 130

5.5 Conclusion 134

Chapter 6: General discussion and future work 135

6.1 General discussion 135

6.1.1 The IRN-loaded PLGA NPs 135

6.1.2 The IRN and PTV co-loaded PLGA NPs 138

6.2 Future work 142

References 144

List of tables

Table 1-1: Molecular subtypes of GBMs and their main characteristics. 7

Table 1-2: Names, molecular formula, molecular weight of IRN forms used in medicine as antitumor agent. 14

Table 1-3: Examples of developed targeted polymer NPs as targeted drug delivery system for treatment of brain tumours malignant gliomas 30

Table 2-1: Levels of variables used in Box–Behnken design (BBD) for preparing IRN-loaded PLGA NPs (5002 and 5004)..... 51

Table 2-2: Design of study and independent variables of Box-Behnken design (BBD) for preparing IRN-loaded PLGA NPs with low intrinsic viscosity PLGA 5002. 52

Table 2-3: Design of study and independent variables of Box-Behnken design (BBD) for preparing IRN-loaded PLGA NPs NPs with high intrinsic viscosity PLGA 5004..... 52

Table 2-4: Design of study and independent variables of Box-Behnken design (BBD) for preparing IRN-loaded PLGA NPs..... 63

Table 2-5: A summary of fitted model analysis for response size and EE of IRN-Loaded PLGA NPs. 68

Table 5.1: The variables in preparing combinations of the IRN and PTV co-loaded PLGA NPs include the amount of drugs, amount of PLGA, percentage of PVA, and type of PLGA. 117

Table 5.2: Characterisation of the IRN and PTV co-loaded PLGA NPs including size, zeta potential, PDI, and EE (n= 3)..... 119

Table 6-1. Characterisation of R13 (IRN-loaded PLGA NPs) and C2 (IRN and PTV co-loaded PLGA NPs) including size, zeta potential, PDI, and EE..... 139

List of figures

Figure 1-1: A schematic depicting GBM a diffusely infiltrative disease and a simple algorithm of GBMS classifications. 5

Figure 1-2: Chemical structures of IRN and SN-38. 13

Figure 1-3: A schematic depicting sections of the brain showing healthy BBB with endothelial cells connected with tight junctions (figure the left) and BBB in tumours with disrupted endothelial cells (figure the right). 18

Figure 1-4: A schematic representation of major pathways of drug transport cross the BBB. 23

Figure 1-5: A schematic representation of EPR effect. 27

Figure 1-6: A schematic illustration non-modified and modified surface of PLGA NPs. 29

Figure 1-7: Chemical structure of **(A)** PGA, **(B)** PLA, and **(C)** PLGA. 39

Figure 1-8: The time dependent of water uptake of polymers with different end groups (capped and uncapped polymers) 41

Figure 1-9: Schematic representation of the single emulsion process. 43

Figure 1-10: Schematic representation of the double emulsion solvent evaporation technique 44

Figure 2-1: Scheme of the preparation method for IRN-loaded PLGA NPs by single emulsion solvent evaporation method. 50

Figure 2-2: Influence the amount of PLGA (40 and 120 mg) on the size (A) zeta potential (B) and polydispersity index (C) of IRN-loaded PLGA 5004 NPs.. 56

Figure 2-3. Influence of the molecular weight of Poly(vinyl alcohol) on the size (A) zeta potential (B) and polydispersity index (C) of IRN-loaded PLGA NPs. 58

Figure 2-4: Influence of the percentage of Poly(vinyl alcohol) on the size (A) zeta potential (B) and polydispersity index (C) of IRN-loaded PLGA NPs. 59

Figure 2-5: Change in particles size (A) and polydispersity index (B) of IRN-loaded PLGA NPs with time of sonication.. 60

Figure 2-6: Change in particle sizes before and after freeze drying..... 61

Figure 2-7: Effect type of PLGA (PLGA 5004 and PLGA 5002) on the EE of IRN-loaded PLGA NPs. 61

Figure 2-8: 3D Response surface plot showing the influence of variables (amount of drug, amount of polymer, percentage of surfactant) on the size of the IRN-loaded NP..... 66

Figure 2-9: 3D Response surface plot showing the influence of variables (amount of IRN, amount of PLGA, percentage of PVA) on the EE of the IRN-loaded NP 67

Figure 2-10: Pareto chart on the effect of variables (amount of IRN, amount of PLGA, percentage of PVA) in order of their effect on size (A) and EE (B) IRN-loaded 5002 PLGA NPs), and on size (C) and EE (B) IRN-loaded 5004 PLGA NPs. 68

Figure 2-11: Zeta potential for all IRN-loaded PLGA NPs. 69

Figure 2-12: Zeta potential of IRN-loaded PLGA NPs, (A) PLGA 5002 and (B) PLGA 5004. 70

Figure 2-13: Number-size distributions of IRN-loaded PLGA NPs (R13) were analysed using dynamic light scattering (DLS). 70

Figure 2-14: Standard curve of IRN (A) using HPLC. 71

Figure 2-15: Morphology evaluation of IRN-loaded PLGA NPs by Transmission Electron Microscopy (TEM)..... 72

Figure 2-16: Differential scanning calorimetry (DSC) thermograms; drug (IRN), polymers (PLGA 5004, PLGA 5002), Surfactants (PVA), and physical mixture (drug, polymers, PVA), and formulations (IRN-loaded PLGA NPs)..... 73

Figure 2-17: X-ray diffraction diffractogram of (A) PLGA 5002, (B) PLGA 5004, (C) PVA, (D) IRN, (E) R13 NPs, and (F) R22 NPs. 74

Figure 2-18: In vitro cumulative release profile of IRN from PLGA NPs of four different NPs (R1, R13, R16, R22). 75

Figure 3-1: Cytotoxicity of two different blank NPs based on the type of PLGA in comparison with IRN- loaded PLGA NPs 86

Figure 3-2: Viability of the primary GBM cells (patient 1) cultured with IRN-loaded NPs (free IRN, R1, R13, R16, and R22)..... 88

Figure 3-3: Viability of the primary GBM cells (patient 2) cultured with IRN-loaded NPs (free IRN, R1, R13, R16, and R22)..... 89

Figure 3-4: Cytotoxicity of IRN-loaded PLGA NPs (R1, R13, R16, R22) and free IRN at 100 μM against four different GBM samples (patient 1 (P1), patient 2 (P2), patient 3 (P3), and patient 4 (P4)) at day 5. 90

Figure 3-5: Cellular uptake of IRN-loaded NPs in the primary GBM cells (patient 1) after incubation time of 3, 6, 24, 120 h 92

Figure 3-6: Comparing cellular uptake of IRN-Loaded PLGA NPs R1, R6, R13, and R22 (10 μM of each) in the primary GBM cells (patient 1) at time 24 and 120 h..... 93

Figure 3-7: In vitro cellular uptake of C6-loaded PLGA NPs evaluated in the primary GBM cells (patient 2) using confocal laser scanning microscopy..... 94

Figure 3-8: Estimation of apoptotic cell population by flow cytometry using Annexin V/PI double-staining assay..... 96

Figure 4-1: Schematic assembly of the BBB model used to study the ability of the IRN-loaded PLGA NPs to cross the BBB. 103

Figure 4-2: TEER measurement with a chopstick electrode using EVOM2 measured in ohm's. 104

Figure 4-3: TEER measurement using ECIS system. 105

Figure 4-4: TEER measurement using cellZscope. 106

Figure 4-5: The phase-contrast microscopy image shows confluency of the hCMEC/D3 cells when the highest resistance was recorded at 168 h. 107

Figure 4-6: The resistance profile of hCMEC/D3 cells over 168 h..... 107

Figure 4-7: Effect of the IRN-loaded PLGA NPs at two different concentrations **(A)** 5mg (≈ 100 μM) and **(B)** 10 mg (≈ 200 μM) on the BBB model permeability at time 0, 6, 24, 48, and 72h. The monoculture was constructed using 8 μM pore size polycarbonate-membrane filters within 24-transwell inserts. The resistance was evaluated by measuring TEER values with EVOM2. 108

Figure 4-8: Changing in resistance values in BBB model (hCMEC/D3 cells) with the IRN-loaded PLGA NPs **(A)** R1 and R6, **(B)** R13 and R22. The cells were seeded on the gold electrode and the resistance was recorded by the ECIS system over 20 h post addition of the NPs. 110

Figure 4-9: Changing in resistance values in co-culturing BBB model (hCMEC/D3 cells and astrocyte) post-addition of the IRN-loaded PLGA NPs (R13). The resistance was recorded by cellZscope system for 82 h after adding NPs. 111

Figure 5-1: Standard curves of PTV using HPLC 119

Figure 5-2: The HPLC chromatogram depicting the peaks of IRN and PTV in the C2 NPs measured at 265 nM wavelength..... 120

Figure 5-3: In vitro cumulative release profile of IRN and PTV from C2 NPs..... 121

Figure 5-4: Viability of GBM primary cells patient 1 **(A)** and patient 2 **(B)** cultured with IRN and PTV co-loaded PLGA NPs (C2) 122

Figure 5-5: Cytotoxicity of IRN and PTV co-loaded PLGA NPs (C2) at 100 μM against four different GBM samples patient 1 (P1), patient 2 (P2), patient 3 (P3), and patient 4 (P3) at day 5. 123

Figure 5-6: Cellular uptake of IRN and PTV co-loaded PLGA NPs (C2) in GBM primary cells (patient 1) after incubation time of 3, 6, 24, 120 h at three different concentrations 0.1, 1, 10 μM observed by flow cytometry. 124

Figure 5-7: Estimation of apoptotic cell population by flow cytometry using Annexin V/PI double-staining assay..... 126

Figure 5-8: Effect of the IRN and PTV co-loaded PLGA NPs (C2) at two different concentration **(A)** 5mg (≈ 100 μM) and **(B)** 10 mg (≈ 200 μM) on the BBB model permeability at time 0, 6, 24, 48, and 72 h. The monoculture was constructed using 8 μM pore size polycarbonate-membrane filters within 24-transwell inserts. The resistance was evaluated by measuring TEER values with EVOM2..... 128

Figure 5-9: Changing in resistance values in BBB model (hCMEC/D3 cells) with the IRN and PTV co-loaded PLGA NPs **(C2)**. The cells were seeded on the gold electrode and the resistance was recorded by the ECIS system over 20h post addition of the NPs.. 129

Figure 5-10: Changing in resistance values in co-culturing BBB model (hCMEC/D3 cells and astrocyte) post-addition of the IRN and PTV co-loaded PLGA NPs (C2). The resistance was recorded by cellZscope system for 82 h after adding NPs. 130

Figure 6-1. Particle sizes and EE of the optimized IRN-loaded PLGA NPs. 136

Figure 6-2. Viability of GBM primary cells (patient 1) cultured with the IRN and PTV co-loaded PLGA NPs (C2) in comparison with IRN-loaded PLGA NPs (R13) and free IRN 140

Figure 6-3. Comparing cellular uptake of the IRN-loaded PLGA NPs (R13), and the IRN and PTV co-Loaded PLGA NPs (C2) (10 μM of each) in GBM primary cells (patient 1) at time 24 and 120 hours determined by flow cytometry..... 141

Figure 6-4. comparing the effect of IRN-loaded PLGA NPs (R13) and the IRN and PIV co-Loaded PLGA NPs (C2) on the BBB permeability at time 0, 6,24,48, and 72h. 142

List of abbreviation

1p/19q	Codeletion of chromosomes 1p and 19q
AC	Alternating current
AGAT	O^6-alkylguanine-DNA alkyltransferase
AMT	Adsorptive mediated transcytosis
ApoE or ApoA-I	Apolipoproteins
ATRX	Alpha thalassemia//mental retardation syndrome X-linked protein/gene
AUC	Area under the curve
BBB	Blood brain barrier
BBBD	blood brain barrier disruption
BBD	Box-Behnken Design
BCEC	Brain capillary endothelial cells
BCNU	Carmustine (bis- chloroethyl nitrosourea
C6	Coumarin 6
CBTRUS	Central Brain Tumour of the United State
CECs	Cerebral endothelial cells
CED	Convection-enhanced delivery
CellZscope	Impedance spectroscopy
CNS	Central nervous system
CPPs	Penetrating peptides
CSF	Cerebrospinal fluid
DCM	dichloromethane
DLS	Dynamic light scattering
DMEM	Dulbecco’s Modified Eagle’s Medium

DMSO	Dimethyl sulfoxide
DoE	Design of experiments
DSC	Differential scanning calorimetry
ECIS	Electric Cell-substrate Impedance Sensing
EE	Encapsulated efficiency
EGFR	Epidermal growth factor receptor
EORTC	European Organization for Research and Treatment of Cancer
EPR	Enhanced permeability and retention
EVOM2	Epithelial volt-ohm meter
FBS	Fetal bovine serum
GBM	Glioblastoma Multiforme
GBM-O	GBM with oligodendroglioma
HBSS	Hanks' Balanced Salt Solution
hCMEC/D3	Human cerebral microvascular endothelial cell line D3
HMG-CoA	3-hydroxy-3-methyl-glutaryl-CoA
hTERT	Human telomerase
IDH	Isocitrate dehydrogenase
IMRT	Intensity modulated RT
IRN	Irinotecan Hydrochloride
KPS	Karnofsky performance scale
LDL	Low-density lipoprotein
LRP	Low density lipoprotein receptor related protein
mAb	Monoclonal antibodies
MDR-1	Multidrug resistant protein 1
MDR-1)	Multidrug resistant protein 1

MGMT	O^6-methylguanine-DNA-methyltransferase
MGMT	O-6-methylguanine-DNA methyltransferase
MPS	Mononuclear phagocyte system
MTIC	3-methyl- (triazen-1-yl) imidazole-4-carboxamide
MTT	Thiazolyl blue tetrazolium bromide
NCIC	National Cancer Institute of Canada Clinical Trials Group
NOS	Not otherwise specified
NPs	Nanoparticles
OLIG2	Oligodendrocyte lineage transcription factor
PBCA	Poly (butylcyanoacrylate)
PBS	Phosphate-buffered saline
PCL	Poly(Ɛ-caprolactone)
PDGFRA	Platelet-derived growth factor receptor-A
PDI	Polydispersity index
PGA	Poly (glycolic acid)
PHDCA	Poly(hexa-decyl cyanoacrylate
PI	Propidium Iodide
PLA	Poly(lactic acid),
PLGA	Poly(lactide-co-glycolide)
PSMA	Prostate specific membrane antigen
PTV	Pitavastatin Calcium
PVA	Poly (vinyl alcohol)
RES	Reticuloendothelial system
RMT	Receptor mediated transcytosis
RMT	Receptor mediated transport

SN-38	7-ethyl-10-hydroxycamptothecin
SRP	Subcutaneous reservoir and pump
SRS	Stereotactic radiosurgery
SSC	Side-scatter
TC	Tumour Cor
TEER	Transendothelial electrical resistance
TEM	Transmission electron microscope
TfR	Transferrin receptors
T_g	Glass transition temperature
VMAT	Volumetric-modulated arc therapy
WHO	World Health Organization
XRD	X-ray diffraction

Chapter 1: Introduction

1.1 Gliomas

Primary brain tumours refer to the different groups of tumours that develop from cells in the central nervous system (CNS). Brain tumours are classified from grade I to grade IV based on histological criteria according to the World Health Organization (WHO) grading system for CNS tumours. In 2016, the classification was updated to incorporate the genetic and molecular alteration of the CNS tumour. The new classification of CNS tumours has influenced the diagnosis criteria, prognosis, and treatment plan of brain tumours. The symptoms of a brain tumour can manifest over weeks, months and even years, depending on its location and growth rate. The location of the tumour can be determined based on the symptoms, which can then be confirmed by imaging such as an MRI or CT scan. For example, numbness and spatial disorientation might be caused by parietal lobe tumours, and visual impairment might be symptoms of temporal or occipital lobe tumours (Lapointe et al., 2018). The symptoms can be more general, which have no connection to the anatomic location of the tumours. 50-80% of brain tumour patients present with seizures, 30% with headaches, and 15% with drowsiness, vomiting, severe headache at night and papilledema, which are due to an increase in the intracranial pressure (Giulioni et al., 2014, Kirby and Purdy, 2014).

Gliomas are the most common form of malignant primary brain tumours and represent 75% of brain tumours in adults (Ostrom et al., 2017). Gliomas develop from glial or precursor cells which include astrocytomas, oligodendrogliomas, and ependymomas (Paw et al., 2015). High-grade gliomas can migrate within the brain through extracellular spaces, however they rarely migrate via the circulatory and lymphatic systems to other organs outside of the brain.

The mobility of glioma cells and their ability to enhance the degradation of extracellular cells are the main contributions for the invasion of gliomas (Cuddapah et al., 2014). According to the 2016 WHO CNS tumours classification, gliomas are classified into four different grades; circumscribed gliomas (grade I), diffusely infiltrating gliomas (grades II-III), and GBM (grade IV). The main molecular markers that are considered in 2016 WHO for gliomas are isocitrate dehydrogenase (IDH) mutations, codeletion of chromosomes 1p and 19q (1p/19q), and the mutation status of alpha thalassemia//mental retardation syndrome X-linked protein/gene (ATRX) (Lapointe et al., 2018, Louis et al., 2016).

1.1.1 Circumscribed glioma (WHO grade I)

This grade of glioma has a more circumscribed growth pattern. It does not have IDH mutations but frequently has BRAF alterations and TSC1/TSC2 mutations which can be used to distinguish circumscribed glioma from diffuse gliomas. This grade of glioma, such as pilocytic astrocytoma and xanthoastrocytoma are curable by complete surgical resection (Louis et al., 2016).

1.1.2 Diffuse gliomas (WHO grades II-III)

Most diffuse gliomas have IDH TP53 and ATRX mutations and are known as astrocytomas (Lapointe et al., 2018). Diffuse gliomas have three different diagnostic and prognostic subgroups based on their molecular alterations including IDH, BRAF, 1p/19q (Eckel-Passow et al., 2015). WHO grade II (diffuse astrocytomas) and WHO grade III (anaplastic astrocytoma) can each be sub-divided into IDH-mutant, IDH-wildtype and not otherwise specified (NOS).

1.2 Glioblastoma Multiforme (GBM) (WHO Grade IV)

GBMs are the most common primary brain tumour in adults, representing 16% of brain and CNS tumours (Dolecek et al., 2012, Filippini, 2012, Thakkar et al., 2014). The rate cases of GBM is 3.2 per 100,000 and more common in men compared to women at the ratio of 1.26:1 according to Europe and North America cancer registry data (Crocetti et al., 2012, Omuro and DeAngelis, 2013). GBM is more common in adult, with 87% of cases in adult patients with a median age of 65 years (Arora et al., 2009). The statistical reports for the period between 2005-2009 from Central Brain Tumour of the United State (CBTRUS), demonstrated that GBM was more common in older patients with an age range between 75 and 84 years, with higher incidence in white males compared to other races (Dolecek et al., 2012). The median survival rate for GBM patients is the lowest at only 14 months when compared to all other cancers, despite an aggressive combination of surgical resection, chemotherapy, and radiotherapy (Stupp et al., 2005, Darefsky et al., 2012). 30% of newly diagnosed GBM patients live 1-2 years, while only 5% live for more than 2 years. The prognosis of recurrent GBM patients is much worse with a median survival rate of 3 to 5 months (Ostrom et al., 2014, Sant et al., 2012, Lamborn et al., 2008). The prognosis of GBM patients is determined based on age, histology of the tumour at the time of diagnosis, Karnofsky performance scale (KPS), and other variables which are related to treatment status such as extent of resection (Curran Jr et al., 1993, Wong et al., 1999) .

GBMs are a malignant glial tumour and the most aggressive form of brain tumour (Schwartzbaum et al., 2006, Rowther et al., 2016). GBMs are mainly located in the cerebellum, spinal cord and brain stem. 61% of GBMs are found in one of the 4 lobes (frontal, temporal, partial, and occipital) with much less incidence in the cerebellum and spinal cord (Lovely et al., 2014). GBMs mainly originate from glial cells of astrocytic origin, while recent studies have been shown that neural stem cells could also be a source of GBMs

(Tomasetti et al., 2017). The most common characteristics of GBMs are resistance to apoptosis, tendency for necrosis, and infiltration of surrounding healthy tissues. GBMs are also characterised by tumour heterogeneity which is one of the greatest challenges when it comes to their treatment. The term multiforme refers to the heterogenicity of GBMs (Furnari et al., 2007, Olar et al., 2012, Florio and Barbieri, 2012, Agarwal et al., 2011a). The invasive, proliferative and angiogenic nature of GBM cells is very high when compared with other normal and cancerous cells (Karcher et al., 2006). The promotion of migration of tumorigenic cells from GBMs to the surrounding tissue has been linked to the interaction between the integrin heterodimer with the extracellular matrix, leading to conformational changes in the cytoskeleton (Louis, 2006) (Figure 1-1).

The causes and possible risk factors of GBMs is not been completely understood. There are some environmental factors such as ionizing radiation, pesticides, solvents, petrochemical industry, and electromagnetic fields that could be described as risk factors for GBMs (Spinelli et al., 2010). Furthermore, there are some genetic diseases such as tuberous sclerosis, Li-Fraumeni syndrome and Turcot syndrome that can be attributed to an increased risk of developing a GBM. Loss of genetic material in chromosomes 10q, amplification of genes, and mutations in certain genes can also be considered as risk factors for the development of GBMs (Network, 2008, Urbańska et al., 2014, Tamimi and Juweid, 2017).

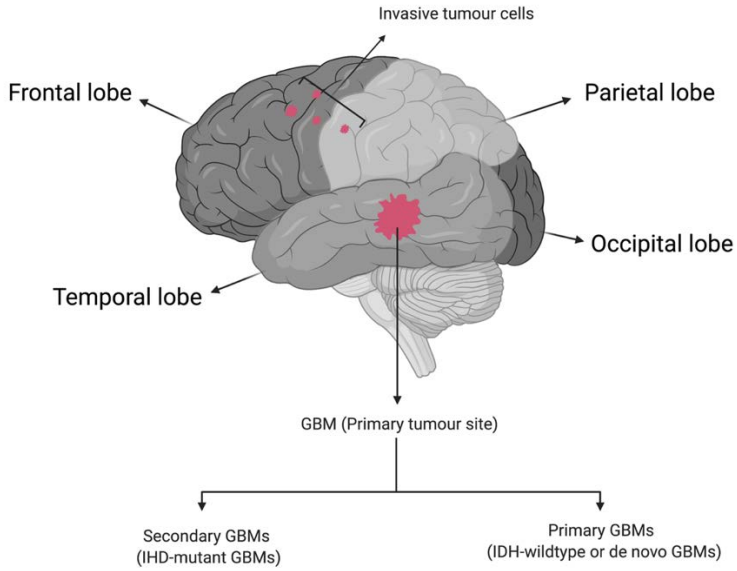


Figure 1-1: A schematic depicting GBM a diffusely infiltrative disease and a simple algorithm of GBMS classifications.

1.2.1 GBM classification

1.2.1.1 Primary and secondary GBMs

In the 2016 WHO CNS tumours classification, GBMs are divided into primary, secondary and NOS. Primary and secondary GBMs have the same clinical and morphological characteristics but they have different histories with different patterns of gene expression, and both of them have the same poor prognosis for patients of equal age (Furnari et al., 2007, Newcomb et al., 1998). NOS GBMs is a graded IV GBM with inconclusive or unavailable IDH mutation status (Louis et al., 2016).

Primary GBMs are the most frequently and represent about 90% of glioblastoma cases, with clinically named as IDH-wildtype or de novo GBMs. In the primary GBMs, the genetic alterations include mutation and amplification of epidermal growth factor receptor (EGFR), mutation of phosphatase and tensin homologue, and loss of chromosome 10q (Reifenberger et al., 2017). There is no evidence of a pre-existing low grade glioma for primary GBMs. The clinical history for patient with primary GBM is quite short at just 3 months or less with the histopathological characteristics presented in the first biopsy. However, after only three

months from initial diagnosis, around 50% of primary GBM patients have significantly larger tumours on their follow up MRI scan (Kleihues and Ohgaki, 1999), emphasising the important of early intervention.

Secondary GBMs or IHD-mutant GBM account for about 10% of GBM cases and more likely to occur in younger patients with a previous low grade glioma (Ohgaki and Kleihues, 2013). Secondary GBMs are characterised by mutations of IDH1 and cellular tumour antigen p53, as well as a loss of chromosome 19q (Reifenberger et al., 2017). These genetic alterations are present in the first biopsy for the majority of patients grade II and III astrocytoma. The progression from low grade glioma to secondary GBMs takes about 5 years, while the time is shorter in the progression from anaplastic astrocytoma to GBMs (Ohgaki and Kleihues, 2007, Ohgaki et al., 2004, Furnari et al., 2007). In general, the development of a secondary GBM is slower than the development of a primary GBM, taking between 10 and 15 years to present with symptoms (Alifieris and Trafalis, 2015).

Recently, a further GBM subtype was added and it is known as a rare GBM with oligodendroglioma (GBM-O) and has been classified in CNS WHO classification. This subtype is characterised by the presence of primitive cells, and MYC or MYCN genes (Louis et al., 2007, Louis et al., 2016). The GBM-O is reported to represent about 20% of GBMs and survival rates have increased in this subgroup, but these increases were lost when the survival rates variables were adjusted for age and gender (Homma et al., 2006). The GBM-O has not yet been identified as a specific subtype of GBM and its diagnostic criteria are still not clear (Laxton et al., 2013).

1.2.1.2 Molecular subtypes

GBMs have been further classified to four molecular subtypes on the basis of gene expression alteration and GBM genomic profiling to determine gene mutations. The four subtypes were identified as Classical, Pro- neural, Neural, and Mesenchymal (Table 1-1). The identification and characteristics of these four subtypes has highlighted the importance to distinguish between them. For example, Verhaak and co-workers have classified most of the previously diagnosed secondary GBMs as the proneural subtype. In comparison to the other three subtypes, the proneural subtype has been linked more to younger patients with no difference in survival rate with the use of aggressive treatments (Verhaak et al., 2010). The prognosis for the proneural subtypes is better than the other subtypes in relation to median survival (Verhaak et al., 2010, Phillips et al., 2006).

Table 1-1: Molecular subtypes of GBMs and their main characteristics (Verhaak et al., 2010).

Subtypes	Molecular characteristics
Classical	- Chromosome 7 amplification with Chromosome 10 loss (100%) - EGFR amplification - CDNK2A loss
Pro- neural	- platelet-derived growth factor receptor-A (PDGFRA) focal amplifications - IDH1 mutations - TP53 and loss of heterozygosity - Chromosome 7 amplification with Chromosome 10 loss (54%) - oligodendrocyte lineage transcription factor (OLIG2) overexpression
Neural	- neuron markers expression (such as neurofilament light polypeptide (NEFL)
Mesenchymal	- NF1 loss - mesenchymal markers expression (such as CH3L1) - Tumour necrosis factor (TNF) overexpression - Nuclear factor-B (NF-κB).

1.2.2 Treatment of GBM

The current standard of care for newly diagnosed GBMs includes surgery resection followed by radiation therapy and then adjuvant chemotherapy with temozolomide. This strategy for the management of GBM is known as the Stupp protocol and was implemented based on a

randomised phase III clinical trial in 2004 (Stupp et al., 2005) performed by the European Organization for Research and Treatment of Cancer (EORTC) and the National Cancer Institute of Canada Clinical Trials Group (NCIC). The median survival was increased from 12.1 months to 14.6 months with the Stupp protocol compared to surgical resection and radiation therapy (Stupp et al., 2005, Stupp et al., 2009a). Pathological diagnosis by surgical biopsy must be established before starting any treatment protocol in order to achieve the optimal management of GBM, except for patients with high potential for surgery (Chamberlain, 2010, Nieder et al., 2006). In recurrent GBM, the options of management are very limited and there is no standard treatment protocol (Wong et al., 1999).

1.2.2.1 Surgical resection

Surgical resection is the first option and cornerstone of the GBM management strategy (Nieder et al., 2006, Lonardi et al., 2005). The main aims of surgical resection are to achieve total resection of tumour without impairment of neurological function, to perform histological and molecular analysis on the tumour tissue and to reduce intracranial pressure (Anton et al., 2012, Ryken et al., 2014). Complete resection of the tumour depends on the grade, site, and morphology of the tumour. However, the complete resection of GBMs is impossible because of its infiltrative and invasive nature. The partial resection for GBM is not ideal because the residual tumour becomes more aggressive with greater neurological impact upon its recurrence. Therefore, the resection surgery is avoided for patients with poor performance status based on KPS score (Wilson et al., 2014). Many studies and randomised clinical trials have reported that more than 98% resection will improve the survival rate and patient's response to radiation therapy and chemotherapy, however, there is no benefit in survival rate for patients over 70 years (Lacroix et al., 2001, Wilson et al., 2014, Ryken et al., 2014). The survival rate has been increased for patients with maximal resection compared to patients with partial resection (Lacroix et al., 2001). Repeated resection surgery many times

may not be possible because of the invasion of GBM cells to vital areas of the brain areas (Mandl et al., 2008, Wong et al., 1999). New advanced surgical imaging techniques such as intraoperative magnetic resonance imaging MRI and diffusion tensor imaging etc. have improved the median survival for a short time (Ryken et al., 2014). These techniques help neurosurgeons to identify the border of the tumour allowing them to achieve maximal resection (Ryken et al., 2014, Hoover et al., 2010).

1.2.2.2 Radiation therapy

External radiation therapy following resection surgery is considered standard protocol for the treatment of high-grade gliomas such as GBM. The median survival has been improved with radiation therapy after resection surgery compared to resection surgery alone (Walker et al., 1978, Van den Bent et al., 2005). The administration of radiation therapy is recommended 2 weeks after resection surgery to provide enough time for wound healing of the surgical resection cavity and surrounding tissues (Leibel and Sheline, 1987). Total administered dose of the radiation is determined by various factors like site, grade, and histology of the tumour, as well as the extent of resection surgery (Chandana et al., 2008). The optimal dose of radiation is 60Gy over a period of 5-7 weeks administered in 30 fractional doses as 2Gy per fraction/5 days per week (Chandana et al., 2008, Leibel and Sheline, 1987, Lonardi et al., 2005, Florio and Barbieri, 2012). The survival rate using a 60Gy radiation dose has improved in comparison with doses of 45 to 55Gy (Walker et al., 1979), however, there is no improvement in survival with radiation dose of 70Gy due to increased toxicity (Chang et al., 1983). According to phase III randomised clinical trials, the survival rates were doubled from 4 to 5 months to 9 to 10 months for GBM patients with radiation therapy, and it is the best treatment choice if surgery resection is not available for elderly patients (Ryu et al., 2014). Radiation therapy can be applied for the whole or partial brain, however, whole brain radiation did not show significant survival benefit compared to the partial brain radiation but

it can be used for multifocal GBM (Shapiro et al., 1989, Leibel and Sheline, 1987). Some techniques have been developed and used to improve targeting of radiation to tumour tissues such as fixed field intensity modulated RT (IMRT), volumetric-modulated arc therapy (VMAT) and stereotactic radiosurgery (SRS), which improve targeting to tumour tissues and reduce toxicity for normal tissues (Scaringi et al., 2018). Radiation therapy is associated with various side effects like necrosis of normal tissues, blood brain barrier (BBB) damage, neurological effect, and headaches (Wilson et al., 2014, Iacob and Dinca, 2009). In the current Stupp protocol for GBM management, the combination treatment of resection surgery, radiation therapy, and temozolomide for GBM has improved survival rate (Stupp et al., 2005) compared to the use of resection surgery and radiation therapy alone (Walker et al., 1978, Group, 2002).

1.2.2.3 Chemotherapy

Various chemotherapeutic agents have been investigated as treatments for GBM since the 1970s (Walker et al., 1978), with most randomised clinical trials ending in a failure to improve survival outcomes (Khasraw and Lassman, 2010). The nitrosoureas have been administered as single or combination therapies with other chemotherapy agents for high grade gliomas (Weller et al., 2013). The main reasons for failure of the nitrosoureas for GBMs is that many serious side effects including neutropenia and thrombocytopenia associated with using these agents (Chamberlain, 2010). Chemotherapy can be administered after surgery and before radiation therapy as neoadjuvant, with radiation therapy as concomitant, or after radiation therapy as adjuvant chemotherapies (Lonardi et al., 2005, Chamberlain, 2010). The current chemotherapeutic agent for GBM is temozolomide and is used in combination with radiation therapy (Stupp et al., 2005). In addition, other chemotherapeutic agents such as irinotecan (methylating agent) (Friedman et al., 1999, Buckner et al., 2003, Raymond et al., 2003), bevacizumab (Anti-angiogenic agent) (Stark-

Vance, 2005, Vredenburgh et al., 2009, Hasselbalch et al., 2010) , and carmustine (alkylating agent) (Walker et al., 1978, Brandes et al., 2004) have shown promise as a treatment for GBM either individually or in combination with other drugs (Stupp et al., 2006, Vredenburgh et al., 2007a, Peters et al., 2015).

1.2.2.3.1 Temozolomide

Temozolomide is the current first line chemotherapy for GBMs based on the results of a phase III randomised clinical trial in 2005 conducted by the EORTC and NCIC. 572 GBM patients were treated with a combination temozolomide and radiation therapy, and then compared with GBM patients with radiation therapy alone. The median survival, at a 28 month follow-up of 28, was increased from 12.1 to 14.6 months and 2 years survival rate was increased from 10.4 to 26.5% (Stupp et al., 2005). Temozolomide is a DNA alkylating agent and a second generation of imidazotetrazine derivative. The mechanism of action of temozolomide is that at physiological pH temozolomide degrades to MTIC (3-methyl-(triazen-1-yl) imidazole-4-carboxamide) and then methylates the DNA resulting in a stop DNA mismatch repair mechanism leading to apoptosis (Villano et al., 2009, Hart et al., 2013). The current dosing regimen for temozolomide for the treatment of GBM is oral administration of 75 mg/m^2/day for 6 weeks followed by a month of radiation therapy, then 150 mg/m^2/day for 5 days of each month for a period of 6 months. If the patient can tolerate a higher dose, 150 mg can be increased up to 200 mg (Stupp et al., 2009b). However, some studies have shown that the efficacy of temozolomide is reduced with GBM patients with O-6-methylguanine-DNA methyltransferase (MGMT) overexpression which leads to temozolomide resistance. Increasing the temozolomide dose can saturate the enzymatic activity of MGMT, and therefore improve the benefit of using temozolomide for those patients (Sarkaria et al., 2008, Hart et al., 2013).

1.2.2.3.2 Gliadel wafer

The Gliadel Wafer is a local drug delivery device consisting of a polymer wafer loaded with carmustine (bis-chloroethylnitrosourea (BCNU)) as the chemotherapeutic agent. It is designed as a wafer or disc of biodegradable copolymer weighting 200 mg with a 1mm thickness and loaded with 3.85% by weight of BCNU (Brem et al., 1995). BCNU is an alkylation agent approved by the FDA for GBM treatment as a potent antineoplastic drug (Ashby et al., 2016). Gliadel Wafers are implanted in the resection cavity where the BCNU is slowly released. The concentration of BCNU in the cavity from local administration with Gliadel was increased 100 times compared to systemic administration of BCNU (Panigrahi et al., 2011). Currently, the Gliadel Wafer is approved for treatment of recurrent GBM and for newly diagnosed GBMs as adjuvant chemotherapy (Panigrahi et al., 2011, Aoki et al., 2007). In a phase I clinical trial, Brem and co-workers investigated the safety and median survival for 21 glioma patients with implanted BCNU polymer and radiotherapy. The median survival for elderly patients with mean age of 60 was 42 weeks (Alexis et al., 2008a). In comparison between patients with Gliadel after resection post-surgery radiation therapy and placebo group, the median survival rate was significantly increased (Westphal et al., 2003). Moreover, some studies have shown that the Gliadel Wafer can be used in combination with other chemotherapeutic drugs such as temozolomide. The median survival rate for GBM patients treated with combined chemotherapies (Gliadel and temozolomide) was increased up to 21 months in a double blind phase III study (McGirt et al., 2009). However, limited penetration of BCNU into tissue after diffusion from the polymeric wafer (1 mm or less) (Fung et al., 1998), cost of the wafers and other side effects like fatal cerebral oedema, and seizures are the main limitations for its use (Gallego et al., 2007, Weber and Goebel, 2005).

1.2.2.3.3 Irinotecan Hydrochloride (IRN)

1.2.2.3.3.1 IRN properties and chemical structure

IRN is a semisynthetic analog of camptothecin isolated from *Camptotheca Acuminata* Chinese trees in 1983 in Japan (Rothenberg, 2001). IRN is known as a potent topoisomerase I inhibitor and it is metabolised into 7-ethyl-10-hydroxycamptothecin (SN-38) as the active form (Figure 1-2), which is 100 to 1000 more potent compared to IRN (Xu and Villalona-Calero, 2002). SN-38 binds to topoisomerase I enzymes which is important for DNA transcription, and therefore the complexation of SN-38 and topoisomerase hinders ligation of the nicked DNA strand resulting in the DNA breaks leading to cell death (Fuchs et al., 2006). SN-38 metabolites are metabolised into the inactive form (SN-38 glucuronide) in the liver (Xu and Villalona-Calero, 2002).

IRN is a water soluble solid pale-yellow powder with a molecular weight of 586.689 g/mol, molecular formulation of $C_{33}H_{38}N_4O_6$ and melting point of 222-223°C. Its chemical structure is similar to camptothecin derivatives having reversibly hydrolysable lactone ring (Robert and Rivory, 1998). The pharmacokinetics of IRN are fully understood with a half- life between 5 and 18 h (Femke et al., 2018). Irinotecan Hydrochloride (IRN), Irinotecan Hydrochloride Trihydrate, and SN-38 lactone are the main medicinal forms of IRN used in medicine (Table 1-2).

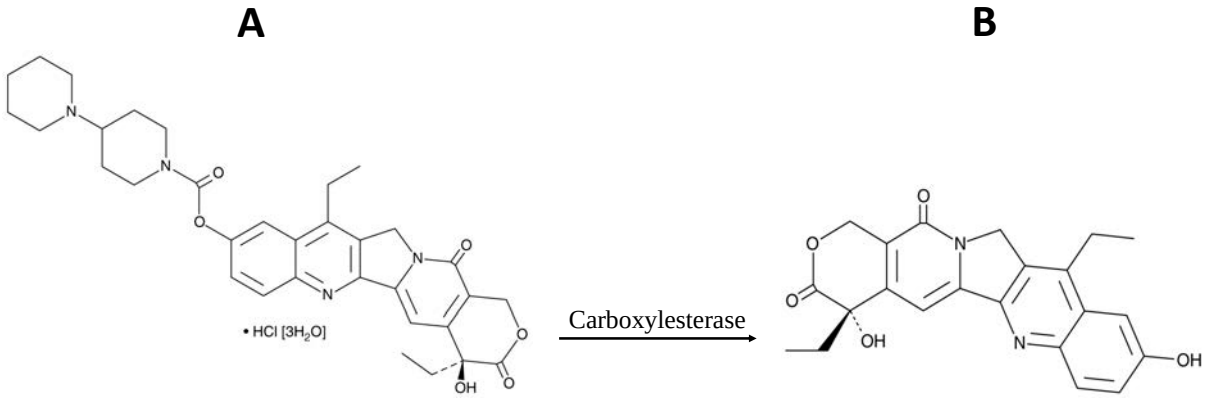


Figure 1-2: Chemical structures of IRN **(A)** and SN-38 **(B)**.

Table 1-2: Names, molecular formula, molecular weight of IRN forms used in medicine as antitumor agents.

IRN forms	Molecular Formula	Molecular weight (g/mol)
IRN Hydrochloride	$C_{33}H_{39}ClN_4O_6$	623.147
IRN Trihydrate	$C_{33}H_{45}ClN_4O_9$	677.192
SN-38 Lactone	$C_{22}H_{20}N_2O_5$	392.411

IRN has been used as a chemotherapeutic agent for a broad spectrum of cancers such as colorectal, ovarian, gastrointestinal tract, and small cell lung cancers (Xu and Villalona-Calero, 2002, Iliescu et al., 2014). Moreover, IRN is established as the first line treatment for metastatic colorectal cancers (Fuchs et al., 2006) and for the treatment of pancreatic cancers in combination with other chemotherapeutic drugs (Fluorouracil, Leucovorin, Oxaliplatin and Gemcitabine) as part of the FOLFIRINOX regimen (Capello et al., 2015). However, IRN is associated with two main adverse side effects; hematologic (neutropenia) and gastrointestinal (diarrhoea) toxicities (Rothenberg, 1998, Hahn et al., 2006). Continuous diarrhoea caused by IRN may lead to the increased residence time of SN-38 in the gastrointestinal tract enhancing the severity of the adverse effects (Fuchs et al., 2006). In addition, IRN is combined with some rare side effects such as anaphylactic reactions, acute renal failure, cardiovascular complication and severe neutropenia (Kweekel et al., 2008).

1.2.2.3.3.2 IRN as a treatment for GBM

IRN has been used as a second or alternative line treatment for GBMs, for those patients who do not respond to the treatment with temozolomide or BCNU (Iacob and Dinca, 2009). The treatment with temozolomide and BCNU may be associated with resistance or serious unwanted side effects. Therefore, the ability of IRN to cross BBB (Hasselbalch et al., 2010) and the different mechanism of action compared to temozolomide is beneficial in overcoming the resistance of GBM to temozolomide as a result , of the methylation of the MGMT enzyme (Vredenburgh et al., 2007b). A study demonstrated that 55% of 60 glioma patients responded for 12 to 42 weeks after intravenous infusion of IRN (Friedman et al.,

1999). A high intravenous dose of IRN is required to improve the therapeutic effect for GBM treatment and that leads to serious side effects of gastrointestinal toxicity such as diarrhoea and neutropenia (Hecht, 1998). All these issues associated with the systemic administration of IRN have prompted the development of novel drug delivery approaches for the delivery of IRN to the brain (Gawley et al., 2020). However. the efficacy of IRN is limited in recurrent and resistant GBMs, but it has improved the response for treatment and survival rate in combination treatment with other chemotherapeutic agents such as temozolomide, and anti-angiogenic bevacizumab for GBMs patients (Hasselbalch et al., 2010, Vredenburgh et al., 2009).

1.3 Challenges of GBM treatment

1.3.1 Toxicity

The toxicity of chemotherapy is the one of the main challenges in the treatment of GBM and the most common toxic side effect is myelosuppression caused by damage to the cells of the bone marrow (Crawford et al., 2004). Neutropenia and thrombocytopenia are induced by myelosuppression, which leads to an increased risk of infection and bleeding (Crawford et al., 2004, Hitron et al., 2011). Generally, myelosuppression is usually associated with high dose chemotherapy and leads to the delay, reduction, and discontinuing of chemotherapy. Consequently, this results in an undesirable impact on survival rate, hospitalisation and quality of life for the patient (Hitron et al., 2011).

1.3.2 Chemotherapy resistance in GBM

Resistance to chemotherapy of GBM is another challenge in the successful treatment which leads to poor prognosis and limited possibilities for chemotherapy treatment (Nakano, 2015). Overexpression of O^6-alkylguanine-DNA alkyltransferase (AGAT) encoded by the O^6-methylguanine-DNA-methyltransferase (MGMT) mediates GBM resistance to alkylating

agents used in chemotherapy. The function of AGAT, is as DNA repair enzymes, in GBM resistance to alkylating agents it is that removal of the alkyl group from O^6 AND O^4 positions of guanine and thymine, respectively, and therefore prompts resistance to alkylating agents (Gerson, 2004). However, reducing AGAT level in the tumour may improve response to chemotherapy by methylation through epigenetic silencing of the MGMT gene (Gerson, 2004, Weller et al., 2013). Studies have demonstrated that response to chemotherapy and survival rate have increased in patients using a methylation promoter in combination with alkylating agents (Hegi et al., 2005). 30 to 60% of GBM cases with methylation of MGMT, are associated with a favourable outcome when treated with alkylating agents, with an increase in survival rate from 12.7 months to 21.7 months. GMB cells are more sensitive to temozolomide if MGMT is methylated via O6-benzylguanine (Alifieris and Trafalis, 2015, Hegi et al., 2005).

1.3.3 Blood brain barrier (BBB)

The BBB is a vascular cellular system in the human and other mammals located in the wall of brain and spinal cord capillaries. The main characteristics of the BBB include continuous physical barriers (such as endothelial cells with tight junctions) and metabolic barriers (such as enzymes and transporters), lacking fenestration, and low activity of pinocytotic (Kniesel and Wolburg, 2000). The combination of these characteristics of physical, metabolic, and transport barriers mediate the functions of the BBB (Abbott et al., 2006a). Nevertheless, owing to its large surface area 12- 20 m^2 and short diffusion distance between capillaries and neurons makes the BBB a potential site to regulate the uptake and delivery of drugs to the brain (Abbott, 2004, Abbott, 2005). The drug molecules that can cross the BBB by passive diffusion is limited; with small molecules having a molecular weight less than 400-600 Da and lipophilic in nature being the most likely (Deeken and Löscher, 2007). Because of the BBB, approximately 98% of small molecules and all large molecules such as peptides and

proteins cannot be delivered to the brain. Almost all chemotherapeutic drugs cannot cross the BBB because they are hydrophilic or larger than 500 Da (Lawrence, 2002, Tam et al., 2016). All Other molecules can access the brain by receptor mediated transcytosis, or specific carrier systems, and that is a huge challenge for drug delivery to the brain for the treatment of CNS diseases such as GBM (Deeken and Löscher, 2007). Therefore, the presence of the BBB in the brain is one of the main limitations for successful treatment of GBM using systemic chemotherapy.

1.3.3.1 Function and structure of BBB

The BBB is a physical and metabolic barrier between the CNS and the general circulatory systems designed to maintain homeostasis in the brain and protect the brain from damage by neurotoxins (Abbott et al., 2006a, Abbott et al., 2010). One of the important functions of the BBB is to provide a stable environment and maintain the ionic composition of the brain (Abbott et al., 2010). Moreover, the BBB protects the brain from tissue damage by preventing the entry of macromolecules such as plasma proteins like albumin, pro- thrombin and plasminogen (Gingrich and Traynelis, 2000).

The BBB is a complex network consisting of endothelial cells, pericytes, astrocytes, and perivascular mast cells with tight junctions (Figure 1-3). The properties of the BBB are mediated by interaction of these different types of cells (Abbott, 2005). An adherence of endothelial cells in the BBB is made of tight junctions which are formed by cadherins and catenin proteins, and therefore this adherence creates high transelectrical resistance of more than 1500 Ω cm^2. The tight junctions have three main proteins which are occludin, claudins, and junctional adhesion molecules. Occludin and claudins proteins support the junction stands, while the junctional adhesion molecules protein mediates the transport of

lymphocytes, neutrophils, and dendritic cells from the vascular system if there is an immunologic response in the brain (Kastin et al., 1999, Mahmoud et al., 2020).

1.3.3.2 Status of the BBB in GBM

In different CNS diseases, such as gliomas, the function and structure of the BBB can be lost or altered. The BBB is altered in GBM patients and is therefore less intact compared to a normal healthy brain (Deeken and Löscher, 2007) (Figure 1-3). By analysis of GBM samples, there is molecular alteration in microvessels through changing in junction protein expression, morphology alteration in pericytes, and alteration in continuous endothelial cells to be intermittent (Liebner et al., 2000). The alteration in the BBB does not occur uniformly throughout the tumour, whereby this disruption in BBB occurs in the core of tumour while remaining intact in other parts of tumour (Deeken and Löscher, 2007). In addition, the changes in BBB are unpredictable between GBM patients, which may limit the development of new chemotherapy treatments.

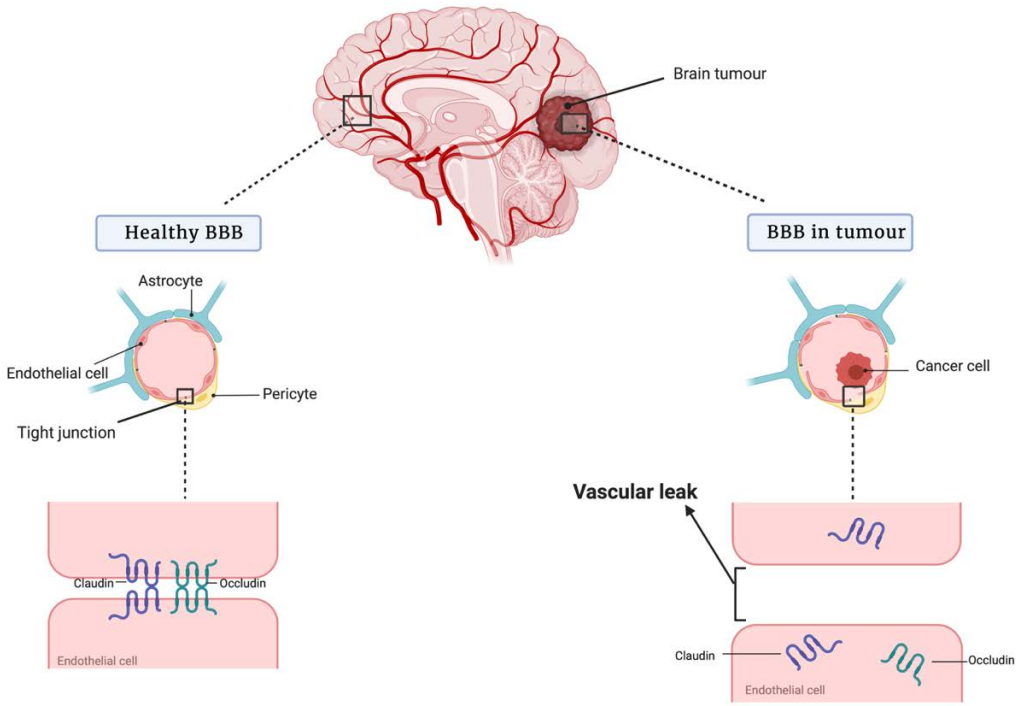


Figure 1-3: A schematic depicting sections of the brain showing healthy BBB with endothelial cells connected with tight junctions (figure the left) and BBB in tumours with disrupted endothelial cells (figure the right).

1.4 Drug delivery to the brain

A number of strategies have been employed to achieve effective delivery of chemotherapeutic drugs to GBMs and can be classified into invasive and non-invasive strategies.

1.4.1 Invasive strategies for drug delivery to the brain

1.4.1.1 Disruption of the BBB

In 1989, Keuwelt and co-workers developed BBB disruption (BBBD) techniques to improve anticancer agent delivery to the brain. This technique uses intra-arterial administration of hypertonic solutions, such as mannitol, to create a temporary disruption of the BBB (Fortin et al., 2005, KrolI et al., 1998). Administering pre-warmed mannitol through the internal carotid artery has increased permeability of some vasoactive molecules like leukotriene and bradykinin (Blanchette and Fortin, 2011). The concentration of chemotherapeutic drugs in the brain has been increased with applying the BBBD technique (Remsen et al., 2000). BBBD technique has been employed with bevacizumab treatment for patients with recurrent glioma, and the result has shown improvement in therapeutic outcomes (Boockvar et al., 2011). This technique has the advantage that the drug can be easily administered to the brain but it is associated with potential risk and leads to changing of vascular pathology and chronic neuropathological in the brain (Blanchette and Fortin, 2011).

1.4.1.2 Intraventricular/Intrathecal administration

This strategy is done by direct injection of drug to cerebrospinal fluid (CSF) through direct intralumbar injection or intraventricular infusion using an implantable reservoir to introduce the drug at constant high concentration in the brain. In 1963, the Ommaya reservoir, as a subcutaneous reservoir and pump (SRP), was introduced to avoid repetition of sampling and introducing drugs into CSF (Ommaya, 1963). The SRP is a plastic reservoir with outlet

catheter within the brain and drugs can be injected to the reservoir and then by manually compressing the reservoir, drugs can be delivered to the brain (Begley et al., 1990). This reservoir was introduced initially for administration of antifungal agents for the treatment of fungal meningitis (Ommaya, 1984). The most common limitations of using SRP include slow drug distribution in the brain, high intracranial pressure, CNS infections, and haemorrhage (Chamberlain et al., 1997, Misra et al., 2003).

1.4.1.3 Convection-enhanced delivery (CED)

Convection enhanced delivery works via fluid convection within the brain by placing a catheter inside the interstitial space. Fluid convection can be created in the brain by interstitial infusion under a pressure gradient leading to better diffusion and enhanced distribution of drug molecules even those with high molecular weight such as proteins (Bobo et al., 1994). CED relies on a concentration and pressure gradient, and is not influenced by the molecular weight of drug (Bobo et al., 1994). The main challenge with CED is achieving an optimal infusion rate as a result of the development of backflow in the catheter (Vogelbaum, 2007). The use of CED for nanoparticles (NP) drug delivery may improve their delivery to the brain by achieving an optimal distribution of NPs, and diffusing NPs to the tumour mass and infiltration cells (Sampson et al., 2008). However, CED is still invasive in nature and can be associated with high risk of infections, tissue injury, air bubbles and leakage into sensitive areas of the brain (Bennewitz and Saltzman, 2009).

1.4.2 Non-invasive strategies for drug delivery to the brain

1.4.2.1 Passive diffusion

Passive diffusion across the BBB occurs when a drug dissolves in the lipid membrane of an endothelial cell and is then released into the brain (Figure 1-4). The physicochemical properties of the drug and concentration gradient between blood and brain mediate passive

diffusion through the BBB. Therefore, low molecular weight, lipid soluble and neutral molecules can cross BBB via passive diffusion. In addition, passive diffusion is also dependent upon the size and lipophilicity of molecules (Fischer et al., 1998). Plain NPs (with no surface modification) and pegylated NPs can be delivered to the brain via passive diffusion. Moreover, they have the ability to diffuse to the brain by enhanced permeability and retention effect (EPR) through leaky vasculature in the tumour tissues. For instance, Paclitaxel-loaded lipid NPs and doxorubicin-loaded liposomes accumulated in the brain with therapeutic efficacy in recurrent glioma patients (Koziara et al., 2004, Hau et al., 2004).

1.4.2.2 Carrier-mediated transport (CMT).

CMT can occur via active or passive diffusion, which occur at the BBB and facilitates transport via a concentration gradient and endocytosis (Garg et al., 2015) (Figure 1-4). The essential polar molecules including glucose, amino acids, and nucleoside are transported to the brain by various carrier transporter (influxes transporters); which are GLUT1 glucose transporter, LAT1 large amino acid transporter, and CNT2 transporter, respectively (Garg et al., 2015, Kumagai et al., 1987, Sai et al., 1998).

Efflux transporter proteins at the BBB remotely remove drug molecules from the brain. The delivery of chemotherapeutic drugs can be improved by inhibition of the efflux mechanism, leading to enhanced concentration of the drug in the brain. Several studies have concluded that the concentration of drugs in the brain have increased by using efflux pumps inhibitors such as p-glycoprotein (P-gp) or breast cancer resistant protein (BCRP) inhibitors (Agarwal et al., 2011a, Agarwal et al., 2011b).

1.4.2.3 Endocytotic transcytosis

Endocytotic transcytosis is the main mechanism of transport for macromolecules such as proteins and peptides to the CNS and consists of two main mechanisms; adsorptive mediated

transcytosis (AMT), and receptor mediated transport (RMT) (Abbott et al., 2010) (Figure 1-4).

1.4.2.3.1 Adsorptive mediated transcytosis (AMT)

AMT is based on electrostatic interactions between negatively charged sites on the brain endothelial site and positively charged molecules (Abbott et al., 2010). Thus, this interaction induces endocytosis followed by transcytosis (Sauer et al., 2005). The AMT transport in the BBB may be facilitated by coupling molecules to short cationic peptides known as penetrating peptides (CPPs) (Drin et al., 2003). This technique was exploited to improve drug delivery to the brain by using drugs and NPs with a positive charge, or conjugating them with positively charged ligands (Wang et al., 2010, Hervé et al., 2008).

1.4.2.3.2 Receptor mediated transcytosis (RMT)

RMT, known also as clathrin-mediated endocytosis, is a highly specific and energy-mediated transport. RMT is the route by which receptor-ligand complexes are internalised within endocytic vesicle (Vyas and Sihorkar, 2000). Macromolecules such as peptides and proteins can cross the BBB by RMT through conjugating the molecules to ligands and then interacting with specific receptors on the membrane of endothelial cells in the BBB (Abbott et al., 2010). Several receptors (such as transferrin receptors (TfR), insulin receptors, and lipoprotein-related protein 1 receptor) are involved in the RMT process and some of these receptors are expressed on the BBB of GBM patients (Pardridge, 2003). A conjugation between ligands and macromolecules binds to the specific receptor on the endothelial cell surface and then it is internalised into the cells and subsequently exocytosed at the abluminal side of the endothelial cells of the brain (Abbott et al., 2010). RMT is considered an interesting transport mechanism for drug delivery. In addition, it has been used to improve delivery of free drug and chemotherapeutic drug-loaded NPs into the brain (Kreuter, 2001).

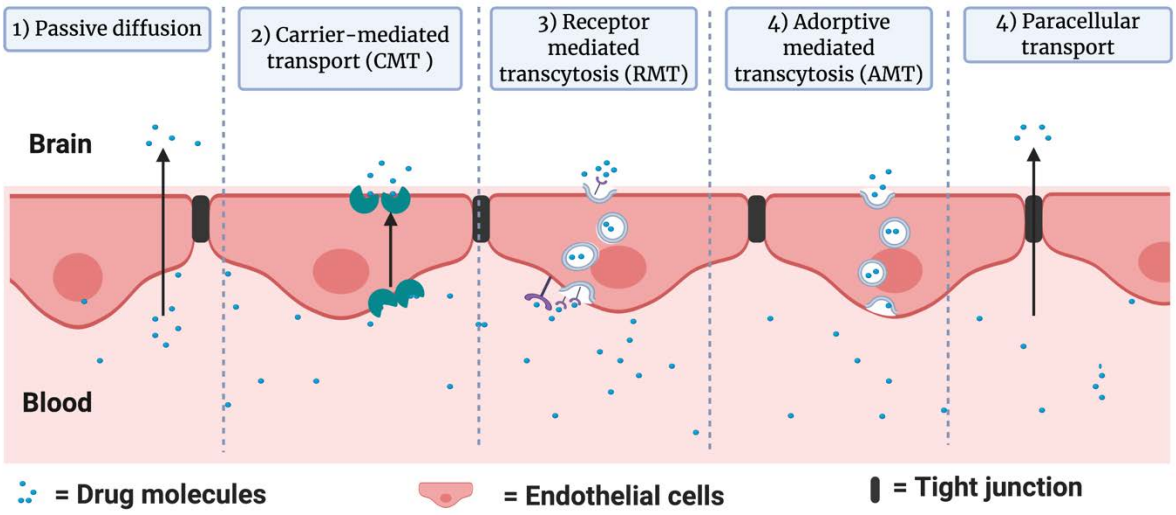


Figure 1-4: A schematic representation of major pathways of drug transport cross the BBB.

1.5 Nanoparticles (NPs) in drug delivery system

NPs are colloidal, submicron-sized drug carriers that carry entrapped drugs to the target and release drugs under certain conditions in the body. The diameter of NPs usually varies from 1 to 1000 nm and the term NP includes nanospheres and nanocapsules. Drugs in the nanosphere, matrix structure, may be absorbed at the surface of the sphere or entrapped within the particle. Nanocapsules consist of an inner liquid core that is surrounded by a polymer. In this case the drugs are usually dissolved in the liquid core and may be adsorbed to the outer surface (Reis et al., 2006). During recent decades, NPs have gained plenty of attention as drug delivery devices. NPs have been used to deliver the drugs to a target tissue and improve the therapeutic effect while reducing side effects. The main goal when designing NPs is the controlled release of the drugs at the target site (Knight, 1981). Liposomes are a similar type of formulation to NPs. Liposomes are small artificial spherical vesicles consisting of an aqueous region surrounded by bilayers of lipids (Akbarzadeh et al., 2013). Polymeric NPs have some advantages over liposomes. Despite the liposomes have unique properties which include protecting the drugs from degradation, improving the targeting, and reducing side effects (Knight, 1981). The clinical use of liposomes has been limited due to poor stability during storage, low encapsulation efficiency (EE) and leakage of drug during

storage or in the blood. On the other hand, NPs help to improve the stability of pharmacologically active agents such as drugs, protein, and peptide and to achieve good controlled release properties (Soppimath et al., 2001). Also, NPs have many advantages over microparticles. Intracellular uptake of NPs are relatively higher than microparticles (Reis et al., 2006, Jung et al., 2000). The ideal NP used for drug delivery should be biodegradable and biocompatible with targeted delivery and controlled release. These properties can be achieved via the manufacturing processes and polymers used to produce NPs as well as any surface modifications used. NPs with no surface modification (conventional NPs) and which were negatively charged are rapidly opsonised and cleared by macrophages. Thus, the most common way to protect these NPs from opsonization is via surface modification with hydrophilic polymers. The type of NPs as well as their charge can influence intestinal uptake. Thus, positively charged polymeric NPs have a high affinity for uptake by follicle-associated epithelium, while negatively charged NPs have low uptake affinity for all types of intestinal tissues (Soppimath et al., 2001, Kumar et al., 2001). Therefore, polymeric composition such as hydrophobicity, outer surface charge, and biodegradation are important parameters for NPs that may affect their absorption, distribution, and elimination(Reis et al., 2006).

Biodegradable polymeric NPs have been extensively studied for drug delivery applications. Both natural and synthetic biodegradable polymers have been used for targeted and controlled release. Natural biodegradable polymers such as collagen, gelatine, and haemoglobin are limited due to cost and purity issues. Synthetic biodegradable polymers do not have these issues, thus they have been used more wildly in drug delivery applications (Jain, 2000, Jalil and Nixon, 1990). Thermoplastic aliphatic polyesters including poly(D,L-lactide) (PDL), poly(lactic acid) (PLA), poly(D,L-glycolide) (PLG), and especially PLGA have generated enormous interest because of their properties. They have good

biocompatibility, biodegradability, mechanical strength, and they are appropriate to carry different classes of drugs such as protein, peptide, and micro-molecules (Jain, 2000).

1.6 Nanoparticles (NPs) for drug delivery to the brain

NPs have proved to be a promising carrier for penetration and enhancing the uptake of drugs across the BBB (Li et al., 2011). A range of different NP formulations have been investigated for delivering chemotherapeutic agents to the brain. The majority of these formulations have utilised polymers that have the desired requirements for biological applications (Adabi et al., 2017). During recent years, NPs for the treatment of GBMs and other CNS diseases have received significant attention (Wong et al., 2012, Saraiva et al., 2016). A small percentage of systemic free drug administration crosses the BBB with non-specific accumulation in off target tissues resulting in serious unwanted side effects. Therefore, the percentage of drug that crosses the BBB has the potential to be increased by formulating them NPs, while reducing non-specific accumulation in other tissues (Chapman et al., 2013, Koo et al., 2006). For example, gadolinium-loaded NPs increased the level of gadolinium 100 fold when compared to free gadolinium (Koffie et al., 2011). Kreuter et al. developed a polymeric system to deliver the drugs to the central nervous system by using poly (butylcyanoacrylate) (PBCA) NPs with dalargin. The penetration of dalargin increased by 3 fold when it was encapsulated in PBCA compared with free drug (Kreuter et al., 1995, Kreuter, 2001).

The manufacture of NPs has improved in the last few years to optimize size, EE and sustained release. Furthermore, stealth capabilities of NPs have been used to protect NPs from protein agglutination in the blood, and to avoid clearance from the blood by the reticuloendothelial system (RES) (Winer et al., 2011, Kelkar and Reineke, 2011). In drug delivery, PEGylation of NPs has been commonly used to protect NPs from blood protein

binding and from the RES (Salvati et al., 2013, Hadjidemetriou et al., 2015). Dawson et al has proved that PEGylation of NPs completely prevented their interaction with plasma proteins. However, other studies have shown that the interaction between proteins and NPs in the blood has not been completely prevented by PEGylation. (Downs et al., 2015). Surface modified NPs with ligands have been used to facilitate imaging of brain tumours (Winer et al., 2011, Kelkar and Reineke, 2011). While coated NPs have been developed for targeted treatment of brain cancers (Grover et al., 2014, Ramalho et al., 2018). Glutathione coated PLGA (poly(lactide-co-glycolide)) NPs containing paclitaxel with a size of approximately 200 nm showed a controlled drug release and had not been effluxed by P-glycoproteins pump across the BBB. In addition, The coated PLGA NPs containing fluorescent dye had improved brain uptake compared to free dye solution (Geldenhuys et al., 2011).

NPs offer a non-invasive method for drug delivery to the brain. However, to improve their effectiveness and ability to cross the BBB, NPs need to be optimised in relation to size, release kinetics, chemical properties as well their ability to protect the drug from the biological environment and enhance drug solubility. Furthermore, modifying their surface could improve their targeting and ability to cross the BBB and accumulation at the site of tumour. (Meyers et al., 2013). In order to be most effective treatment for brain tumour, with decreased toxicity , NPs need to fulfil certain criteria, which include non-toxic, biodegradable, extended circulation time, no blood aggregation, high EE and the ability to cross the BBB (Tian et al., 2014).

The ability of NPs to be loaded with single or multi drugs and targeted with several ligands makes them a promising tool to improve the treatment of GBM. Moreover, the crossing of the BBB by NPs depends on their physicochemical properties with no alteration to the

structure of the drugs needed. NPs can enhance passive diffusion of drugs into the brain by increasing the concentration gradient between blood and brain resulting in concentrating of the drug at the surface or inside of BBB (Haque et al., 2012). NPs can diffuse and accumulate in the tumour by the EPR effect because of the leaky vasculature in the tissues of tumours increasing the concentration of the drug in the tumour compared to the plasma (Figure 1-5). NPs may help to achieve an effective treatment for GBMs by improving the ability of the drugs to cross the BBB, reducing side effects, achieving sustained release, and avoiding rapid clearance of the drugs (Wicki et al., 2015).

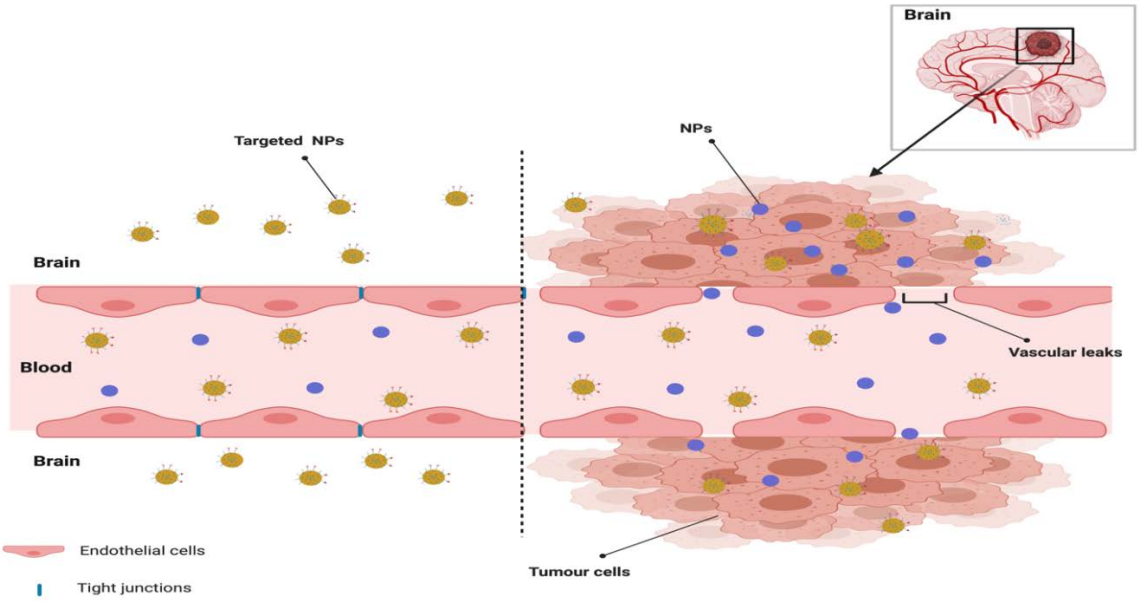


Figure 1-5: A schematic representation of EPR effect. Healthy BBB are surrounded with intact endothelial cells with tight junction and in contrast, BBB in tumour BBB with loss tight junction between endothelial cells. Only targeted NPs can cross both healthy and disrupted BBB, while non-modified NPs can pass to the tumour based on EPR effect.

1.7 Polymeric Nanoparticles (NPs) for drug delivery to the brain

Polymeric NPs are known as colloidal submicron NPs and are used as carriers of various drugs such as chemotherapeutic drugs, either adsorbed on the surface or encapsulated within the NPs (Reis et al., 2006). Many types of polymers such as poly(lactic acid) (PLA), poly(Ɛ-caprolactone) (PCL), Poly(butyl-cyanoacrylate) (PBCA), poly (glycolic acid) (PGA), PLGA and poly (amino acids) have been used in the manufacture of NPs. Due to their

biocompatibility and low toxicity relative to other polymers, PLGA, PGA, and PLA are the most extensively utilised polymers in drug delivery to the brain, (Béduneau et al., 2007). They all degrade into lactic acid and glycolic acid which enter into the Krebs cycle where their metabolites are extracted from the body as carbon dioxide and water. (Crotts and Park, 1998). The advantages of Polymeric NPs over other types of NPs include improved release kinetics, better compatibility with some active agents, no oxidation issues as with phospholipids and improved shelf-life (Shi et al., 2011, Davis, 2009, Drummond et al., 1999). An understanding of the molecular weight, crystallinity and stability of the polymers and physicochemical properties of the drug would be very important for the successful production of polymeric NPs for drug delivery to the brain. (Masood, 2016).

The first polymeric NPs developed to deliver drugs to the brain was performed by Kreuter *et al*. The BBB penetration of dalargin was significantly increased by formulating it into PBCA NPs (Kreuter et al., 1995). In 2001, Kreuter *et al.* used the same dalargin-loaded PBCA NPs coated with p80, to increase penetration into brain tissue. This NP formulation was utilised for the delivery of other chemotherapeutic drugs, such as doxorubicin and loperamide into the brain (Kreuter, 2001). Calvo *et al* prepared PEG-PHDCA (poly(hexa-decyl cyanoacrylate)) NPs that displayed greater accumulation in the brain when compared to the p80 formulation, which could be due to passive diffusion or intake via macrophage (Calvo et al., 2001). The density of the PEG coating on the surface of the NPs can influence the level at which they cross the BBB. Vila *et al* developed PEG-PLA NPs with different densities of PEG coating and showed that a greater accumulation in the brain of the smaller NPs, has achieved with the highest PEG density (Gao et al., 2006).

1.7.1 Targeted polymeric NPs for the Treatment of GBM

The active targeting of polymeric NPs via surface modification with ligands that bind to target molecules on the surface of cancer cells or other cells within the body is a significant development in nanotechnology (Kamaly et al., 2012) (Figure 1-4). Table 1-3 shows examples of targeted polymer NPs as treatments for GBM. The affinity ligands bind directly to antigens that are differentially overexpressed on the plasma membrane of cells or to extracellular proteins on the target tissue (Kamaly et al., 2012). Active targeting of NPs can be used for either extracellular or intracellular delivery of drugs. NPs are more effective if they are targeted to intracellular sites (Shi et al., 2011, Sugano et al., 2000).

Targeted NPs can have either single or multi ligands attached to their surfaces. To date, most researchers have preferred to use a single ligand as multi-ligands are associated with some disadvantages, particularly when used for penetration of the BBB and tumour cells. For example, multi-ligands influence drug release as well as the mobility of the NPs. Furthermore, competitive binding and/or an interaction between ligands may reduce the targeting efficiency of the NPs (Jain et al., 2015).

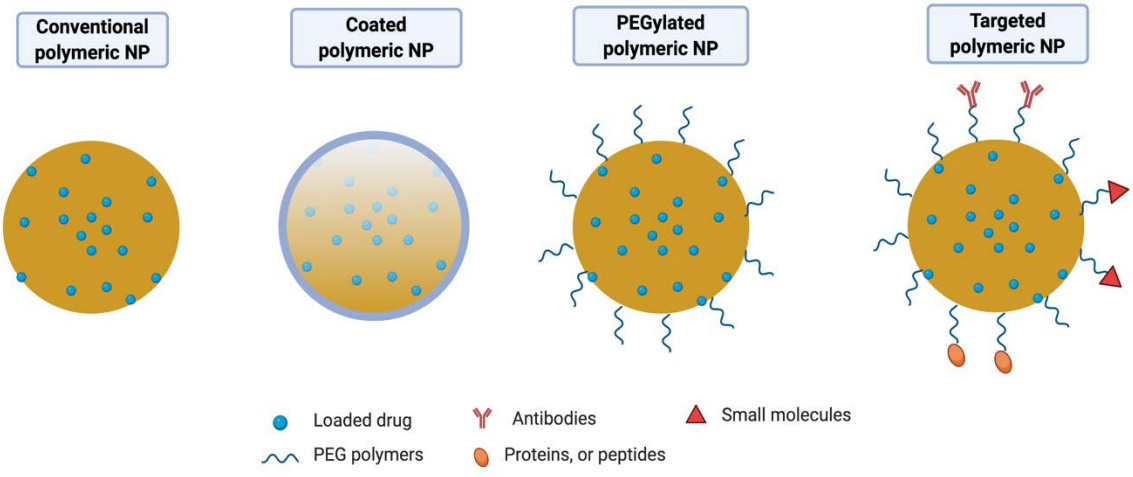


Figure 1-6: A schematic illustration non-modified and modified surface of PLGA NPs.

Table 1-3: Examples of developed targeted polymer NPs as targeted drug delivery system for treatment of brain tumours malignant gliomas (Mahmoud et al., 2020).

Polymer type	Drug-Loaded	Size (nm)	Targeting strategy	Targeted site	Ref.
PLGA	Dil	90	Transferrin	TfR	(Chang et al., 2009)
PMLA	Antisense ON	25	mAbs-antisense oligonucleotides (AONs)	(proteins) laminin-411	(Ding et al., 2010)
PEG-PCL	Paclitaxel	<100	Angiopep	LRP	(Xin et al., 2011)
PEG-PLGA	Coumarin 6	125	peptide (12 amino-acid)	Peptide	(Li et al., 2011)
PEG-PCL	Paclitaxel Rhodamine	90	Angiopep	LRP	(Xin et al., 2012)
PLGA	methotrexate	85	Transferrin	TfR	(Jain et al., 2015)
PEG-PLGA	doxorubicin	100-300	endogenous tripeptide thiol (glutathione)	Glutathione transporter	(Geldenhuys et al., 2015)
PLGA	loperamide	100	mAbs (8D3)	TfR	(Fornaguera et al., 2015)
PLGA	Curcumin	100	Magnetic guidance Peptide (T7)	TfR	(Cui et al., 2016)
PLGA	doxorubicin	120	poloxamer 188	LRP	(Malinovskaya et al., 2017)
PEG-PLGA	TMZ	190	mAbs (OX26)	TfR	(Ramalho et al., 2018)
PLGA	Paclitaxel	230-255	Tripeptide (RGD) Superparamac iron oxide	αvβ3 integrin	(Ganipineni et al., 2019)

1.7.2 Application of targeted polymeric NPs in drug delivery to the brain

1.7.2.1 Ligand-polymeric NPs

Alexis *et al* demonstrated increased cytotoxicity of paclitaxel-loaded NPs using a ligand targeted to the extracellular domain of the trans-membrane human epidermal growth factor receptor 2 (HER-2) when compared with non-targeted NPs. This improvement in cytotoxicity was due to the targeted NPs increased cellular uptake (Alexis et al., 2008b). Studies have also reported that the most effective function in using targeted NPs is to increase cellular uptake (Kirpotin et al., 2006, Bartlett et al., 2007).

Low density lipoprotein receptor related protein (LRP) and TfR are known to be overexpressed on glioma cells (Jain et al., 2015). These two receptors were used to target glioma cells with polymeric NPs by binding the anti-transferrin and angiopep ligands to their surface. Anti-transferrin can cross the BBB through TfR while the angiopep ligand binds to LRP on the surface of glioma cells (Jain et al., 2015, Xin et al., 2012). The TfR is the most widely characterised receptor-mediated transport system, which provides successful cellular uptake and it is overexpressed in numerous tumours cells (Chang et al., 2009). BBB targeting of an *in-vitro* model has increased 20-fold with TfR-PLGA NPs compared to targeted PLGA NPs. Chang *et al* demonstrated that TfR-PLGA NPs had a 20-fold increase in uptake by the BBB, using an in vitro model of the BBB, when compared to un-modified PLGA NPs. The cellular uptake of the TfR-PLGA NPs by the BBB model was by endocytosis mechanism (Chang et al., 2009). The major disadvantages of using TfR as a ligand for NPs is the competition with endogenous TfR for receptor binding. This may result in reducing the cellular uptake and thus the effectiveness of the NPs (Georgieva et al., 2014). An antibody directed against the TfR has been used as an alternative ligand to the endogenous TfR as it binds to an epitope of the TfR which is located at a different location from TfR binding.

Therefore, the NPs have less binding competition as they do not interfere with the TfR intake mechanism. This will increase their cellular uptake and thus their effectiveness (Chen and Liu, 2012). Different monoclonal antibodies (mAb) such as OX26 (anti-rat TfR mAbs), R17-217 and 8D3 (both anti-mouse TfR mAbs) have been developed for enhancing brain uptake. OX26 mAbs has been shown to have a high affinity for cells that overexpress TfR, including GBM cells (Loureiro et al., 2014, Calzolari et al., 2010). The level of brain uptake for each of the antibodies is different. For example, the brain uptake of 8D3 mAbs was relatively high compared to R17-217 mAbs. 8D3 and R17-217 mAbs were more selective for the brain than liver and kidney (Lee et al., 2000). Rmalho *et al* developed receptor mediated TMZ-loaded PLGA NPs for GBM treatment functionalized with an OX26 mAbs. The cellular internalization of the OX26mAbs NPs was significantly enhanced compared to the PLGA NPs with no mAbs (Ramalho et al., 2018).

Another promising LPR ligand for delivering NPs to the CNS and BBB penetration is angiopep. It is from a peptide family that is derived from aprotinin and human proteins (Demeule et al., 2008b). The transcytosis capacity and parenchymal accumulation of angiopep-2 is much greater compared to transferrin (Demeule et al., 2008a). The ability of angiopep to facilitate penetration of the BBB of polymeric NPs has been confirmed in a number of studies (Shao et al., 2010, Xin et al., 2011). Xin *et al* fabricated dual targeting NPs to improve the drug delivery of paclitaxel to glioma cells. Angiopep-PEG-PCL NPs were highly endocytosed by U87 GBM cells compared with non-targeted PEG-PCL NPs. These NPs have also shown higher penetration, distribution, and accumulation in 3D glioma spheroids as well as increased efficacy in U87 tumour bearing mice (Xin et al., 2011, Xin et al., 2012).

1.7.2.2 Coated-polymeric NPs

Another approach to enhancing the uptake of NPs by the BBB is to coat them with a polymer that will facilitate cellular uptake. As discussed earlier about the role of surfactants in coating, Kreuter demonstrated that intravenously injected doxorubicin-loaded p80-coated NPs had a 40% cure rate in rats with intracranially transplanted GBMs. Although not fully elucidated, they hypothesised that the most likely mechanism for transport of the NPs across the BBB was endocytosis by the endothelial cells lining the brain blood capillaries. Coating the NPs with p80 lead to the adsorption of apolipoprotein E from blood plasma onto the NPs surface. The particles then mimicked low-density lipoprotein (LDL) particles and could thus interact with the LDL receptor leading to their enhanced uptake by the endothelial cells (Kreuter, 2001). The first polymeric NPs for penetration of the BBB were investigated by Schröder *et al* in 1995. PBCA NP coated with p80 enhanced BBB penetration of hexapeptide dalargin-loaded NPs (Schröder and Sabel, 1996). Wohlfart *et al* demonstrated, using a rat glioma model, that poloxamer 188-coated PLGA NPs enabled the delivery of doxorubicin across the BBB in therapeutically effective concentrations. The basis for their transport across the BBB was hypothesised to be adsorption of blood apolipoproteins (ApoE or ApoA-I) onto the NPs surface due to the poloxamer 188 coating, followed by RMT of the NPs (Wohlfart et al., 2011). Manlioovskaya *et al* demonstrated that these same NPs entered U87 human GBM cells via clathrin-mediated endocytosis. They also demonstrated that the NPs released their doxorubicin via diffusion rather than by intracellular degradation (Malinovskaya et al., 2017). These studies prove that PLGA NPs coated with poloxamer 188 could improve the delivery of doxorubicin and potentially other chemotherapeutic drugs into brain tumours.

1.8 Routes of Administration of NPs in the Treatment of Malignant Gliomas

There are three main routes of administration for NPs designed to treat brain tumours: 1. direct delivery to the brain; 2. direct systemic delivery to the brain and 3. indirect systemic delivery to the brain.

1.8.1 Direct delivery

Direct delivery to the brain offers a way of bypassing the BBB by direct injection of the NPs into the brain. CED has been used to infuse a NP suspension directly into brain tissue. Lollo *et al* used CED to deliver 10 µl of paclitaxel-loaded lipid nanocapsules directly into the brain of mice. The results showed that the overall survival of mice treated with the lipid nanocapsules was significantly increased in comparison with mice treated with free paclitaxel (Lollo et al., 2015, Allard et al., 2010). Fourniols *et al.* described the direct injection of photo-polymerizable hydrogel containing TMZ-loaded micelles to the brain using a syringe to inject through an incision drilled in the skull. The TMZ-loaded micelles and injection were well tolerated while the hydrogel improved the drug release profile (Fourniols et al., 2015). The major limitations of direct delivery to the brain is its invasive nature, the risk of infection and the need to control critical parameters such as pH and osmolarity which if not optimised may lead to brain damage (Huynh et al., 2012).

1.8.2 Direct systemic delivery

Direct systemic delivery to the brain is where NPs are directly administered into blood stream through the carotid artery and transported to the brain avoiding the majority of the systemic circulation. This technique has shown improved survival compared to CED with reduced risk of brain damage (Laine et al., 2012). Huynh *et al.* administered ferrociphekunol-loaded NPs to the brain of GBM inflicted rats using both CED and direct systemic delivery. Direct systemic delivery provided a survival of 28 days compared to 24 days for the CED group.

The results indicated that direct systemic delivery could provide a modest increase in survival when compared to direct delivery to the brain (Huynh et al., 2012, Huynh et al., 2011).

1.8.3 Indirect systemic delivery

Indirect systemic delivery involves the delivery of NPs into the systemic circulation via routes of administration that require absorption such as oral, topical, nasal, and peritoneal administration. The major advantages of oral administration are the convenience, non-invasiveness, and patient compliance. Kumar *et al* administered two curcumin formulations (NPs and plain suspension) orally to a rat intestinal ex-vivo model. The results showed that the bioavailability of NPs formulation was 12 times greater than the plain suspension (Kumar et al., 2016). Intraperitoneal administration is widely used as an indirect systematic delivery method by injecting the drug into peritoneal tissue. It is used when administering large doses or when it is difficult to locate a vein for direct systemic delivery (Verreault et al., 2015).

1.9 Additional challenges to using NPs as in the treatment of GBMs

In additional to the BBB and multi drug resistance there are other challenges associated with using NPs as drug delivery systems in the treatment of GBM which include the reticuloendothelial system, the renal system and pathophysiological barrier in tumours.

1.9.1 The reticuloendothelial system (RES)

NPs can be cleared from the blood stream by the RES which is also known as the mononuclear phagocyte system (MPS), through phagocytes-NPs binding and stimulating a cytokine cascade (von Roemeling et al., 2017). In addition, NPs can be recognised by the immune system and then cleared from the blood because of the attachment of proteins and peptides in the bloodstream (Choi et al., 2007). The surface modification of the NPs could

protect NPs from being recognised by the RES could solve this challenge and increase their circulation time in the bloodstream (von Roemeling et al., 2017).

1.9.2 The renal system

The process of blood filtration in the renal system is considered as one of the main challenges of using NPs. NPs with a size range of 70 to 100 nm can pass through the fenestrated endothelium, however, will face difficulty crossing the glomerular filtration barrier which clears particles sized between 2 to 8 nm (von Roemeling et al., 2017). The shape and charge of the NPs could influence the process of renal clearance. Since the glomerular basement membrane has a negative charge, cationic NPs can display increased renal clearance compared to the same sized neutral or anionic NPs (von Roemeling et al., 2017, Ruggiero et al., 2010).

1.9.3 Pathophysiological barrier in tumours

Deep penetration of NPs through tumour tissue is difficult due to the composition and structure of the extracellular matrix, and vasculature difference of the tumour which is dependent on the location and stage of the tumour (von Roemeling et al., 2017). The microenvironment of the tumour is usually characterised by leaky vessels, abnormal blood flow, and interstitial hypertension which are caused by dysfunction of the lymphatic vessels and vascular hyperpermeability (Boucher et al., 1990, Jain, 2005). All these characteristics could hinder the diffusion process of NPs into the tumour. There are several strategies to overcome this challenge and improve drug delivery into the tumour. For example, using antiangiogenic agents to normalize the tumour vasculature, reduce vessel size and vascular permeability in GBM patients (Jain, 2005). Moreover, degrading components of the tumour matrix such as collagen and glycosaminoglycan by using bacterial collagenase treatment to

normalize the extracellular matrix of the tumour and resulting in improving NPs penetration (Alexandrakis et al., 2004).

1.10 Clinical Transition of Polymeric NPs

Polymeric NP formulations utilizing different polymers, coatings and targeting ligands have been introduced into the clinic. The FDA has approved a range of different routes of administration for NPs, such as systemic, local, and oral administration (Anselmo and Mitragotri, 2016). The main route of administration used in most preclinical and clinical studies is intravenous administration due to the NPs being able to reach all parts of the body giving them a high potential to influence clinical care by targeting both the primary cancer and any associated metastasis (Dobrovolskaia et al., 2008, Moghimi et al., 2001). All of the NP formulations approved for cancer treatment are liposomal formulations. The first approved NP formulation was Doxil (PEG functionalized liposomal doxorubicin) in 1995, and the most recently approved NP is Onivyde (Irinotecan liposomal formulation) (Barenholz, 2012, Carnevale and Ko, 2016). The majority of all approved liposomal NP formulations are not PEGylated except for Doxil and Onivyde, which have been shown to have advantages over non-PEGylated NP formulations even with their low amount of PEG (Anselmo and Mitragotri, 2016, Chang et al., 2015). Preclinical research performed in the 1970s, 1980s, and 1990s, using polymers as controlled release systems for drug delivery has led to a number of clinically approved products (Kamaly et al., 2012). The clinical success of using polymers for controlled release, and the ability to manufacture polymeric formulations on the nanoscale have driven the research of polymeric depots away from the macro/micro scale to the nanoscale (Kreuter, 1978). A Number of PEGylated polymeric NP formulations such as SP1049C, NK911, and Genexol-PM are in early phase clinical trials for various types of cancers (Valle et al., 2011, Andrade et al., 2018, Matsumura et al., 2004, Ahn et al., 2014,

Kim et al., 2004). SP1049C is a pluronic polymeric micelle NP containing entrapped doxorubicin, that is currently evaluated for patients with esophagus and esophageal junction metastatic cancer in a phase II/III clinical trial (Valle et al., 2011, Shah et al., 2021, Fatima et al., 2021). The other two polymeric NPs, K911 (Doxorubicin-loaded PEG-poly(aspartic acid)) is in phase II clinical trials for various cancers (Andrade et al., 2018, Ahn et al., 2014, Shah et al., 2021), while Genexol-PM (Paclitaxel-loaded PEG-PLA) has been approved and is already commercially available (Chen et al., 2021). These first generation, polymeric NPs have shown promising efficacy against various cancers with wider therapeutic windows and lower side effects. However, these NPs are associated with a number of limitations related to targeting, therefore targeted polymeric NPs are now under preclinical and clinical investigation (Kamaly et al., 2012). The first targeted polymeric NPs to reach the clinic is BIND-014, which is composed of a prostate specific membrane antigen (PSMA) conjugated to a docetaxel-loaded PLGA NPs (Ahn et al., 2014, Kamaly et al., 2012). There are only two other targeted polymeric NPs currently in clinical trials, CALAA-01 (phase II, (Shah et al., 2021)), and SEL-068 (phase I, (Hu et al., 2019)) (Autio et al., 2018, Chakraborty et al., 2017, Giri et al., 2017). The synthesis of targeted NPs is complex and difficult to scale-up. The tuning of ligand density is very difficult because the target ligands attach to the surface of the pre-prepared NPs through post-coupling processes. In order to achieve a high efficiency of the coupling of the ligands excess amounts of reagents and purification techniques for removing unbound ligands are needed. These issues have led to batch-to-batch variability and difficulty in reproducing the surface properties. Consequently, the clinical transition for targeted NPs will be difficult unless they are prepared using pre-functionalized polymeric materials and a minimum number of components (Gu et al., 2008, Kamaly et al., 2012). However, this will require the development and registration of new polymeric excipients.

1.11 Poly(lactide-co-glycolide) (PLGA) in drug delivery

PLGA is a thermoplastic aliphatic polyester that has been used in biomedical and pharmaceutical applications (De Jong et al., 2001). The biodegradation and biocompatibility of PLGA has been investigated by a number of researchers (Jain, 2000, Elmowafy et al., 2019). They are influenced by the physical, chemical, and biological properties of the PLGA. Therefore, understanding these properties before formulating PLGA as a NP is very important for the choice of PLGA and the selection of the manufacturing processes (Jain, 2000, Jalil and Nixon, 1990)).

1.11.1 Physio-chemical properties of PLGA

1.11.1.1 Structure, synthesis, and general properties of PLGA

The polymer PLA is a linear aliphatic polyester which is derived from lactic acid monomers (Figure 1-7). There are two optical forms of PLA; an active stereoregular form (L-PLA) and inactive racemic form (D,L-PLA) . L-PLA is a semicrystalline form because its polymer chain is highly regular while the form of D,L-PLA is amorphous due to irregularities of structure of its polymer chain. The polymeric of D,L-PLA is commonly used because of the highly homogeneous of the drugs within the polymer itself (Södergård and Stolt, 2002, Wu, 1995). Poly(glycolic acid) PGA lacks the methyl groups of the PLA, thus PGA is highly crystalline (Jain, 2000).

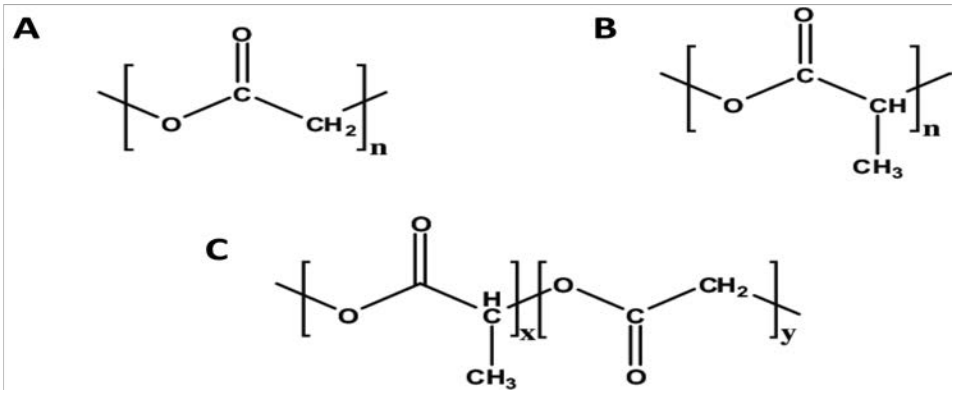


Figure 1-7: Chemical structure of **(A)** PGA, **(B)** PLA, and **(C)** PLGA. N refers to the repeated number of the PLA and PGA, while x and y refer to number of lactic and glycolic units in PLGA, repectively.

When the polymer is synthesised only by glycolide or lactic acid, the polymer may demonstrate semicrystalline form. On the other hand, the random sequence of backbone of polymer which contains a ratio of between lactide and glycolide prevents the forming of crystalline structure with high regularity. Similarly, the mixture of D- and L- lactic will prevent the semicrystalline behaviour from being observed. PLGA is a synthetic polymer which consists of a mixture of D- and L- of lactic acid (Figure 1-7), and thus PLGA at room or physiological temperature is usually an amorphous solid (De Jong et al., 2001). The PLGA polymers containing less than 70% glycolide are amorphous in nature (Reed and Gilding, 1981) and the risk of producing a crystalline form during manufacturing and degradation may be reduced by using a PLGA with intermediate ratios of lactide and glycolide (De Jong et al., 2001). Thus, the rate of hydrolysis of PLGA polymers containing 50:50 ratio of lactic and glycolic acids is faster than the hydrolysis of PLGA polymers containing a higher ratio of either of the two monomers. The mechanical strength of the PLGA, the ability of the PLGA to work as a drug delivery system, the rate of biodegradation, and hydrolysis are influenced and controlled by the physical properties of the PLGA and other factors. The melting point and the level of crystallinity are related to the molecular weight of the polymer (Wu, 1995, Lewis, 1990, Kitchell and Wise, 1985). At the same time, the molecular weight of the polymers and their chain composition determine the physical properties of the polymers (De Jong et al., 2001). The hydrolysis of the polyesters is strongly influenced by pH because the hydrolysis is catalysed by acid and base (De Jong et al., 2001). The PLGA copolymer has a fairly rigid chain structure because their glass transition temperature (T_g) is above the physiological temperature. Therefore, the glassy form in nature gives enough mechanical strength for the PLGA copolymers to be used as drug delivery devices (Jain, 2000). Jamshidi and co-worker have pointed to the correlation related between the T_g of PLGA and the lactide

and molecular weight. The T_g of PLGA is decreased with low content of lactide in copolymer composition and low molecular weight (Jamshidi et al., 1988).

1.11.1.2 Degradation of PLGA

The degradation of PLGA occurs first by the uptake of water followed by hydrolysis of the ester bonds. This process continues throughout the PLGA matrix. The degradation of the PLGA matrix was shown to proceed randomly via hydrolytic chain cleavage of swollen polymers (Thies and Bissery, 1984). During biodegradation of the PLGA, the number of the carboxylic end groups present in the PLGA chains are increased as a cleaving process of the individual polymer chain (Wu, 1995, Lewis, 1990). Thus, the degradation of the polymers was found to degrade at different rates based on the polymer end group. The rate of the degradation of the uncapped PLGA which has free carboxyl group at terminus is faster than capped PLGA which has alkyl ester linkage at terminus because the uncapped PLGA takes up water at a faster rate. Figure 1-8 shows that there is a difference in the water uptake between capped and uncapped polymers. Also, the degradation of uncapped polymers took more percentage of water in the first 10 days (>100%), hence the degradation of uncapped polymer was faster because of the increased production of acidic groups.

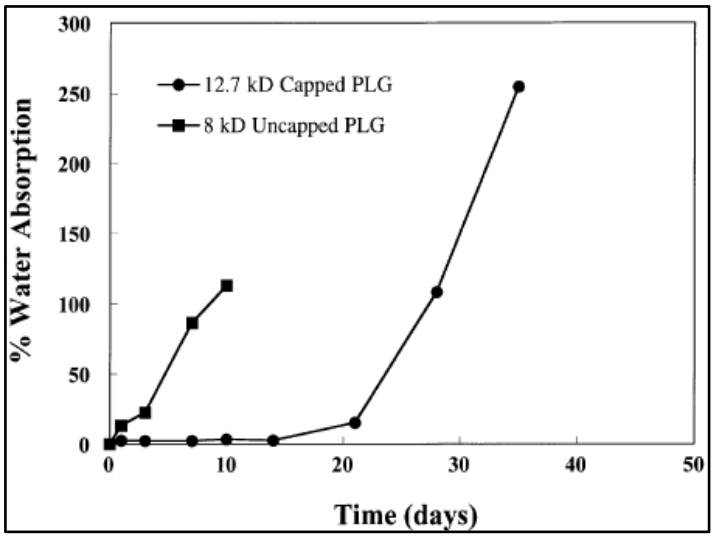


Figure 1-8: The time dependent of water uptake of polymers with different end groups (capped and uncapped polymers) (Tracy et al., 1999).

The PLGA molecular weight is one of the most important factors that influences the degradation of the PLGA polymer. The effect of the molecular weight on the degradation of polymer had a smaller effect compared with the effect of the polymer end group. Tracy *et al* have carried out extensive studies on the degradation of the PLGA with different molecular weights through in vitro and in vivo studies. The degradation of low molecular weight polymer was faster in vivo compared to high molecular weight but there was no difference in vitro. The higher molecular weight took longer for complete degradation because a longer time was required to break the matrix polymer by hydrolysis. This difference in the degradation between in vivo and in vitro may be due in part to the body's response to a foreign body. (Tracy et al., 1999). The PLGA polymer degrades into lactic and glycolic acid monomers that are subsequently metabolised. The lactic acid is metabolised by entering the tricarboxylic acid cycle, and is eliminated as carbon dioxide and water from the body. On the other hand, glycolic acid is either eliminated as carbon dioxide and water or excreted via the kidneys (Jain, 2000, Brady et al., 1973).

1.11.2 PLGA NPs preparation

1.11.2.1 Preparation of NPs by dispersion of pre-formed polymers.

There are currently a number of preparation methods for the manufacture of NPs. The choice of method depends on the properties of the polymers, the drug, the intended use, and desired release profile (Jain, 2000). Generally, NPs are prepared by two main techniques; dispersion from pre-formed polymers or polymerization of monomers. The dispersion of preformed polymers technique has two main methods; (i) the single emulsion and (ii) the double emulsion method (Soppimath et al., 2001). The dispersion of pre-formed polymers method is the most convenient method to prepare NPs. This method is perfect for soluble and insoluble drugs and is good for laboratory scale processes (Alimohammadi and Joo, 2014).

1.11.2.2 Single emulsion technique

This process includes oil-in-water emulsification to prepare NPs. The polymer is first dissolved in an organic solvent such as dichloromethane then the drug dissolved or dispersed into the solution of the pre-formed polymer. The mixture of drug and polymer in the organic solvent is emulsified to the aqueous solution to make o\w emulsion by using a surfactant such as poly (vinyl alcohol) (PVA). After that the organic solvent is evaporated either by stirring or increasing the temperature under pressure (Figure 1-9) (Scholes et al., 1993).

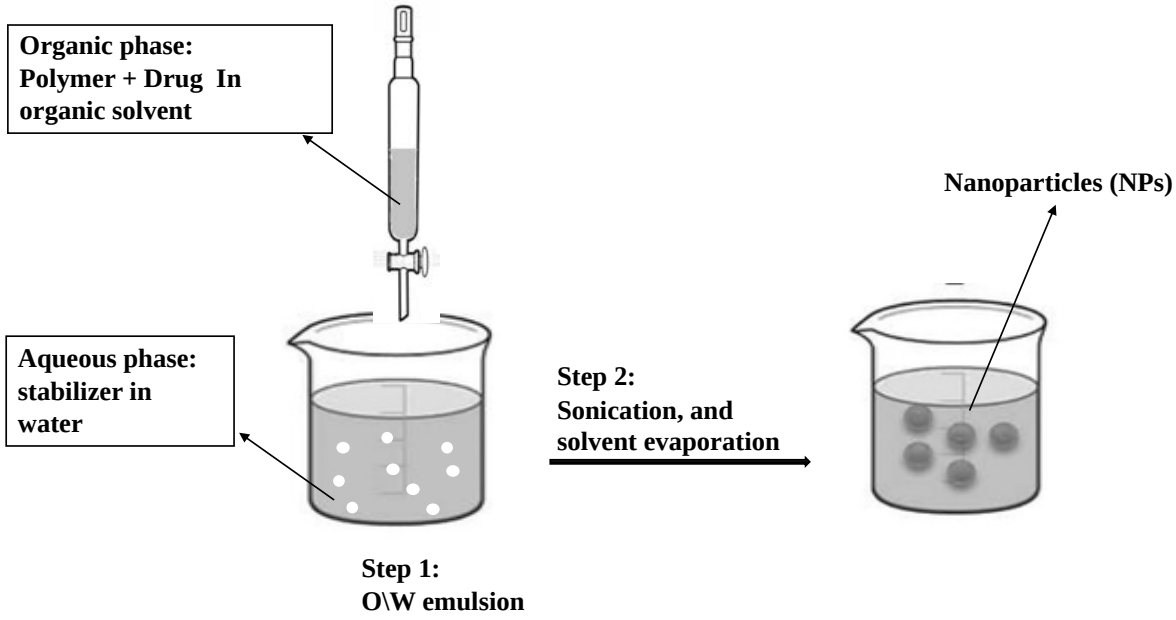


Figure 1-9: Schematic representation of the single emulsion process.

During this process, the dispersed phase must first diffuse out completely to the dispersion medium before evaporation. The evaporation step is a very critical step because it strongly affects the final NP formulation. This step is influenced by different factors like solubility of polymer, type of organic solvent and the dispersion phase. NPs with a porous structure are produced when the solvent evaporation step is done very rapidly. This is due to the rapid evaporation of the solvent rupturing the droplets. The main disadvantage of the single emulsion method is low EE for highly or moderately water-soluble drugs (Arshady, 1991). The poor encapsulation and burst effect of the hydrophilic drug during this method is due to

it diffusing from the dispersed phase to the continuous phase (Jalil and Nixon, 1990, Wada et al., 1988). The other factors that influence EE and the final NPs formulation are polymer concentration, stabilizer type, stabilizer concentration, stabilizer molecular weight, and time of sonication (Arshady, 1991, Jain, 2000).

1.11.2.3 Double emulsion technique

The double emulsion method is the most appropriate method for water-soluble drugs (Figure 1-10). Generally, the first emulsion of the organic solvent containing the polymer and aqueous solution of the drug is added gently with stirring to the large volume of water containing a stabilizer. Then the removal of solvent is done by evaporation or extraction (Alonso et al., 1994). Quite a number of hydrophilic drugs have been successfully formulated as NPs using this method including the peptide leuprolide acetate (Kamijo et al., 1996), proteins (Gutierro et al., 2002), and vaccines(Malik et al., 2019). With this method there are also many factors that influence the final NPs such as concentration of the polymer, stabilizer concentration, and stabilizer molecular weight (Jain, 2000, Zambaux et al., 1998).

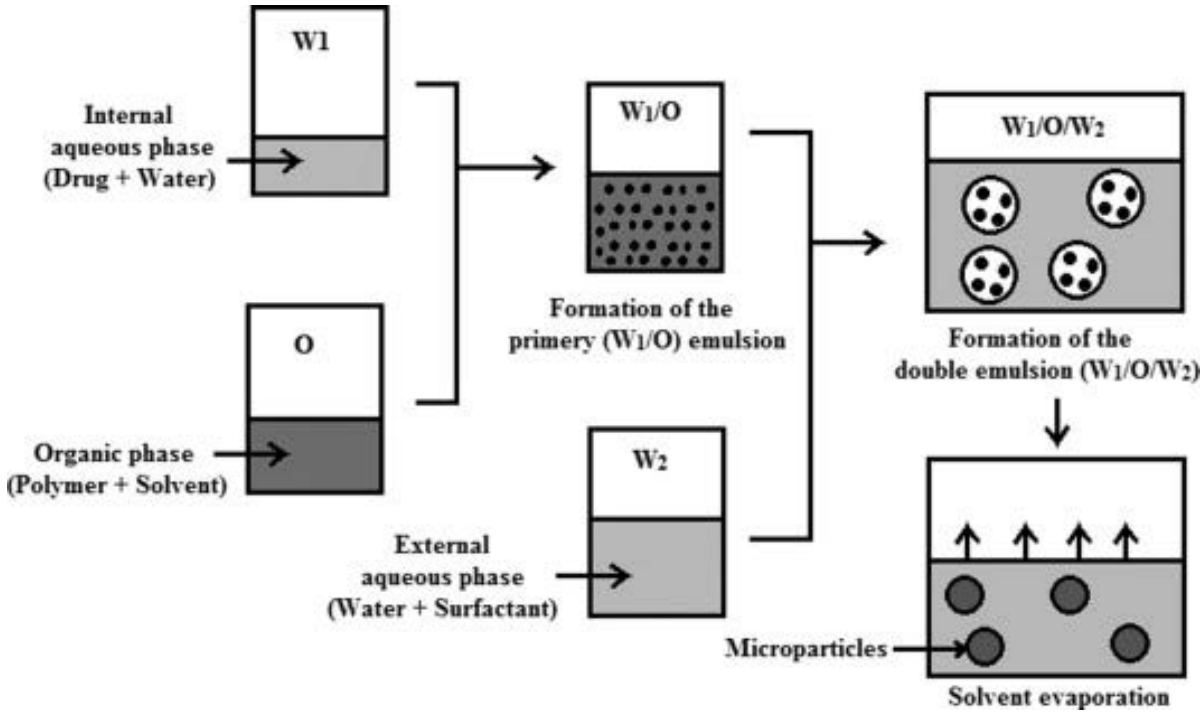


Figure 1-10: Schematic representation of the double emulsion solvent evaporation technique (Giri et al., 2013).

1.11.3 PVA as a surfactant

In the dispersion of pre-formed polymers preparation method, a surfactant is essential to stabilize the dispersed phase (Florence and Whitehill, 1982). PVA has been commonly used as a polymer surfactant in the solvent evaporation method. The PVA remains on the surface of the NPs and is difficult to remove (Carrio et al., 1995). The surface properties of the NPs are influenced by the concentration, molecular weight, degree of hydrolysation and polymerisation of the PVA (Murakami et al., 1997, Scholes et al., 1993, Zambaux et al., 1998). Boury *et al* have proposed that increasing the concentration of PVA results in an increase in the residual PVA in the NPs (Boury et al., 1995). Therefore, the size and polydispersity index (PDI) of the NPs are influenced by the concentration of PVA. Increasing the concentration PVA leads to a size reduction and a low PDI (Zambaux et al., 1998, Scholes et al., 1993). The lower the molecular weight of PVA has produced the smaller size of the NPs (Scholes et al., 1993).

1.12 Aims and objectives

The aim of this study is to develop and characterise IRN-loaded as well as IRN and PTV co-loaded PLGA NPs and demonstrate their potential as a treatment for GBM via their cytotoxicity against primary GBM cells as their ability to cross the BBB. These aims will be achieved through the following objectives;

1. To prepare and characterise IRN-loaded PLGA NPs using low and high intrinsic viscosity PLGA
2. To develop and optimize the IRN-loaded PLGA NPs, in addition, to determine the effect of the main variables on the characterisation using Box-Behnken design of experiments approach.
3. To prepare and characterise the IRN and PTV co-loaded PLGA NPs.

4. To assess cytotoxicity of the free IRN, Blank NPs, IRN-loaded PLGA NPs, and IRN and PTV co-loaded PLGA NPs against primary GBM cells.
5. To study the cellular uptake and apoptotic ability of the IRN-loaded PLGA NPs and IRN and PTV co-loaded PLGA NPs using primary GBM cells.
6. To assess the ability of IRN-loaded PLGA NPs, and IRN and PTV co-loaded PLGA NPs to promote apoptosis and necrosis in the primary GBM cells.
7. To optimised and culture mono- and co-culture BBB models using hCMEC/D3 cells and astrocytes
8. To investigate the ability of the IRN-loaded PLGA NPs and IRN and PTV co-loaded PLGA NPs to cross the vitro mono- and co-culture BBB models based on the TEER measurement technique using different approaches.

Chapter 2: Development and characterisation of Irinotecan hydrochloride-loaded PLGA NPs

2.1 Introduction

NPs offer a non-invasive systemic drug delivery strategy for improving the delivery of drugs to the brain. NPs have been extensively studied and have been shown to improve drug delivery to the brain by facilitating crossing of the BBB (Re et al., 2012). The ability to achieve a high drug loading as well as the potential to modify their surface make NPs a promising strategy for the treatment of GBM (Haque et al., 2012). NPs have the ability to penetrate the BBB and accumulate in brain tissue based on the EPR effect (Wicki et al., 2015).

Polymeric NPs are the most preferred for drug delivery because of their biocompatibility, biodegradation, high encapsulation efficiency, sustained release and compatibility with chemotherapeutic drugs (Mahmoud et al., 2020). An understanding of the properties of polymers such as molecular weight, stability and crystallinity are required when using polymeric NPs for drug delivery to the brain (Masood, 2016). PLGA is a synthetic, amorphous copolymer that consists of different ratios of lactic acid and glycolic acid monomers (De Jong et al., 2001). PLGA polymers with a 50:50 ratio of lactic and glycolic acid have a faster hydrolysis compared to other PLGA polymers containing higher ratios of either lactic or glycolic acid. The physical properties of PLGA such as melting point, molecular weight and glass transition temperature (T_g) impact its mechanical strength, biodegradation, and hydrolysis, which are important features when it comes to its use in drug delivery (Wu, 1995, Lewis, 1990, Kitchell and Wise, 1985). It's biodegradation and wide range of erosion times make PLGA suitable as a controlled release polymer for drug delivery (Dhal and Mishra, 2019). The ability of NPs to be targeted to specific tissues as well as cross

biological membranes and barriers, such as the BBB, is impacted by their physicochemical properties including particle size, shape and zeta potential (Malikmammadov et al., 2018). These physicochemical properties plus PDI and EE have an impact on the ability of NPs to be used as drug delivery systems. Size is an essential factor that enables NPs to be transported via the bloodstream and allows NPs to be delivered to the tumour site (Malikmammadov et al., 2018). The small size of the NPs means they can be easily delivered to the tumour via the EPR effect through leaky blood vessels (Bregoli et al., 2016). Optimizing the size of the NPs and ensuring they have a spherical can improve their tumour uptake via improved fluid dynamics (Truong et al., 2015). Moreover, the distribution of NPs in the bloodstream as well as their stability is influenced by their surface charge.

In this chapter, the preparation, optimisation and characterisation of IRN-loaded PLGA NPs is described. IRN-loaded PLGA NPs were prepared through a single emulsion solvent evaporation method. A range of variables were studied during the pre-screening, including the amount and type of PLGA, molecular weight and percentage of PVA, sonication time, and lyophilization process. Then, three factors and three levels of Box-Behnken Design (BBD) were used as a design of experiment (DoE) to develop and optimize the IRN-loaded PLGA NPS. The BBD comprised 15 runs for PLGA 5002 (low intrinsic viscosity) and and 15 runs for PLGA 5004 (high intrinsic viscosity) with each having three central points. IRN-loaded PLGA NPs were characterised for their size, zeta potential, and PDI by using dynamic light scattering (DLS), morphology by using Transmission Electron Microscope (TEM), EE, and release profile. In addition, the crystallinity of the NPs was evaluated using differential scanning calorimetry (DSC) and X-ray diffraction (XRD).

2.2 Materials, Instruments and Methods

2.2.1 Materials

PLGA polymers (PURASORB PDLG 5002A, 50:50 DL-lactide/glycolide copolymer, Mw 17 Kg/mol), (PURASORB PDLG 5004, 50:50 DL-lactide/glycolide copolymer, Mw 44 Kg/mol), were purchased from Corbion (Amsterdam, The Netherlands). Irinotecan Hydrochloride was obtained from LGM Pharma (Georgia, USA). Poly(vinyl alcohol), Mw 89,000-98,000, 99+% hydrolysed and Poly(vinyl alcohol) Mw 13,000-23,000, 98+% hydrolysed, were purchased from Sigma-Aldrich Company Ltd (Dorset, UK). Potassium dihydrogen orthophosphate HiPerSolv CHROMANORM, Octanesulphonic acid sodium salt ≥99% HiPerSolv CHROMANORM®, and Phosphate buffered saline (PBS) 1X, for biotechnology were purchased from VWR (Leicestershire, UK). Acetonitrile, and Dichloromethane were purchased from Fisher Scientific (Leicestershire, UK).

2.2.2 PLGA IRN-NPs preparation and characterisation

2.2.2.1 Preparation of blank and IRN-loaded PLGA NPs using the single emulsion solvent evaporation method

The PLGA and IRN were dissolved in 10 mL of DCM. The dispersed phase was added dropwise to the aqueous phase containing PVA under stirring. The mixture was sonicated using a microtip probe sonicator (VWR, UK) at 60% amplitude. The emulsion was gently stirred for 4 h and the residual dichloromethane (DCM) evaporated off. The NPs solution was recovered by centrifugation at 9,500 rpm for 20 min and the supernatant removed. The NPs were washed twice by being suspended in distilled water, centrifuged and the supernatant removed. The purified NPs were suspended in 10 mL of 5% sucrose and placed in the freezer at -80℃ overnight. The frozen solution was freeze dried for 48 h at 0.01 mbar and -85℃ (Figure 2-1).

2.2.2.2 Pre-screen study for the IRN-loaded PLGA NPs

The pre-screening study was performed to investigate the influence of the amount of PLGA, molecular weight of PVA, percentage of PVA, sonication time, type of PLGA, lyophilisation process, and percentage of cryoprotectant on the size, zeta potential, and PDI of the IRN-loaded PLGA NPs. These results were used to select the three main factors for the design of the experiment study.

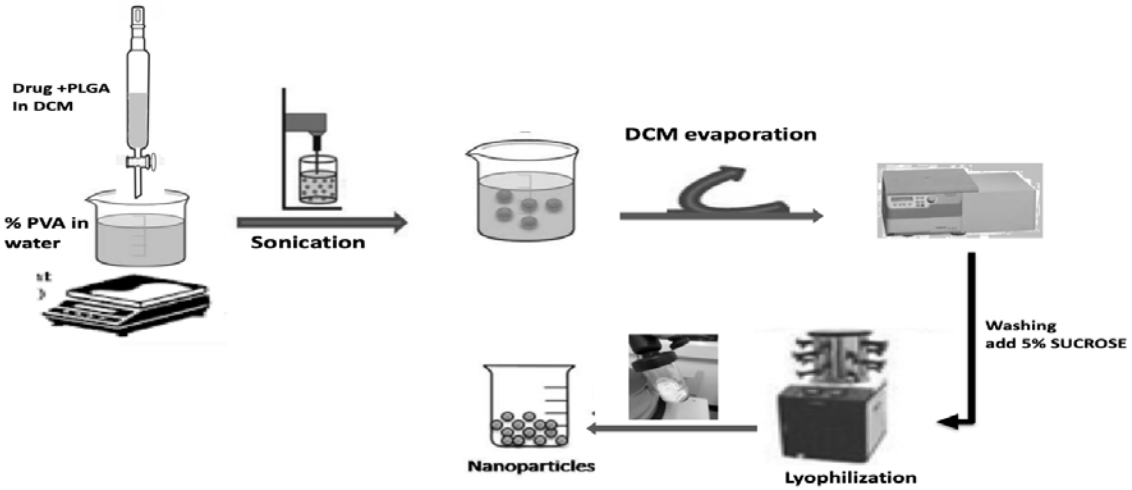


Figure 2-1: Scheme of the preparation method for IRN-loaded PLGA NPs by single emulsion solvent evaporation method.

2.2.2.3 Design of Experiments (DoE) for the IRN-loaded PLGA NPs using a Box-Behnken design (BBD).

Three factors and three levels of BBD were employed to construct polynomial models and to determine the most influential factors affecting the preparation and characterisation of the IRN-loaded PLGA NPs (Table 2-1). Response surface methodology was based on the BBD using the Minitab software. The independent variables were as follows: the amount of IRN (X_1), amount of PLGA (X_2), and percentage of PVA (X_3). All three factors were employed to minimize the particle size of NPs and increase the EE of IRN. The dependent variables were particle size (nm), zeta potential, PDI and EE. The BBD comprises 15 runs for PLGA 5002 (Table 2-2) and another 15 runs for PLGA 5004 (Table 2-3) with each having three central points. The nonlinear equation for the quadratic model is given in equation 1.

Equation 1

$$R= \beta_0 + \beta_1X_1 + \beta_2X_2 + \beta_3X_3 + \beta_{12}X_1X_2 + \beta_{13}X_1X_3 + \beta_{23}X_2X_3 + \beta_{11}(X_1)^2 + \beta_{22}(X_2)^2 + \beta_{33}(X_3)^2$$

Where R is a response, β_0 is intercept and β_1, β_2, β_3, β_{11}, β_{12}, β_{13}, β_{22}, β_{23}, and β_{33} are the regression coefficients. The three independent variables are the amount of IRN (X_1), amount of PLGA (X_2), and percentage of PVA (X_3). X_1X_2, X_1X_3, and X_2X_3 are interaction terms, while $(X_1)^2$, $(X_2)^2$, and $(X_3)^2$ are the quadratic terms of the models. The three levels (low, medium, and high) of each factor were chosen based on the results of the pre-screening study. Fitting response factors to the models of linear, second, and quadratic were performed for statistical validation of the polynomial equation. The fitness of the models and the effectiveness of the process variables on the response were evaluated using the statistical value of β-coefficient and coefficient of determination (R-squared). A significance level of $p < 0.05$ was accepted to denote significance in all cases.

Table 2-1: Levels of variables used in Box–Behnken design (BBD) for preparing IRN-loaded PLGA NPs (5002 and 5004).

Type of PLGA	**Levels of design**			**Independents variables**
	-1	**0**	**+1**	
PLGA 5002	6	8	10	Drug amount (mg)
	120	180	240	PLGA 5002 polymer amount (mg)
	2	4	8	PVA Surfactant (%)
PLGA 5004	6	8	10	Drug amount (mg)
	120	180	240	PLGA 5004 polymer amount (mg)
	2	4	8	PVA Surfactant (%)

Table 2-2: Design of study and independent variables of Box-Behnken design (BBD) for preparing IRN-loaded PLGA NPs with low intrinsic viscosity PLGA 5002.

Run	Variables		
	IRN (mg)	PLGA (mg)	PVA (%)
R1	6	120	4
R2	6	240	4
R3	10	120	4
R4	10	240	4
R5	6	180	2
R6	6	180	8
R7	10	180	2
R8	10	180	8
R9	8	120	2
R10	8	120	8
R11	8	240	2
R12	8	240	8
R13	8	180	4
R13a	8	180	4
R13b	8	180	4

Table 2-3: Design of study and independent variables of Box-Behnken design (BBD) for preparing IRN-loaded PLGA NPs NPs with high intrinsic viscosity PLGA 5004.

Run	Variables		
	IRN (mg)	PLGA (mg)	PVA (%)
R15	6	120	4
R16	6	240	4
R17	10	120	4
R18	10	240	4
R19	6	180	2
R20	6	180	8
R21	10	180	2
R22	10	180	8
R23	8	120	2
R24	8	120	8
R25	8	240	2
R26	8	240	8
R27	8	180	4
R28	8	180	4
R29	8	180	4

2.2.3 HPLC analysis

2.2.3.1 HPLC assay condition

IRH was analysed using an Agilent LC System (Agilent Technologies, Santa Clara, California, United States) equipped with a quadratic pump and autosampler. The separation was performed using a Luna® 5 µm, C18, 100 Å analytical HPLC column (150 mm *4.6 cm)

at 25℃ with a mobile phase consisting of a 30:30:40 mixture of solution A (ion-pair solution), solution B (KH_2PO_4) and acetonitrile. The pH of mobile phase was adjusted to 3.0 by phosphoric acid and a flow rate of 1 mL/min was used. An injection volume of 20 µL and run time of 10 min was used, with UV detection performed at a wavelength of 265nm.

2.2.3.2 Stock solution and calibration curve.

5 mg of IRH was transferred into a 50 mL volumetric flask and dissolved in acetonitrile to produce a stock solution with a final concentration of 100 µg/mL. The stock solution was subsequently used to prepare standard solutions with concentrations of 2, 10, 30, 50, 70, 90,100 µg/mL. The calibration curve was prepared by plotting the area under the curve (AUC) versus the concentration.

2.2.4 Size, PDI, zeta potential and EE of IRN-loaded PLGA NPs.

The mean particle size, PDI, and zeta potential of the NPs were determined by dynamic light scattering (DLS) using a zetasizer (Malvern Zetasizer, UK). The dried NPs were suspended in deionised water then sonicated for 3 min. The homogenous suspension was analysed for size, PDI, and zeta potential. The entrapped drug in the NPs was determined by dissolving a 5 mg sample of NP formulation in acetonitrile. The acetonitrile containing dissolved NPs was filtered using 0.45 µm and subsequently analysed by HPLC for IRN concentration. EE was calculated using equation 2.

Equation 2

$$\mathrm{EE\%} = \frac{\text{amount of IRN per amount of NPs} * 100}{\text{amount of IRN per amount of polymer in formulation}}$$

2.2.5 In vitro release

25 mg of the IRN-loaded PLGA NPs (n = 3) was suspended in 30 mL of PBS at either pH 7.4 and 4.5 and placed in an orbital shaking incubator (Unitron HT infors) at 37℃ and 100 rpm. A 0.5 mL sample was collected and replaced with 0.5 mL of fresh media, every day for 9 days and the collected samples stored at 4℃ until analysed. The free IRN was separated by centrifugation at 13000 rpm for 30 min and analysed by HPLC.

2.2.6 Transmission Electron Microscope (TEM)

The morphology of the IRN-loaded PLGA NPs was analysed by TEM with a JEM 1010 electron microscope at a voltage of 80 kV. The NPs were suspended in distilled water and deposited on a copper grid and dried before measurement.

2.2.7 Differential scanning calorimetry (DSC)

Thermal analysis of IRN, PLGA 5002, PLGA 5004, PVA and IRN-loaded PLGA NPs was conducted using a DSC250 TA Instruments DSC. Approximately 7.5 mg of each sample was added to a DSC pan and placed in the thermal chamber of the DSC. The DSC analysis was performed between 25 and 300 °C at a heating rate of 10 °C/min under nitrogen.

2.2.8 Powder X-ray diffraction (PXRD)

The PXRD analysis was performed on IRN, PLGA, PVA, IRN-loaded PLGA NPs and physical mixture (IRN, PLGA, and PVA) using a Panalytical Empyrean diffractometer (PANanalyical, Almelo, The Netherlands) with Cu Kα radiation (λ = 1.54060) at 40 kV and 40 mA between 5° and 80° (2Theta) at 25 °C.

2.2.9 Statistical analysis

Statistical analysis was performed using a one-way or two-ways analysis of variance (ANOVA) (GraphPad Prism version 9.0.0 (86) for Windows, GraphPad Software, San

Diego, CA). Post-hoc comparisons of the means were performed using Tukey's Honestly Significance Difference test. A significance level of $p < 0.05$ was accepted to denote significance in all cases.

2.3 Results

2.3.1 Pre-screening of the key parameters involved in the development of IRN-loaded PLGA NPs using the single emulsion solvent evaporation technique

During the pre-screening stage many variables were investigated to determine those which have the greatest impact on producing NPs with acceptable characteristics for them to be a suitable drug delivery system. The variables investigated were amount of PLGA, molecular weight of surfactant PVA, percentage of PVA, sonication time, type of PLGA (based on the intrinsic viscosity), the lyophilisation process.

2.3.1.1 The amount of PLGA

The influence of the amount (40 mg and 120 mg) of PLGA on the size, zeta potential, PDI of the IRN-loaded PLGA 5004 NPs was investigated. The 40 mg of PLGA produced particles outside the nanometre range, while with the 120 mg of PLGA produced NPs with a size of less than 500 nm (Figure 2-2A). In addition, there was no significant ($p > 0.05$) difference in zeta potential and PDI between IRN-loaded PLGA NPs produced using the 40 or 120 mg of PLGA 5004 (Figure 2-2B and C).

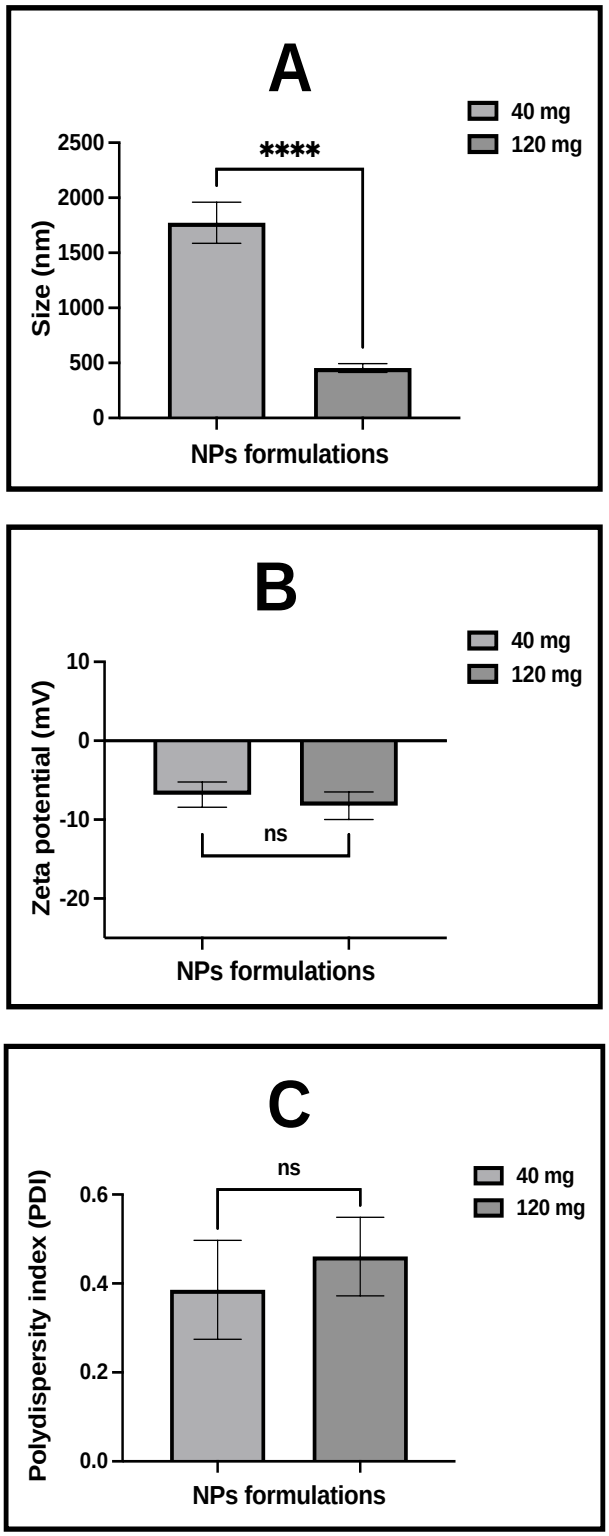


Figure 2-2: Influence the amount of PLGA (40 and 120 mg) on the size (A) zeta potential (B) and polydispersity index (C) of IRN-loaded PLGA 5004 NPs. Results shown as mean ± SD, n= 3, significance found using a one-way ANOVA with a Tukey's post-hoc test, * = P<0.05 ** = P<0.01, *** = P<0.001, **** = P<0.0001.

2.3.1.2 Effect the molecular weight of PVA as surfactant

The effect of the molecular weight of the surfactant (PVA) on the size, zeta potential, and PDI of IRN-loaded PLGA NPs produced using PLGAs of different inherent viscosities (5002 = 0.2 and 5004 = 0.4) was investigated using two different (13-23 K and 89-98 K) molecular weights of PVA. The size of both sets of IRN-loaded NPs produced using the high molecular weight of PVA were more than 500 nm in size, while those prepared using the low molecular weight PVA were around 200 nm (Figure 2-3A). The zeta potential of the IRN-loaded PLGA 5004 NPs was -6.4±1.5 with higher molecular weight of PVA and -16.5±0.4 with the low molecular weight PVA. A similar trend was seemed with the PLGA 5002 NPs, zeta potential was lower with the high molecular weight of PVA (Figure 2-3B). PVA molecular weight clearly influences PDI with both PLGA NPs having higher PDIs with the higher molecular weight PVA (Figure 2-3C). With the low molecular weight PVA the PDI was around 0.2 and 0.4 for PLGA 5004 and 5002, respectively. In comparison, with the high molecular weight PVA the PDIs of the PLGA 5004 and 5002 NPs were around 0.7 and 0.5, respectively.

2.3.1.3 Percentage PVA

Another variable that was investigated during the pre-screening study was the percentage of PVA. A low percentage of PVA (0.50%) produced NPs with an approximate size of 500 nm and 850 nm with PLGA 5004 and 5002, respectively. The sizes of both types of NPs were significantly decreased with an increase in the percentage of PVA from 0.50 to 4.0%. The PLGA 5004 NPs had an approximate size of 152.0±1.8 nm, while the PLGA 5002 NPs had an approximate size of 454.7±32.5 nm (Figure 2-4A). The Zeta potential values of either type IRN-loaded PLGA NPs were not influenced by the percentage of PVA (Figure 2-4B), while the PDI was significantly ($p < 0.05$) increased by reducing the percentage of PVA from 4 to 0.50% (Figure 2-4C).

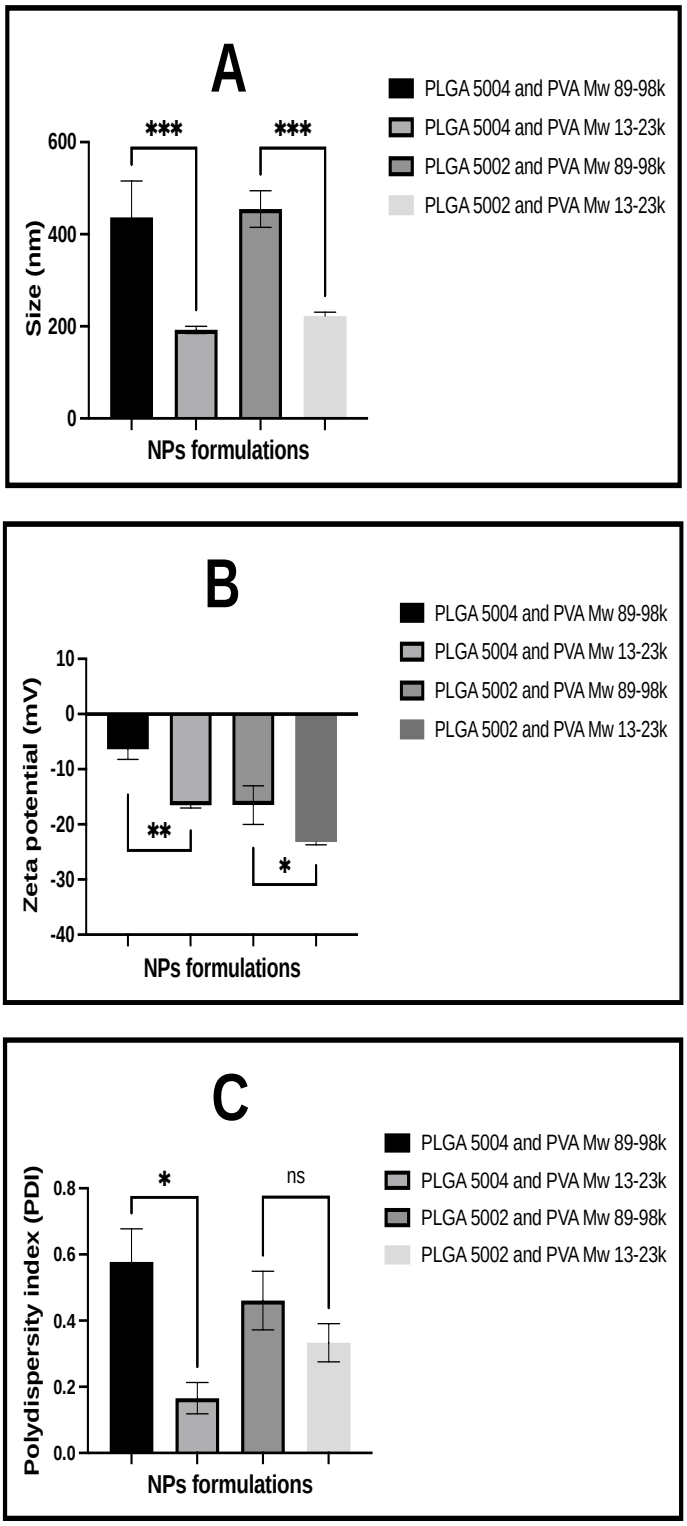


Figure 2-3. Influence of the molecular weight of the PVA on the size (A) zeta potential (B) and polydispersity index (C) of IRN-loaded PLGA NPs made of PLGA 5004 and PLGA 5002 using two different molecular weight of PVA (89-98k and 13-23k). Results shown as mean ± SD, n= 3, significance found using a 2way ANOVA with a Tukey's post-hoc test, * = P<0.05 ** = P<0.01, *** = P<0.001, **** = P<0.0001.

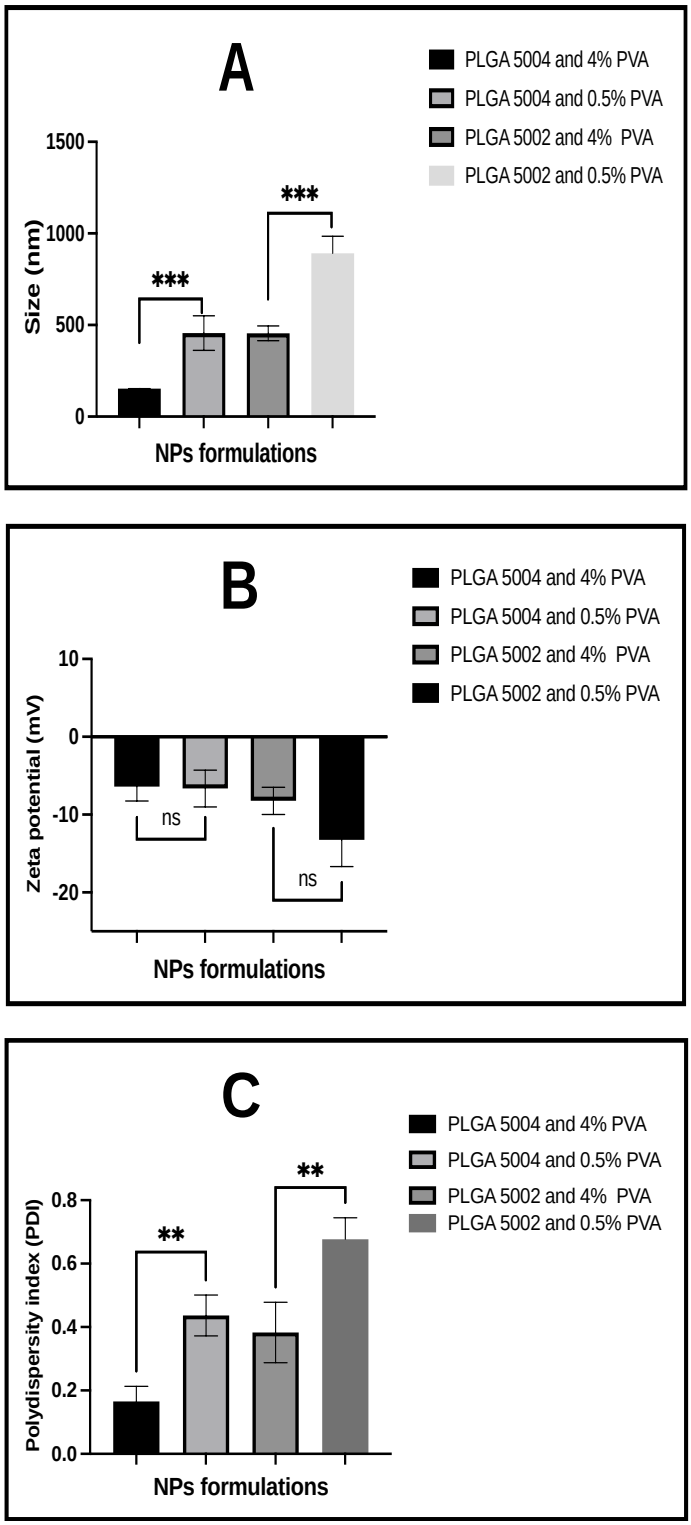


Figure 2-4: Influence of the percentage of the PVA on the size (A) zeta potential (B) and polydispersity index (C) of IRN-loaded PLGA NPs made of PLGA 5004 and PLGA 5002 using two different percentage of PVA (4 and 2%). Results shown as mean ± SD, n= 3, significance found using a 2way ANOVA with a Tukey's post-hoc test, * = P<0.05 ** = P<0.01, *** = P<0.001, **** = P<0.0001.

2.3.1.4 Influence of sonication time on the size and PDI of the NPs

The influence of long (10 min) and short (5 min) sonication times on the size and PDI of IRN-loaded PLGA 5004 NPs was investigated (Figure 2-5). A sonication time of 5 min resulted in NPs with a size of 764.3±44.6 nm and a PDI of 0.7, while a sonication time of 10 min resulted in the NPs have a s size of 370±8.8 nm and a PDI of 0.3 (Figure 2-5A and B). Therefore, increasing the sonication time results in a reduction in both the size and PDI of the NPs.

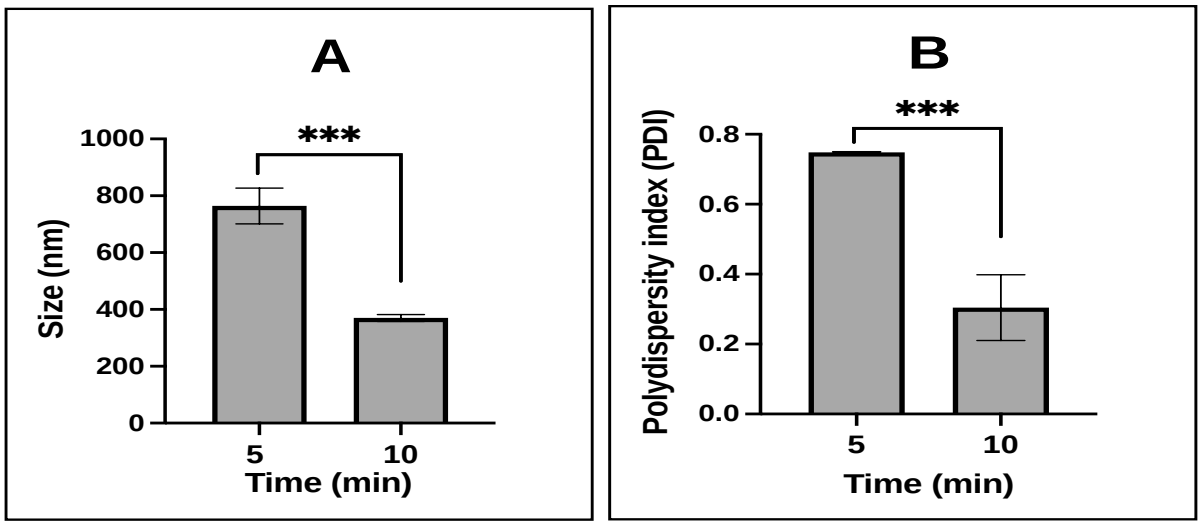


Figure 2-5: Change in particles size (A) and polydispersity index (B) of IRN-loaded PLGA NPs with time of sonication (5 and 10 min). Results shown as mean ± SD, n= 3, significance found using a 2way ANOVA with a Tukey's post-hoc test, ($p < 0.05$).

2.3.1.5 Influence of freeze drying on the size of NPs

The effect of freeze drying on the particle size of NPs was investigated to see if there is any significant change in their size before and after freeze drying. The sizes of IRN-loaded PLGA NPs with both PLGAs were significantly ($p < 0.05$) increased after freeze drying. The size of IRN-loaded PLGA 5004 NPs before and after freeze drying were 185.7±4.1 nm and 226.6±31.1 nm respectively, while the size of the PLGA 5002 were 200.3±2.1 nm and 222.2±7.1 nm (Figure 2-6)

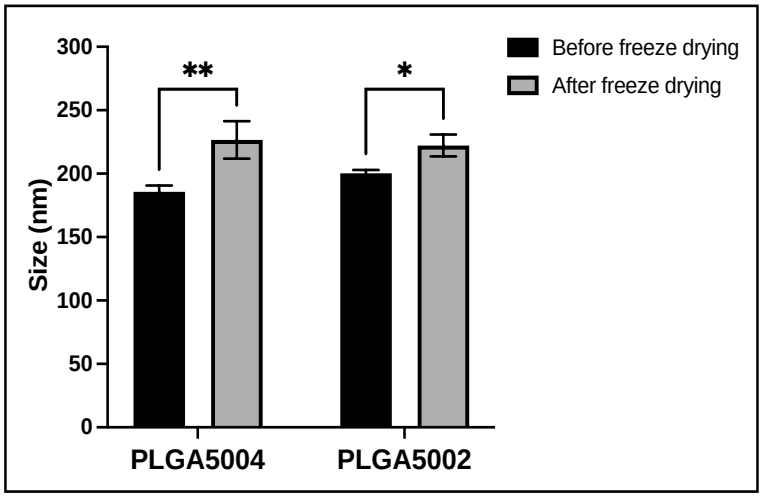


Figure 2-6: Change in particle sizes before and after freeze drying with using 5% sucrose as cryoprotectant for two different NPs; NPs performed with PLGA 5004 and PLGA 5002. Results shown as mean ± SD, n= 3, significance found using a one-way ANOVA with a Tukey's post-hoc test, ($p < 0.05$).

2.3.1.6 Effect the type of the PLGA on the EE of NPs

The EE of the IRN-loaded PLGA NPs demonstrate that the IRN-loaded PLGA 5002 NPs have a significantly ($p < 0.05$) higher EE than the PLGA 5004 NPs (Figure 2-7). Both formulations have the same initial amounts of IRN and PLGA as well as the same percentage of PVA, however, the EE for IRN-loaded PLGA 5004 NPs was 39.78±3.67, while it was 87.79±1.62 with PLGA 5002 NPs (Figure 2-7).

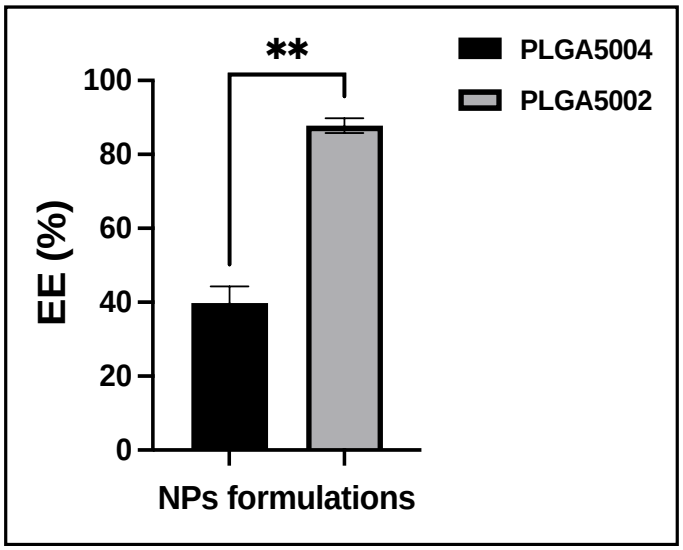


Figure 2-7: Effect type of PLGA (PLGA 5004 and PLGA 5002) on the EE of IRN-loaded PLGA NPs. Results shown as mean ± SD, n= 3, significance found.

2.3.2 DoE process to determine the key quality parameters for the IRN-loaded PLGA NPs.

In the present study, a BBD was applied during the development and optimization of the IRN-loaded PLGA NPs using the single emulsion solvent evaporation technique. A total of 15 confirmatory runs with 3 centre points for each type of PLGA (PLGA 5002 and PLGA 5004) were performed (Table 2-2 and 2-3). The DoE included 3 factors (independent variables): 1) the amount of IRN (X_1), 2) the amount of PLGA (X_2), 3) the percentage of PVA (X_3), and 2 responses (dependent variables); 1) particle size and 2) EE. All NPs were characterised for particle size, zeta potential, PDI and EE (Table 2-4). Polynomial equations were determined based on the statistical estimation of different parameters. The factors X_1, X_2, and X_3 represent the effect on the responses with changing one factor at a time, while the interaction terms ($(X_2)^2$, $(X_2)^2$, $(X_3)^2$, X_1X_2, X_1X_3, and X_2X_3) show the effect on response of changing two factors at a time. The effect of the factors on the responses was plotted in three-dimension (3D) surface graphs (Figure 2-8 and 2-9). The 3D response surface plots are used to investigate the changes in the response related to 2 different factors (Hao et al., 2011).

2.3.2.1 Effect of the independent variables on the particle size of IRN-loaded PLGA NPs.

The average particle size for all IRN-loaded NPs with both low intrinsic viscosity 5002 PLGA ($Y_{1\text{-}02}$) NPs R1-R13b and high (PLGA 5004) intrinsic viscosity PLGA ($Y_{1\text{-}04}$) formulation R15-R28 were determined. The particle size of the NPs was found to be in the range of 158.2 nm (R3) to 1050 nm (R11) for PLGA 5002 and 193.4 nm (R15) to 420.5 nm (R25) for PLGA 5004 (Table 2-4). Equations 3 and 4 were used to explain the effect of each independent variable on particle size.

Equation 3

$$Y_{1\text{-}02} = 1951 + 10\,X_1 - 19.0X_2 - 294X_3 + 10.50(X_1)^2 + 0.06(X_2)^2 + 43.40(X_3) - 0.04X_1X_2 + 3.60X_1X_3 - 0.92X_2X_3$$

Equation 4

$$Y_{1\text{-}04} = 654 + 34.80X_1 - 2.38X_2 - 104.20X_3 - 4.60(X_1)^2 + 0.01(X_2)^2 + 13.84(X_3)^2 - 0.01X_1X_2 + 2.12X_1X_3 - 0.34X_2X_3$$

Table 2-4: Design of study and independent variables of Box-Behnken design (BBD) for preparing IRN-loaded PLGA NPs.

Run	Characterisation			
	Size (nm)	Zeta potential	PDI	EE (%)
R1	222.2±7.1	-23.2±0.4	0.3	88.9
R2	158.2±3.3	-37.3±1.2	0.2	40.8
R3	946.7±36.8	-20.7±0.9	0.2	98.5
R4	1022.0±17.8	-26.7±0.8	0.4	97.4
R5	235.5±3.4	-30.2±0.6	0.4	60.6
R6	184.1±7.1	-30.9±7.5	0.3	80.1
R7	1002.0±36.8	-22.7±0.9	0.4	92.3
R8	1002.0±117.1	-20.1±09	0.5	85.7
R9	615.1±10.5	-18.5±0.4	0.5	97.1
R10	1056.0±18.1	-7.7±18.8	0.1	76.2
R11	1046.3±178.1	-22.8±0.5	0.9	88.2
R12	705.4±195.3	-22.8±0.9	0.9	34.0
R13	290.6±24.8	-22.8±0.9	0.2	65.4
R13a	232.0±15.7	-20.8±0.4	0.2	61.5
R13b	262.0±12.4	-22.0±0.5	0.2	66.0
R15	193.4 ± 4.9	-8.9±0.5	0.2	5.8
R16	246.8 ± 5.6	-11.1±0.4	0.3	16.8
R17	200.9±7.4	-11.0±0.5	0.2	4.5
R18	224.6±4.1	-11.4±0.8	0.3	10.8
R19	363.8±24.9	-19.2±0.3	0.4	4.9
R20	208.5±10.2	-9.9±0.2	0.3	8.3
R21	289.6±5.3	-10.5±0.5	0.2	8.2
R22	226.6± 14.7	-10.0±1.1	0.4	42.8
R23	384.8±22.3	-13.1±0.4	0.3	4.0
R24	388.5±9.1	-7.2±0.2	0.3	5.4
R25	420.6±21.6	-14.2±0.7	0.3	5.1
R26	201.8±2.2	-11.9±0.7	0.2	22.4
R27	207.3±15.7	-11.6±0.6	0.2	5.1
R28	232.8±6.5	-13.0±0.3	0.3	5.6
R29	217.7±4.6	-11.0±0.8	0.3	5.8

Positive or negative values for a factor in the polynomial equation indicate either a synergistic or antagonistic effect, respectively. The values of the regression coefficient (r^2) were 0.92 for the PLGA 5002 NPs (R1-R13) and 0.96 for the PLGA 5004 NPs (R15-R29), indicating a good fit and good correlation between response and the selected factor. The adjusted R^2 of 0.73 for the PLGA 5002 NPs and 0.84 for the PLGA 5004 NPs were in close agreement with the predicted R^2 (Table 2-6). From the equations, it is obvious that factor X_1 (amount of IRN) influenced the particle size of IRN-loaded PLGA NPs, with an increase in the amount of IRN increasing the particle size. The mean particle size of the PLGA 5002 NPs prepared using 6 mg of IRN ranged between 150 and 250 nm, while those prepared using 8 mg ranged from 200 to 600 nm, with particle sizes above 600 nm achieved when the amount

of IRN was increased to 10 mg. Typically, the amount of IRN that can be incorporated into a polymer is fixed. The negative value for factor X_3 (percentage of PVA) demonstrates that increasing the percentage of PVA with a high amount of PLGA results in a decrease in the particle size of all NPs (Figure 2-8C and F). For example, R5 and R6 have the same amount of IRN but they have different percentages (2 and 8%, respectively) of PVA. The particle size of R5 was 235.5±3.4 nm, while the particle size of R6 was significantly ($p < 0.05$) decreased to 184.1±7.1 nm with an increase in the percentage of PVA. The particle size of the IRN-loaded PLGA 5002 NPs increased by increasing the amount of IRN and PLGA (X_1X_2) simultaneously (Figure 2-8A), while the particle size of the IRN-loaded PLGA NPs decreased by increasing the amount of PLGA and the percentage of PVA (X_2X_3) simultaneously (Figure 2-8C and F).

2.3.2.2 Effect of the independent variables on the EE of the IRN-loaded PLGA NPs.

The EE for all IRN-loaded NPs with both low intrinsic viscosity PLGA 5002 ($Y_{2\text{-}02}$) NPs R1-R13b and high intrinsic viscosities PLGA 5004 ($Y_{2\text{-}04}$) formulation R15-R28 were determined. The EEs were found to be in the range of 34.0 (R12) to 98.5% (R3) for the PLGA 5002 NPs and 4.0 (R23) to 42.8 (R22) for the PLGA 5004 NPs (Table 2-4). Equations 5 and 6 were used to explain the effect of each independent variable on EE;

Equation 5

$$Y_{2\text{-}02} = 577 - 74.4X_1 - 2.875X_2 + 3.7X_3 + 3.54(X_1)^2 + 0.004(X_2)^2 + 0.30(X_3)^2 + 0.18X_1X_2 - 0.28X_1X_3 - 0.06X_2X_3$$

Equation 6

$$Y_{2\text{-}04} = -51.3 - 10.70X_1 + 0.86X_2 + 6.20X_3 + 0.25(X_1)^2 - 0.002(X_2)^2 - 0.29(X_3)^2 + 0.02\ X_1X_2 + 0.63\ X_1X_3 - 0.02\ X_2X_3$$

According to Equation 5, factor X_3 (percentage of PVA) had a positive effect on the EE of the PLGA 5002 NPs while factor X_1 (amount of IRN) and X_2 (amount of PLGA) showed a less positive or negative effect on their EE (Table 4). Thus, an increase in the percentage of

surfactant enhanced the EE of IRN in PLGA 5002 NPs (Figure 2-9B and E). When the amount of PLGA or IRN is increased individually they either increase the EE slightly or reduce their EE. However, when they are increased simultaneously (X_1X_2) they increase the EE of the PLGA 5002 NPs (Figure 2-9A). Equation 6 demonstrates that the factors X_2 (amount of PLGA) and X_3 (percentage of PVA) had a positive effect on the EE of the PLGA 5004 NPs. Simultaneously increasing the amount of PLGA and PVA leads to a high EE in these NPs (Figure 2-9F). Furthermore, the EE is increased by simultaneously increasing the amount of IRN and PLGA (X_1X_2) as well as the amount of IRN and surfactant (X_1X_3) (Figure 2-9D and E).

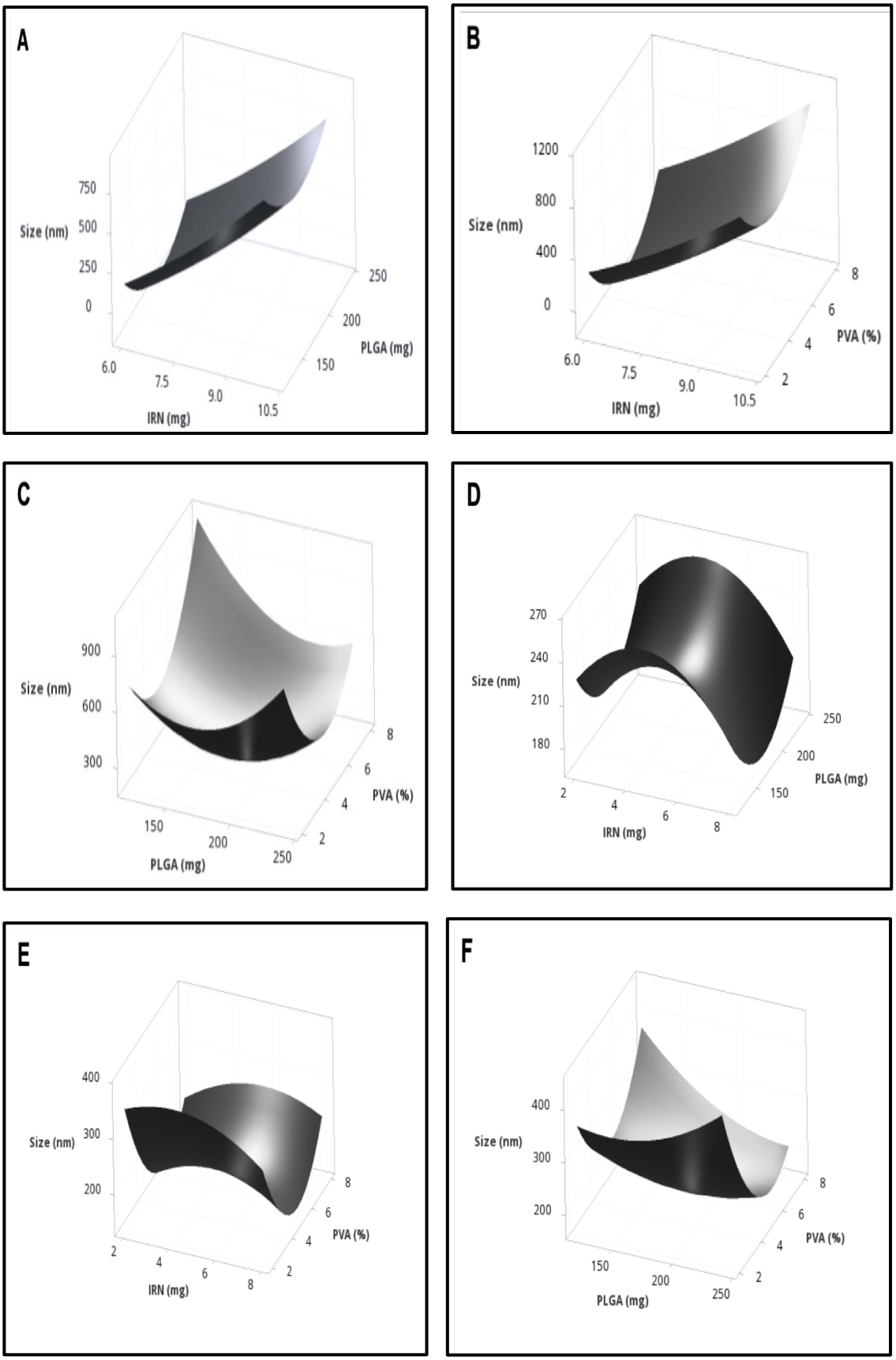


Figure 2-8: 3D Response surface plot showing the influence of variables (amount of drug, amount of polymer, percentage of surfactant) on the size of the IRN-loaded NP with PLGA 5002 (A, B, and C) and with PLGA 5004 (D, E, and F).

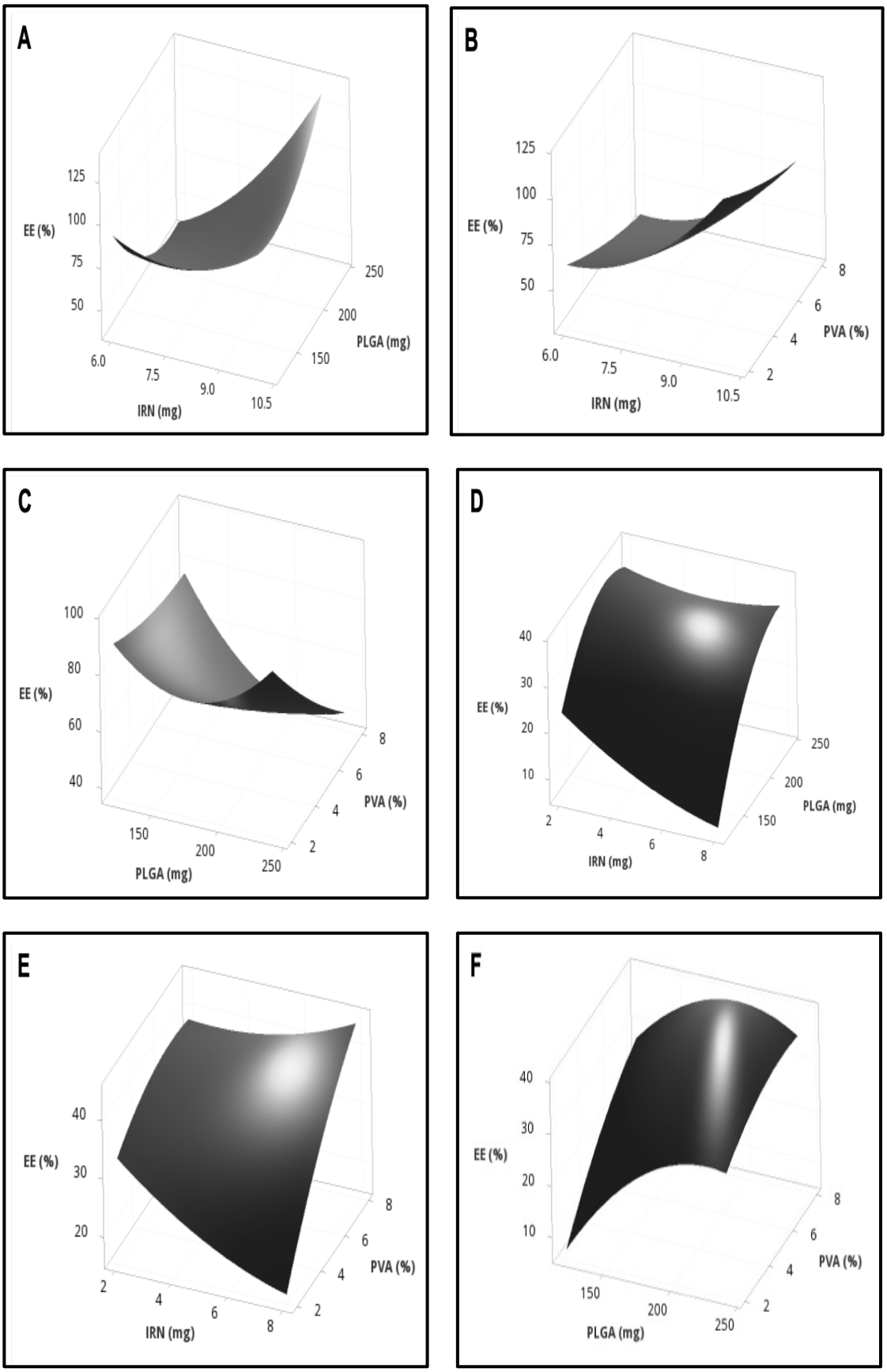


Figure 2-9: 3D Response surface plot showing the influence of variables (amount of IRN, amount of PLGA, percentage of PVA) on the EE of the IRN-loaded NP with PLGA 5002 (A, B, and C) and with PLGA 5004 (D, E, and F).

Table 2-5: A summary of fitted model analysis for response size and EE of IRN-Loaded PLGA NPs.

Source	Size (nm)				EE (%)			
	PLGA 5002		PLGA 5004		PLGA 5002		PLGA 5004	
	Coeff	P-Value	Coeff	P-Value	Coeff	P-Value	Coeff	P-Value
Intercept	204	0.156	189.0	0.000	56.75	0.001	33.43	0.000
IRN	378	0.021	-5.7	0.607	26.34	0.008	-2.62	0.234
PLGA	-70.3	0.424	-19.8	0.123	-7.90	0.128	8.86	0.007
PVA	8.2	0.925	-51.0	0.004	-16.58	0.018	8.48	0.007
IRN*IRN	42	0.773	-41.4	0.060	14.18	0.116	2.27	0.512
PLGA*PLGA	227	0.097	38.0	0.051	15.85	0.044	-7.33	0.047
PVA*PVA	390	0.034	124.6	0.001	2.70	0.696	-2.63	0.450
IRN*PLGA	-4	0.977	-1.3	0.931	21.52	0.045	4.16	0.172
IRN*PVA	22	0.873	19.1	0.218	-1.68	0.812	5.65	0.077
PLGA*PVA	-165.3	0.148	-61.8	0.007	-9.96	0.107	-3.58	0.228
R^2	0.918		0.955		0.941		0.921	
R^2(adjusted)	0.732		0.874		0.808		0.779	

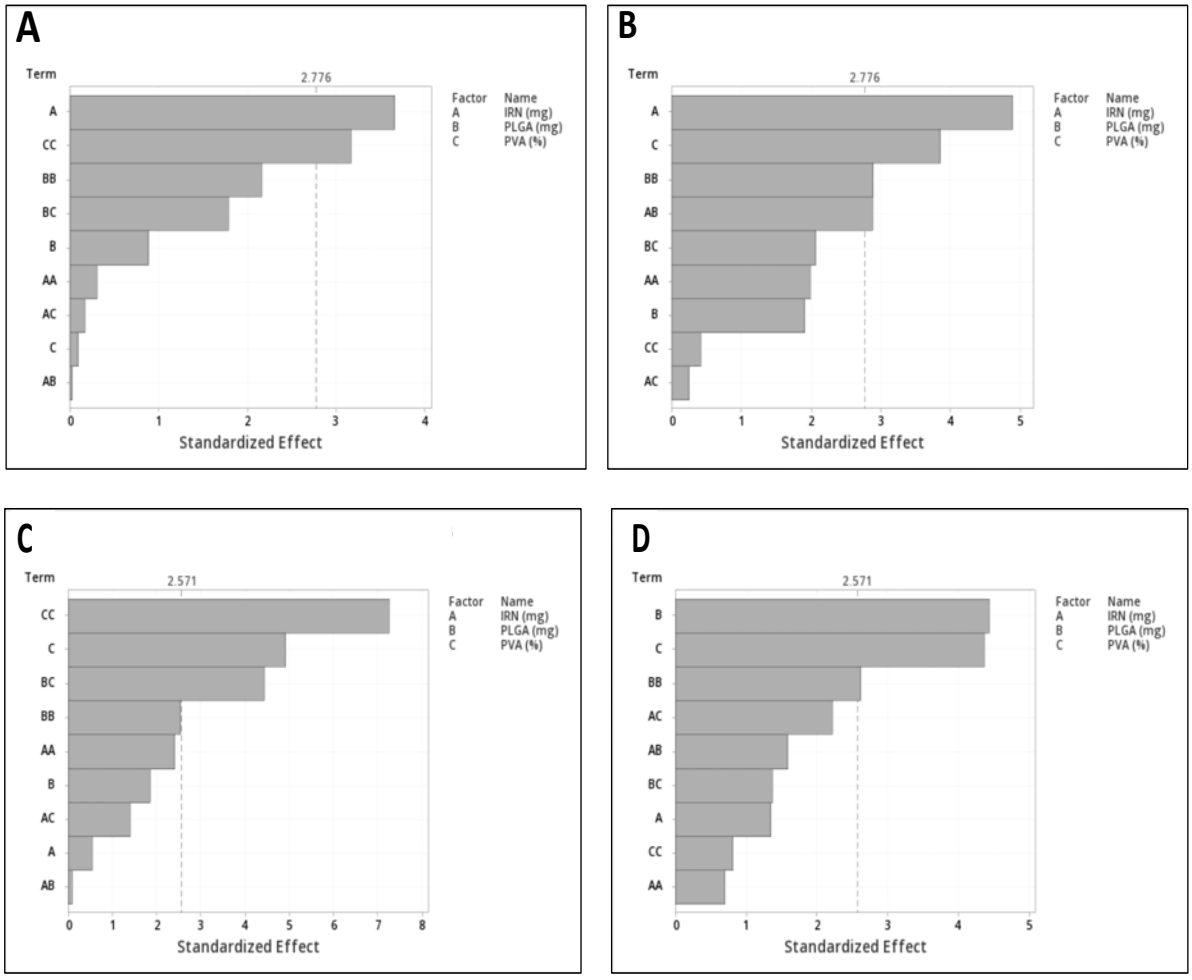


Figure 2-10: Pareto chart on the effect of variables (amount of IRN, amount of PLGA, percentage of PVA) in order of their effect on size (A) and EE (B) IRN-loaded 5002 PLGA NPs), and on size (C) and EE (B) IRN-loaded 5004 PLGA NPs.

2.3.3 Zeta potential and PDI.

Zeta potential was dependent on the type and amount of the PLGA (Figure 2-11). The zeta potential of the PLGA 5002 NPs was in the range of -7.7 (R10) to -37.3 (R2). The R2 formulation had 240 mg of PLGA 5002, while the R10 formulation had 120 mg of the same PLGA. For the PLGA 5004 NPs, the zeta potential ranged from -8.9 (R15) and -14.2 (R25) with formulation R25 having the highest amount of PLGA (Table 2-4).

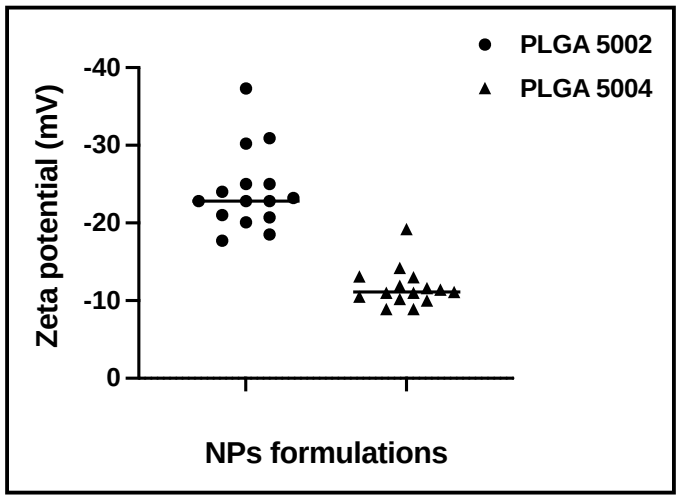


Figure 2-11: Zeta potential for all IRN-loaded PLGA NPs. (●) IRN-loaded PLGA NPs with PLGA 5004, (▲) IRN-loaded PLGA NPs with PLGA 5002.

Figure 2-12 shows the change in zeta potential with increasing the amount of PLGA. Zeta potentials of IRN-loaded PLGA NPs have significantly increased with increasing amounts of PLGA. In NPs with PLGA 5002, The zeta potentials of NPs were -22.5±1.3 with 120 mg and -37.3±1.7 with 240 mg of PLGA 5002. On the other hand, the zeta potentials with 120 and 240 mg of PLGA 5004 were -18.2±0.9 and -24.7±1.0, respectively.

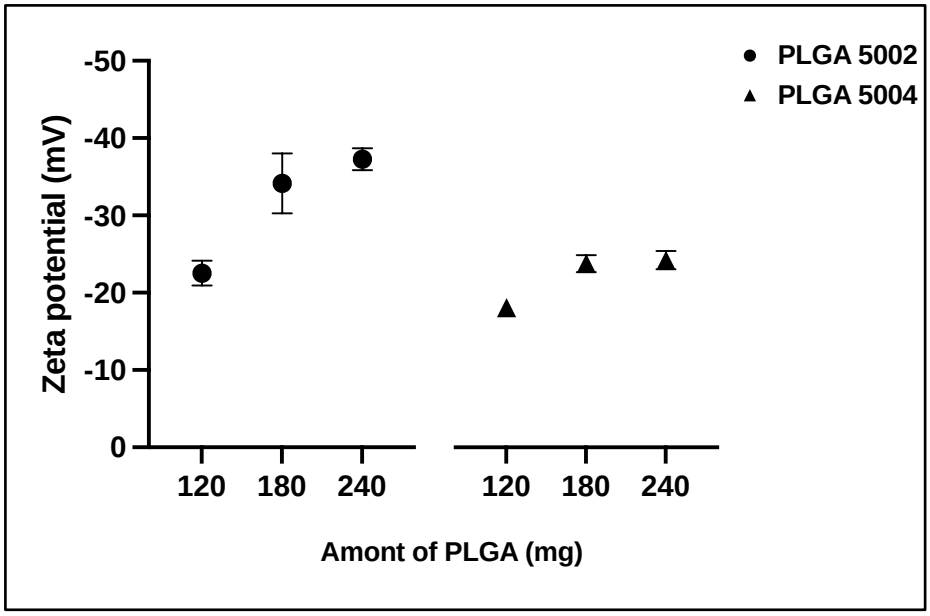


Figure 2-12: Zeta potential of IRN-loaded PLGA NPs, (A) PLGA 5002 and (B) PLGA 5004. The NPs formulation in each type of PLGA have the same amount of IRN and % of PVA but with three different levels of PLGA amount (120, 180, 240 mg).

DLS size measurements for NPs formulation revealed the average size and PDI of IRN-loaded PLGA NPs (Figure 2-13).

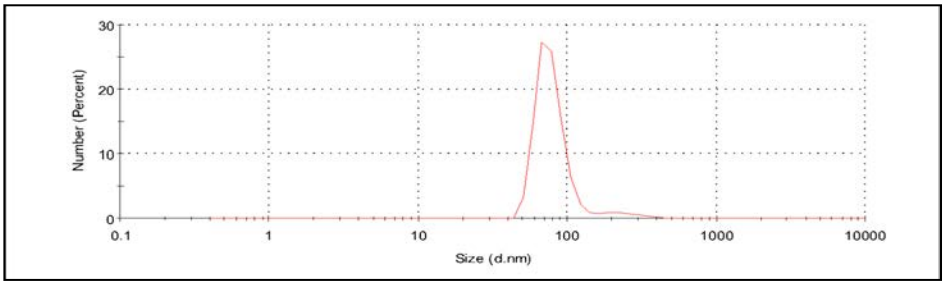


Figure 2-13: Number-size distributions of IRN-loaded PLGA NPs (R13) were analysed using dynamic light scattering (DLS).

2.3.4 HPLC analysis for IRN

Figure 2-14 shows the IRN standard curve at 7 different concentrations of IRN quantified by HPLC. The correlation between the IRN concentrations and the HPLC area under the curve AUC was excellent with the R value at 0.09997 from 2 to 100 μg/ml. The retention time was approximately 1.80 min.

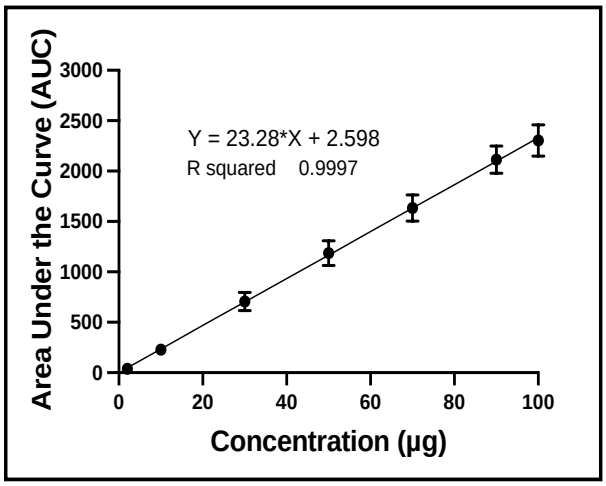


Figure 2-14: Standard curve of IRN using HPLC (n= 3).

2.3.5 Optimization of the IRN-loaded PLGA NPs

The optimised NP formulations for each type of PLGA were determined based on a set criteria of minimum particle size and maximum EE. The statistical tools and response surface analysis allowed us to determine that the optimised formulation for PLGA 5004 (high intrinsic viscosity) was R22, which consisted of 10 mg of IRN, 120 mg of PLGA, and 8% PVA. The EE and particle size for these NPs were 42.8% and 226.6±14.7, respectively. The optimised formulations for PLGA 5002 (low intrinsic viscosity), were R1, R6, and R13. The EE values were 88, 80, and 65%, while the particle sizes were 222.2±7.1, 184.1±7.2, and 290.6±24.8 nm, respectively.

2.3.6 Transmission Electron Microscopy (TEM).

Morphological evaluation of the IRN-loaded PLGA NPs was performed by TEM (Figure 1-15) and demonstrated that the IRH-loaded NPs are a group of uniform spherical particles with smooth edges that are within the nanometer range.

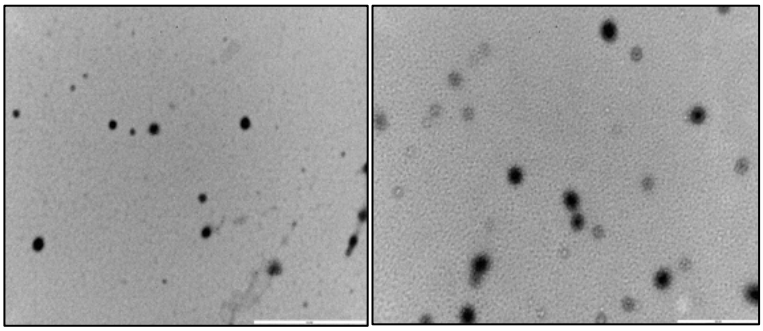


Figure 2-15: Morphology evaluation of IRN-loaded PLGA NPs by Transmission Electron Microscopy (TEM).

2.3.7 Differential scanning calorimetry (DSC)

Figure 2-16 shows the DSC thermographs for IRN, PLGA, PVA, physical mixtures, and IRN-loaded PLGA NPs. The thermograph for IRN exhibited two different endothermic peaks. The first was observed as a broad peak over the range of 70-120℃. The second peak was exhibited at 272℃ as a distinctive endothermic melt peak and was followed immediately by thermal decomposition. The DSC thermographs demonstrated that PLGA was amorphous with a Tg of 45℃, while PVA had a broad melting peak from 200 to 230°C. The melting peak of IRN disappears in a 1:2 physical mixture of IRN and PVA. A physical mixture of 1:1:1 IRN, PLGA, and PVA exhibited a Tg at 45℃, for PLGA and broad melting peak between 200 and 230℃ for PVA and a melting peak at 272℃ for IRN. The DSC thermographs for both the IRN-loaded and blank PLGA NPs show a broad melting peak between 150 and 190 °C which is due to the sucrose used in the freeze drying process. The Tg for PLGA and melting peak for PVA are detected in both the blank and IRN-loaded PLGA NPs, while the IRN melting peak has disappeared in the IRN-loaded PLGA NPs. However, the 1:2 physical mixture of IRN and PVA demonstrated that the IRN can dissolve in the PVA during the DSC analysis. Therefore, XRD will be used to try and determine the physical nature of the IRN in the NPs.

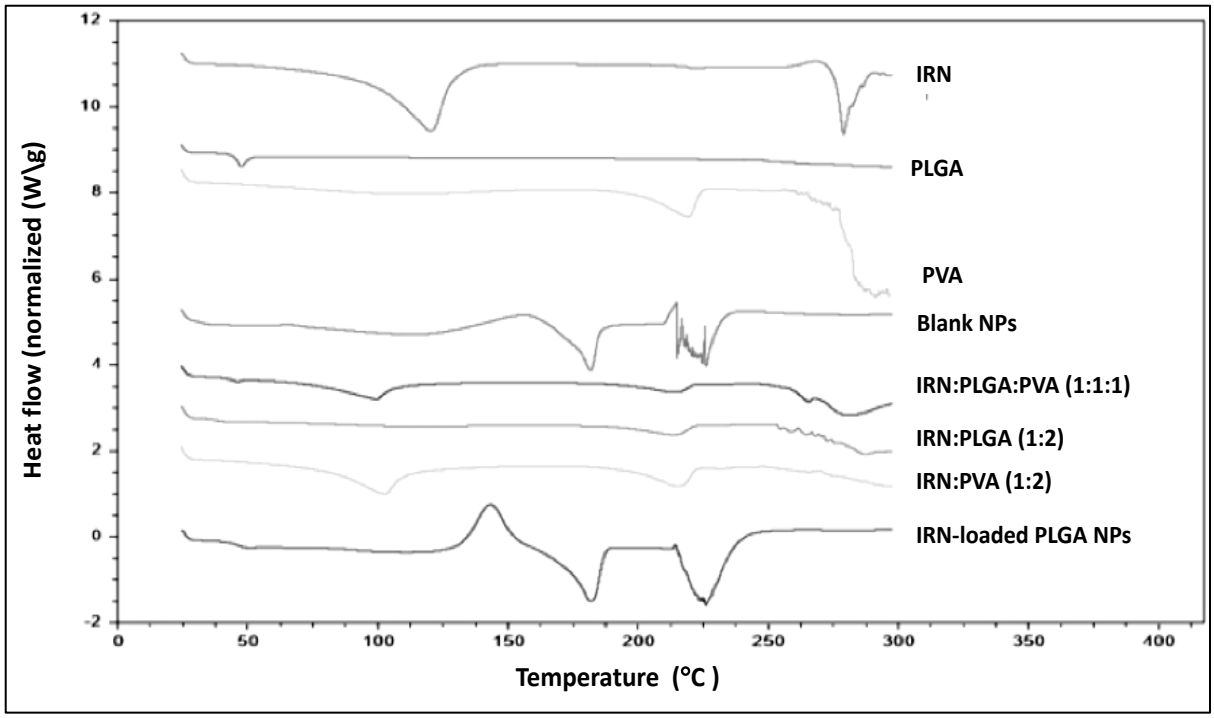


Figure 2-16: Differential scanning calorimetry (DSC) thermograms; drug (IRN), polymers (PLGA 5004, PLGA 5002), Surfactants (PVA), and physical mixture (drug, polymers, PVA), and formulations (IRN-loaded PLGA NPs).

2.3.8 X-ray diffraction (XRD)

The XRD patterns for PLGA 5002, PLGA 5004, PVA, IRN and IRN-loaded PLGA NPs (R13 and R22) are presented in Figure 2-17B to G. Both PLGAs were completely amorphous, while the PVA consisted of both amorphous and crystalline regions, with IRN being completely crystalline. However, the XRD patterns for the IRN-loaded PLGA NPs do not contain any of the diffraction peaks belonging to IRN, which confirms that the IRN within the NPs is in its amorphous state.

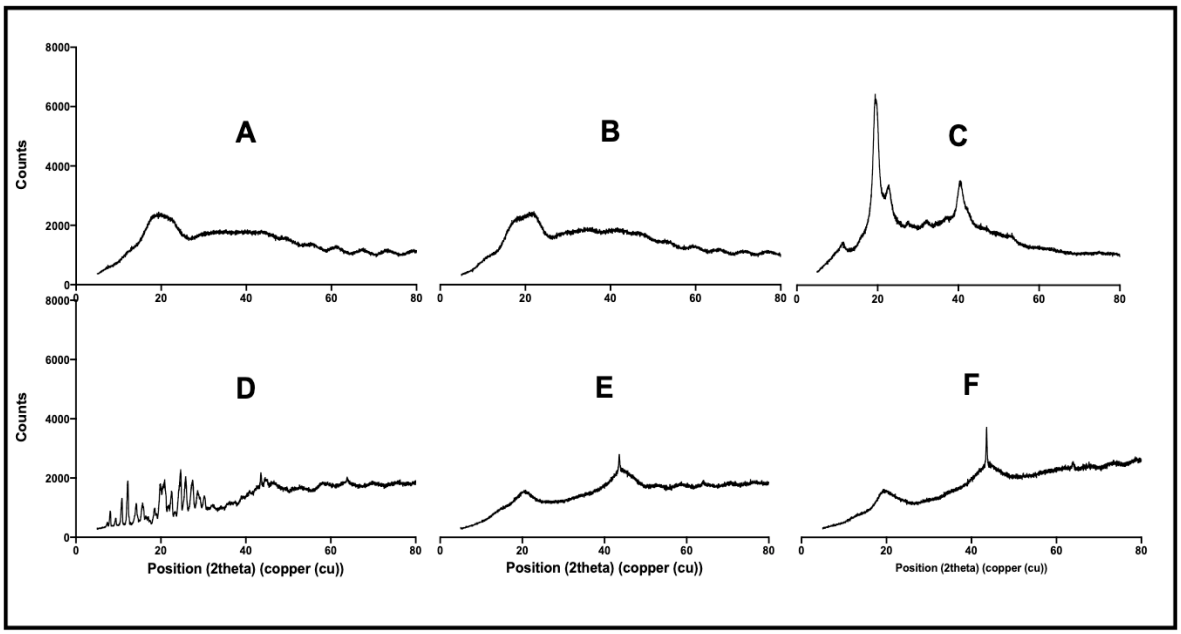


Figure 2-17: X-ray diffraction diffractogram of (A) PLGA 5002, (B) PLGA 5004, (C) PVA, (D) IRN, (E) R13 NPs, and (F) R22 NPs.

2.3.9 pH-dependent drug release

The release of IRN from the optimised NPs was performed in PBS at two different pHs (7.4 and 4.5) at 37℃. The percentage cumulative in vitro release profiles for the NPs is presented in figure 2-18. The release profile for all NPs exhibited a typical biphasic release profile over the 9 days. The initial phase of release involved a 'burst' release at day 1, followed by the second phase of release which provided slower and constant release up to day 9. At pH 7.4 (Figure 2-18A), the NPs with the high intrinsic viscosity PLGA 5004 (R22) released approximately three times more IRN than the NPs with the low intrinsic viscosity PLGA 5002 (R1, R13). The R22 NPs released approximately 80% of their IRN content over the 9 days, while R1, R6 and R13 released approximately 32.2±1.8, 37.4±4.6 and 37.2±3.0% of their IRN content respectively over the same time period. The release of IRN from R1 increased two fold when acidic (pH 4.5) PBS was used (Figure 2-18B). The percentage cumulative release of IRN from R1 was 32.2±1.8% at pH of 7.4 and 74.0±2.0% at pH of 4.5 over 9 days.

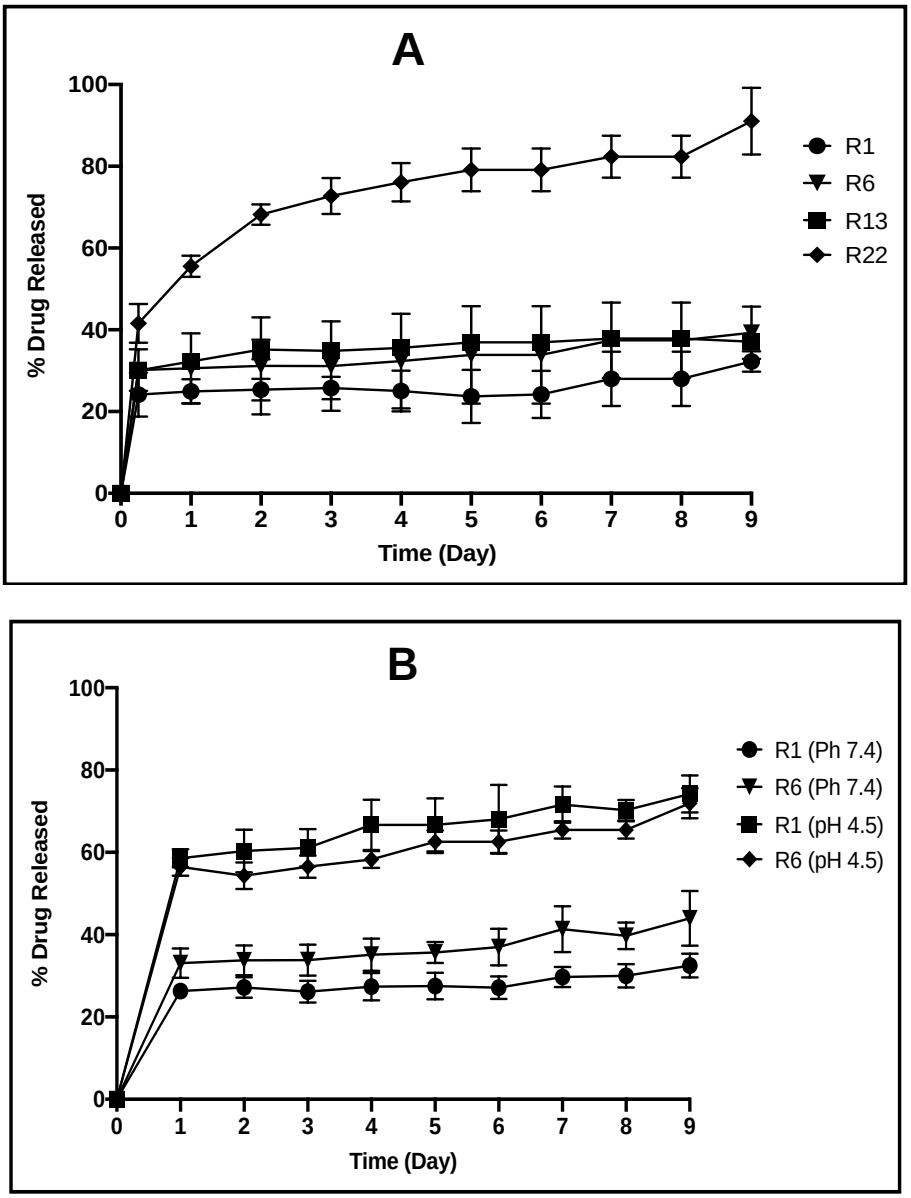


Figure 2-18: In vitro cumulative release profile of IRN from PLGA NPs of four different NPs (R1, R13, R16, R22), in the PBS at normal pH **(A)** and acidic pH (4.5) pH **(B)**, during 9 days in the shaking incubator at 100 rpm and 37°C. Results shown as mean ± SD, n= 3, significance found using a two-way ANOVA with a Tukey's post-hoc test, * = P<0.05 ** = P<0.01, *** = P<0.001, **** = P<0.0001.

2.4 Discussion

The single emulsion solvent evaporation technique has been used in this study to prepare IRN-loaded PLGA NPs. It produced spherical NPs with sizes range of 150 - 1100 nm with the low intrinsic viscosity PLGA (5002) and 190 - 425 nm with the high intrinsic viscosity PLGA (5004). Many variables were investigated during the pre-screening and development of the IRN-loaded PLGA NPs including the effect of the amount of PLGA, molecular weight

and percentage of PVA, sonication time, and lyophilization process on the size, zeta potential, and PDI. In addition, the effect of intrinsic viscosity of the PLGA on the EE was also investigated. In the DoE, the impact of the variables (amount of IRN, amount of PLGA, and percentage of PVA) was investigated using a Box-Behnken Design.

Particle size and EE are critical in the development of NPs for drug delivery to ensure that they deliver enough drug to the target area to induce a therapeutic effect (Almeida et al., 2019). The pre-screening study demonstrated that the low amounts (40 mg or less) of PLGA and high molecular weight PVA did not produce NPs. The reduction in particle size by lowering the molecular weight of the PVA may be related to the viscosity of the continuous phase. A continuous phase with lower viscosity is produced by using a low molecular weight PVA during preparation of the NPs, and this effect may reduce the particle size and PDI of IRN-loaded PLGA NPs (Scholes et al., 1993). A longer sonication time of 10 min significantly reduced the size of the PLGA NPs when compared to a shorter 5 min sonication time. The reduction in the size of IRN-loaded NPs with the 10 min sonication time can be attributed to more energy released in the process of emulsification resulting in smaller droplets during preparation of the NPs (Madani et al., 2018). A sonication time of 10 min was not been exceeded so to avoid de-emulsification or agglomeration during the preparation processes (Español et al., 2016, Tripathi et al., 2010). The size of IRN-loaded PLGA 5002 NPs increased with increasing the initial amount of IRN. Increasing the amount of drug can increase the viscosity of the dispersed phase, producing larger NPs (Sharma et al., 2016, Mao et al., 2008). PVA acts as a surfactant and enhances the interfacial stabilization of the emulsion nanodroplets preventing them from aggregating (Budhian et al., 2007). The concentration of PVA must be high enough to cover the interfacial area of all nanodroplets. The decrease in particle size with a high concentration of PVA has been reported by

Allemann *et al* (Allémann et al., 1992). The increase in particle size by increasing both PLGA and IRN simultaneously can be explained via consideration of the viscosity of the organic phase. By increasing the PLGA, the viscosity of the organic phase increases, consequently, the viscous forces resisting droplet breakdown are increased, which leads to a larger droplet, resulting in the increased particle size of NPs (Sharma et al., 2016, Zweers et al., 2003). Furthermore, the high viscosity of organic solution can slow down the diffusion of the organic phase into the aqueous phase, leading to the formation of larger NPs (Tefas et al., 2015). The EE of the IRN-loaded NPs was increased by increasing the percentage of PVA and PLGA. The increase in the EE with higher percentage of PVA can be explained by an increase in the viscosity of the aqueous phase, which decreases the diffusion of the IRN from the organic phase, promoting IRN entrapment in NPs. Furthermore, increasing the amount of PLGA increases the viscosity of the organic phase further decreasing the diffusion of the IRN from the organic to the aqueous phase resulting in a higher EE (Budhian et al., 2007). Moreover, the electrostatic interaction between the IRN and acidic termination of the low intrinsic viscosity PLGA 5002 is most likely the reason for their high EE when compared to high intrinsic viscosity PLGA 5004, which was not acid terminated.

DSC analysis was conducted to investigate the physical properties (crystalline or amorphous) of the NPs and to determine if there was an interaction between IRN, PLGA or PVA (Dillen et al., 2004). The thermograph for IRN exhibited two endothermic peaks; the first one represents the dehydration peak of water (Rajpoot and Jain, 2019), and the second one represented the endothermic melt peak of IRN. In the physical mixture of IRN and PVA (1:2), the peak of IRN disappeared which suggests that IRN is completely dissolved in the PVA, which is due to them both being hydrophilic and the fact that there is twice as much PVA as IRN, on the other hand, in physical mixture of IRN, PLGA, and PVA (1:1:1), all

peaks of IRN, PVA, and PLGA were observed, which demonstrates there is no interaction between the PLGA, PVA and IRN due to a lack of shift in Tg or melting peaks, while IRN retains some level of its crystallinity in this physical mixture (Wang et al., 2019). The reason IRN retains its crystallinity in the 1:1:1 IRN, PLGA, and PVA physical mixture is due to the 1:1 ratio of PVA to IRN and there is not enough PVA to dissolve all of the IRN. The IRN melt peak disappeared in the IRN-loaded PLGA NPs which suggests that the IRN is its amorphous form within the NPs, which was confirmed by XRD.

The release profile of the IRN-loaded PLGA NPs is biphasic with a 'burst' release at day 1 and then slower release up to day 9. The 'burst' release corresponds with the IRN on the surface of the NPs being released, while the second phase was due to the diffusion of the IRN through the PLGA polymer, mediated by erosion and degradation of the polymer and resulting in a slow and more constant release rate (Tewes et al., 2007, Kumskova et al., 2020). The release of IRN from the PLGA 5002 NPs was much slower than the release from the PLGA 5004 NPs. This is due to the low intrinsic viscosity PLGA 5002 being acid terminated, which results in an electrostatic interaction between the HCL group of the IRN and the PLGA, slowing down the diffusion of IRN through the polymer. This is further evident in the second phase of release, with R22 having a significantly ($p < 0.05$) faster rate of release than either R1 or R13 between day 1 and 9. It is during this phase of diffusion controlled release that the electrostatic interaction would have most impact. The release of IRN from the NPs was faster at acidic pH due to an increase the solubility of IRN in the acidic media. The IRN is a HCL salt, which means the IRN is a base. Therefore, at low pH it will be ionised, which will increase its solubility (Ramchandani and Robinson, 1998, Ci et al., 2014, Sawada et al., 1995). Designing NPs with lower release at physiological pH and higher release at the low pH of the tumour microenvironment may help to reduce side effects

by limiting off-target toxicity through the reduction of drug release in normal tissue coupled with an increase in release in the tumour tissue (Wang et al., 2015). The pH of the normal tissue is in the range of 7.2 - 7.4, while tumour tissue ranges from 5.7 to 8.7, and the pH of the subcellular endosomes and lysosomes in tumour tissue ranges from 4.5 to 5.5 (Gerweck and Seetharaman, 1996, Stubbs et al., 2000).

2.5 Conclusion

The IRN-loaded PLGA NPs using two PLGAs of different inherent viscosities (5002 = 0.2 and 5004 = 0.4) were successfully developed single emulsion solvent evaporation method. In the pre-screening, various variables were studied including the amount and type of PLGA, molecular weight and percentage of PVA, sonication time, and lyophilization process. The IRN-loaded PLGA NPs were optimised using 3-factors and 3-level Box-Behnken statistical design software for each type of PLGA. The independent variables were amount of PLGA, and drug (IRN) and percentage of surfactant (PVA) and the dependent response were size and EE. 30 formulations of IRN-loaded PLGA NPs were prepared and characterised for their size, zeta potential, PDI, and EE. 4 IRN-loaded PLGA NPs formulations (R1, R6, R13, R22) were determined as the optimised NP formulations for further studies based on the minimum particle size with high EE. The IRN-loaded PLGA NPs showed a biphasic release pattern of the burst and sustained release. The release of IRN was affected by the type of the PLGA and the pH of the media, which was much faster from PLGA 5004 and in acidic PBS. The crystallinity of the NPs was evaluated using differential scanning calorimetry (DSC) and X-ray diffraction (XRD).

Chapter 3: Evaluation of the cytotoxicity of the IRN-loaded PLGA NPs using primary High Grade Glioma cells.

3.1 Introduction

IRN is a semisynthetic pro-drug that is a potent inhibitor of topoisomerase I which is involved in the transcription of DNA. IRN is converted into its active metabolites 7-ethyl-10-hydroxycamptothecin (SN-38) in glioblastoma cells, which is approximately 100 times more potent than the IRN pro-drug (Xu and Villalona-Calero, 2002). IRN has proven antitumor activities against different types of cancer such as colorectal cancer, gastrointestinal tract tumours, and glioblastoma (Xu and Villalona-Calero, 2002). In advanced colorectal cancer, IRN in combination with 5-fluorouracil (5-FU) and folinic acid is used as part of standard treatment regimen (Saunders and Iveson, 2006). IRN either on its own or in combination with other chemotherapeutic drugs such as temozolomide and bevacizumab has demonstrated therapeutic benefit in the treatment of GBM (Friedman et al., 1999, Yung et al., 2005, Vredenburgh et al., 2007a). A high systemic dose of IRN is required in order for it to demonstrate any therapeutic benefit as a treatment for GBM resulting in serious side effects such as diarrhoea and neutropenia (Hecht, 1998). The side effects associated with the systemic administration of IRN have prompted research into the development of novel drug delivery strategies to improve the delivery of IRN into the brain (Gawley et al., 2020). Thus, the IRN-loaded NPs have been developed to increase the concentration of IRN that crosses the BBB while reducing the unwanted side effects that are associated with systemic administration of IRN.

In vitro cell culture is fundamental to cancer research in order to provide information on tumour biology and therapeutic cytotoxicity. It allows for tumour cells to be studied in a controlled environment, and has been an attractive method for high-throughput screening of

drugs because of its ease of scale up and low cost (Seidel et al., 2015). However, the phenotypic genetic characteristic of primary cells isolated from human cancer tissue samples are much more representative of the original tumour compared to cancer lines (Seidel et al., 2015). This has resulted in cell lines being used in many successful pre-clinical studies that have failed in the clinic, due to misleading information about genetic pathways in cancers (Millau et al., 2010, Zhang et al., 2008). In GBM, the heterogenicity is the most important characteristic that needs to be maintained during tissue culture. This genetic diversity is maintained in primary GBM cells compared to GBM cell lines (Aum et al., 2014). Flow cytometry can be used to measure light scattering and fluorescence in single cells to evaluate cellular uptake and the apoptotic effect of NPs (Zucker et al., 2013). The detection of their cellular association using the side-scattered (SSC) intensity is more suitable for NPs that do not have fluorescence but have high scattering efficiency instead, as the SSC intensity is related to the inner granularity of cells (Suzuki et al., 2007, Zucker et al., 2010).

In this chapter, four primary GBM cell lines isolated from patients undergoing craniotomies at the Queen Elizabeth Hospital were used to assess the cytotoxicity, cellular uptake and apoptotic ability of the IRN-loaded PLGA NPs (R1, R6, R13, R22). The cytotoxicity of the IRN-loaded PLGA NPs has been investigated over 11 days with three different concentrations of 1, 10, and 100 μM. The cellular uptake of the IRN-loaded PLGA NPs (R1, R6, R13, R22) in the primary GBM cells (patient 1) at 3, 6, 24, 120 h after treatment were evaluated by flow cytometry. Confocal laser scanning microscopy was used to evaluate internalization of the fluorescent coumarin 6 (C6)-loaded PLGA NPs by the primary GBM cells (patient 1). In addition, flow cytometry was used to quantify cellular apoptosis in the primary GBM cells (patient 1) at day 5 after treatment with the IRN-loaded PLGA NPs (R13).

3.2 Materials and methods

3.2.1 Materials

Irinotecan Hydrochloride were obtained from Jiangsu Hengrui Medicine Co Ltd (Jiangsu, China). Dulbecco's Modified Eagle's Medium (DMEM-F12), sodium pyruvate, sodium bicarbonate solution ($NaHCO_3$), fetal bovine serum (FBS), thiazolyl blue tetrazolium bromide (MTT) powder, dimethyl sulfoxide (DMSO), Triton X-100, Coumarin 6 ≥99%, and trypsin replacement enzyme 1X were all purchased from Merck Life Science UK Limited (Dorset, UK). Collagenase, Pronase, antibiotic- antimycotic (containing penicillin, streptomycin and fungizone), and hank's balanced salt solution (HBSS) were all purchased from Gibco. 1.077 +/- 0.001 g/mL Ficoll-Paque density gradient cushions was purchased from GE Healthcare Life Sciences (Amersham, UK). Phosphate buffered saline (PBS) 1X, for biotechnology were purchased from VWR (Leicestershire, UK). Wheat Germ Agglutinin, Alexa Fluor™ 594 Conjugate, and Hoechst 33342, Trihydrochloride, Trihydrate - 10 mg/mL Solution in Water, and Dead Cell Apoptosis Kit with Annexin V Alexa Fluor™ 488 & Propidium Iodide (PI) were purchased from Thermofisher (Stafford).

3.2.2 Biopsy collection and dispersion

Unfixed Tumour Core (TC) tissue was collected directly from recurrent GBM patients undergoing craniotomies at the Queen Elizabeth Hospital in accordance with ethical approval (application number: 19-337) from the Human Biomaterials Resource Centre (HBRC). The samples were immediately placed in collection fluid and transported to the laboratory. Extraction of the tumour cells from the tissue and culturing of the subsequent cells was performed using standard methods. The GBM samples were removed from the patient by surgical resection. The collected samples were placed in fluid and transferred immediately to the laboratory and the cells extracted for future experiments.

The biopsy dispersion of the sample was done completely on the collection day. The tumour samples were immersed in and then rinsed with Hanks' Balanced Salt Solution (HBSS) to remove the blood clots. After rinsing the samples with HBSS, the samples were sliced using sterile crossed scalpels into approximately $1mm^3$ fragments. The fragments were suspended in 30 mL of HBSS, then transferred to a small conical flask using a sterile Pasteur pipette. The fragments were stirred for 30 min at 37℃ and then for 30 min at 4℃ with 0.25 mg/mL collagenase, 0.40 mg/mL DNAse, and 0.50 mg/mL pronase enzymes to digest the tumour fragments. The undigested materials were sieved out using 100 μM pore nylon mesh. The remaining suspension was layered onto 12 mL Ficoll-Paque™ density gradient cushions (Density: 1.077 +/- 0.001 g/mL) using two 50 mL tubes. The tubes were weighted and balanced using HBSS droplets then centrifuged at 1200 rpm at room temperature for 30 min. The cells from the digested sample appeared as a band at the interface while the Erythrocytes settled at the bottom of the tube. The band at the interface was removed and placed in a15 mL tube and 15 ml of HBSS added. The tube was centrifuged for 5 min at 1200 rpm, the supernatant discarded and the cells resuspended in the media for further studies.

3.2.3 Cell viability (MTT assay)

The primary GBM cells were seeded at a density of 10,000 cells per well in 96 well plate using DMEM containing 10% FBS and incubated for 48 h at 37℃ with 5% CO_2. After 48 h, the medium was removed and replaced with a free IRN solution or a NP suspension at different concentrations (1, 10, and 100 μM). The plates were incubated for 1, 3, 5, 7, 9, and 11 days. The MTT solution (0.50 mg\mL) 5mg of 3-(4,5-Dimethylthiazol-2-yl)-2,5-Diphenyltetrazolium Bromide per ml of PBS was added to each well and the plates incubated for 3 h when the media was replaced with 100 μl of DMSO. The Absorbance of control cells and treated cells was measured at 570 nm. The cell viability was calculated by a percentage

of absorbance of the treated cells to the control cells and expressed as percentage of the cell viability. All experiments were performed in triplicate and the data displayed as mean ± SD.

3.2.4 Cellular uptake by flow cytometry

Cellular uptake was determined using flow cytometry. The primary GBM cells were seeded at a density of $5x10^4$ cells per well in 24 well plates using DMEM containing 10% FBS and incubated for 48 h at 37℃ with 5% CO_2. After 48 h, the medium was removed and replaced with a NP suspension at different concentrations (0.1, 1, and 10 μM), and the plates were incubated for 3, 6, 24, 120 h. After each exposure time, the cells were washed twice with PBS then detached using trypsin. The detached cells were transferred to Eppendorf tubes then centrifuged at 1500 rpm for 5 min. The non-treated cells (control) and NP treated cells were re-suspended in 0.50 mL of PBS for flow cytometry analysis. Light-scattered intensity was monitored on side scattering (SSC), and a gating process was undertaken based on the intensity of SSC-A and FSC-H (forward-scattering). The data gating and visualization were performed using FlowJo™ software (FlowJo, LLC., USA).

3.2.5 Confocal laser scanning microscopy

The primary GBM cells were seeded at a density of $5x10^4$ cells per well in 24 well plates using DMEM containing 10% FBS and incubated for 48 h at 37℃ with 5% CO_2. After 48 h, the medium was removed and replaced with a coumarin 6 (C6)-loaded PLGA NP suspension at concentrations of 50 μM, and the plates were incubated for 2 h. The C6-loaded PLGA NP remaining in the media were removed and the cells were washed three times with PBS. The cells were fixed with 4% formaldehyde at room temperature for 15 min then washed three times with PBS, then permeabilised with ice cold 0.1% Triton X-100 for 20 min. Subsequently, the cells were stained with Hoechst dye (1 mg/mL) and Alexa Fluor® 594 (500 μg/mL) for 30 min and the stained cells washed three times with PBS. Finally, the cells

were mounted using a mounting medium and observed using a confocal laser scanning microscope (LSM 780, Zeiss, Germany).

3.2.6 Apoptosis assay labelling with Alexa® Fluor 488 annexin V and PI

The primary GBM cells were seeded at a density of $2x10^5$ cells per well in 12 well plate using DMEM containing 10% FBS and incubated for 48 h at 37℃ with 5% CO_2. After 48 h, the medium was removed and replaced with a NP suspension (R13) at different concentrations (1 and 10 μM), and the plates were incubated for 3 days. After 3 days. The DMEM media was collected, the cells detached using trypsin and then collected. The collected DMEM media and cells were centrifuged at 1500 rpm for 5 min at 4℃. The supernatant was discarded and cells were suspended in a 100 μl annexin-binding buffer. Then, 5 μL Alexa Fluor® 488 annexin V and 1 μL 100 μg/mL PI labelling solution were added to each 100 μL of cell suspension and incubated for 15 min. After incubation time, 400 μl of annexin binding buffer was added. A negative and positive control were used by using DMSO and staurosporine, respectively. Then, analysed to identify each type of cell death (necrosis or apoptosis) using flow cytometry. A statistical fit and cell cycle analysis were performed using FlowJo™ software (FlowJo, LLC., USA).

3.2.7 Statistical analysis

Statistical analysis was performed using a one-way or two-ways analysis of variance (ANOVA) (GraphPad Prism version 9.0.0 (86) for Windows, GraphPad Software, San Diego, CA). Post-hoc comparisons of the means were performed using Tukey's Honestly Significance Difference test. A significance level of $p < 0.05$ was accepted to denote significance in all cases.

3.3 Results

3.3.1 Cytotoxicity of the IRN-loaded PLGA NPs against primary GBM cells

The cytotoxicity of blank and IRN-loaded PLGA NPs at a concentration of 10 μM against primary GBM cells and after 5 days incubation is presented in Figure 3-1. The cell viability of the blank PLGA 5002 and 5004 NPs were 76.0±3.5 and 88.4±1.3%, respectively, while the cell viabilities of the IRN-loaded PLGA NPs were significantly ($p < 0.05$) decreased to 41.0±1.0 and 53.9±1.3%.

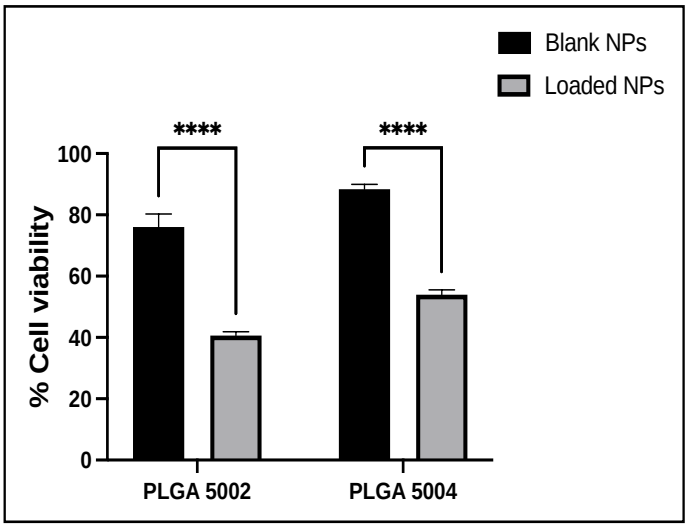
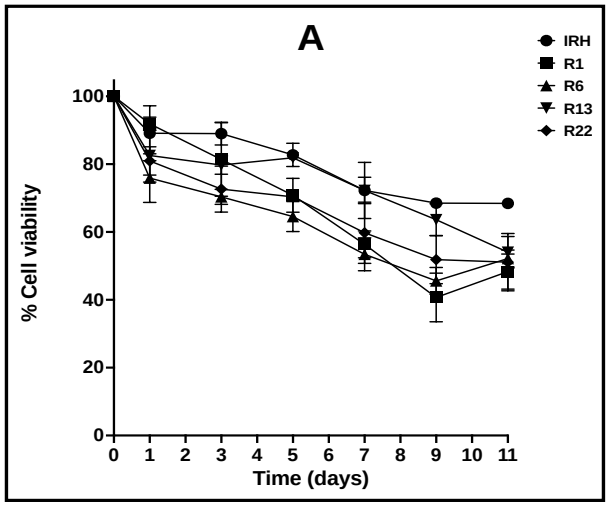


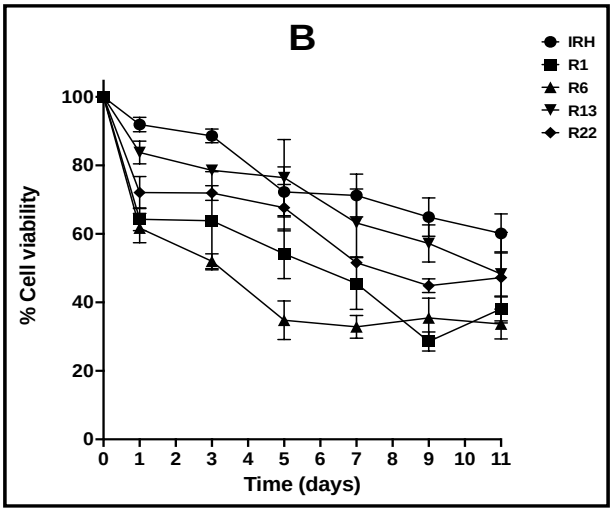
Figure 3-1: Cytotoxicity of two different blank NPs based on the type of PLGA in comparison with IRN- loaded PLGA NPs. The cytotoxicity of each blank NPs was compared with cytotoxicity of loaded PLGA NPs that have the same type of PLGA (PLGA 5002 or PLGA 5004) and same amount of NPs (equal 10 μM of IRN-Loaded NPs) in the same patient. Results shown as mean ± SD, (n= 3), significance found using a 2way ANOVA with Tukey's post-hoc test,($P < 0.05$).

The cytotoxicity of IRN-loaded PLGA NPs at different concentrations (1, 10, and 100 μM) against primary GBM cells for two patients over 11 days of treatment is presented in Figure 3-2 and Figure 3-3. In patient 1, the 1 and 10 μM concentrations (Figure 3-2A and B) of free IRN achieved a cell viability of 68.4±1.1 and 60.1±4.7% 11 days after treatment, respectively, while the 100 μM concentration (Figure 3-2C) achieved a cell viability below 10% 3 days after treatment. At concentrations of 1 μM and 10 μM, the IRN-loaded NPs achieved a significantly ($p < 0.05$) lower cell viability than the free IRN 11 days after treatment (Figure 3-2A and B). The lowest cell viabilities were 40 and 28% achieved with the

R1 NPs compared to the other NPs (R6, R13, R22) at a concentration of 1 and 10 μM on day 9 (Figure 3-2A and B). At a concentration 100 μM, the IRN-loaded PLGA NPs (R1, R6, R13, R22) reduced cell viability to below 35% at day 9 and 11. The lowest cell viabilities were 10 and 16% achieved by the R13 NPs compared to R1, R16, and R22 at a concentration of 100 μM on day 9 and 11 post treatment, respectively (Figure 3-2C). At day 11 post treatment, the cytotoxicity of IRN-loaded PLGA NPs was similar to day 9 at all three concentrations (1, 10, and 100 μM).

In patient 2, the 1 and 10 μM concentrations (Figure 3-3A and B) of free IRN achieved a cell viability of 74.7±6.1 and 49.1±0.2% 11 days after treatment, respectively, while the 100μM concentration (Figure 3-3C) achieved a cell viability 19.7±2.4% 3 days after treatment. At concentration of 1 and 10 μM the R1 and R6 NPs achieved a significantly ($p < 0.05$) lower cell viability than the free IRN 11 days after treatment, with the R13 NPs achieving this at 10 μM (Figure 3-3A and B). The lowest cell viabilities were 49 and 32% achieved by the R6 NPs at a concentration of 1 and 10 μM on day 9 (Figure 3-3A and B). At concentrations of 100 μM, all of the IRN-loaded PLGA NPs reduced the cell viability to below 20% at day 5. The lowest cell viabilities at 100 μM were 18 and 16% achieved by the R13 NPs on day 9 and 11 post treatment, respectively (Figure 3-3C). At day 11 post treatment, the cytotoxicity of IRN-loaded PLGA NPs was similar to day 9 at concentrations of 1 and 10 μM.





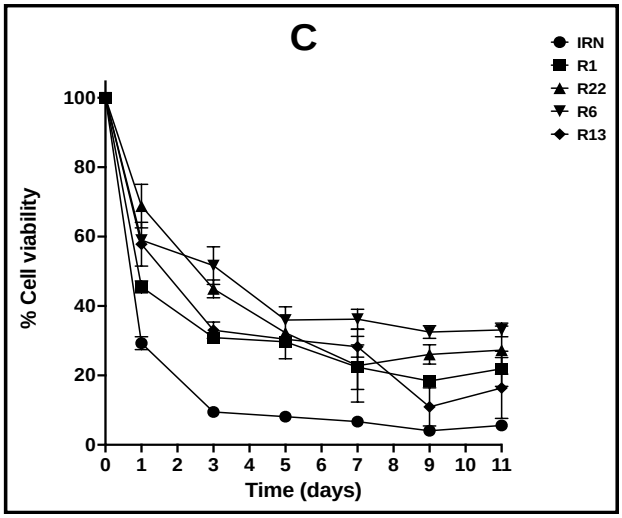


Figure 3-2: Viability of the primary GBM cells (patient 1) cultured with IRN-loaded NPs (free IRN, R1, R13, R16, and R22) at three different concentration for each (A) 1 μM, (A) 10 μM, (C) 100 μM) at day 1, 3, 5, 7, 9, 11. Results shown as mean ± SD, n= 3, significance found using a 2way ANOVA with a Tukey's post-hoc test, * = P<0.05 ** = P<0.01, *** = P<0.001, **** = P<0.0001.

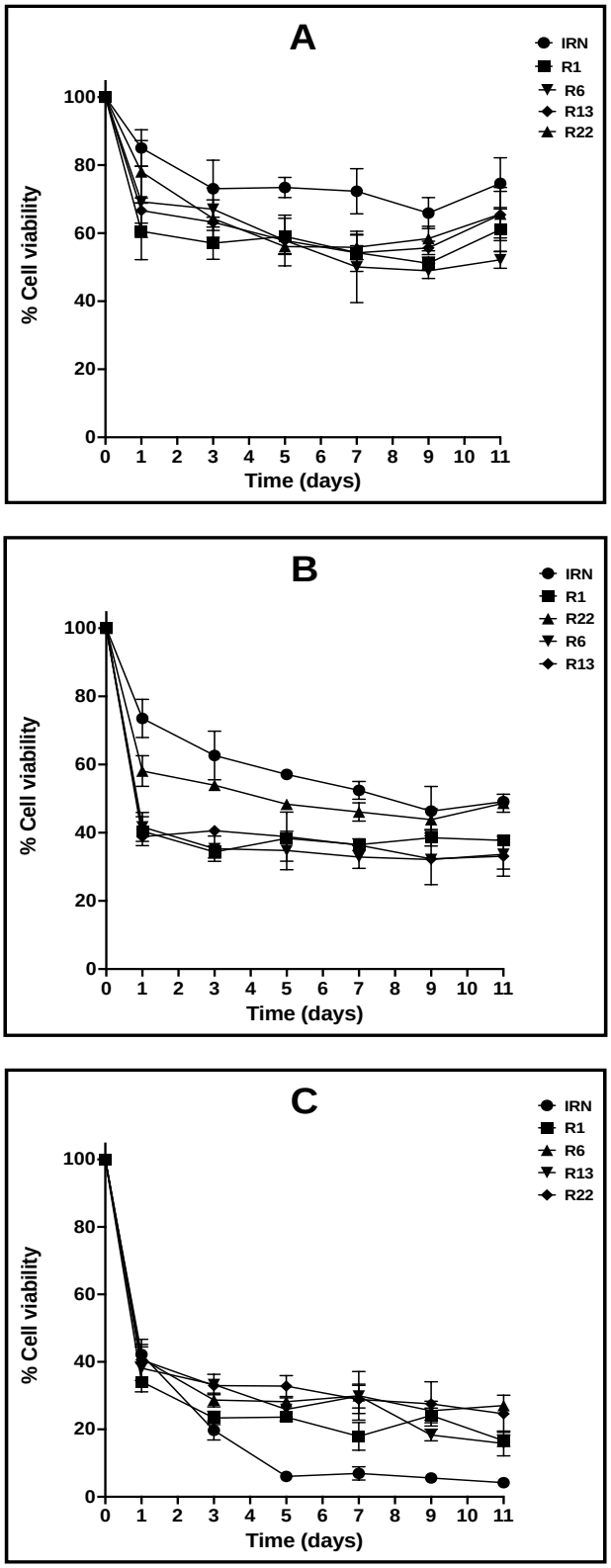


Figure 3-3: Viability of the primary GBM cells (patient 2) cultured with IRN-loaded NPs (free IRN, R1, R13, R16, and R22) at three different concentration for each (A) 1 μM, (A) 10 μM, (C) 100 μM) at day 1, 3, 5, 7, 9, 11. Results shown as mean ± SD, n= 3, significance found using a 2way ANOVA with a Tukey's post-hoc test, * = P<0.05 ** = P<0.01, *** = P<0.001, **** = P<0.0001.

Figure 3-4 presents the cytotoxicity of free IRN and the IRN-loaded PLGA NPs (R1, R6, R13, R22) at concentration of 100 μM against primary GBM cells of 4 different patients (P1, P2, P3, P4) 5 days post treatment. The cell viability of the free IRN was below 10% for patient 1 and 2, while for patient 3 and 4 it was approximately 22%. At concentration of 100 μM, the free IRN achieved a significantly ($p < 0.05$) lower cell viability than the IRN-loaded PLGA NPs for all 4 patients, except for the R13 NPs in patient 4, were there was no significant difference between pure IRN and the NPs. There was no significant difference ($p > 0.05$) in cell viability across the IRN-loaded PLGA NPs in patients 1, 2, and 4 except R13 in patient 4. With patient 3 the IRN-loaded PLGA NPs had a significant ($p < 0.05$) cell viability when compared to the other patients. For example, the R1 NPs achieved a significantly ($p < 0.05$) higher cell viability in patient 3 compared to patients 1, 2, and 4.

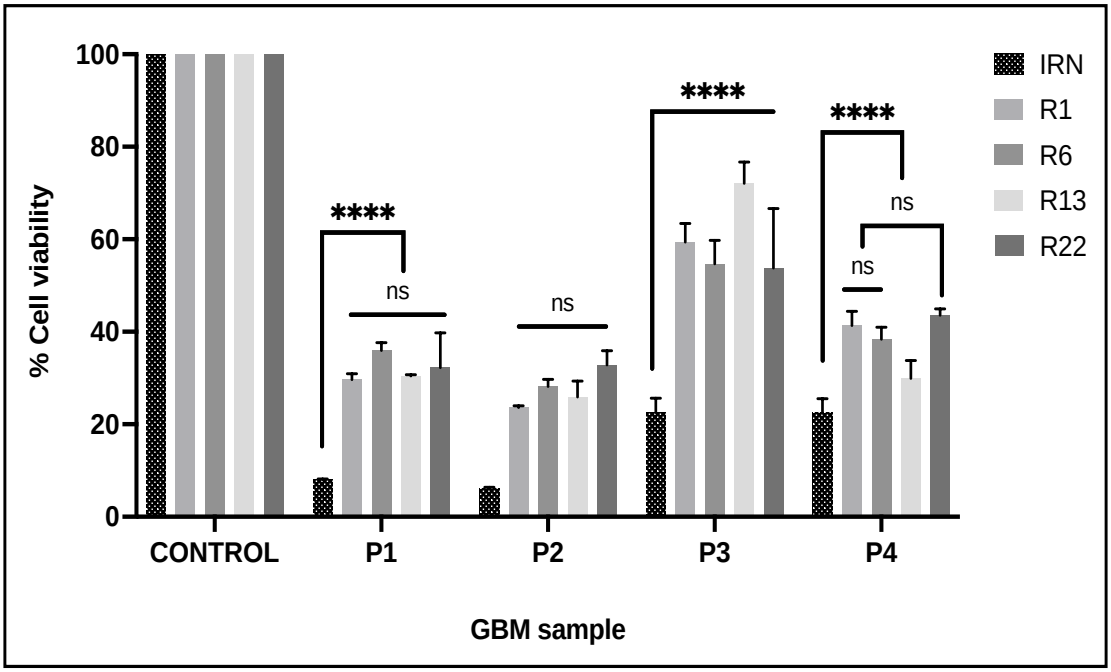


Figure 3-4: Cytotoxicity of IRN-loaded PLGA NPs (R1, R13, R16, R22) and free IRN at 100 μM against four different GBM samples (patient 1 (P1), patient 2 (P2), patient 3 (P3), and patient 4 (P4)) at day 5. Results shown as mean ± SD, n= 3, significance found using a 2way ANOVA with a Tukey's post-hoc test, * = P<0.05 ** = P<0.01, *** = P<0.001, **** = P<0.0001.

The cellular uptake of the IRN-loaded PLGA NPs (R1, R6, R13, and R22) at different concentrations of (0.1, 1, and 10 μM) were investigated in primary GBM cells at times of 3,

6, 24, 120 h after treatment (Figure 3-5). The control was untreated primary GBM cells and they were monitored also at times of 3, 6, 24, and 120 h. The results show that the cellular uptake of the IRN-loaded PLGA NPs was influenced by the time of treatment and concentration of the NPs. There was no significant difference ($p > 0.05$) in SSC intensity between control and treatment with different concentrations (0.1, 1, and 10 μM) of R6 and R22 at 3 h of treatment, while there was a significant ($p < 0.05$) difference with R1 and R13. In terms of SSC, the intensities of SSC in the primary GBM cells treated with NPs were higher than in the untreated primary GBM cells. However, with an increase in the time after treatment, the uptake of IRN-loaded PLGA NPs in the primary GBM cells (patient 1) were significantly ($p < 0.05$) increased. At a concentration of 0.1 μM of R6, R13, and R22 NPs there was no difference in cellular uptake at 3 h and 6 h post treatment. For each concentration, the cellular uptake of the IRN-loaded PLGA NPs significantly increased ($p < 0.05$) with an increase in time post treatment. For example, the uptake of 1 μM of the R13 NPs at 120 h post treatment in the primary GBM cells was significantly higher than the uptake of the same concentration of the R13 NPs at either 6 or 24 h (Figure 3-5B). Furthermore, the uptake of the IRN-loaded PLGA NPs in the primary GBM cells was significantly ($p < 0.05$) increased with an increase in the concentration of NPs. The highest cellular uptake was achieved with 10 μM of the IRN-loaded PLGA NPs (R1, R6, R13, and R22).

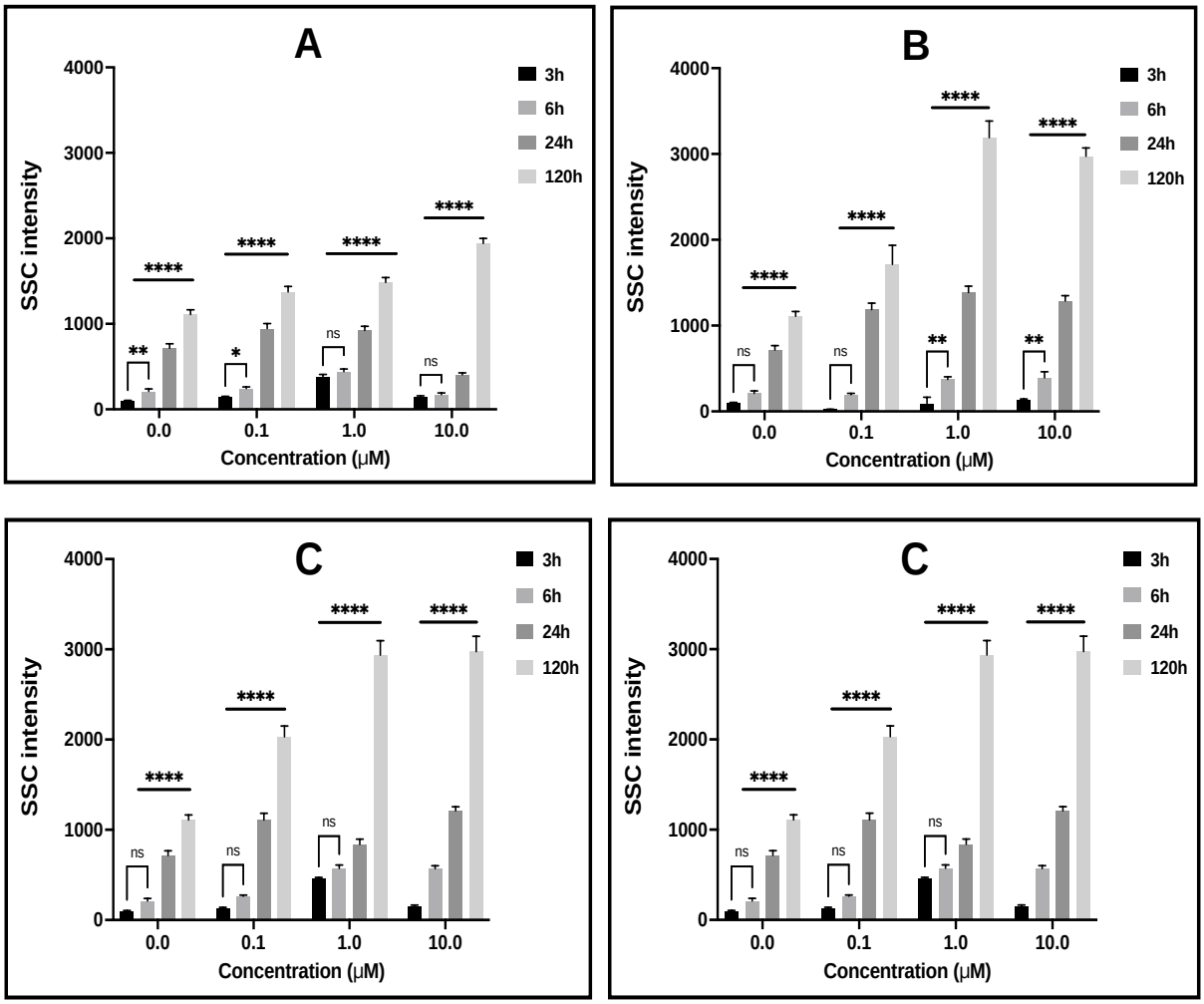


Figure 3-5: Cellular uptake of IRN-loaded NPs in the primary GBM cells (patient 1) after incubation time of 3, 6, 24, 120 h at three different concentrations 0.1, 1, 10 μM for formulation; R1 (A), R6 (B), R13 (C), R22 (D) observed by flow cytometry. Results shown as mean ± SD, (n= 3), significance found using a 2way ANOVA with a Tukey's post-hoc test, * = P<0.05 ** = P<0.01, *** = P<0.001, **** = P<0.0001.

Figure 3-6 shows a comparison of cellular uptake in the primary GBM cells for the different IRN-loaded PLGA NPs (R1, R6, R13, and R22) at a concentration of 10 μM 24 and 120 h post treatment. The R1 NPs had the lowest cellular uptake at both of 24 and 120 h, while the R22 NPs had the highest cellular uptake at both 24 and 120 h post treatment. There was no significant difference in cellular uptake between R6 and R13 at 24 and 120 h post treatment as well as R6, R13 and R22 at 120 h post treatment.

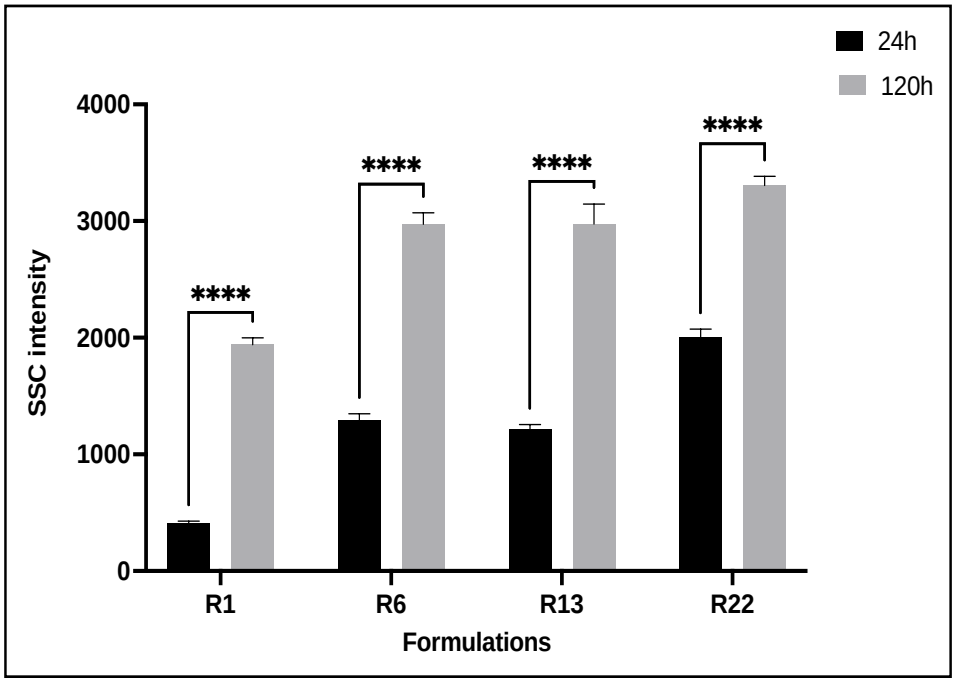


Figure 3-6: Comparing cellular uptake of IRN-loaded PLGA NPs R1, R6, R13, and R22 (10 μM of each) in the primary GBM cells (patient 1) at time 24 and 120 h determined by flow cytometry Results shown as mean ± SD, (n= 3), significance found using a 2way ANOVA with a Tukey's post-hoc test, * = P<0.05 ** = P<0.01, *** = P<0.001, **** = P<0.0001.

3.3.2 Confocal laser scanning microscopy

Confocal laser scanning microscopy images of the primary GBM cells 2 h post incubation with coumarin 6 (C6)-loaded PLGA NPs at a concentration of 50 μM are presented in Figure 3-8. The cells nuclei are shown in blue (Hoechst dye), the cytoplasm in red (Alexa Fluor® 594) and the C6-loaded PLGA NPs in green (coumarin 6). Figure 3-7A-a to d shows the untreated control primary GBM cells for each of the different stains, while figure 3-7A-e shows a merged image of a to d. The primary GBM cells treated with C6-loaded PLGA NPs for each of the stains and the merged image are presented in figure 3-7B-a to e. The result show that the green C6-loaded PLGA NPs have aggregated in the cell cytoplasm with some of NPs penetrating into the nuclei as shown in in the merged image (Figure 3-7.B-e), while there was no aggregation of C6-loaded PLGA NPs in the spaces between the primary GBM cells(Figure3-7B-e).

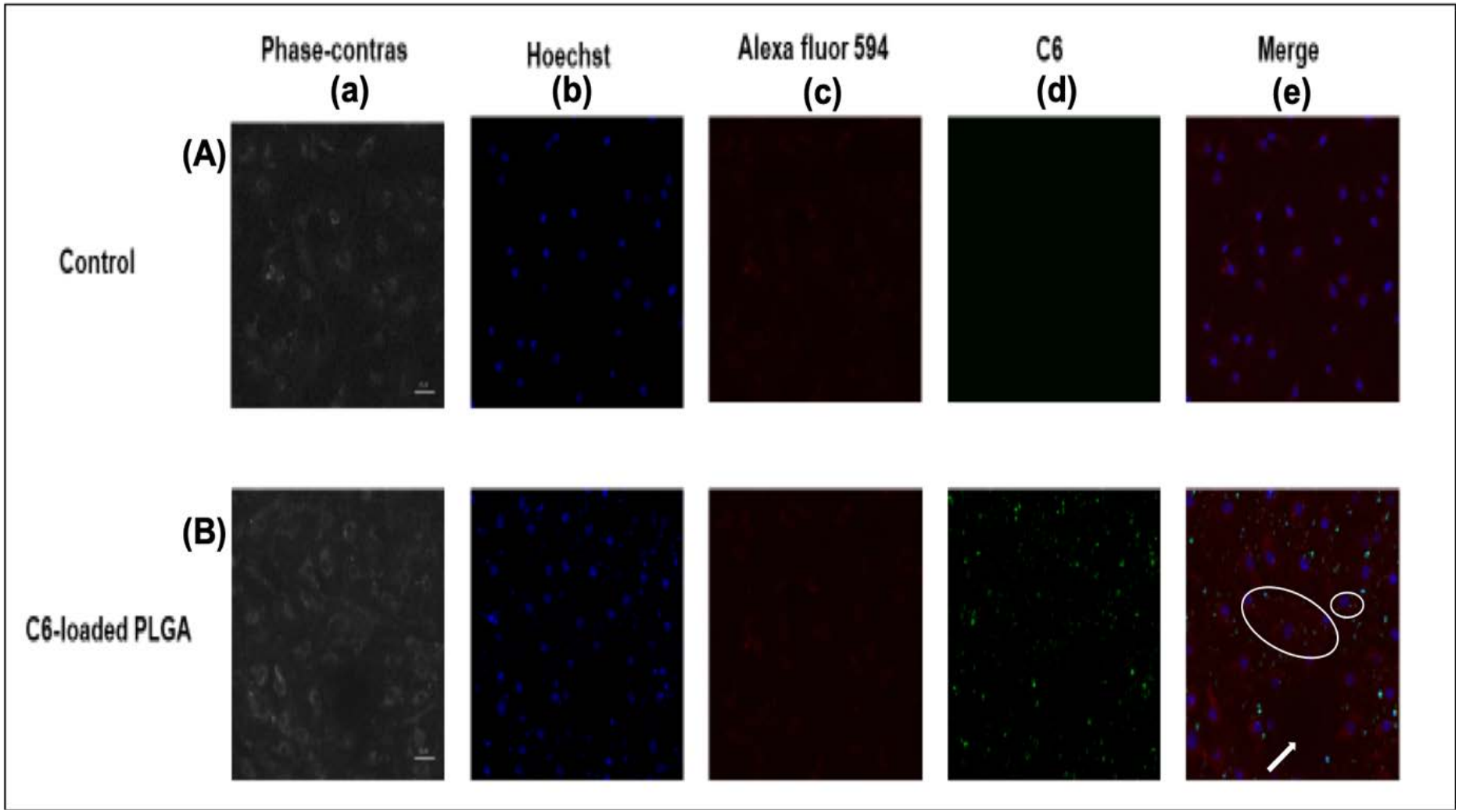


Figure 3-7: In vitro cellular uptake of C6-loaded PLGA NPs evaluated in the primary GBM cells (patient 2) using confocal laser scanning microscopy. The cells were treated with coumarin 6 (C6)-Loaded PLGA NPs 50 µM for 2 h. (A) untreated primary GBM cells and (B) treated primary GBM cells; (a) unstained (b) stained with Hoechst dye for cells nuclei (c) stained with Alexa Fluor® 594 for cells cytoplasm (d) without and with C6- loaNPs (e) the foure merged images.

3.3.3 Quantitative analysis of apoptosis using the Annexin V/PI double-staining assay and flow cytometry calculations.

Apoptotic primary GBM cells after treatment with the IRN-loaded PLGA NPs (R13) were identified by flow cytometry using the Annexin V/PI double-staining assay. The primary GBM cells were treated with staurosporine as a positive control, DMSO as a negative control, and R13 at concentrations of 1 and 10 μM. Figure 3-8A represents the percentage of the apoptotic primary GBM cells relative to controls and R13 concentrations, and Figure 3-8B represents dot plots of annexin V/PI staining of the primary GBM cells. The total percentage of apoptotic primary GBM cells after treatment with staurosporine (positive control) was less than 0.1%, with 69.3% dead cells, while the total apoptotic cells with DMSO (negative control) was 52%. The untreated control cells had only 10.6% total apoptotic (early and late apoptotic) primary GBM cells, which was significantly increased to 64.8 and 74.9% when treated with 1 and 10μM of R13 for 3 days (Figure 3-8A). The increase in the total apoptotic primary GBM cells was principally in the late apoptotic stage. At a concentration of 10 μM, the percentage of early and late apoptotic cells was 10.2 and 64.7% respectively.

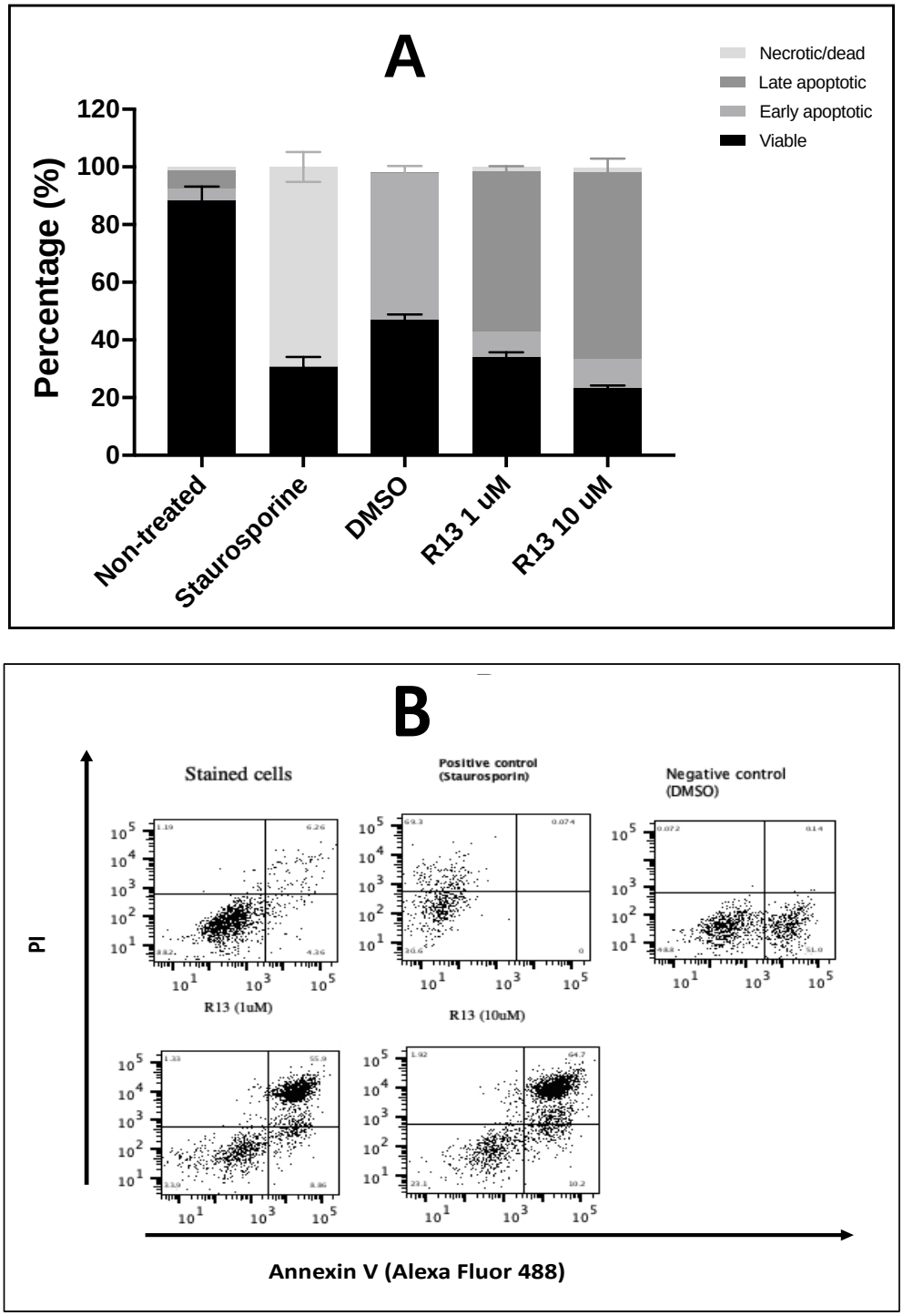


Figure 3-8: Estimation of apoptotic cell population by flow cytometry using Annexin V/PI double-staining assay. (A) Graphical representation of Viable (Annexin V-/PI-), early apoptotic (Annexin V+/PI-), late apoptotic (Annexin V+/PI+), and necrotic/dead (Annexin V-/PI+) cells obtained from flow cytometry. The primary GBM cells (patient 1) were treated with Staurosporine (positive control), DMSO (negative control), and R13. (B) Representative dot plot obtained from Annexin V/PI double-staining after three days treatment with R13 in two different concentrations of 1, 10 μM; Viable cells (Lower left), Annexin V positive early apoptotic cells (Lower Right), Annexin V and PI dual positive (Upper Right), and only PI positive necrotic cells (Upper Left) (n= 3).

3.4 Discussion

The cytotoxicity of the blank PLGA NPs and the optimised IRN-loaded PLGA NPs (R1, R6, R13, and R22) were investigated against primary GBM cells using the MTT assay. The cytotoxicity of the blank PLGA NPs demonstrates that although the NPs are slightly cytotoxic themselves (Altındal and Gümüşderelioğlu, 2016), loading them with IRN makes them significantly ($p < 0.05$) more cytotoxic. For the IRN-loaded PLGA NPs, there was no significant difference ($p > 0.05$) in the cytotoxicity of the R1, R6, R13, and R22 in 3 of the 4 patients despite the differences in their EE (Table 2-4). R22 with an EE of 40% had a similar cytotoxicity profile as R1, R6 and R13, which had EEs of 88.9, 80.1 and 65.4, respectively. This can be explained by the release profile of the NPs (Figure 2-18). The release rate of IRN from R22 was significantly ($p < 0.005$) higher than either R1 or R13. At a concentration of 100 μM (Figure 3-3C), the IRN-loaded PLGA NPs reduced cell viability to below 40% at day 5, where it remained for 11 days post treatment.

The cellular uptake of the IRN-loaded PLGA NPs by the primary GBM cells was analysed by flow cytometry and confocal microscopy. In terms of SSC intensity in flow cytometry, the IRN-loaded PLGA NPs were observed inside the primary GBM cell by increased side scatter. The average of SSC intensity in the primary GBM cells treated with IRN-loaded PLGA NPs was increased with an increase in the time post treatment as well as the concentration of the NPs. That can be explained by that the cellular association and cellular uptake of NPs in the primary GBM cells being proportional to the concentration of the NPs as well as the exposure time to the NPs (Danhier et al., 2009). The relationship between the cellular uptake of the NPs and the increase in the side scatter suggests that the amount of NPs inside the cells is related to the mass concentration of NPs applied to the cells (Zucker et al., 2013). The IRN-loaded PLGA NPs could be internalised into the cells via different pathways such as passive diffusion or endocytosis. The increase SSC intensity with an increase in incubation time

indicates the time-dependent transfer of the NPs into the cells by passive diffusion, which has time dependent characteristics (Lee et al., 2015). The cellular uptake efficiency of the NPs could be influenced by their size and surface charge (Bannunah et al., 2014, Fröhlich, 2012, He et al., 2010). The results demonstrate that the cellular uptake of the IRN-loaded PLGA NPs is be influenced by both the surface charge and concentration of NPs. The uptake of NPs with a low negative surface charge of -10 (R22) was much higher than those NPs with a higher negative surface charge of -22 (R1), -30 (R6), and -22 (R13). This result suggests that the IRN-loaded PLGA NPs with a lower negative surface charge accumulate at the cellular membrane due to the higher affinity for electrostatic interaction with the cell membrane (He et al., 2010). This phenomenon reflects the influence of the surface charge on the cellular internalization of the NPs which was also observed by other authors (Malinovskaya et al., 2017, Hillaireau and Couvreur, 2009, Bannunah et al., 2014, Kumar et al., 2013). The R1 NPs had a low cellular uptake compared to the other NPs (R1, R6, and R13) and that could be explained by the lower concentration of the R1 NPs was used due to its high EE.

The cellular uptake of C6-loaded PLGA NPs is easily visualised by confocal laser scanning microscopy. The images support that the C6-loaded PLGA NPs can be internalised into the primary GBM cells, which is consistent with the data obtained by flow cytometry. To further analyse NPs- induced cytotoxicity, the apoptotic effect of the IRN-loaded PLGA NPs on the primary GBM cells was investigated using the Annexin V/PI double-staining assay by flow cytometry. The results showed that the IRN-loaded PLGA NPs were able to significantly promote apoptosis and necrosis in the primary GBM cells, especially in the late stage apoptosis, in dose dependent manner. After the induction of apoptosis, phosphatidylserine is translocated from the inner membrane leaflet of viable cells to the exposed membrane surface and that is the early event in apoptosis stage. Annexin V has a very affinity to bind to

phosphatidylserine on the outer plasma membrane and that can be used to determine the population of apoptotic cells (Kekre et al., 2005, Tousi et al., 2021).

3.5 Conclusion

Four primary GBM cells isolated from patients were used to assess the cytotoxicity, cellular uptake and apoptotic ability of the optimised IRN-loaded PLGA NPs (R1, R6, R13, R22). The cytotoxicity study confirms that the optimised NPs showed toxicity effect as pure IRN at 1 and 10μM against the primary GBM cells. The cellular uptake of the IRN-loaded PLGA NPs was increased with time of treatment and concentrations of NPs. Low negative charge NPs has shown better cellular uptake compared to high negative. The results of flow cytometry and confocal microscopy have shown the ability of the NPs to be internalised in the primary GBM cells. Thus, we propose that the IRN-loaded PLGA NPs could be efficiently used for treatment of GBM.

Chapter 4: The ability of the IRN-loaded PLGA NPs to cross in vitro mono- and co-culture BBB models

4.1 Introduction

In vitro BBB models are very useful and allow to develop a reliable prediction of the brain penetration of a drug or carrier, such as a nanoparticle. Early models initially involved isolated primary brain capillary endothelial cells (BCEC) co-cultured with astrocytes (Rubin et al., 1991, Huwyler et al., 1996, Török et al., 2003). This model was limited due to the isolation process being very time consuming. Therefore, immortalised rat or mouse cell line BBB models such as the RBE4 (Roux et al., 1994), GPNT (Régina et al., 1999), and End3 (Omidi et al., 2003) were developed. However, most of these models were characterised with a high permeability and therefore needed to be co-cultured with astrocytes or glial cells (Markoutsa et al., 2011). The Human cerebral microvascular endothelial cell line D3 (hCMEC/D3) cells, which are a well characterised human brain endothelial cell line, were used as a BBB cellular model. Endothelial cells have a unique feature of forming a monolayer with tight junctions producing an intact barrier of endothelial cells as a continuous membrane (Abbott et al., 2006b). This model has been shown to mimic the main characteristics of the BBB in humans (Weksler et al., 2005), even in the absence of co-cultured glial cells. The hCMEC/D3 cells under appropriate culturing conditions have been shown to form tight junction complexes (Weksler et al., 2005). This model has been proven to be reliable for screening drugs and/or carriers for CNS diseases (Poller et al., 2008).

The hCMEC/D3 cell line was derived from human temporal lobe microvessels during surgery for the control of epilepsy and enriched with cerebral endothelial cells (CECs). The hCMEC/D3 cells were sequentially immortalised by lentiviral vector transduction with the catalytic subunit of human telomerase (hTERT) and SV40 large T antigen in the first

passage. The CEC were selectively isolated by limited dilution cloning. The clones were extensively characterised for phenotype of brain endothelial with typical endothelial markers such as CD31, VE-cadherin, and von Willebrand factor expressed in the hCMEC/D3 cells. The cells remain as contact inhibited monolayers in culture, are able to form capillary tubes in matrix and show a stable normal karyotype. These cells demonstrate the main characteristics of the BBB such as the capacity to exclude drugs and the formation of tight junctions. Therefore, the hCMEC/D3 cells represent one such human BBB model that can grow easily and is amenable to study drug transport into the CNS (Weksler et al., 2005, Weksler et al., 2013, Poller et al., 2008).

Transendothelial electrical resistance (TEER) is the measurement of electrical resistance of the cellular monolayer. TEER is used to confirm the integrity and permeability of the monolayer and it is a very sensitive and reliable method (Srinivasan et al., 2015). Measuring the resistance of the barrier according to Ohm's law is one of the main methods for achieving this. TEER measurements are based on the qualitative measurement of electric resistance of the barrier and the maximum, maintained value of the TEER measurement reflects the cellular barrier integrity (Benson et al., 2013, Srinivasan et al., 2015). Applying direct alternating current (AC) (I) square wave with a frequency of 12.5 Hz with defined voltage (U) is applied in this method to measure the resistance. The resistance of the barrier can be calculated according to Ohm's law: were Resistance (R) = Voltage (U) / Current (I) (Benson *et al.*, 2013).

In this chapter, TEER measurement was used to measure the resistance of the BBB according to Ohm's law. Two methods; An epithelial volt-ohm meter (EVOM2) and Electric Cell-substrate Impedance Sensing (ECIS) were used to study the changes in the resistance of the

brain endothelial cells monolayer (hCMEC/D3) after adding the IRN-loaded PLGA NPs (R1, R6, R13, and R22). Impedance spectroscopy (CellZscope) was used to investigate the change in resistance in a co-culture of hCMEC/D3 cells and astrocytes after adding the IRN-loaded PLGA NPs (R13). The CellZscope approach was a more sophisticated model, which has the correct oxygen level and pressure normally seen in the brain. The EVOM model was used as a high throughput screening model and then the most promising NPs was advanced to the CellZscope model. The results will be used as a suggestive indicator on the ability of the IRN-loaded PLGA NPs to cross the BBB in humans.

4.2 Materials and Methods

4.2.1 Materials

Sterile 6.5 mm transwell plates with an 8.0 μm pore size polycarbonate membrane insert, were purchased from Corning (Flintshire, UK). ECIS culture ware 8W10E+ lexan (PC) 8 well arrays with 40 electrodes (1.96 mm^2 total area) per well were purchased from Ibidi (UK). The ECIS model 1600R was purchased from Applied Biophysics (USA). Human cerebral microvascular endothelial cell line D3 (hCMEC/D3) cells, and EndoGRO-MV complete culture media kit were purchased from Merck Life Science UK Limited (Hertfordshire, UK).

4.2.2 Monoculture of human BBB models using the hCMEC/D3 cells

The hCMEC/D3 cells were cultured using the EndoGRO™-MV complete media kit supplemented with 1 ng/mL FGF-2. A monoculture BBB model was constructed using hCMEC/D3 cells plated on polycarbonate membrane transwell inserts (24 well tissue culture plate, 8 μm porosity, and wells were pre-coated with human perlecan) (Figure 4-1). The hCMEC/D3 cells were seeded at a density of 7.5 X 10^4 cells/well and incubated for 60 to 72 h at 37°C, 5% CO^2.

4.2.3 Co-culture of the human BBB model using hCMEC/D3 cells and human astrocytes

Polycarbonate membrane transwell inserts (24 well inserts, 8 µm pore size) were used and coated with 10 µg/ml human perlecan on the apical side and 5 µg/ml human fibronectin on the basal side of the filter. $2.5x10^4$ cells/well of astrocytes were seeded and left to adhere and grow for 72 h in a 37 ºC, 5% CO_2 humidified incubator. $7.5x10^4$ of hCMEC/D3 were then seeded on the apical side (Figure 4-1) of the filter before placing the cellZscope module in a sterile, humidified, 37ºC and 5% CO_2 incubator.

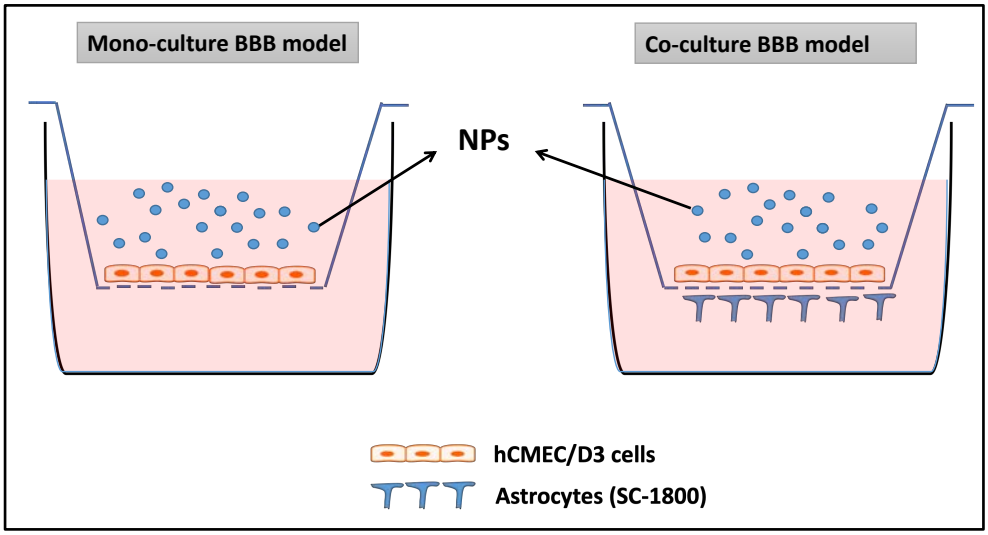


Figure 4-1: Schematic assembly of the BBB model used to study the ability of the IRN-loaded PLGA NPs to cross the BBB. A monoculture BBB model of the hCMEC/D3 cell (left) and a coculture BBB model of the hCMEC/D3 cell and astrocyte (right). 24 well plates, (8 µm porosity, and polycarbonate membrane transwell inserts) were used and the filters were coated with 10µg/mL perlecan.

4.2.4 EVOM2 method for TEER measurement of the monoculture BBB model (hCMEC/D3 cells)

EVOM2 with an STX2 electrode (Figure 4-2) was used to measure TEER. Initially, EVOM2 resistance was measured manually every 30 min for 6 h directly after seeding the cells in the insert, then every 24 h up to 168 h or until a constant resistance value was achieved, which is deemed to be a reflection of the formation of a tight barrier. Once a tight barrier was formed, the media on the apical side was replaced with NPs (R1, R6, R13, and R22) suspended in the

media two different concentrations (100 µM and 200 µM) and the resistance values measured at 0, 6, 24, 48, and 72 h.

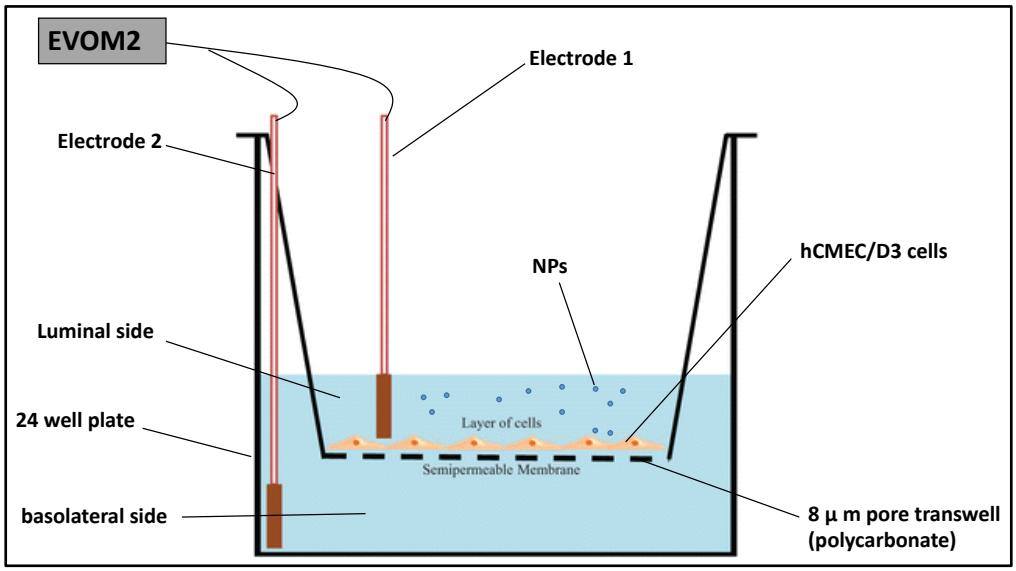


Figure 4-2: TEER measurement with a chopstick electrode using EVOM2 measured in ohm's. The monoculture BBB model consists of a monolayer of the hCMEC/D3 cells cultured on the semipermeable membrane inserts. For the TEER measurement, the shorter electrode placed in the upper compartment and the longer electrode placed in the lower compartment and the ohmic resistance was determined by applying AC voltage to the electrodes. Schematic adapted from ref. (Srinivasan et al., 2015).

4.2.5 ECIS method of TEER measurement on the mono-culture BBB model (hCMEC/D3 cells)

The ECIS system consisted of an eight well cell culture dish arrays (8W10E+PC), with each well equipped with a gold large counter and 40 small sensing electrodes with a diameter of 250 µm. The tissue culture dish arrays with 0.9 cm^2 in basal area and 0.4 mL total volume were washed with HBSS. 10 mM of L-cysteine was added for 10 min at 37°C in an humidified incubator to activate the arrays. After being activated by L-cysteine, wells were washed with HBSS and then incubated with 10 µg/mL of perlecan for 2 h. $7.5x10^4$ hCMEC/D3 in 300µL of EBM+ EGM-2 +2% HS were seeded per well (Figure 4-3). The arrays were then connected to the instrument after which AC was applied through a 1-MΩ resistor to monitor the development of an intact endothelial cell monolayer. Once the resistance plateaued, 300 µL of R1, R6, R13 and R22 were added on top of the endothelial

cell monolayer and electrical resistance measured for any changes. Time series data was collected and analysed using an ECIS core software. Resistance values were obtained in Ω.

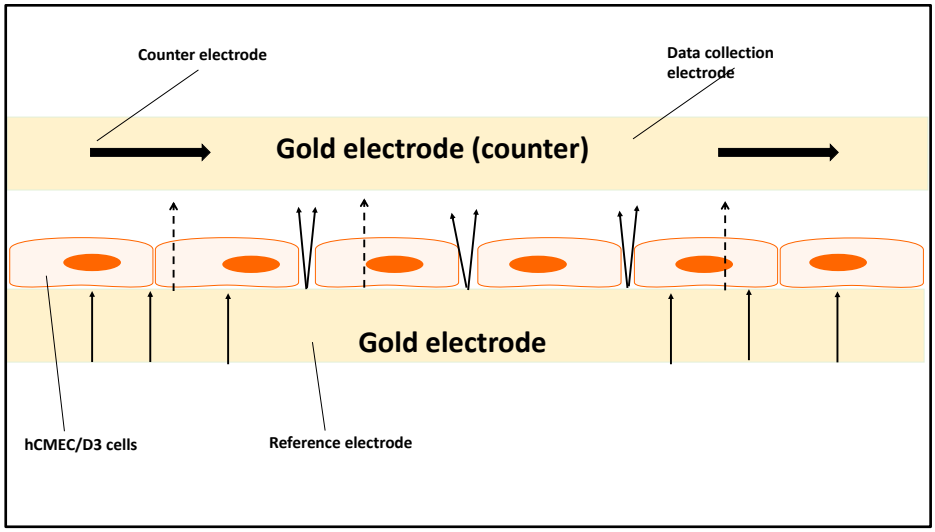


Figure 4-3: TEER measurement using ECIS system. The hCMEC/D3 cells were directly adhered on electrodes and the current was passed through the monoculture cells.

4.2.6 CellZscope method for TEER measurement of co-culture BBB model (hCMEC/D3 cells and astrocytes)

CellZscope was used to measure the resistance of the co-culture BBB model consisting of hCMEC/D3 cells on the apical and astrocytes on the basal side of the permeable membranes in the transwells. The electric resistance of the BBB model was measured by an electric equivalent circuit and the data analysed as TEER via a corresponding mathematical model. $2.5x10^4$ cells/well of astrocytes were seeded and left to adhere and grow for 72 h in a 37°C, 5% CO_2 humidified incubator. $7.5x10^4$ of hCMEC/D3 cells were then seeded on the apical side of the filter before placing the cellZscope module in a sterile, humidified, 37°C and 5% CO_2 incubator and connected to the cellZscope external controller, which in turn was connected to the cellZscope 1.5.0 software throughout a USB port. Once resistance values plateaued, 300µL of the IRN-loaded PLGA NPs (R13) was added on top of the endothelial cell monolayer and electrical resistance recorded for any changes. TEER values were collated and analysed using the same operating software. Resistance values were expressed as $\Omega.cm^2$ (Figure 4-4).

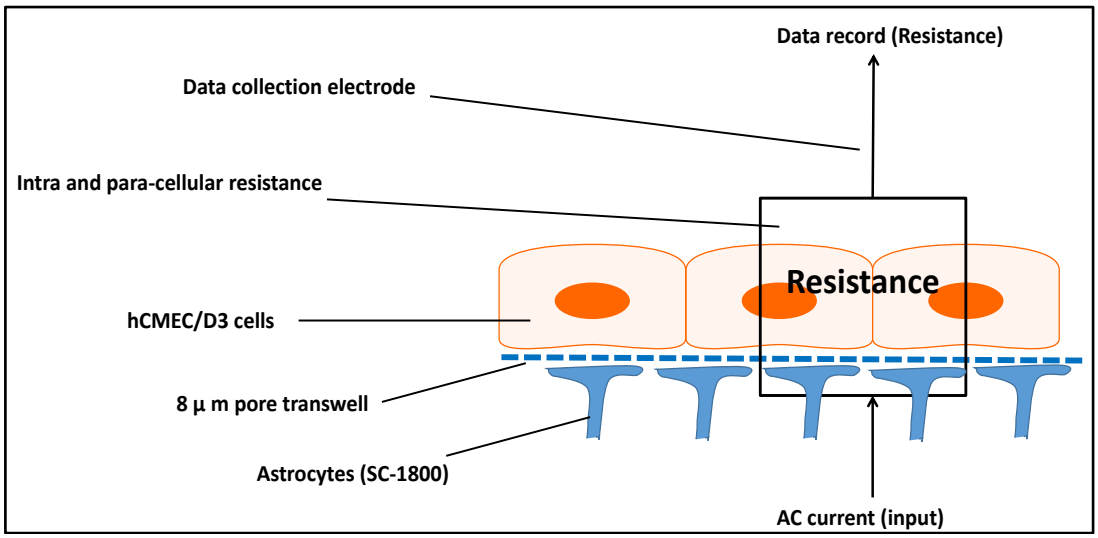


Figure 4-4: TEER measurement using cellZscope. The hCMEC/D3 and astrocyte were grown on the transwell membrane and non-invasive AC current pass through the co-culture BBB model of cells and astrocyte.

4.2.7 Statistical analysis

Statistical analysis was performed using a one-way analysis of variance (ANOVA) (GraphPad Prism version 9.0.0 (86) for Windows, GraphPad Software, San Diego, CA). Post-hoc comparisons of the means were performed using Tukey's Honestly Significance Difference test. A significance level of $p < 0.05$ was accepted to denote significance in all cases.

4.3 Results

4.3.1 Monitoring the change in resistance of the monoculture BBB model using EVOM2

After seeding the hCMEC/D3 cells, the resistance was monitored until a maximum resistance (200 – 225 Ω/cm^2) was recorded after 3 consecutive readings. Figure 4-5 shows the phase contrast microscopy of highly confluent hCMEC/D3 cells at 168 h when the cells achieved the highest resistance of 218.3±1.0 Ω/cm2 (Figure 4-6). The image of the hCMEC/D3 cells shows that the cells adhered well to the polycarbonate membrane.

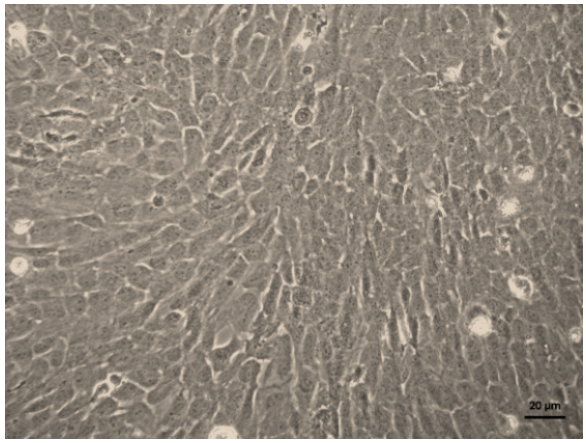


Figure 4-5: The phase-contrast microscopy image shows confluency of the hCMEC/D3 cells when the highest resistance was recorded at 168 h.

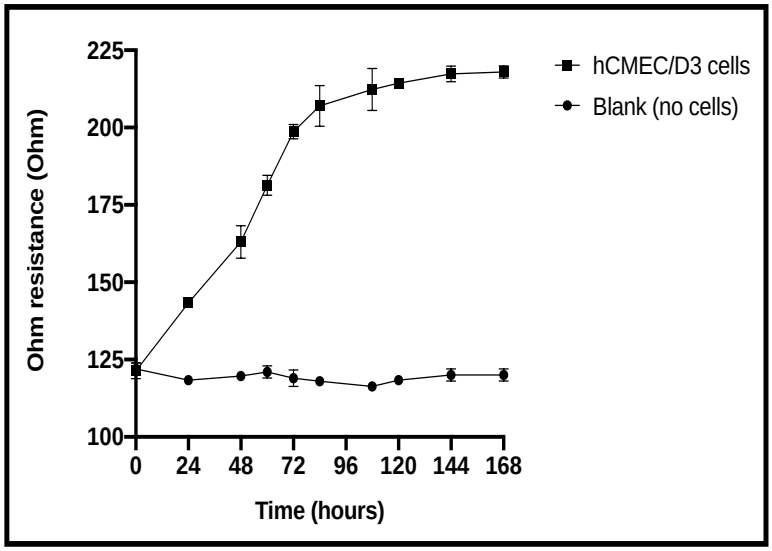


Figure 4-6: The resistance profile of hCMEC/D3 cells over 168 h starting immediately after seeding the cells (time 0) until the highest resistance (time 168 h) was reached, presented as Ohm's resistance. The density of cells was 7.5 X 10^4 cells/well. A monoculture BBB model was constructed using 8 µm pore size polycarbonate-membrane filters in 24-transwell inserts. The resistance was evaluated by measuring TEER values with EVOM2. Results shown as mean ± SD, n= 3, significance found using a one-way ANOVA with a Tukey's post-hoc test, ($p < 0.05$).

The IRN-loaded PLGA NPs (R, R6, R13 and R22) were added at two different concentrations (≈100 and ≈200 µM) at t=168 h and the resistance recorded over 3 days with readings acquired at 0, 6, 24, 48, 72 h. At 100 µM, the R1 and R13 NPs induced a slight reduction to the resistance value after 6 h exposure, which was maintained for 24 h, with further significant ($p < 0.05$) reductions at 48 and 72 h (Figure 4-7A). For the R22 NPs a significant ($p < 0.05$) reduction was seen after 48 h, followed by a further reduction ($p <$

0.05) at 72 h (Figure 4-7A). At 200 µM a similar trend is seen (Figure 4-7B), with all NPs causing a slight decrease in resistance at 6 and 24 h, with significant ($p < 0.05$) decreases in resistance at 48 and 72 h. In the control well (only cell with no adding NPs), no significant difference ($P > 0.05$) was observed over 72 h.

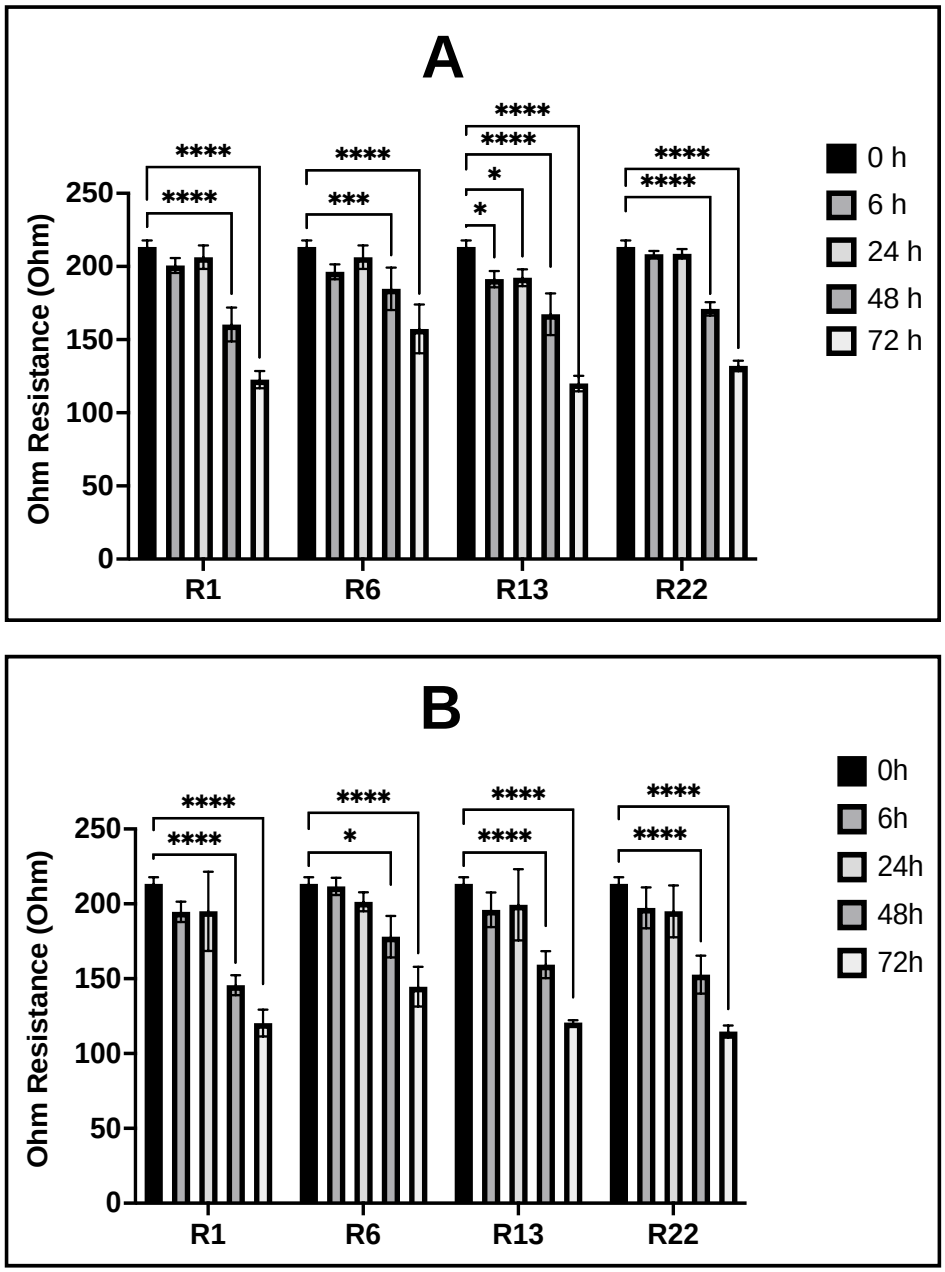


Figure 4-7: Effect of the IRN-loaded PLGA NPs at two different concentrations **(A)** 5mg (≈ 100 µM) and **(B)** 10 mg (≈ 200 µM) on the BBB model permeability at time 0, 6, 24, 48, and 72h. The monoculture was constructed using 8 µM pore size polycarbonate-membrane filters within 24-transwell inserts. The resistance was evaluated by measuring TEER values with EVOM2. A significant decrease ($p < 0.05$) in resistance was shown at 48 h after adding NPs for all IRN-loaded PLGA NPs (R1, R6, R13, R22) compared to the control (time 0). Results shown as mean ± SD, n= 3, significance found using a 2way ANOVA with a Tukey's post-hoc test, * = P<0.05 ** = P<0.01, *** = P<0.001, **** = P<0.0001.

4.3.2 Monitoring the change in resistance of the mono-culture BBB model using the ECIS system

The ECIS system was used to investigate the change in resistance after adding the IRN-loaded PLGA NPs to the mono-culture BBB model (hCMEC/D3 cells). The ECIS histograms in Figure 4-8 show the resistance of the monoculture BBB model per time point. The R1, R6, R13, and R22 NPs were added to the mono-culture BBB model after 70-72 h of seeding the hCMEC/D3 cells and once the resistance had plateaued, and the resistance values recorded in Ω. The IRN-loaded PLGA NPs reduced the endothelial barrier integrity as demonstrated by a decrease in the resistance post-addition of NPs. The resistance values were recorded over 20 h post-addition, with the resistance of the BBB model was gradually and significantly decreased ($P < 0.05$) within the first hour of addition of the R1 and R6 NPs (Figure 4-8A). The resistance decreased from approximately 1100 Ω to between 950 and 1000 Ω. The resistance slightly increased over the next two hours, and then decreased significantly over following 20 h ($P < 0.05$). The resistance 20 h post addition of the R1 and R6 NPs was approximately 800 Ω and 700 Ω, respectively (Figure 4-8A). The resistance of the mono-culture BBB model 20 h after the addition of the R13 and R22 NPs decreased from approximately 1500 Ω to approximately 850 and 1300 Ω respectively (Figure 4-8B).

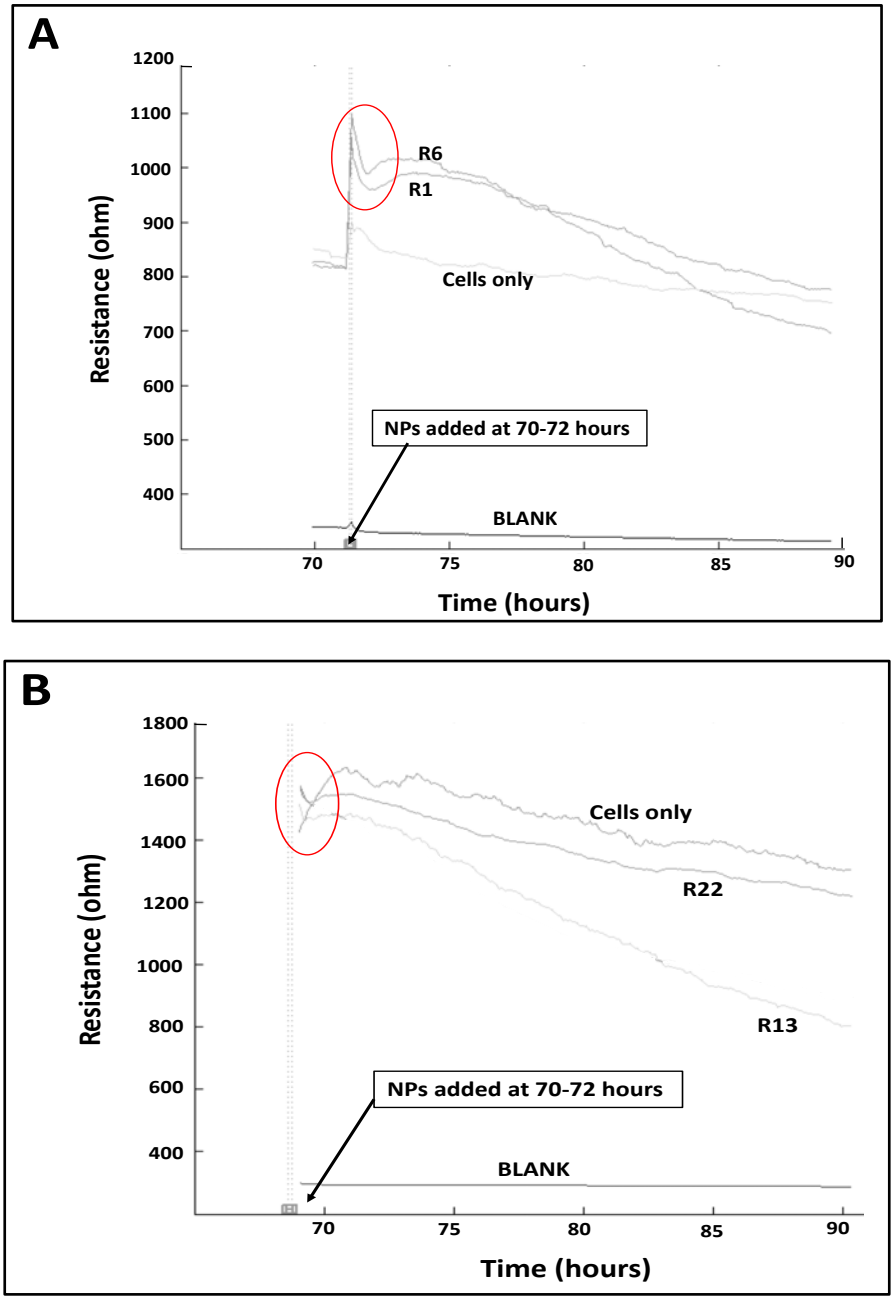


Figure 4-8: Changing in resistance values in BBB model (hCMEC/D3 cells) with the IRN-loaded PLGA NPs **(A)** R1 and R6, **(B)** R13 and R22. The cells were seeded on the gold electrode and the resistance was recorded by the ECIS system over 20 h post addition of the NPs. The NPs were added at 70-72 h once resistance values plateaued. Significance found using a one-way ANOVA with a Tukey's post-hoc test, ($p < 0.05$), (n=3).

4.3.3 Monitoring the change in resistance of the co-culture BBB model using the cellZscope system

A cellZscope system was used to record the change in the resistance of the co-culture BBB model. Once the resistance value plateaued, the R13 NPs were added and the resistance measured over 82 h by the cellZscope system (Figure 4-9). The result demonstrate that the

plateaued resistance was achieved after 48 h of culturing BBB model and the resistance was 27 $\Omega.cm^2$. The resistance of the co-culture BBB model gradually decreased over the first 10 h after the addition of the R13 NPs, when it then increased over the following 10 to 15 h, decreasing again until a final resistance value of 15 $\Omega.cm^2$ was achieved after 82 h.

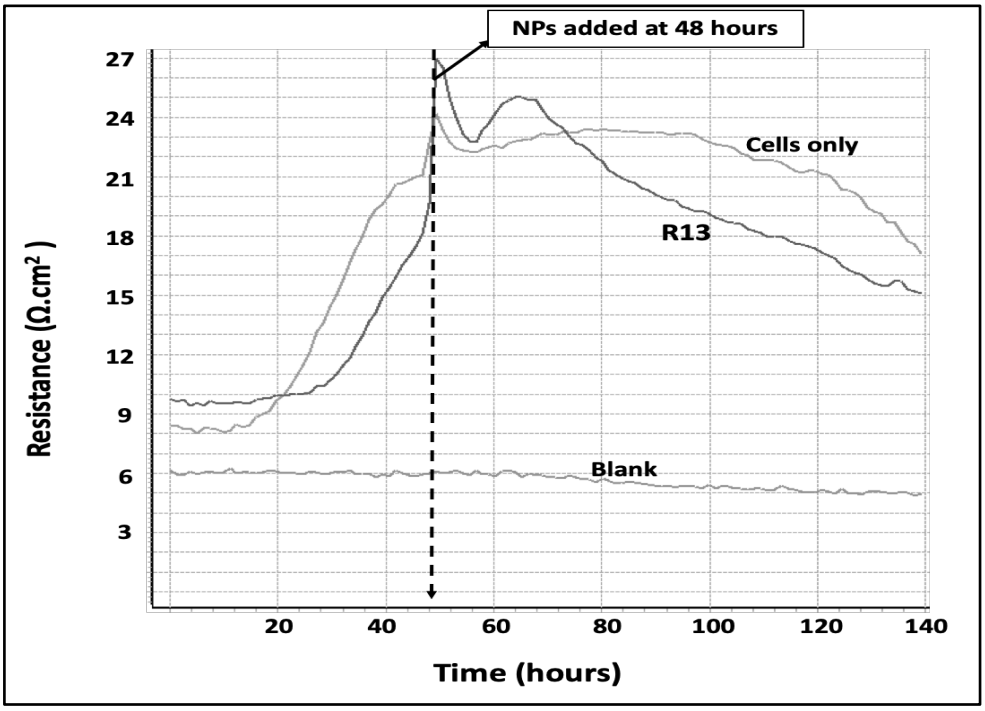


Figure 4-9: Changing in resistance values in co-culturing BBB model (hCMEC/D3 cells and astrocyte) post-addition of the IRN-loaded PLGA NPs (R13). The resistance was recorded by cellZscope system for 82 h after adding NPs. The NPs were added at 48h once resistance values plateaued. Significance found using a one-way ANOVA with a Tukey's post-hoc test, ($p < 0.05$), (n=3).

4.4 Discussion

In order for the IRN-loaded PLGA NPs to be an effective treatment for GBM they need to cross the BBB and deliver therapeutic concentrations of IRN to the tumour tissue. The mono-culture of the hCMEC/D3 cells and their co-culture with astrocytes were used as BBB models to evaluate the ability of the IRN-loaded PLGA NPs to cross the BBB. The main advantages of the hCMEC/D3 cells are that they provide a stable, easily to culture, transferable population of human microvascular CECs that maintain a normal BBB phenotype (Weksler et al., 2013). This BBB model has been shown to be well adapted for drug uptake or transport studies (Weksler et al., 2013). TEER is a quantitative method to

investigate the integrity of endothelial cells in a monolayer cell culture model (Srinivasan et al., 2015). A high resistance value indicates the tightness and integrity of the BBB, while a low resistance value indicates opening of the tight junctions of the BBB and an increased permeability (Chen et al., 2016). A decrease in TEER values is suggestive of opening of the tight junction of the BBB by the NPs, which will increase their permeability across the BBB into the brain (Chen et al., 2016). Upon validating the ability of the IRN-loaded PLGA NPs to cross the BBB, we used two BBB models (mono- and coculture) and three different approaches (EVOM2, ECIS, and cellZscope) to measure the TEER values.

The TEER values obtained from these instruments cannot be compared between each other, because they are different in various parameters such as the height and surface area of the inserts, and the AC frequencies (Maherally et al., 2018). The resistance of the mono-culture BBB model was monitored using the EVOM2 and ECIS systems, while the cellZscope system was used for co-culture BBB model. In the EVOM2 work, the mono-culture BBB model was constructed using polycarbonate membrane transwell inserts (24 well inserts, 8µm pore size). The TEER values for EVOM were significantly decreased ($P < 0.05$) at 48 and 72 h with the IRN-loaded PLGA NPs (R1, R6, R13, and R22). This decrease in TEER value indicates that the tight junctions of the BBB model were opened by the NPs and therefore the NPs can cross the BBB model. The EVOM2 technique is a manual instrument and the TEER values may be influenced by different variables such as position and angles of electrodes (Maherally et al., 2018). Hence, further evidence instruments with less variability such as ECIS and cellZscope was performed to confirm the permeability of the IRN-loaded PLGA NPs across the BBB model. The effect of the NPs on the integrity and resistance of brain endothelial monolayers was also assessed using the ECIS system at a two-dimensional level.

The ECIS is an automated, real-time, label free impedance-based instrument to monitor and record many cellular activities on the cell layer by recording non-invasive AC signals (Giaever and Keese, 1991). The result demonstrate that the resistance of mono-culture BBB model decreased within the first hour after addition of the NPs, which indicates that the tight junction of the BBB model was opened by the IRN-loaded PLGA NPs and thus their permeability through the monoculture BBB model was increased. The results of the cellZscope demonstrated that the IRN-loaded PLGA NPs were able to cross the co-culture BBB models within 1 h post-addition. As can be seen from Figures 4-8 and 4-9 the decrease in resistance is gradual post addition of the NPs, which indicates that the NPs did not destroy the tight junctions between the endothelial cells as there is no sharp decrease in the resistance. Moreover, there was a slight increase in resistance over a period of approximately 10 h, which would indicate recovering of the tight junction after the NPs crossed the BBB models. Therefore, the NPs could have a reversible effect on the tight junction of the BBB, which is ideal for safe and effective treatment. The results of the three methods were consistent, a noticeable decrease in the resistance was recorded post addition of the IRN-loaded PLGA NPs to both the mon-culture and coculture BBB models when compared to the control (only cells with no addition of NPs). According to the EVOM2, ECIS, and cellZscope results, there was no impact of particle size of the ability of the IRN-loaded PLGA NPs to reduce the TEER value and thus cross the BBB. However, the size range of the particles was 184 to 291 nm and thus there may not be enough of a difference between their size to see an impact.

4.5 Conclusion

The hCMEC/D3 cells as BBB model showed that the cells adhered well and the resistance increased with the cells growing. The co-culture BBB model was constructed of the

hCMEC/D3 cells and astrocyte and showed high resistance within 48 h. The TEER measurement was used to investigate the change in the resistance of the BBB models after adding the NPs using three different instruments (EVOM2, ECIS, and cellZscope). All these instruments showed a decrease in the TEER values of the BBB models with the addition of the IRN-loaded PLGA NPs. Therefore, the optimised IRN-loaded PLGA NPs can efficiently cross the mono- and co-culture BBB models. Overall, The IRN-loaded PLGA NPs are promising treatment for GBM that could potentially cross the BBB and deliver the therapeutic levels IRN to the tumour tissue.

Chapter 5: Dual formulation of Irinotecan hydrochloride and Pitavastatin calcium into PLGA NPs

5.1 Introduction

Pitavastatin (PTV) is a synthetic lipid lowering agent, and belongs to the statin family. PTV inhibits HMG-CoA (3-hydroxy-3-methyl-glutaryl-CoA) reductase in the liver and therefore controls the synthesis of cholesterol (Ose, 2011). Numerous studies have concluded that statin drugs, including PTV, have efficacy in reducing the growth of tumours (Jiang et al., 2014, Thurnher et al., 2012, Nielsen et al., 2012). A study showed that PTV induced cellular autophagy and suppressed multidrug resistant protein 1 (MDR-1) in GBM tumour cells (Jiang et al., 2014). The mechanism of action was suggested to be the influence of PTV on the metabolism of cholesterol, a component of the cell membrane, as well as signalling in tumour cells both of which are important for tumour growth. Therefore, highly proliferative cells such as GBMs require a lot of cholesterol and this could make GBM cells respond to statin therapy (Jiang et al., 2014). Further studies have implicated that statins can induce apoptosis of GBM cells by targeting LDL cells and resulting in GBM cell apoptosis through the ERK/AKT pathway (Jiang et al., 2014, Yanae et al., 2011).

The aforementioned studies on the cytotoxicity of statins against GBM cells, has encouraged researchers to investigate the cytotoxicity of the combination therapy of IRN and PTV. The potency of IRN was significantly enhanced against tumours when combined with PTV. The cytotoxicity of IRN was significantly increased in combination with PTV and its IC_{50} values against GBMs were decreased 40 to 70 fold compared to IRN alone (Jiang et al., 2014, Matusewicz et al., 2015). The suggested rationale for the increased cytotoxicity of IRN in combination with PTV is due to PTV being a substrate for the overexpressed MDR-1 protein in GBM cells which eliminates IRN from the cells. Therefore the suppression of MDR-1

glycosylation by PTV increases IRN accumulation in the GBMs cells making it more effective (Anjum et al., 2017, Matusewicz et al., 2015). This combination therapy makes IRN more cytotoxic against GBM cells at lower concentrations, which could help to reduce the systemic dose of IRN avoiding the serious unwanted side effects associated with high dose IRN (Jiang et al., 2014).

In this chapter, the preparation and characterisation of PLGA NPs co-loaded with both IRN and PTV is described. The type and amount of PLGA, IRN, and PVA were chosen based on the optimised IRN loaded PLGA NPs (Chapter 2). IRN and PTV co-loaded PLGA NPs were characterised for their size, zeta potential, PDI, EE, and release profile. Four primary GBM cell lines isolated from patients undergoing craniotomies at the Queen Elizabeth Hospital were used to assess their cytotoxicity, cellular uptake and apoptotic ability. The cytotoxicity of the IRN and PTV co-loaded PLGA NPs (C2) was investigated over 11 days at three different concentrations of 1, 10, and 100 μM. The cellular uptake of the IRN and PTV co-loaded PLGA NPs (C2) in the primary GBM cells (patient 1) at 3, 6, 24, 120 h after treatment was evaluated by flow cytometry. In addition, flow cytometry was used to quantify cellular apoptosis in the primary GBM cells (patient 1) 5 days after treatment with the IRN and PTV co-loaded PLGA NPs (C2). The ability of IRN and PTV co-loaded PLGA NPs (C2) to cross in vitro monoculture and co-culture BBB models was evaluated based on the TEER measurement technique using EVOM2 and ECIS methods for monoculture BBB model, and cellZscope method for co-culture BBB model.

5.2 Materials and Methods

5.2.1 Materials

Pitavastatin calcium was obtained from LGM Pharma (Georgia, USA). All others materials and patient samples used were the same as those used in chapters two, three and four.

5.2.2 Preparation of IRN and PTV-loaded PLGA NPs using single emulsion solvent evaporation method

The preparation method is explained in detail in Chapter 2, section 2.2.2.1 Preparation of Blank and IRN-loaded PLGA NPs using single emulsion solvent evaporation method. The IRN and PTV were dissolved in organic phase (DCM). Table 5.1 shows the amount of PLGA, IRN, PTV, and the percentage of the PVA that were used for the IRN and PTV co-loaded PLGA NPs formulations.

Table 5.1: The Variables in preparing combinations of the IRN and PTV co-Loaded PLGA NPs include the amount of drugs, amount of PLGA, percentage of PVA, and type of PLGA.

Run	Drugs (mg)		Type of PLGA	PLGA (mg)	PVA (%)
	IRN	PTV			
C1	4	4	PLGA 5002	120	2
C2	4	4	PLGA 5002	180	4
C3	4	4	PLGA 5002	240	4

5.2.3 HPLC analysis, size, zeta potential, EE, and in vitro release.

The methods are the same as those described in Chapter 2, section 2.2.3 HPLC analysis.

5.2.4 Biopsy collection and dispersion, cell viability study, cellular uptake, and apoptosis assay labelling with Alexa® Fluor 488 annexin V and PI.

The methods are the same as those described in Chapter 3, sections 3.2.2 Biopsy collection and dispersion, 3.2.3 Cell viability, 3.2.4 Cellular uptake by flow cytometry, and 3.2.6 Apoptosis assay labelling with Alexa® Fluor 488 annexin V and PI.

5.2.5 Monoculture and coculture BBB models, EVOM2, ECIS, and cellZscope methods

The methods are the same as those described in Chapter 4, sections 4.2.1 Monoculture of human BBB models using the hCMEC/D3 cells, 4.2.3 Co-culture of the human BBB model using hCMEC/D3 cells and human astrocytes (SC-1800), 4.2.4 EVOM2 method for TEER measurement of the monoculture BBB model (hCMEC/D3 cells), 4.2.5 ECIS method of TEER measurement on the mono-culture BBB model (hCMEC/D3 cells), and 4.2.6CellZscope method for TEER measurement of co-culture BBB model (hCMEC/D3 cells and astrocytes)

5.2.6 Statistical analysis

Statistical analysis was performed using a one and two way analysis of variance (ANOVA) (GraphPad Prism version 9.0.0 (86) for Windows, GraphPad Software, San Diego, CA). Post-hoc comparisons of the means were performed using Tukey's Honestly Significance Difference test. A significance level of $p < 0.05$ was accepted to denote significance in all cases.

5.3 Results

5.3.1 Preparation IRN and PTV co-loaded PLGA NPs by single emulsion solvent evaporation method

IRN and PTV co-loaded PLGA NPs were prepared using the single emulsion solvent evaporation technique. The PLGA 5002 (low intrinsic viscosity) at three different levels (120, 180, 240) were used to prepare C1, C2, and C3 NPs, respectively. The percentages of PVA were 2% with C1, while 4% with C2, and C3. The Initial amount of IRN and PTV in the NPs was 4 mg of each in all IRN and PTV co-loaded PLGA NPs. The smallest size 70.30±0.16 nm was achieved with C2 NPs which has the highest EE of PTV (18.50%) compared to C1 and C3 NPs (5.50 and 9.70%, respectively). The size of C3 NPs was

162.10±1.63 and the EE of IRN was 59.54% while the EE of PTV was 9.72%. The zeta potential of the IRN and PTV co-loaded PLGA NPs was found to be in the range of -22 to -24, and the PDIs were less than 2.9 (Table 5.2).

Table 5.2: Characterisation of the IRN and PTV co-loaded PLGA NPs including size, Zeta potential, PDI, and EE (n= 3).

Formulation	size (nm)	Zeta potential	PDI	EE (%)		Total EE (%)
				IRN	PTV	
C1	93.3±0.8	-22.7±0.9	0.3	29.4	5.5	34.9
C2	70.3±0.2	-24.6±1.8	0.2	44.6	18.5	63.1
C3	162.1±1.6	-23.2±0.5	0.2	59.6	9.7	69.2

5.3.2 HPLC analysis for IRN and PTV

Figure 5.1 shows the PTV standard curve at 5 different concentrations of each quantified by the HPLC. The correlation between the PTV concentration and the HPLC AUC was excellent with the R values at 0.9996 from 0.01 to 100 µg/ml. The retention times were approximately 3.90 min for PTV. The HPLC chromatogram of the IRN and PTV co-loaded PLGA NPs (C2) is shown in Figure 5-2. As can be seen, the HPLC chromatogram of the C2 NPs reveal a peak at 1.8 min which refers to the presence of IRN and peak at 3.9 min which refers to the presence of PTV.

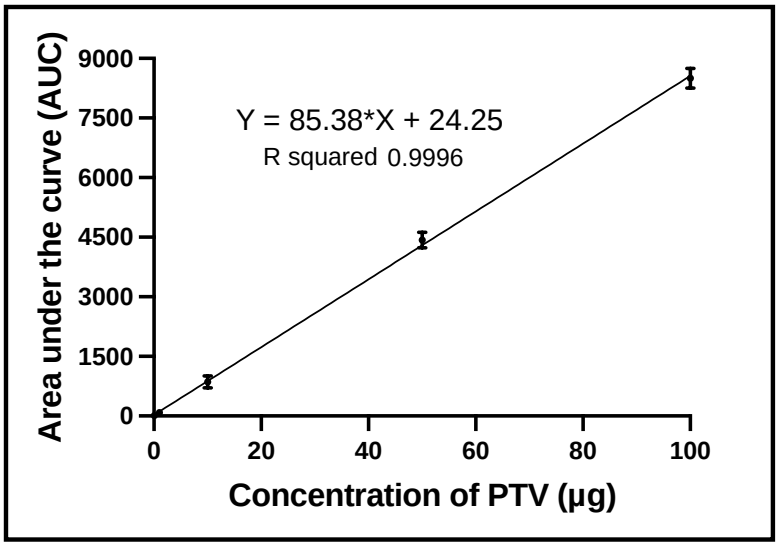


Figure 5-1: Standard curves of PTV using HPLC (n= 3).

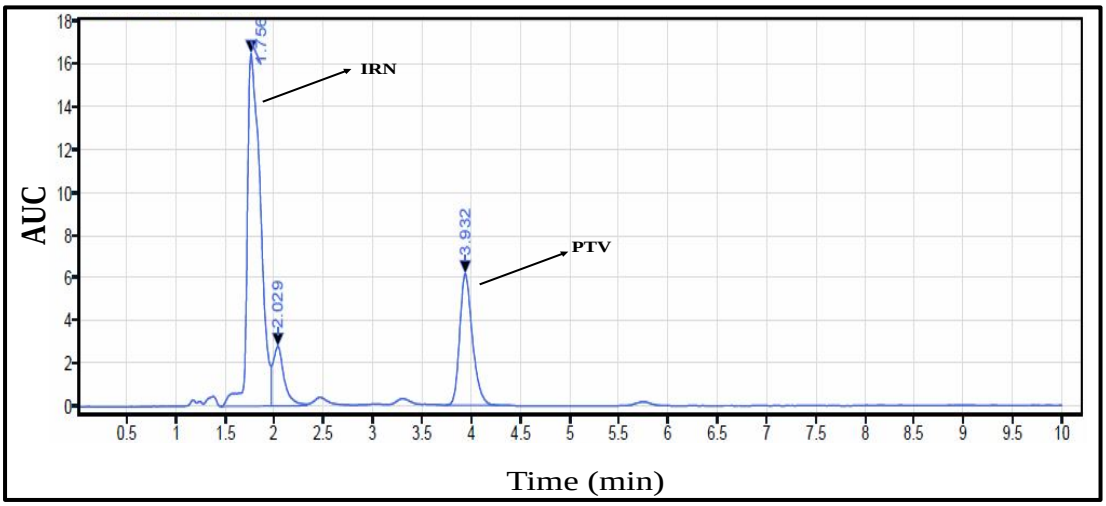


Figure 5-2: The HPLC chromatogram depicting the peaks of IRN and PTV in the C2 NPs measured at 265 nM wavelength.

5.3.3 pH-dependent drug release

The release of IRN and PTV from the C2 NPs was performed in PBS at two different pH values (7.4 and 4.5) at 37℃ and the percentage cumulative in vitro release for the C2 NPs is presented in Figure 5-3A and B. The release for the C2 NPs at both pH values exhibited a biphasic release profile over the 9 days. The initial phase of release involved a 'burst' release at day 1, followed by the second phase of release which provided slower and constant release up to day 9. At pH 7.4, the C2 NPs released approximately 43% of their IRN content and 30% of their PTV content over 9 days (Figure 5-3A). The release of IRN from C2 significantly ($p < 0.05$) increased when acidic (pH.4.5) PBS was used. On the other hand, there was no significant difference ($P > 0.05$) in the release of PTV from the C2 in normal and acidic PBS (Figure 5-3B). The percentage cumulative release of PTV from C2 was 30.9±5.5 at pH of 7.4 and 32.6±1.8 at pH of 4.5 over 9 days.

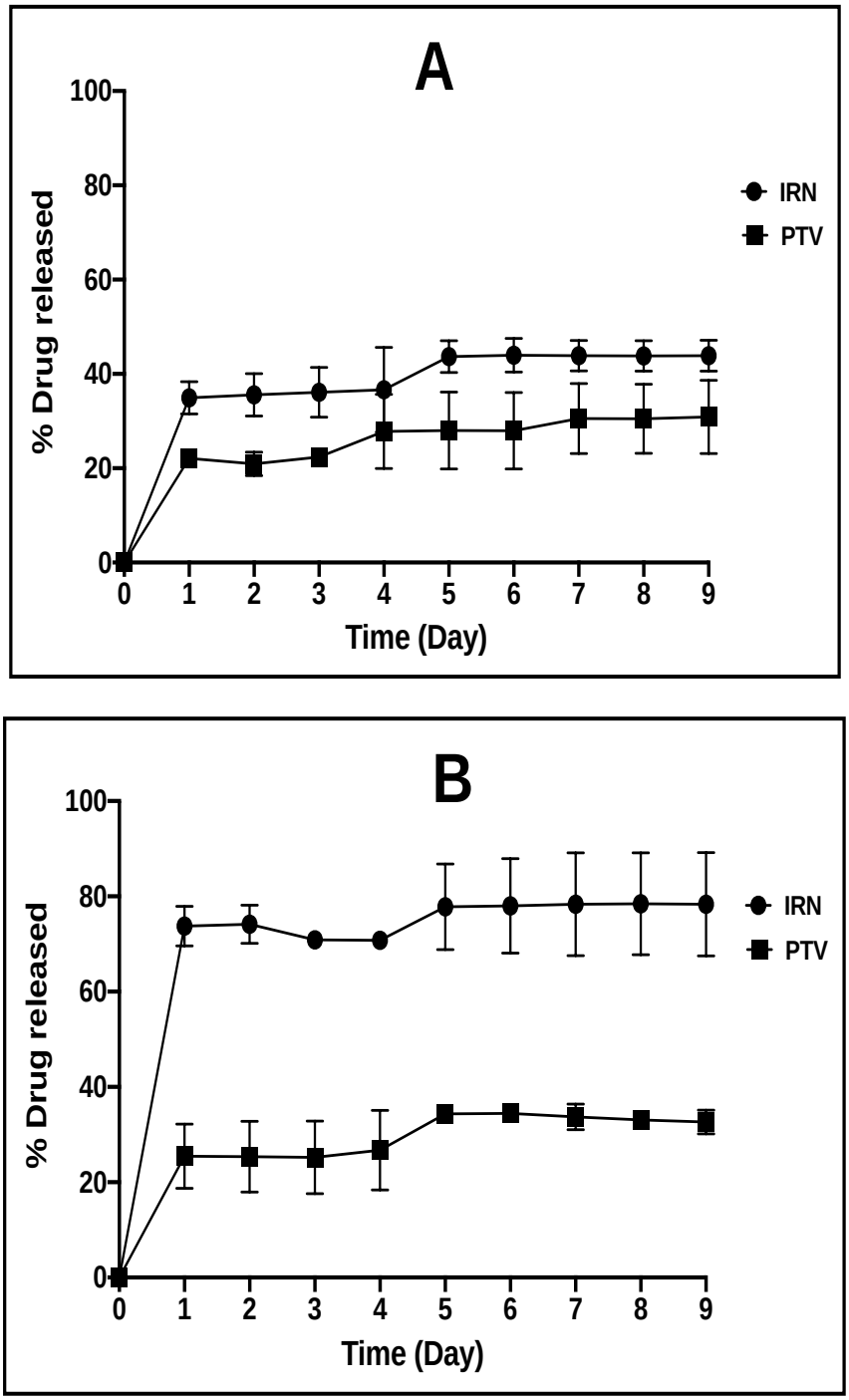


Figure 5-3: In vitro cumulative release profile of IRN and PTV from C2 PLGA NPs, in the PBS at pH 7.4 **(A)** and pH=4.5 **(B)**, during 9 days in the shaking incubator at 100 rpm and 37°C. Results shown as mean ± SD, n= 3, significance found using a 2way ANOVA with a Tukey's post-hoc test, ($p < 0.05$).

5.3.4 Cytotoxicity study using MTT assay for IRN and PTV co-loaded PLGA NPs against the primary GBM cells

The cytotoxicity of IRN and PTV co-loaded PLGA NPs (C2) at different concentrations (1, 10, and 100 μM) against primary GBM cells for two patients over 11 days is presented in

Figure 5-4. In patient 1, the lowest cell viabilities were 51 and 39.6% achieved with C2 at a concentration of 1 and 10 μM on day 9, respectively. The 100 μM concentration achieved a cell viability below 20 and 13% 3 and 11 days after treatment, respectively (Figure 5-4A). In patient 2, the 1 and 10 μM concentration of C2 achieved cell viabilities of 65.3±6.5 and 21.3±2.3%, respectively, while 100μM concentration achieved a cell viability 4.6±0.3% 11 days after treatment (Figure 5-4B).

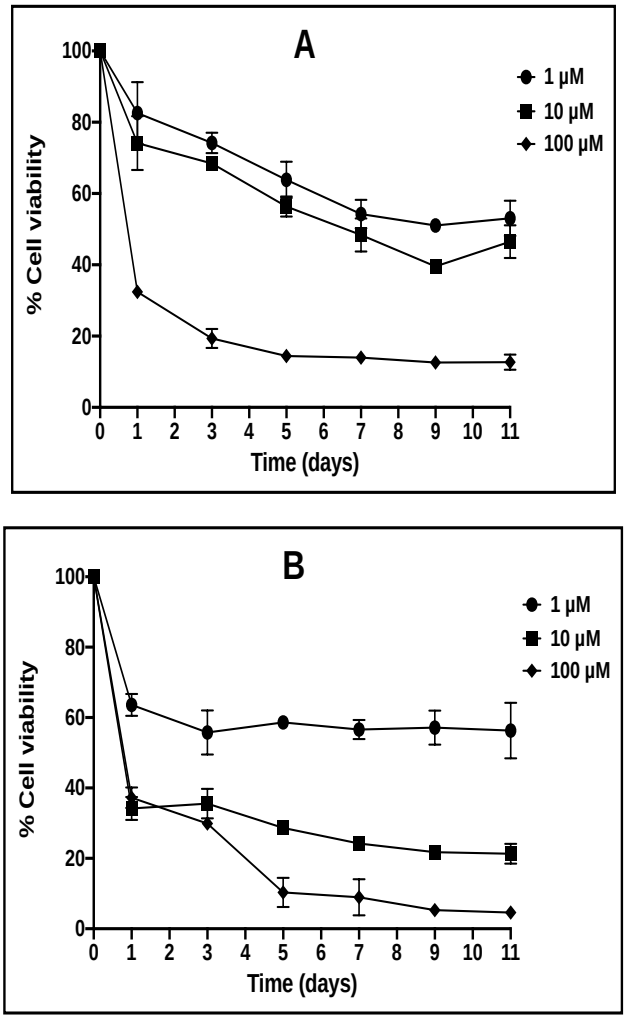


Figure 5-4: Viability of GBM primary cells patient 1 **(A)** and patient 2 **(B)** cultured with IRN and PTV co-loaded PLGA NPs (C2) at three different concentration (1 μM, 10 μM, 100 μM) at day 1, 3, 5, 7, 9, 11. Results shown as mean ± SD, n= 3, significance found using a 2way ANOVA with a Tukey's post-hoc test, ($p < 0.05$).

Figure 5-5 presents the cytotoxicity of IRN and PTV co-loaded PLGA NPs (C2) at concentration of 100 μM against primary GBM cells of 4 different patients (P1, P2, P3, P4) 5

days post treatment. The cell viability for all patients was found to be in the range of 10% (P1) to 23% (P4) 5 days post treatment. In patient 1 and 2, C2 NPs achieved significantly ($P < 0.05$) lower cell viabilities than for patients 3 and 4. There was no significant difference ($P > 0.05$) in cell viabilities of the C2 NPs between P1 and P2 as well as between P3 and P4.

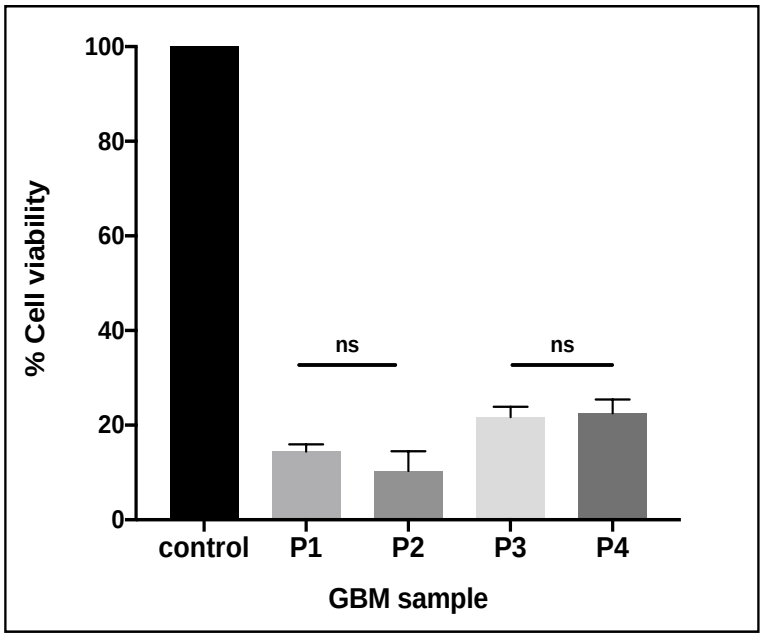


Figure 5-5: Cytotoxicity of IRN and PTV co-loaded PLGA NPs (C2) at 100 μM against four different GBM samples patient 1 (P1), patient 2 (P2), patient 3 (P3), and patient 4 (P3) at day 5. Results shown as mean ± SD, n= 3, significance found using a 2way ANOVA with a Tukey's post-hoc test, * = P<0.05 ** = P<0.01, *** = P<0.001, **** = P<0.0001.

5.3.5 Cellular uptake using flow cytometry

The cellular uptake of the IRN and PTV co-loaded PLGA NPs (C2) at different concentrations (0.1, 1, and 10 μM) were investigated in the primary GBM cells at times of 3, 6, 24, 120h after treatment. The control was untreated primary GBM cells, which were also monitored at times of 3, 6, 24, and 120 h. The SSC intensity reflects the change in the cellular uptake and the increase in the SSC intensity indicates an increase in the uptake of C2 NPs. Figure 5-6 presents the change in the cellular uptake of C2 NPs and control cells with no NPs in the primary GBM cells at time 3, 6, 24, 120h post treatment. The results show that the cellular uptake of C2 NPs was influenced by the time of treatment and the concentration of the NPs. At 3 h post treatment, there was no significant difference ($p > 0.05$) in the cellular

uptake between different concentrations (0.1, 1, and 10 μM) of the C2 NPs. At a concentration of 0.1 μM of C2 NPs, there was no significant difference in the cellular uptake at 3 and 6 h post treatment, while there was a significant increase ($p < 0.05$) with the concentration of 1 and 10 μM. The higher cellular uptake was achieved at 120 h post treatment for all concentrations (0.1, 1, and 10 μM) of the C2 NPs. The SSC intensity of the C2 NPs was increased from 1325, 1814.3 and 2153.3 at 24h to 2029, 2772.7 and 2758.7 at 120 h for the 0.1, 1 and 10 μM concentrations, respectively. There was no significant difference ($p > 0.05$) in the cellular uptake at 120 h post treatment between the concentrations of 1 and 10 μM.

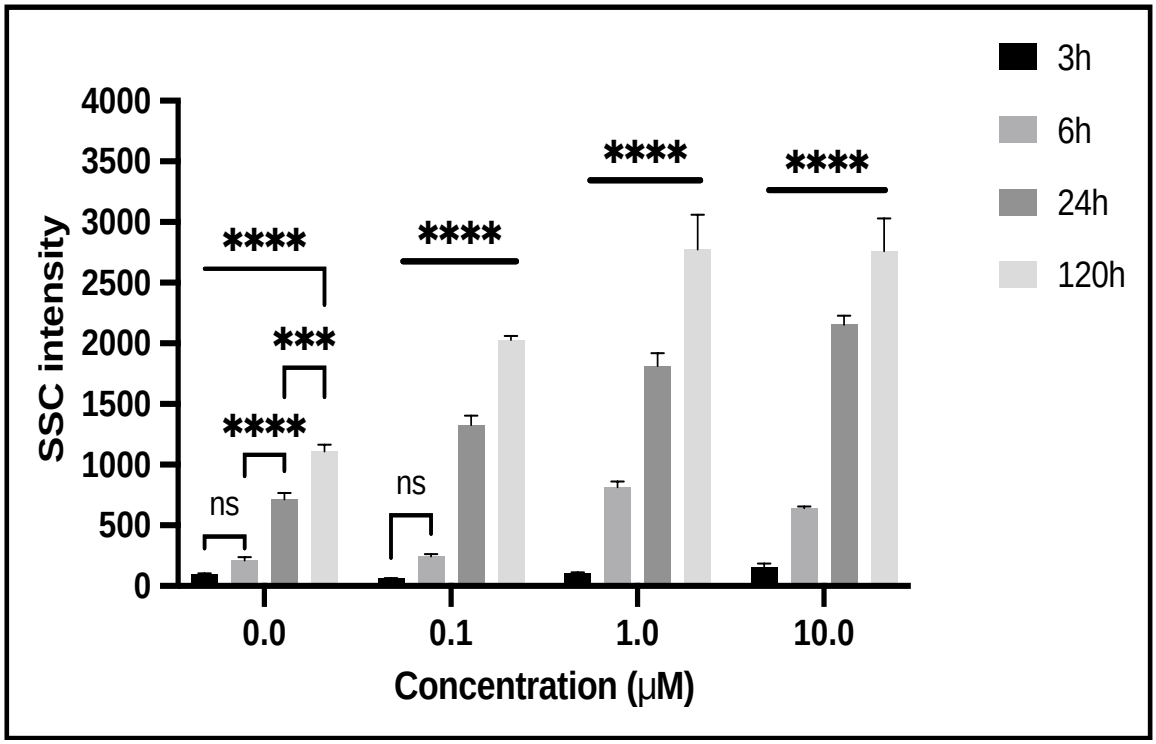


Figure 5-6: Cellular uptake of IRN and PTV co-loaded PLGA NPs (C2) in GBM primary cells (patient 1) after incubation time of 3, 6, 24, 120 h at three different concentrations 0.1, 1, 10 μM observed by flow cytometry. Results shown as mean ± SD, n=3, significance found using a 2way ANOVA with a Tukey's post-hoc test, * = P<0.05 ** = P<0.01, *** = P<0.001, **** = P<0.0001.

5.3.6 Quantitative analysis of apoptosis using the Annexin V/PI double-staining assay and flow cytometry calculations.

Apoptotic primary GBM cells after treatment with IRN and PTV co-loaded PLGA NPs (C2) were identified by flow cytometry using the Annexin V/PI double-staining assay. The primary GBM cells were treated with staurosporine as a positive control, DMSO as a negative control, and C2 NPs at concentration of 1 and 10 μM. Figure 5-7A represents the percentage of the apoptotic primary GBM cells relative to controls and C2 NPs concentrations, and Figure 5-7B represents dot plots of annexin V/PI staining of the primary GBM cells. The untreated control cells had only 10.6% of total apoptotic (early and late apoptotic) primary GBM cells, which was significantly increased ($p < 0.05$) to 53.2 and 72.3% when treated with 1 and 10 μM of the C2 NPs. The viable cells were significantly decreased ($p < 0.05$) with C2 NPs compared to the untreated cells. The percentage of viable primary GBM cells in the untreated groups was 88.2%, compared to 35.6 and 16% with the 1 and 10 μM C2 NP groups, respectively.

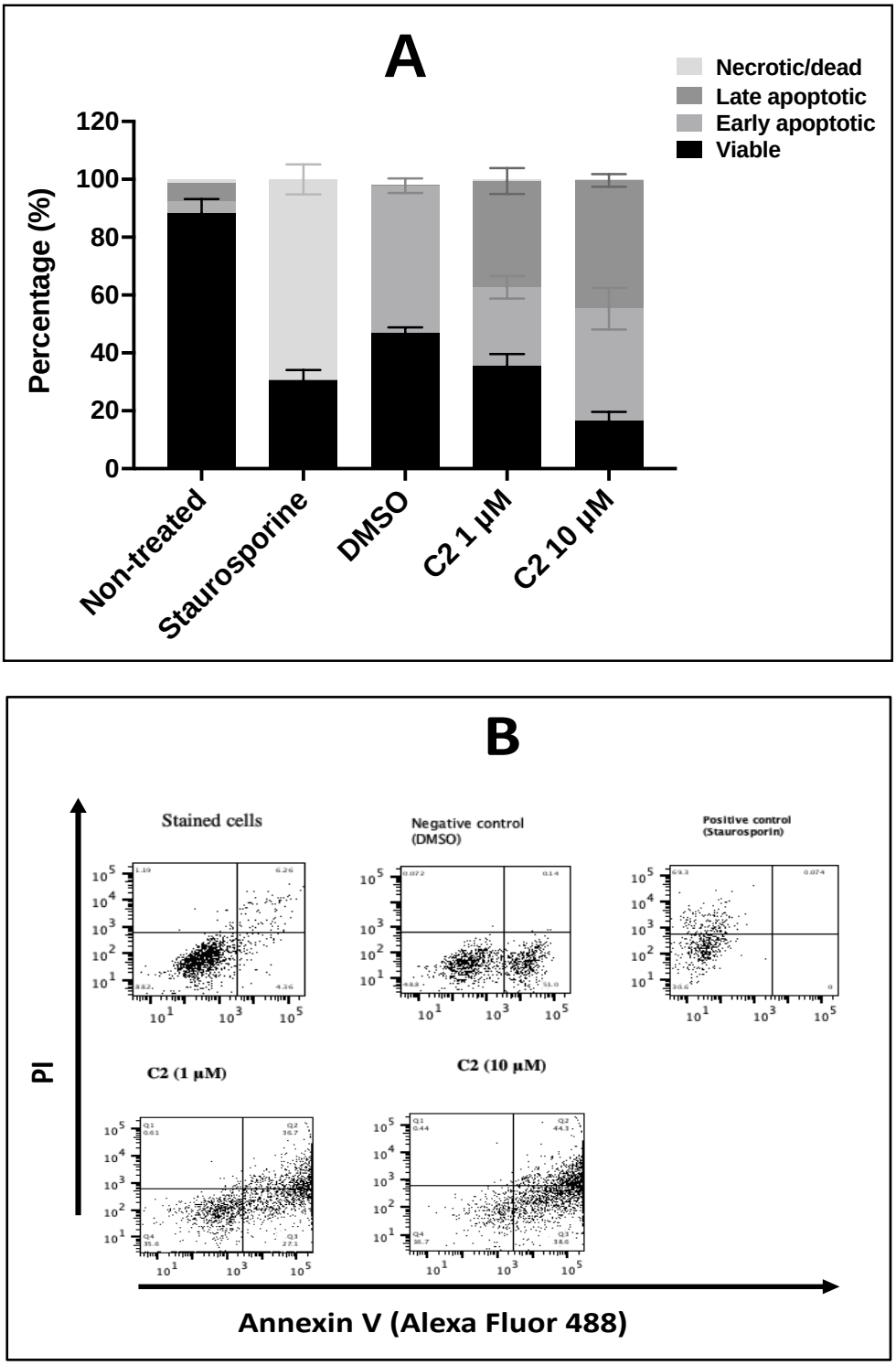


Figure 5-7: Estimation of apoptotic cell population by flow cytometry using Annexin V/PI double-staining assay. **(A)** Graphical representation of Viable (Annexin V-/PI-), early apoptotic (Annexin V+/PI-), late apoptotic (Annexin V+/PI+), and necrotic/dead (Annexin V-/PI+) cells obtained from flow cytometry.GBM Primary cells (patient 1) were treated with Staurosporine (positive control), DMSO (negative control), and the IRN and PTV co-loaded PLGA NPs (C2). **(B)** Representative dot plot obtained from Annexin V/PI double-staining after three days treatment with C2 in two different concentration 1, 10 µM; Viable cells (Lower left), Annexin V positive early apoptotic cells (Lower Right), Annexin V and PI dual positive (Upper Right), and only PI positive necrotic cells (Upper Left). Results shown as mean ± SD, n= 3, significance found using a 2way ANOVA with a Tukey's post-hoc test, ($p < 0.05$).

5.3.7 Permeability of the IRN and PTV co-loaded PLGA NPs across in vitro monoculture and coculture BBB models

The ability of IRN and PTV co-loaded PLGA NPs (C2) to cross the monoculture and coculture BBB models were evaluated using three different approaches (EVOM2, ECIS, and cellZscope). The monoculture and coculture BBB models and TEER measurement methods were fully described in chapter 4. Briefly, the monocultured consisted of a monolayer of the hCMEC/D3 cells, while the coculture BBB models consisted of two layers of the hCMEC/D3 cells and astrocytes. The change in the resistance of monoculture BBB model was monitored using EVOM2 and ECIS systems, while the cellZscope system was used for coculture BBB model.

5.3.7.1 Monitoring the change in resistance of the monoculture BBB model using EVOM2

EVOM2 system was used to investigate the change in resistance after adding the IRN and PTV co-loaded PLGA NPs (C2) to monoculture BBB model (hCMEC/D3 cells). Once the resistance plateaued, C2 NPs were added at two different concentrations (≈100 and ≈200 μM) at t=168 h and the resistance recorded over 3 days with readings acquired at 0, 6, 24, 48, 72 h (Figure 5-8). At 100 μM, the C2 NPs induced a slight reduction to the resistance value after 6 h exposure, and further significant ($p < 0.05$) reductions at 24, 48 and 72 h. At 200 μM a significant ($p < 0.05$) reduction in resistance was observed after 6 h exposure. There was no significant difference ($p > 0.05$) in the resistance between 48 and 72 h post-addition of the C2 NPs (Figure 5-8). In the control well cells only, there was no significant difference ($P > 0.05$) observed over 72 h.

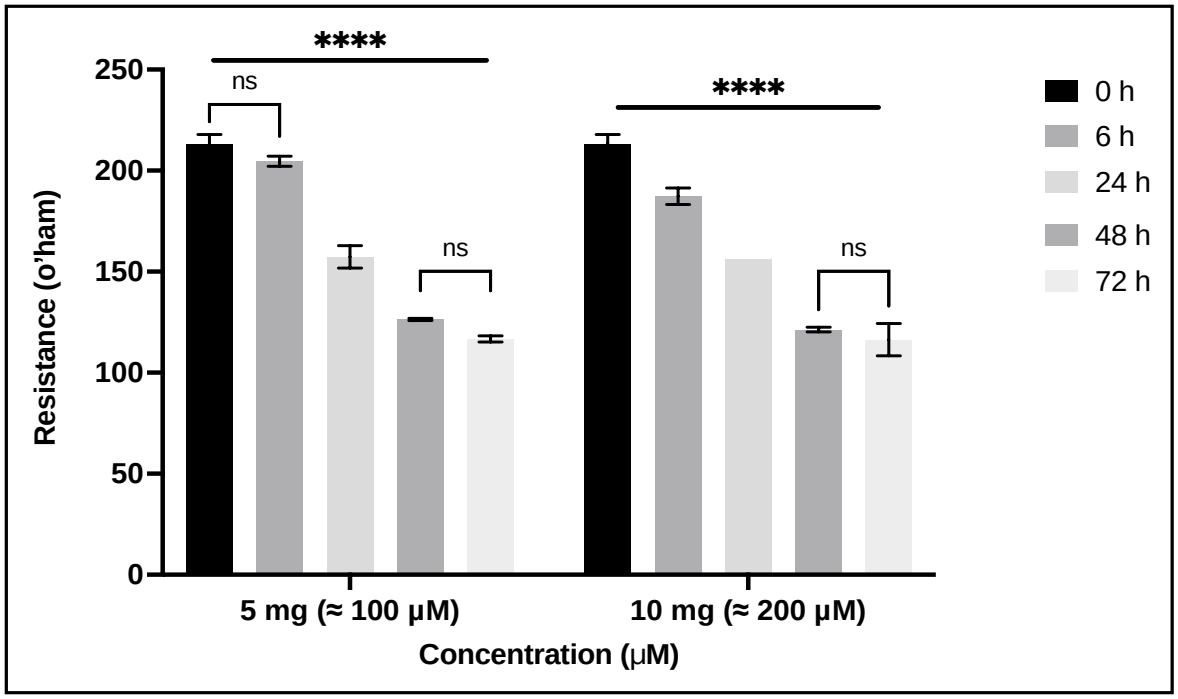


Figure 5-8: Effect of the IRN and PTV co-loaded PLGA NPs (C2) at two different concentration **(A)** 5mg (≈ 100 µM) and **(B)** 10 mg (≈ 200 µM) on the BBB model permeability at time 0, 6, 24, 48, and 72 h. The monoculture was constructed using 8 µM pore size polycarbonate-membrane filters within 24-transwell inserts. The resistance was evaluated by measuring TEER values with EVOM2. A significant decrease ($p < 0.05$) in resistance was showed at 24h after adding NPs for IRN and PTV co-loaded PLGA NPs (C2) compared to the control (time 0). Results shown as mean ± SD, n= 3, significance found using a 2way ANOVA with a Tukey's post-hoc test, * = P<0.05 ** = P<0.01, *** = P<0.001, **** = P<0.0001.

5.3.7.2 Monitoring the change in resistance of the mono-culture BBB model using ECIS system

ECIS system was used to investigate the change in resistance after adding the IRN and PTV co-loaded PLGA (C2) NPs to monoculture BBB model (hCMEC/D3 cells). The ECIS histogram in Figure 5-9 shows the resistance of the monoculture BBB model per time point. The C2 NPs were added to the mono-culture BBB model after 70-72 h of seeding the hCMEC/D3 cells and once the resistance had plateaued, and the resistance values recorded in Ω. The IRN and PTV co-loaded PLGA NPs reduced the endothelial barrier integrity as demonstrated by a decrease in the resistance post-addition of NPs. The resistance values were recorded over 20 h post-addition, with the resistance of the BBB model gradually decreased from approximately 1600 Ω to the range of approximately 1400-1450 Ω within first two

hours of addition of the C2 NPs and continued to decrease over the remaining 18 h until it reached approximately 950 Ω.

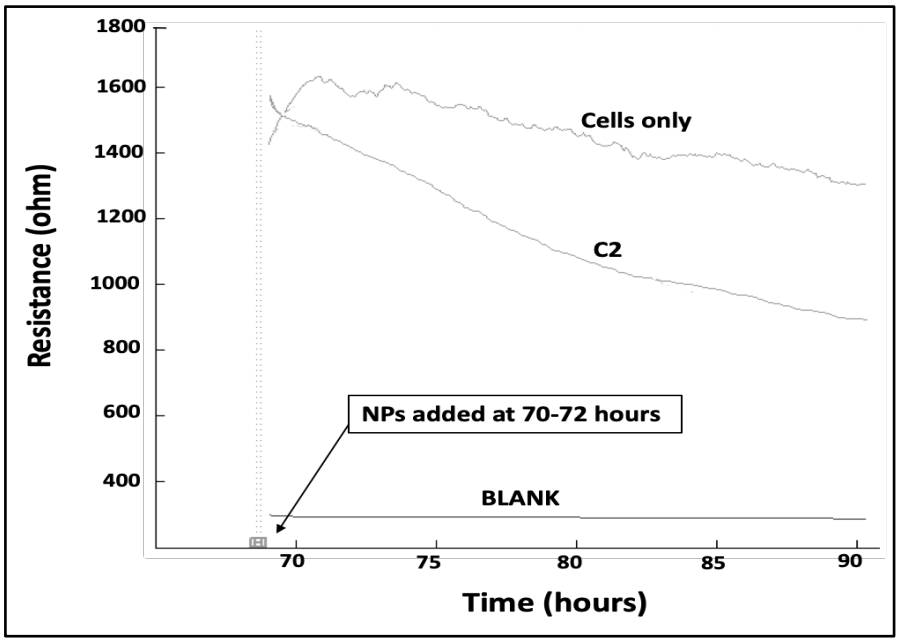


Figure 5-9: Changing in resistance values in BBB model (hCMEC/D3 cells) with the IRN and PTV co-loaded PLGA NPs **(C2)**. The cells were seeded on the gold electrode and the resistance was recorded by the ECIS system over 20 h post addition of the NPs. The NPs were added at 70-72 h once resistance values plateaued. Significance found using a one-way ANOVA with a Tukey's post-hoc test, ($p < 0.05$), (n=3).

5.3.7.3 Monitoring the change in resistance of the co-culture BBB model using cellZscope system

A cellZscope system was used to record the change in the resistance of the coculture BBB model after adding IRN and PTV co-loaded PLGA NPs (C2). Once the resistance value plateaued, the C2 NPs were added and the resistance measured over 82 h by the cellZscope system (Figure 5-10). The results demonstrate that the plateaued resistance (27 $\Omega.cm^2$) was achieved after 48 h of culturing the BBB model. The resistance of the coculture BBB model gradually decreased over the first 8 h after the addition of the C2 NPs, when it then increased over the following 5 to 10 h, decreasing again until a final resistance value of 17 $\Omega.cm^2$ was achieved after 82 h. The resistance in the control (only cells) increased slightly from 22 to 23.50 $\Omega.cm^2$ over the time between 60 and 100 h, While the resistance with C2 NPs gradually decreased from 25 to 22 $\Omega.cm^2$ over the same period (Figure 5-10).

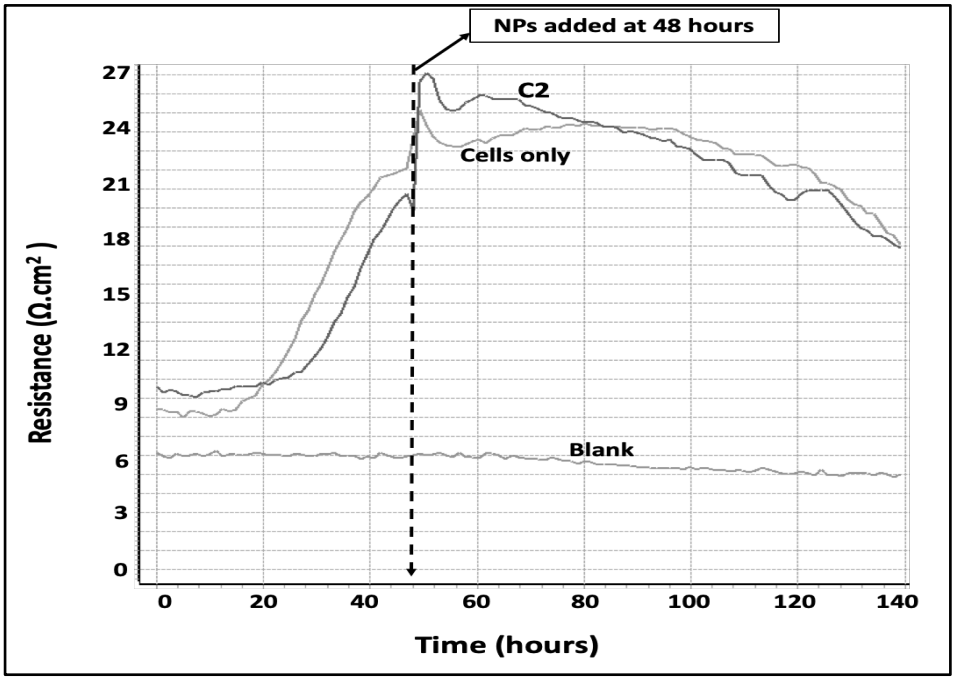


Figure 5-10: Changing in resistance values in co-culturing BBB model (hCMEC/D3 cells and astrocyte) post-addition of the IRN and PTV co-loaded PLGA NPs (C2). The resistance was recorded by cellZscope system for 82 h after adding NPs. The NPs were added at 48h once resistance values plateaued. Significance found using a one-way ANOVA with a Tukey's post-hoc test, ($p < 0.05$), (n=3).

5.4 Discussion

Many studies have investigated the combination of IRN and PTV in the treatment of tumours, and the potency of IRN was significantly enhanced against GBM tumours when combined with PTV (Jiang et al., 2014, Matusewicz et al., 2015). The increase in the cytotoxicity of IRN in combination with PTV is possible due to PTV being a substrate for the overexpressed MDR-1 protein in GBM cells which increases IRN accumulation in the GBMs cells making it more effective (Anjum et al., 2017, Matusewicz et al., 2015).

In this chapter, a novel dual-loaded IRN and PTV co-loaded PLGA NPs were developed, characterised and investigated for their cytotoxicity against GBM cells in vitro. The amount of drugs, PLGA, and PVA were chosen based on the DoE of the IRN-loaded PLGA NPs formulations. Three formulations of IRN and PTV co-loaded PLGA NPs were prepared with the same amount of IRN and PTV (4 mg of each) but different amounts of PLGA 5002 (120,

180, and 240 mg). The single emulsion solvent evaporation technique was used in this study to prepare the IRN and PTV co-loaded PLGA NPs (C1, C2, and C3). It produced spherical NPs with particle sizes below 200 nm. The C2 NPs were chosen for further evaluation based on their low size (70 nm) and highest EE (18.5%) of PTV. The size of C3 NPs was much larger than C2 NPs, which is due to them being prepared with 240 mg of PLGA compared to the 180 mg used with C2. Therefore, the size of IRN and PTV co-loaded PLGA NPs increased with increasing the amount of PLGA 5002, and this result agreed with that from Chapter 2. By increasing the PLGA, the viscosity of the organic phase increases, consequently, the viscous forces resisting droplet breakdown are increased, which leads to a larger droplet, resulting in the increased particle size of the NPs (Sharma et al., 2016, Zweers et al., 2003). On the other hand, the size of C2 NPs was lower than C1 NPs even though the C1 NPs have a lower amount of PLGA 5002, but they have only 2% of the PVA. The concentration of PVA must be high enough to cover the interfacial area of all nanodroplets. The decrease in particle size with a high concentration of PVA has been reported by Allemann *et al* (Allémann et al., 1992).

The release profile of the IRN and PTV co-loaded PLGA NPs is biphasic with a ‘burst’ release at day 1 and then slower release up to day 9. The ‘burst’ release of IRN and PTV corresponds with drug on the surface of the NPs being released, while the second phase was due to their diffusion through the PLGA polymer, mediated by erosion and degradation of the polymer and resulting in a slow and more constant release rate (Tewes et al., 2007, Kumskova et al., 2020). The release of IRN was faster at acidic pH due to increased solubility of the IRN. The IRN has been ionised in low pH, which increased its solubility. The release profile of IRN from the IRN and PTV co-loaded PLGA NPs and from IRN-loaded PLGA NPs were consistent in both acidic and normal PBS.

The cytotoxicity of the IRN and PTV co-loaded PLGA NPs (C2) was investigated against primary GBM cells using the MTT assay. The cytotoxicity of the blank PLGA 5002 NPs (Figure 3-2) demonstrates that although the NPs are slightly cytotoxic themselves, loading them with IRN and PTV makes them significantly ($p < 0.05$) more cytotoxic. The cell viability of the blank PLGA 5002 NPs at day 5 after treatment was 76.03±3.48%, while the cell viabilities of the IRN-loaded PLGA NPs (R13) and IRN and PTV co-loaded PLGA NPs (C2) were significantly ($p < 0.05$) decreased to 38.86±5.88 and 28.66±1.24%, respectively. Studies on the cytotoxicity effect of statins against GBM cells demonstrated that the cytotoxicity of IRN was significantly enhanced when combined with PTV (Anjum et al., 2017, Matusewicz et al., 2015, Jiang et al., 2014). The IC_{50} values of IRN in combination with PTV against GBM were decreased 40 to 70 fold compared to IRN alone (Jiang et al., 2014, Matusewicz et al., 2015).

The cellular uptake of the IRN and PTV co-loaded PLGA NPs by the primary GBM cells was analysed by flow cytometry. The average of SSC intensity in the primary GBM cells treated with IRN and PTV co-loaded PLGA NPs was increased with an increase in the time post treatment as well as the concentration of the NPs. That can be explained via the cellular association and cellular uptake of C2 NPs in the primary GBM cells being proportional to the concentration of the NPs as well as their exposure time to the NPs (Xiong et al., 2011, Malinovskaya et al., 2017). The relationship between the cellular uptake of the NPs and the increase in the side scatter suggests that the amount of NPs inside the cells is related to the mass concentration of NPs applied to the cells (Zucker et al., 2013). The C2 NPs could be internalised into the cells via different pathways such as passive diffusion or endocytosis. The increased SSC intensity with an increase in incubation time indicates the time-dependent

transfer of the NPs into the cells by passive diffusion, which has time dependent characteristics (Lee et al., 2015).

The ability of the IRN and PTV co-loaded PLGA NPs (C2) to cross the BBB was evaluated using models of mono-culture of the hCMEC/D3 cells and their co-culture with astrocytes. The hCMEC/D3 cells as BBB model has been shown to be well adapted for drug uptake or transport studies (Weksler et al., 2013). TEER is a quantitative method to investigate the integrity of endothelial cells in a monolayer cell culture model (Srinivasan et al., 2015). Upon validating the ability of the IRN and PTV co-loaded PLGA NPs to cross the BBB, we used two BBB models (mono- and coculture) and three different approaches (EVOM2, ECIS, and cellZscope) to measure the TEER values. The resistance of the mono-culture BBB model was monitored using the EVOM2 and ECIS systems, while the cellZscope system was used for co-culture BBB model. The TEER values for EVOM were significantly decreased ($P < 0.05$) at 24, 48 and 72 h with the IRN and PTV co-loaded PLGA NPs (C2). This decrease in TEER value indicates that the tight junctions of the BBB model were opened by the NPs within 24 h and therefore the NPs can cross the BBB model. In the ECIS work, the result demonstrate that the resistance of mono-culture BBB model decreased after addition of the C2 NPs, which indicates that the tight junction of the BBB model was opened by the IRN and PTV co-loaded PLGA NPs and thus their permeability through the monoculture BBB model was increased. The results of the cellZscope demonstrated that the C2 NPs were able to cross the co-culture BBB models within 1 h post-addition. There was a slight increase in resistance over a period of approximately 5 h, which would indicate recovering of the tight junction after the C2 NPs crossed the BBB models. Therefore, the C2 NPs could have a reversible effect on the tight junction of the BBB, which is ideal for safe and effective treatment. The results of the three methods were consistent, with a noticeable decrease in the resistance

recorded post addition of the IRN and PTV co-loaded PLGA NPs (C2) to both the mon-culture and coculture BBB models when compared to the control.

5.5 Conclusion

The IRN and PTV co-loaded PLGA NPs were prepared with the low intrinsic viscosity (PLGA 5002) PLGA polymer using the single emulsion solvent evaporation technique. Three formulations (C1, C2, and C3) of IRN and PTV co-loaded PLGA NPs were prepared and characterised for their size, zeta potential, and EE. The lowest size was achieved with the C2 NPs which also had the highest EE of PTV compared to the C1 and C3 NPs. The C2 NPs were chosen for further evaluation of their release, cytotoxicity, cellular uptake, and ability to cross the BBB. The release profile of IRN and PTV from co-loaded PLGA NPs demonstrated sustained release over 9 days in both normal and acidic pH. The release of IRN was higher at acidic pH, while the release of PTV was not affected by changing the pH. The cytotoxicity and cellular uptake of the C2 NPs on the primary GBM cells were concentration and time dependent. The TEER measurements were used to investigate the change in the resistance of the BBB models after adding the IRN and PTV co-loaded PLGA NPs (C2 NPs) using three different instruments (EVOM2, ECIS, and cellZscope). All these instruments showed a decrease in the TEER values of the BBB models with the addition of the C2 NPs. Therefore, the IRN and PTV co-loaded PLGA NPs can efficiently cross the mono- and co-culture BBB models. Based on these results, the IRN and PTV co-loaded PLGA NPs are a promising treatment for GBM that could potentially cross the BBB in humans and deliver therapeutic levels of both IRN and PTV to the tumour tissue.

Chapter 6: General discussion and future work

6.1 General discussion

GBMs are the most common primary brain tumour in adults with poor prognosis despite the amount of research into this terrible disease. This calls for the development of novel strategies for the delivery of chemotherapeutic drugs at sufficient concentrations to the brain in order to yield better treatment outcomes. IRN is currently used as a second line treatment for GBMs (Iacob and Dinca, 2009). The drug delivery system in this study was designed for passive and controlled delivery of IRN to GBM tumours. This drug delivery carrier consisted of NPs of biodegradable PLGA polymers and PVA as surfactant. These NPs were expected to improve drug delivery of IRN to the brain by crossing the BBB, increasing IRN circulating time in the blood, increasing the accumulation of IRN in the GBM tumour by EPR effect, and minimizing toxic effect of IRN in healthy tissue.

In this project, the IRN-loaded PLGA NPs and the IRN and PTV co-loaded PLGA NPs were developed to enhance the delivery of IRN and PTV to the brain to improve the treatment of GBM. These NPs have been characterised and assessed for their cytotoxicity against primary GBM cells as well as their ability to cross the BBB models.

6.1.1 The IRN-loaded PLGA NPs

The single emulsion solvent evaporation technique was used to prepare the IRN-loaded PLGA NPs. During their development process many variables were investigated in the pre-screening study and then three variables chosen to investigate their impact on the particle size and EE using a BBD for the DoE. The BBD comprised 15 runs for PLGA 5002 (low intrinsic viscosity) and another 15 runs for PLGA 5004 (high intrinsic viscosity) with each having three central points. Based on the statistical and response surface analysis from the DoE, the

size and EE of the IRN-loaded PLGA NPs were most affected by changes in the mount of IRN, PLGA, and PVA. Generally, the particle size of the IRN-loaded PLGA NPs increased with increasing the viscosity of the organic phase (dispersed phase) by increasing the amount of IRN or/and PLGA. By increasing the viscosity of the organic phase, the resistance droplet breakdown is increased resulting in the increased particle size of NPs (Sharma et al., 2016, Zweers et al., 2003). The concentration of PVA must be high enough to cover the interfacial area of all nanodroplets with the purpose of preventing the NPs from aggregation (Allémann et al., 1992, Budhian et al., 2007). The type of PLGA clearly impacted on the EE of the IRN which was higher with low intrinsic viscosity PLGA 5002. The reason for the high EE with PLGA 5002 is due to the existence of acidic termination which leads to an electrostatic interaction with IRN. From the 30 IRN-loaded PLGA NP formulations, the optimised formulations (R1, R6, R13 and R22) were chosen for further analysis in this project (Figure 6-1). The minimum particle size with the highest EE were the main criteria to determine the optimised IRN-loaded PLGA NPs formulation to take forward.

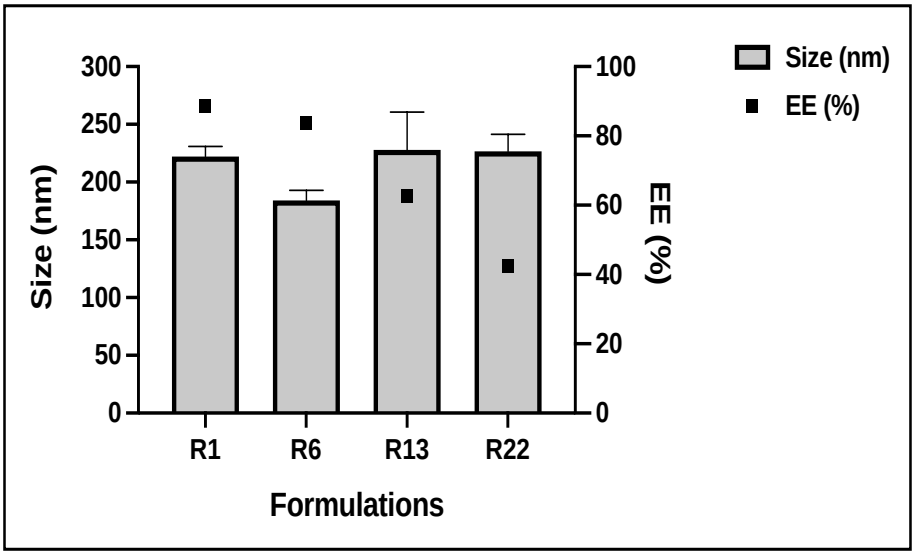


Figure 6-1. Particle sizes and EE of the optimised IRN-loaded PLGA NPs. Results shown as mean ± SD, n= 3, significance found using a one-way ANOVA with a Tukey's post-hoc test, ($p < 0.05$).

The physical properties of the optimised IRN-loaded PLGA NPs were investigated using DSC and XRD. The results of the DSC and XRD showed that the IRN is in its amorphous

form within the NPs and there is no interaction between the PLGA, PVA, and IRN. The release of IRN from both sets of NPs showed a burst release on day one followed by sustained release up to day 9. The sustained release of IRN through the optimised NPs was due to the erosion and degradation of the PLGA polymers (Tewes et al., 2007, Kumskova et al., 2020). The release of IRN in the PLGA 5004 was much faster compared to the PLGA 5002 due to an electrostatic interaction between acidic termination in the PLGA 5002 and the HCL group in the IRN. The release of IRN from the optimised NPs with PLGA 5002 was faster in acidic media (pH 4.5) due to the IRN being ionised in the low pH which increased its solubility.

The Primary GBM cells isolated from four patients were used to investigate the cytotoxicity, cellular uptake, and apoptotic ability of the optimised IRN-loaded PLGA NPs. The NPs showed a toxic effect against all GBM cells and the effect increased by increasing the concentration of the NPs and the time of treatment (Jain et al., 2014). Flow cytometry and confocal microscopy were used to analyse the cellular uptake of the optimised IRN-loaded PLGA NPs and C6-loaded PLGA NPs, respectively. The results of the flow cytometry showed the cellular uptake increased by increasing the concentration of the NPs and the time of treatment and that indicates the time-dependent transfer of the NPs into the cells by passive diffusion (Lee et al., 2015, Danhier et al., 2009). The IRN-loaded PLGA NPs were able to induce apoptosis and necrosis in the primary GBM cells, the apoptotic effect of the NPs was concentration dependent which the apoptosis stage increased by increasing concentration of the NPs (Mansourizadeh et al., 2020). The ability of the IRN-loaded PLGA NPs to cross the mono-culture BBB model and co-culture BBB models was evaluated using the TEER measurement technique. The EVOM2, ECIS, and cellZscope approaches were used to measure the TEER values and monitor the change in the resistance of the BBB

models after addition of the NPs. The TEER values of the mono- and co-culture BBB models were decreased after adding the IRN-loaded PLGA NPs which indicates that the NPs can cross the BBB by opening the tight junctions increasing the permeability of the BBB (Chen et al., 2016, Nafee et al., 2009).

6.1.2 The IRN and PTV co-loaded PLGA NPs

PTV has been chosen in this project based on the various studies that have shown the combination of IRN and PTV enhanced the cytotoxicity of IRN against tumours including GBM (Jiang et al., 2014, Matusewicz et al., 2015, Anjum et al., 2017). The IRN and PTV co-loaded PLGA NPs were developed using the single emulsion solvent technique. The smallest NPs with the highest EE of PTV was achieved with C2 NPs which were prepared using 180 mg of PLGA 5002, 4% of PVA, and 4 mg of both IRN and PTV. The size of C2 NPs was much smaller than the R13 NPs which have the same total amount of drug (8 mg), PLGA 5002 (180 mg), and percentage of PVA (4%) (Table 1-6). The EE of both R13 and C2 were similar, while there was a significant ($P < 0.05$) difference in the particle size. The decrease in the size of C2 compared to the R13 could be explained by the viscosity of the organic phase having IRN and PTV during C2 NPs preparation process was lower than the viscosity of organic phase (only IRN) with R13 NPs. The high viscosity of the organic phase leads to reducing in the net shear stress and producing droplets with larger size. In addition, the high viscosity of the organic phase could delay the dispersion of organic phase to the aqueous phase, which leads to larger droplets and formed NPs with large size after evaporation of organic phase (Song et al., 2008, Budhian et al., 2007).

Table 6-1. Characterisation of R13 (IRN-loaded PLGA NPs) and C2 (IRN and PTV co-loaded PLGA NPs) including size, zeta potential, PDI, and EE.

Formulation	size (nm)	Zeta potential	PDI	Total EE (%)
R13	290.6±24.8	-22.8±0.9	0.2	65.4
C2	70.3±0.2	-24.6±1.8	0.2	63.1

The cytotoxicity and cellular uptake of the IRN and PTV co-loaded PLGA NPs (C2) were investigated using the primary GBM cells. In comparison with the R13 NPs, the C2 were shown to be more cytotoxic against the primary GBM cells during the 11 days of treatment (Figure 6-2). The combination treatment of IRN and PTV could be the reason for the higher cytotoxicity of the C2 NPs compared to the R13 NPs (Jiang et al., 2014, Matusewicz et al., 2015).

The cellular uptake of C2 were significantly higher at 24 h post treatment compared to the R13 NPs (Figure 6-3). The difference in the cytotoxicity effect and the cellular uptake between C2 and R13 NPs could be related to their particle size. The size of the NPs has been shown to have a clear effect on the cellular uptake of different types of NPs (He et al., 2010). Choi et al. investigated the effect of the particle size between different sizes between 70 and 600 nm, and in the study the maximum cellular uptake occurred with the smallest NPs (Choi et al., 2014). Therefore, the high cellular uptake of the C2 NPs within the first 24 h could be the responsible for higher cytotoxicity of the C2 NPs compared to the R13 NPs (Chen et al., 2011).

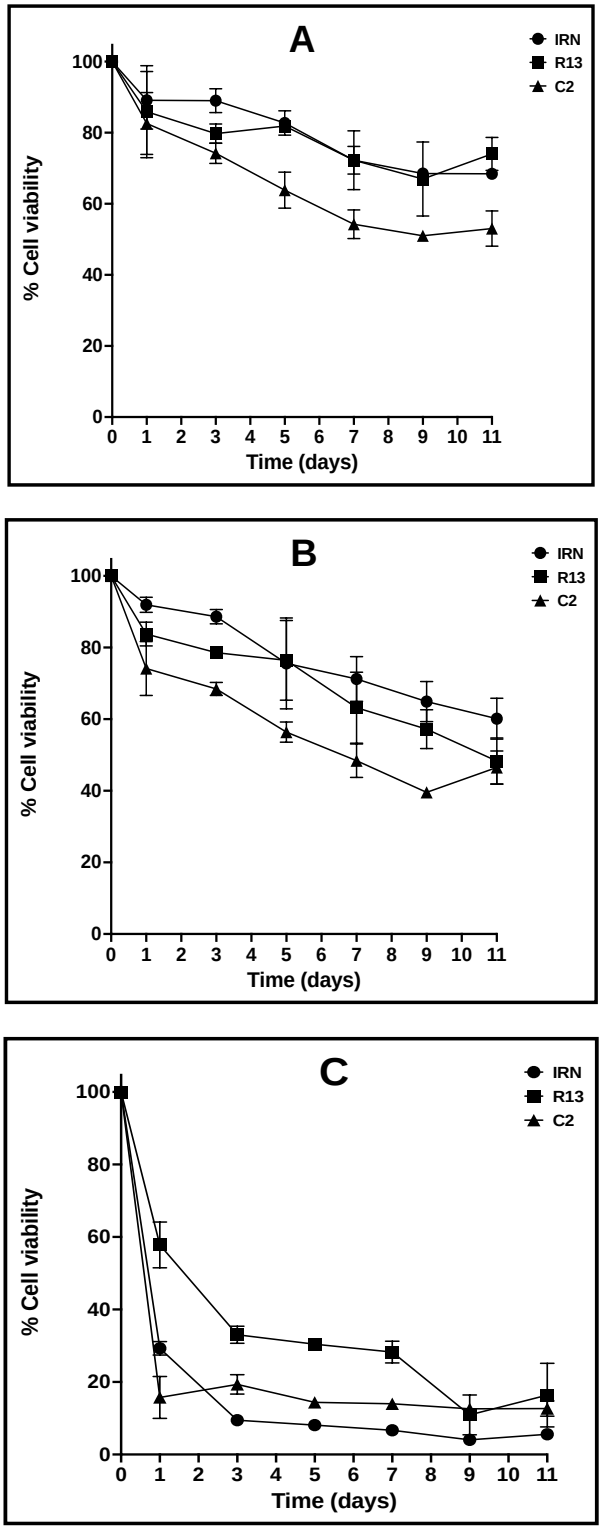


Figure 6-2. Viability of GBM primary cells (patient 1) cultured with the IRN and PTV co-loaded PLGA NPs (C2) in comparison with IRN-loaded PLGA NPs (R13) and free IRN at three concentration of each (A) 1 μM, (A) 10 μM, (C) 100 μM) at day 1, 3, 5, 7, 9, 11. Results shown as mean ± SD, n= 3, significance found using a 2way ANOVA with a Tukey's post-hoc test, * = $P<0.05$ ** = $P<0.01$, *** = $P<0.001$, **** = $P<0.0001$.

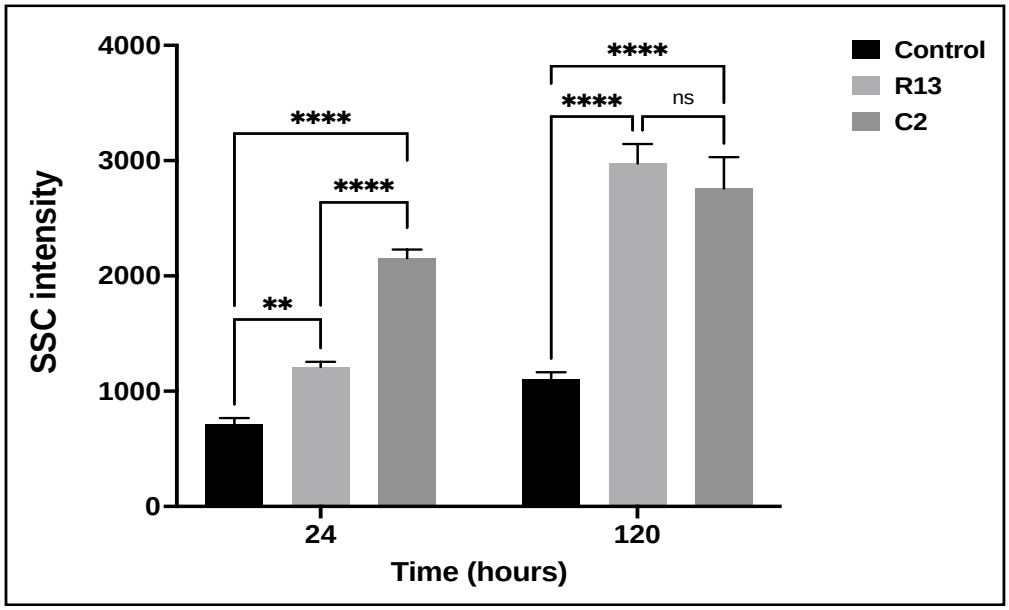


Figure 6-3. Comparing cellular uptake of IRN-loaded PLGA NPs formulations (R13), and the IRN and PTV co-Loaded PLGA NPs (C2) (10 μM of each) in GBM primary cells (patient 1) at time 24 and 120 hours determined by flow cytometry. Results shown as mean ± SD, n= 3, significance found using a 2way ANOVA with a Tukey's post-hoc test, * = P<0.05 ** = P<0.01, *** = P<0.001, **** = P<0.0001.

The ability of the IRN and PTV co-loaded PLGA NPs to cross mono- and co-culture BBB models was investigated using three different instruments (EVOM2, ECIS, and cellZscope) to measure the change in the TEER values after adding the NPs. The results showed a decrease in the TEER values for both BBB models after the addition of the C2 NPs, consequently, the C2 NP can efficiently cross the BBB models. In the EVOM2 work with mono-culture BBB model, the C2 NPs were able to cross the BBB model faster than the R13 NPs. The significant decrease in the TEER values occurred within 6 h post addition of the C2 NPs, while 48 h with R13 NPs. It has shown that the size of the NPs seems to have an impact on the ability of the NPs to cross BBB. The permeability through the BBB model is increased with smaller size of the NPs (Hanada et al., 2014). The smaller NPs under 100 nm can be endocytosed by cells more easily and diffuse more efficiently through the BBB (Lombardo et al., 2020).

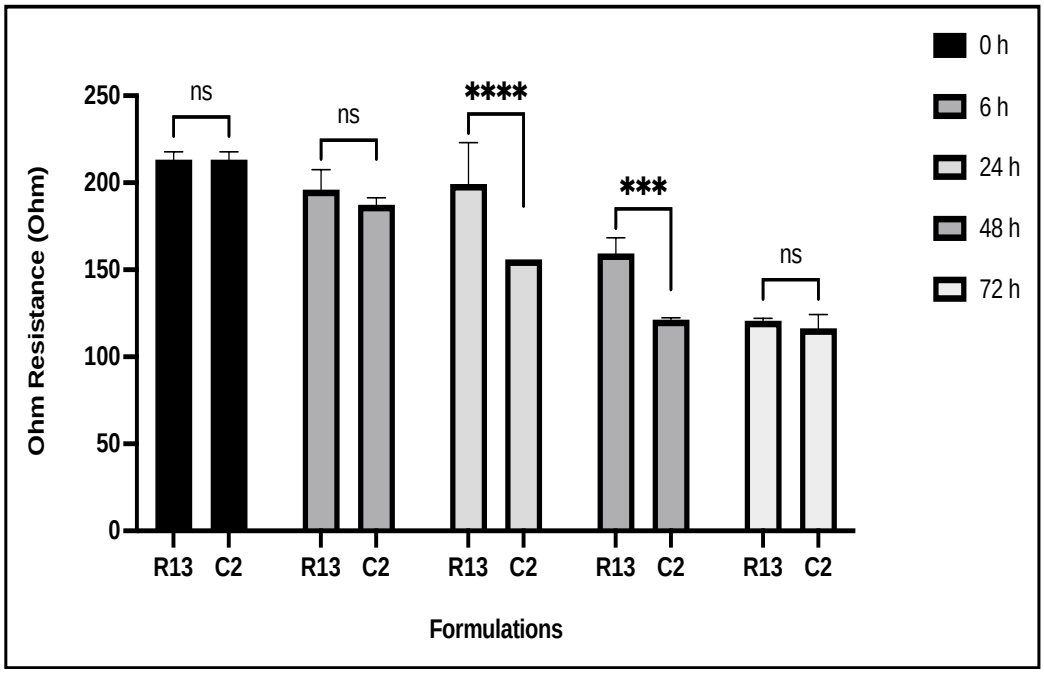


Figure 6-4. comparing the effect of IRN-loaded PLGA NPs (R13) and the IRN and PIV co-Loaded PLGA NPs (C2) on the BBB permeability at time 0, 6,24,48, and 72h. The significant decrease in resistance was shown with C2 at 6h, and it was shown at 48 h with R13 compared to the control (time 0). At time 24h and 48h after adding nanoparticles, there are significant difference in resistance between R13 and C2, but no significant difference at 6h and 72h. Results shown as mean ± SD, n= 3, significance found using a 2way ANOVA with a Tukey's post-hoc test, * = P<0.05 ** = P<0.01, *** = P<0.001, **** = P<0.0001.

6.2 Future work

The animal study using mice to investigate the toxicity and efficacy of the IRN-loaded PLGA, we are about to perform. This study is ongoing and would have been included in the thesis only for the delay due to the COVID-19 pandemic. The primary 3D GBM spheroids should be optimised and used to evaluate the cytotoxicity and cellular uptake of the NPs. Modification on the surface of the NPs could improve the delivery of the IRN into the brain. The NPs need to be attached with PEG on their surface to provide stealth properties in order to prolong circulation time, delay opsonization process, and reduce uptake by reticuloendothelial system. Some experiments should be carried out to synthesis PEG-PLGA complex, and measure the quantity and purity of the attached PEG after synthesis using NMR and Fourier transform infrared (FTIR). The effects of the PEGylation on the size, zeta potential and EE of the NPs should be determined as well as the release profile of IRN from

the PEG-PLGA NPs. Also, the surface of the NPs could be modified by incorporating targeting ligands such as monoclonal antibody (mAb) which are specific and expressed in GBM cells to improve the targeting delivery of the IRN to treat the GBM. The targeting ligand could be attached to the surface of IRN-loaded PEG-PLGA NPs to improve delivery to the GBM cells, and increase the accumulation of the NPs at the site of the tumour. The NPs could be functionalised with an OX26 mAb for transferrin receptor in the GBM cells which are known for overexpressing this type of receptor. The affinity of the transferrin receptors to the mAb need to be carried out using enzyme-linked immunosorbent assay (ELISA). The EE of IRN and release of the mAb-PEG-PLGA NPs must be studied and compared to the IRN-loaded PLGA NPs. To confirm that the mAb-PEG-PLGA can internalize in the GBM cells through transferrin receptor-mediated endocytosis, transferrin competitive binding needs to be carried out. The ability of the mAb-PEG-PLGA to cross the BBB models should be investigated using the same approaches in this study. Further in vivo studies should also be carried out to investigate the toxicity and biodistribution of the targeted NPs attached with a mAb.

References

Abbott, N. J. 2004. Evidence for bulk flow of brain interstitial fluid: significance for physiology and pathology. *Neurochemistry international,* 45**,** 545-552.

Abbott, N. J. 2005. Dynamics of CNS barriers: evolution, differentiation, and modulation. *Cellular and molecular neurobiology,* 25**,** 5-23.

Abbott, N. J., et al. 2010. Structure and function of the blood–brain barrier. *Neurobiology of disease,* 37**,** 13-25.

Abbott, N. J., et al. 2006a. Astrocyte–endothelial interactions at the blood–brain barrier. *Nature reviews neuroscience,* 7**,** 41-53.

Adabi, M., et al. 2017. Biocompatibility and nanostructured materials: applications in nanomedicine. *Artificial cells, nanomedicine, and biotechnology,* 45**,** 833-842.

Agarwal, S., et al. 2011a. Delivery of molecularly targeted therapy to malignant glioma, a disease of the whole brain. *Expert reviews in molecular medicine,* 13**,** e17.

Agarwal, S., et al. 2011b. The role of the breast cancer resistance protein (ABCG2) in the distribution of sorafenib to the brain. *Journal of Pharmacology and Experimental Therapeutics,* 336**,** 223-233.

Ahn, H. K., et al. 2014. A phase II trial of Cremorphor EL-free paclitaxel (Genexol-PM) and gemcitabine in patients with advanced non-small cell lung cancer. *Cancer chemotherapy and pharmacology,* 74**,** 277-282.

Akbarzadeh, A., et al. 2013. Liposome: classification, preparation, and applications. *Nanoscale research letters,* 8**,** 1-9.

Alexandrakis, G., et al. 2004. Two-photon fluorescence correlation microscopy reveals the two-phase nature of transport in tumors. *Nature medicine,* 10**,** 203-207.

Alexis, F., et al. 2008a. HER-2-Targeted Nanoparticle–Affibody Bioconjugates for Cancer Therapy. *ChemMedChem: Chemistry Enabling Drug Discovery,* 3**,** 1839-1843.

Alexis, F., et al. 2008b. Factors affecting the clearance and biodistribution of polymeric nanoparticles. *Molecular pharmaceutics,* 5**,** 505-515.

Alifieris, C. & Trafalis, D. T. 2015. Glioblastoma multiforme: Pathogenesis and treatment. *Pharmacology & therapeutics,* 152**,** 63-82.

Alimohammadi, Y. H. & Joo, S. W. 2014. PLGA-based nanoparticles as cancer drug delivery systems. *Asian Pac J Cancer Prev,* 15**,** 517-535.

Allard, E., et al. 2010. Local delivery of ferrociphenol lipid nanocapsules followed by external radiotherapy as a synergistic treatment against intracranial 9L glioma xenograft. *Pharmaceutical research,* 27**,** 56-64.

Allémann, E., et al. 1992. Preparation of aqueous polymeric nanodispersions by a reversible salting-out process: influence of process parameters on particle size. *International Journal of Pharmaceutics,* 87**,** 247-253.

Almeida, K. B., et al. 2019. PLGA nanoparticles optimized by Box-Behnken for efficient encapsulation of therapeutic Cymbopogon citratus essential oil. *Colloids and Surfaces B: Biointerfaces,* 181**,** 935-942.

Alonso, M. J., et al. 1994. Biodegradable microspheres as controlled-release tetanus toxoid delivery systems. *Vaccine,* 12**,** 299-306.

Altındal, D. Ç. & Gümüşderelioğlu, M. 2016. Melatonin releasing PLGA micro/nanoparticles and their effect on osteosarcoma cells. *Journal of microencapsulation,* 33**,** 53-63.

Andrade, F., et al. 2018. Micellar-Based Nanoparticles for Cancer Therapy and Bioimaging. *Nanooncology.* Springer.

Anjum, K., et al. 2017. Current status and future therapeutic perspectives of glioblastoma multiforme (GBM) therapy: A review. *Biomedicine & Pharmacotherapy,* 92**,** 681-689.

Anselmo, A. C. & Mitragotri, S. 2016. Nanoparticles in the clinic. *Bioengineering & translational medicine,* 1**,** 10-29.

Anton, K., et al. 2012. Glioblastoma multiforme: overview of current treatment and future perspectives. *Hematology/Oncology Clinics,* 26**,** 825-853.

Aoki, T., et al. 2007. Management of glioblastoma. *Expert opinion on pharmacotherapy,* 8**,** 3133-3146.

Arora, R. S., et al. 2009. Age–incidence patterns of primary CNS tumors in children, adolescents, and adults in England. *Neuro-oncology,* 11**,** 403-413.

Arshady, R. 1991. Preparation of biodegradable microspheres and microcapsules: 2. Polyactides and related polyesters. *Journal of Controlled Release,* 17**,** 1-21.

Ashby, L. S., et al. 2016. Gliadel wafer implantation combined with standard radiotherapy and concurrent followed by adjuvant temozolomide for treatment of newly diagnosed high-grade glioma: a systematic literature review. *World journal of surgical oncology,* 14**,** 1-15.

Aum, D. J., et al. 2014. Molecular and cellular heterogeneity: the hallmark of glioblastoma. *Neurosurgical focus,* 37**,** E11.

Autio, K. A., et al. 2018. Safety and efficacy of BIND-014, a docetaxel nanoparticle targeting prostate-specific membrane antigen for patients with metastatic castration-resistant prostate cancer: a phase 2 clinical trial. *JAMA oncology,* 4**,** 1344-1351.

Bannunah, A. M., et al. 2014. Mechanisms of nanoparticle internalization and transport across an intestinal epithelial cell model: effect of size and surface charge. *Molecular pharmaceutics,* 11**,** 4363-4373.

Barenholz, Y. C. 2012. Doxil®—the first FDA-approved nano-drug: lessons learned. *Journal of controlled release,* 160**,** 117-134.

Bartlett, D. W., et al. 2007. Impact of tumor-specific targeting on the biodistribution and efficacy of siRNA nanoparticles measured by multimodality in vivo imaging. *Proceedings of the National Academy of Sciences,* 104**,** 15549-15554.

Béduneau, A., et al. 2007. Active targeting of brain tumors using nanocarriers. *Biomaterials,* 28**,** 4947-4967.

Begley, D. J., et al. 1990. Permeability of the blood-brain barrier to the immunosuppressive cyclic peptide cyclosporin A. *Journal of neurochemistry,* 55**,** 1222-1230.

Bennewitz, M. F. & Saltzman, W. M. 2009. Nanotechnology for delivery of drugs to the brain for epilepsy. *Neurotherapeutics,* 6**,** 323-336.

Benson, K., et al. 2013. Impedance-based cell monitoring: barrier properties and beyond. *Fluids and Barriers of the CNS,* 10**,** 1-11.

Blanchette, M. & Fortin, D. 2011. Blood-brain barrier disruption in the treatment of brain tumors. *The Blood-Brain and Other Neural Barriers.* Springer.

Bobo, R. H., et al. 1994. Convection-enhanced delivery of macromolecules in the brain. *Proceedings of the National Academy of Sciences,* 91**,** 2076-2080.

Boockvar, J. A., et al. 2011. Safety and maximum tolerated dose of superselective intraarterial cerebral infusion of bevacizumab after osmotic blood-brain barrier disruption for recurrent malignant glioma. *Journal of neurosurgery,* 114**,** 624-632.

Boucher, Y., et al. 1990. Interstitial pressure gradients in tissue-isolated and subcutaneous tumors: implications for therapy. *Cancer research,* 50**,** 4478-4484.

Boury, F., et al. 1995. Dynamic properties of poly (DL-lactide) and polyvinyl alcohol monolayers at the air/water and dichloromethane/water interfaces. *Journal of colloid and interface science,* 169**,** 380-392.

Brady, J. M., et al. 1973. Resorption rate, route of elimination, and ultrastructure of the implant site of polylactic acid in the abdominal wall of the rat. *Journal of Biomedical Materials Research Part A,* 7**,** 155-166.

Brandes, A., et al. 2004. How effective is BCNU in recurrent glioblastoma in the modern era?: A phase II trial. *Neurology,* 63**,** 1281-1284.

Bregoli, L., et al. 2016. Nanomedicine applied to translational oncology: a future perspective on cancer treatment. *Nanomedicine: Nanotechnology, Biology and Medicine,* 12**,** 81-103.

Brem, H., et al. 1995. The safety of interstitial chemotherapy with BCNU-loaded polymer followed by radiation therapy in the treatment of newly diagnosed malignant gliomas: phase I trial. *Journal of neuro-oncology,* 26**,** 111-123.

Buckner, J. C., et al. 2003. Irinotecan in the treatment of glioma patients: current and future studies of the North Central Cancer Treatment Group. *Cancer: Interdisciplinary International Journal of the American Cancer Society,* 97**,** 2352-2358.

Budhian, A., et al. 2007. Haloperidol-loaded PLGA nanoparticles: systematic study of particle size and drug content. *International journal of pharmaceutics,* 336**,** 367-375.

Calvo, P., et al. 2001. Long-circulating PEGylated polycyanoacrylate nanoparticles as new drug carrier for brain delivery. *Pharmaceutical research,* 18**,** 1157-1166.

Calzolari, A., et al. 2010. Transferrin receptor 2 is frequently and highly expressed in glioblastomas. *Translational oncology,* 3**,** 123-134.

Capello, M., et al. 2015. Carboxylesterase 2 as a determinant of response to irinotecan and neoadjuvant FOLFIRINOX therapy in pancreatic ductal adenocarcinoma. *JNCI: Journal of the National Cancer Institute,* 107, 1-9.

Carnevale, J. & Ko, A. H. 2016. MM-398 (nanoliposomal irinotecan): emergence of a novel therapy for the treatment of advanced pancreatic cancer. *Future Oncology,* 12**,** 453-464.

Carrio, A., et al. 1995. Preparation and degradation of surfactant-free PLAGA microspheres. *Journal of controlled release,* 37**,** 113-121.

Chakraborty, C., et al. 2017. Therapeutic miRNA and siRNA: moving from bench to clinic as next generation medicine. *Molecular Therapy-Nucleic Acids,* 8**,** 132-143.

Chamberlain, M. C. 2010. Temozolomide: therapeutic limitations in the treatment of adult high-grade gliomas. *Expert review of neurotherapeutics,* 10**,** 1537-1544.

Chamberlain, M. C., et al. 1997. Complications associated with intraventricular chemotherapy in patients with leptomeningeal metastases. *Journal of neurosurgery,* 87**,** 694-699.

Chandana, S. R., et al. 2008. Primary brain tumors in adults. *American family physician,* 77**,** 1423-1430.

Chang, C., et al. 1983. Comparison of postoperative radiotherapy and combined postoperative radiotherapy and chemotherapy in the multidisciplinary management of malignant gliomas. A joint Radiation Therapy Oncology Group and Eastern Cooperative Oncology Group study. *Cancer,* 52**,** 997-1007.

Chang, J., et al. 2009. Characterization of endocytosis of transferrin-coated PLGA nanoparticles by the blood–brain barrier. *International journal of pharmaceutics,* 379**,** 285-292.

Chang, T., et al. 2015. Phase I study of nanoliposomal irinotecan (PEP02) in advanced solid tumor patients. *Cancer chemotherapy and pharmacology,* 75**,** 579-586.

Chapman, C. D., et al. 2013. Intranasal treatment of central nervous system dysfunction in humans. *Pharmaceutical research,* 30**,** 2475-2484.

Chen, I.-C., et al. 2016. Influence of silver and titanium dioxide nanoparticles on in vitro blood-brain barrier permeability. *Environmental toxicology and pharmacology,* 47**,** 108-118.

Chen, J., et al. 2011. Enhanced cellular uptake of folic acid–conjugated PLGA–PEG nanoparticles loaded with vincristine sulfate in human breast cancer. *Drug development and industrial pharmacy,* 37**,** 1339-1346.

Chen, Y. & Liu, L. 2012. Modern methods for delivery of drugs across the blood–brain barrier. *Advanced drug delivery reviews,* 64**,** 640-665.

Chen, Y., et al. 2021. Recent progress in nanoformulations of cabazitaxel. *Biomedical Materials, 16,3, 032002.*

Choi, H. S., et al. 2007. Renal clearance of quantum dots. *Nature biotechnology,* 25**,** 1165-1170.

Ci, T., et al. 2014. Tumor regression achieved by encapsulating a moderately soluble drug into a polymeric thermogel. *Scientific reports,* 4**,** 1-13.

Crawford, J., et al. 2004. Chemotherapy-induced neutropenia: risks, consequences, and new directions for its management. *Cancer,* 100**,** 228-237.

Crocetti, E., et al. 2012. Epidemiology of glial and non-glial brain tumours in Europe. *European journal of cancer,* 48**,** 1532-1542.

Crotts, G. & Park, T. G. 1998. Protein delivery from poly (lactic-co-glycolic acid) biodegradable microspheres: release kinetics and stability issues. *Journal of microencapsulation,* 15**,** 699-713.

Cuddapah, V. A., et al. 2014. A neurocentric perspective on glioma invasion. *Nature Reviews Neuroscience,* 15**,** 455-465.

Cui, Y., et al. 2016. Dual-targeting magnetic PLGA nanoparticles for codelivery of paclitaxel and curcumin for brain tumor therapy. *ACS applied materials & interfaces,* 8**,** 32159-32169.

Curran Jr, W. J., et al. 1993. Recursive partitioning analysis of prognostic factors in three Radiation Therapy Oncology Group malignant glioma trials. *JNCI: Journal of the National Cancer Institute,* 85**,** 704-710.

Danhier, F., et al. 2009. Paclitaxel-loaded PEGylated PLGA-based nanoparticles: in vitro and in vivo evaluation. *Journal of controlled release,* 133**,** 11-17.

Darefsky, A. S., et al. 2012. Adult glioblastoma multiforme survival in the temozolomide era: A population-based analysis of Surveillance, Epidemiology, and End Results registries. *Cancer,* 118**,** 2163-2172.

Davis, M. E. 2009. The first targeted delivery of siRNA in humans via a self-assembling, cyclodextrin polymer-based nanoparticle: from concept to clinic. *Molecular pharmaceutics,* 6**,** 659-668.

De Jong, S., et al. 2001. New insights into the hydrolytic degradation of poly (lactic acid): participation of the alcohol terminus. *Polymer,* 42**,** 2795-2802.

Deeken, J. F. & Löscher, W. 2007. The blood-brain barrier and cancer: transporters, treatment, and Trojan horses. *Clinical cancer research,* 13**,** 1663-1674.

Demeule, M., et al. 2008a. Involvement of the low-density lipoprotein receptor-related protein in the transcytosis of the brain delivery vector Angiopep-2. *Journal of neurochemistry,* 106**,** 1534-1544.

Demeule, M., et al. 2008b. Identification and design of peptides as a new drug delivery system for the brain. *Journal of Pharmacology and Experimental Therapeutics,* 324**,** 1064-1072.

Dhal, C. & Mishra, R. 2019. Formulation development and in vitro evaluation of gentamicin sulfate-loaded PLGA nanoparticles based film for the treatment of surgical site infection by Box–Behnken design. *Drug development and industrial pharmacy,* 45**,** 805-818.

Dillen, K., et al. 2004. Factorial design, physicochemical characterisation and activity of ciprofloxacin-PLGA nanoparticles. *International journal of pharmaceutics,* 275**,** 171-187.

Ding, H., et al. 2010. Inhibition of brain tumor growth by intravenous poly (β-L-malic acid) nanobioconjugate with pH-dependent drug release. *Proceedings of the National Academy of Sciences,* 107**,** 18143-18148.

Dobrovolskaia, M. A., et al. 2008. Preclinical studies to understand nanoparticle interaction with the immune system and its potential effects on nanoparticle biodistribution. *Molecular pharmaceutics,* 5**,** 487-495.

Dolecek, T. A., et al. 2012. CBTRUS statistical report: primary brain and central nervous system tumors diagnosed in the United States in 2005–2009. *Neuro-oncology,* 14**,** v1-v49.

Downs, M. E., et al. 2015. Blood-brain barrier opening in behaving non-human primates via focused ultrasound with systemically administered microbubbles. *Scientific reports,* 5**,** 15076-15088.

Drin, G., et al. 2003. Studies on the internalization mechanism of cationic cell-penetrating peptides. *Journal of Biological Chemistry,* 278**,** 31192-31201.

Drummond, D. C., et al. 1999. Optimizing liposomes for delivery of chemotherapeutic agents to solid tumors. *Pharmacological reviews,* 51**,** 691-744.

Eckel-Passow, J. E., et al. 2015. Glioma groups based on 1p/19q, IDH, and TERT promoter mutations in tumors. *New England Journal of Medicine,* 372**,** 2499-2508.

Elmowafy, E. M., et al. 2019. Biocompatibility, biodegradation and biomedical applications of poly (lactic acid)/poly (lactic-co-glycolic acid) micro and nanoparticles. *Journal of Pharmaceutical Investigation,* 49**,** 347-380.

Español, L., et al. 2016. Dual encapsulation of hydrophobic and hydrophilic drugs in PLGA nanoparticles by a single-step method: drug delivery and cytotoxicity assays. *RSC advances,* 6**,** 111060-111069.

Fatima, S., et al. 2021. Polymeric nanoparticles for potential drug delivery applications in cancer. *Nanoformulation strategies for cancer treatment.* , 65-88.

Femke, M., et al. 2018. Individualization of irinotecan treatment: a review of pharmacokinetics, pharmacodynamics, and pharmacogenetics. *Clinical pharmacokinetics,* 57**,** 1229-1254.

Filippini, G. 2012. Epidemiology of primary central nervous system tumors. *Handbook of clinical neurology.* 104, 3-22.

Fischer, H., et al. 1998. Blood-brain barrier permeation: molecular parameters governing passive diffusion. *The Journal of membrane biology,* 165**,** 201-211.

Florence, A. & Whitehill, D. 1982. The formulation and stability of multiple emulsions. *International Journal of Pharmaceutics,* 11**,** 277-308.

Florio, T. & Barbieri, F. 2012. The status of the art of human malignant glioma management: the promising role of targeting tumor-initiating cells. *Drug discovery today,* 17**,** 1103-1110.

Fornaguera, C., et al. 2015. PLGA nanoparticles prepared by nano-emulsion templating using low-energy methods as efficient nanocarriers for drug delivery across the blood–brain barrier. *Journal of controlled release,* 211**,** 134-143.

Fortin, D., et al. 2005. Enhanced chemotherapy delivery by intraarterial infusion and blood-brain barrier disruption in malignant brain tumors: The Sherbrooke experience. *Cancer,* 103**,** 2606-2615.

Fourniols, T., et al. 2015. Temozolomide-loaded photopolymerizable PEG-DMA-based hydrogel for the treatment of glioblastoma. *Journal of Controlled Release,* 210**,** 95-104.

Friedman, H. S., et al. 1999. Irinotecan therapy in adults with recurrent or progressive malignant glioma. *Journal of Clinical Oncology,* 17**,** 1516-1516.

Fröhlich, E. 2012. The role of surface charge in cellular uptake and cytotoxicity of medical nanoparticles. *International journal of nanomedicine,* 7**,** 5577-5591.

Fuchs, C., et al. 2006. Irinotecan in the treatment of colorectal cancer. *Cancer treatment reviews,* 32**,** 491-503.

Fung, L. K., et al. 1998. Pharmacokinetics of interstitial delivery of carmustine, 4-hydroperoxycyclophosphamide, and paclitaxel from a biodegradable polymer implant in the monkey brain. *Cancer research,* 58**,** 672-684.

Furnari, F. B., et al. 2007. Malignant astrocytic glioma: genetics, biology, and paths to treatment. *Genes & development,* 21**,** 2683-2710.

Gallego, J., et al. 2007. Fatal outcome related to carmustine implants in glioblastoma multiforme. *Acta neurochirurgica,* 149**,** 261-265.

Ganipineni, L. P., et al. 2019. Paclitaxel-loaded multifunctional nanoparticles for the targeted treatment of glioblastoma. *Journal of drug targeting,* 27**,** 614-623.

Gao, X., et al. 2006. Lectin-conjugated PEG–PLA nanoparticles: preparation and brain delivery after intranasal administration. *Biomaterials,* 27**,** 3482-3490.

Garg, T., et al. 2015. Current strategies for targeted delivery of bio-active drug molecules in the treatment of brain tumor. *Journal of drug targeting,* 23**,** 865-887.

Gawley, M., et al. 2020. Development and in vivo evaluation of Irinotecan-loaded Drug Eluting Seeds (iDES) for the localised treatment of recurrent glioblastoma multiforme. *Journal of Controlled Release,* 324, 1-16.

Geldenhuys, W., et al. 2011. Brain-targeted delivery of paclitaxel using glutathione-coated nanoparticles for brain cancers. *Journal of drug targeting,* 19**,** 837-845.

Geldenhuys, W., et al. 2015. Brain-targeted delivery of doxorubicin using glutathione-coated nanoparticles for brain cancers. *Pharmaceutical development and technology,* 20**,** 497-506.

Georgieva, J., et al. 2014. Smuggling drugs into the brain: an overview of ligands targeting transcytosis for drug delivery across the blood–brain barrier. *Pharmaceutics,* 6**,** 557-583.

Gerson, S. L. 2004. MGMT: its role in cancer aetiology and cancer therapeutics. *Nature Reviews Cancer,* 4**,** 296-307.

Gerweck, L. E. & Seetharaman, K. 1996. Cellular pH gradient in tumor versus normal tissue: potential exploitation for the treatment of cancer. *Cancer research,* 56**,** 1194-1198.

Giaever, I. & Keese, C. R. 1991. Micromotion of mammalian cells measured electrically. *Proceedings of the National Academy of Sciences,* 88**,** 7896-7900.

Gingrich, M. B. & Traynelis, S. F. 2000. Serine proteases and brain damage–is there a link? *Trends in neurosciences,* 23**,** 399-407.

Giri, T. K., et al. 2013. Prospects of pharmaceuticals and biopharmaceuticals loaded microparticles prepared by double emulsion technique for controlled delivery. *Saudi Pharmaceutical Journal,* 21**,** 125-141.

Giri, V. P., et al. 2017. Anti-nicotine vaccine: current status. *International Journal of Basic & Clinical Pharmacology,* 4**,** 1309-1313.

Giulioni, M., et al. 2014. Epilepsy associated tumors. *World Journal of Clinical Cases: WJCC,* 2**,** 623-641.

Group, G. M.-a. T. G. 2002. Chemotherapy in adult high-grade glioma: a systematic review and meta-analysis of individual patient data from 12 randomised trials. *The Lancet,* 359**,** 1011-1018.

Grover, A., et al. 2014. Brain-targeted delivery of docetaxel by glutathione-coated nanoparticles for brain cancer. *Aaps Pharmscitech,* 15**,** 1562-1568.

Gu, F., et al. 2008. Precise engineering of targeted nanoparticles by using self-assembled biointegrated block copolymers. *Proceedings of the National Academy of Sciences,* 105**,** 2586-2591.

Gutierro, I., et al. 2002. Size dependent immune response after subcutaneous, oral and intranasal administration of BSA loaded nanospheres. *Vaccine,* 21**,** 67-77.

Hadjidemetriou, M., et al. 2015. In vivo biomolecule corona around blood-circulating, clinically used and antibody-targeted lipid bilayer nanoscale vesicles. *ACS nano,* 9**,** 8142-8156.

Hahn, K. K., et al. 2006. Pharmacogenetics and irinotecan therapy. *American journal of health-system pharmacy,* 63**,** 2211-2217.

Hanada, S., et al. 2014. Cell-based in vitro blood–brain barrier model can rapidly evaluate nanoparticles' brain permeability in association with particle size and surface modification. *International journal of molecular sciences,* 15**,** 1812-1825.

Hao, J., et al. 2011. Development and optimization of solid lipid nanoparticle formulation for ophthalmic delivery of chloramphenicol using a Box-Behnken design. *International journal of nanomedicine,* 6**,** 683-692.

Haque, S., et al. 2012. Nanostructure-based drug delivery systems for brain targeting. *Drug Development and Industrial Pharmacy,* 38**,** 387-411.

Hart, M. G., et al. 2013. Temozolomide for high grade glioma. *Cochrane Database of Systematic Reviews, 4, CD007415*.

Hasselbalch, B., et al. 2010. Cetuximab, bevacizumab, and irinotecan for patients with primary glioblastoma and progression after radiation therapy and temozolomide: a phase II trial. *Neuro-oncology,* 12**,** 508-516.

Hau, P., et al. 2004. Pegylated liposomal doxorubicin-efficacy in patients with recurrent high-grade glioma. *Cancer: Interdisciplinary International Journal of the American Cancer Society,* 100**,** 1199-1207.

He, C., et al. 2010. Effects of particle size and surface charge on cellular uptake and biodistribution of polymeric nanoparticles. *Biomaterials,* 31**,** 3657-3666.

Hecht, J. R. 1998. Gastrointestinal toxicity of irinotecan.*Oncology*,12, 72-78

Hegi, M. E., et al. 2005. MGMT gene silencing and benefit from temozolomide in glioblastoma. *New England Journal of Medicine,* 352**,** 997-1003.

Hervé, F., et al. 2008. CNS delivery via adsorptive transcytosis. *The AAPS journal,* 10**,** 455-472.

Hillaireau, H. & Couvreur, P. 2009. Nanocarriers' entry into the cell: relevance to drug delivery. *Cellular and molecular life sciences,* 66**,** 2873-2896.

Hitron, A., et al. 2011. Incidence and risk factors of clinically significant chemotherapy-induced thrombocytopenia in patients with solid tumors. *Journal of Oncology Pharmacy Practice,* 17**,** 312-319.

Homma, T., et al. 2006. Correlation among pathology, genotype, and patient outcomes in glioblastoma. *Journal of Neuropathology & Experimental Neurology,* 65**,** 846-854.

Hoover, J. M., et al. 2010. Clinical trials in brain tumor surgery. *Neuroimaging Clinics,* 20**,** 409-424.

Hu, Y., et al. 2019. Nicotine Vaccines: The Past, the Present, and the Future. *Neuroscience of Nicotine.* 475-482.

Huwyler, J., et al. 1996. Evidence for P-glycoprotein-modulated penetration of morphine-6-glucuronide into brain capillary endothelium. *British journal of pharmacology,* 118**,** 1879-1885.

Huynh, N. T., et al. 2011. Treatment of 9L gliosarcoma in rats by ferrociphenol-loaded lipid nanocapsules based on a passive targeting strategy via the EPR effect. *Pharmaceutical research,* 28**,** 3189-3198.

Huynh, N. T., et al. 2012. Administration-dependent efficacy of ferrociphenol lipid nanocapsules for the treatment of intracranial 9L rat gliosarcoma. *International journal of pharmaceutics,* 423**,** 55-62.

Iacob, G. & Dinca, E. B. 2009. Current data and strategy in glioblastoma multiforme. *Journal of medicine and life,* 2**,** 386-393.

Iliescu, R. I., et al. 2014. Montmorillonite–alginate nanocomposite as a drug delivery system–incorporation and in vitro release of irinotecan. *International journal of pharmaceutics,* 463**,** 184-192.

Jain, A., et al. 2015. Surface engineered polymeric nanocarriers mediate the delivery of transferrin–methotrexate conjugates for an improved understanding of brain cancer. *Acta biomaterialia,* 24**,** 140-151.

Jain, D. S., et al. 2014. Unraveling the cytotoxic potential of Temozolomide loaded into PLGA nanoparticles. *DARU Journal of Pharmaceutical Sciences,* 22**,** 1-9.

Jain, R. A. 2000. The manufacturing techniques of various drug loaded biodegradable poly (lactide-co-glycolide)(PLGA) devices. *Biomaterials,* 21**,** 2475-2490.

Jain, R. K. 2005. Normalization of tumor vasculature: an emerging concept in antiangiogenic therapy. *Science,* 307**,** 58-62.

Jalil, R. & Nixon, J. 1990. Biodegradable poly (lactic acid) and poly (lactide-co-glycolide) microcapsules: problems associated with preparative techniques and release properties. *Journal of microencapsulation,* 7**,** 297-325.

Jamshidi, K., et al. 1988. Thermal characterization of polylactides. *Polymer,* 29**,** 2229-2234.

Jiang, P., et al. 2014. Novel anti-glioblastoma agents and therapeutic combinations identified from a collection of FDA approved drugs. *Journal of translational medicine,* 12**,** 1-13.

Jung, T., et al. 2000. Biodegradable nanoparticles for oral delivery of peptides: is there a role for polymers to affect mucosal uptake? *European Journal of Pharmaceutics and Biopharmaceutics,* 50**,** 147-160.

Kamaly, N., et al. 2012. Targeted polymeric therapeutic nanoparticles: design, development and clinical translation. *Chemical Society Reviews,* 41**,** 2971-3010.

Kamijo, A., et al. 1996. In vitro release test system of (D, L-lactic-glycolic) acid copolymer microcapsules for sustained release of LHRH agonist (leuprorelin). *Journal of controlled release,* 40**,** 269-276.

Karcher, S., et al. 2006. Different angiogenic phenotypes in primary and secondary glioblastomas. *International journal of cancer,* 118**,** 2182-2189.

Kastin, A. J., et al. 1999. Peptides crossing the blood–brain barrier: some unusual observations. *Brain research,* 848**,** 96-100.

Kekre, N., et al. 2005. Pancratistatin causes early activation of caspase-3 and the flipping of phosphatidyl serine followed by rapid apoptosis specifically in human lymphoma cells. *Cancer chemotherapy and pharmacology,* 56**,** 29-38.

Kelkar, S. S. & Reineke, T. M. 2011. Theranostics: combining imaging and therapy. *Bioconjugate chemistry,* 22**,** 1879-1903.

Khasraw, M. & Lassman, A. B. 2010. Advances in the treatment of malignant gliomas. *Current oncology reports,* 12**,** 26-33.

Kim, T.-Y., et al. 2004. Phase I and pharmacokinetic study of Genexol-PM, a cremophor-free, polymeric micelle-formulated paclitaxel, in patients with advanced malignancies. *Clinical cancer research,* 10**,** 3708-3716.

Kirby, S. & Purdy, R. A. 2014. Headaches and brain tumors. *Neurol Clin,* 32**,** 423-32.

Kirpotin, D. B., et al. 2006. Antibody targeting of long-circulating lipidic nanoparticles does not increase tumor localization but does increase internalization in animal models. *Cancer research,* 66**,** 6732-6740.

Kitchell, J. P. & Wise, D. L. 1985. Poly (lactic/glycolic acid) biodegradable drug—polymer matrix systems. *Methods in Enzymology,* 112, 436-448.

Kleihues, P. & Ohgaki, H. 1999. Primary and secondary glioblastomas: from concept to clinical diagnosis. *Neuro-oncology,* 1**,** 44-51.

Kniesel, U. & Wolburg, H. 2000. Tight junctions of the blood–brain barrier. *Cellular and molecular neurobiology,* 20**,** 57-76.

Knight, C. G. 1981. *Liposomes, from physical structure to therapeutic applications,* sole distributors for the USA and Canada, Elsevier North-Holland.

Koffie, R. M., et al. 2011. Nanoparticles enhance brain delivery of blood–brain barrier-impermeable probes for in vivo optical and magnetic resonance imaging. *Proceedings of the National Academy of Sciences,* 108**,** 18837-18842.

Koo, Y.-E. L., et al. 2006. Brain cancer diagnosis and therapy with nanoplatforms. *Advanced drug delivery reviews,* 58**,** 1556-1577.

Koziara, J. M., et al. 2004. Paclitaxel nanoparticles for the potential treatment of brain tumors. *Journal of controlled release,* 99**,** 259-269.

Kreuter, J. 1978. Nanoparticles and nanocapsules--new dosage forms in the nanometer size range. *Pharmaceutica Acta Helvetiae,* 53**,** 33-39.

Kreuter, J. 2001. Nanoparticulate systems for brain delivery of drugs. *Advanced drug delivery reviews,* 47**,** 65-81.

Kreuter, J., et al. 1995. Passage of peptides through the blood-brain barrier with colloidal polymer particles (nanoparticles). *Brain research,* 674**,** 171-174.

Kroli, R. A., et al. 1998. Outwitting the blood-brain barrier for therapeutic purposes: osmotic opening and other means. *Neurosurgery,* 42**,** 1083-1099.

Kumagai, A., et al. 1987. Absorptive-mediated endocytosis of cationized albumin and a beta-endorphin-cationized albumin chimeric peptide by isolated brain capillaries. Model system of blood-brain barrier transport. *Journal of Biological Chemistry,* 262**,** 15214-15219.

Kumar, A., et al. 2016. Curcumin-loaded lipid nanocarrier for improving bioavailability, stability and cytotoxicity against malignant glioma cells. *Drug delivery,* 23**,** 214-229.

Kumar, N., et al. 2001. Biodegradable block copolymers. *Advanced drug delivery reviews,* 53**,** 23-44.

Kumar, R., et al. 2013. Facile synthesis of PEGylated PLGA nanoparticles encapsulating doxorubicin and its in vitro evaluation as potent drug delivery vehicle. *Drug delivery and translational research,* 3**,** 299-308.

Kumskova, N., et al. 2020. How subtle differences in polymer molecular weight affect doxorubicin-loaded PLGA nanoparticles degradation and drug release. *Journal of Microencapsulation,* 37**,** 283-295.

Kweekel, D., et al. 2008. Clinical and pharmacogenetic factors associated with irinotecan toxicity. *Cancer treatment reviews,* 34**,** 656-669.

Lacroix, M., et al. 2001. A multivariate analysis of 416 patients with glioblastoma multiforme: prognosis, extent of resection, and survival. *Journal of neurosurgery,* 95**,** 190-198.

Laine, A.-L., et al. 2012. Brain tumour targeting strategies via coated ferrociphenol lipid nanocapsules. *European Journal of Pharmaceutics and Biopharmaceutics,* 81**,** 690-693.

Lamborn, K. R., et al. 2008. Progression-free survival: an important end point in evaluating therapy for recurrent high-grade gliomas. *Neuro-oncology,* 10**,** 162-170.

Lapointe, S., et al. 2018. Primary brain tumours in adults. *The Lancet,* 392**,** 432-446.

Lawrence, R. N. 2002. William Pardridge discusses the lack of BBB research. *Drug Discovery Today,* 7**,** 223-226.

Laxton, R. C., et al. 2013. Primary glioblastoma with oligodendroglial differentiation has better clinical outcome but no difference in common biological markers compared with other types of glioblastoma. *Neuro-oncology,* 15**,** 1635-1643.

Lee, H. J., et al. 2000. Targeting rat anti-mouse transferrin receptor monoclonal antibodies through blood-brain barrier in mouse. *Journal of Pharmacology and Experimental Therapeutics,* 292**,** 1048-1052.

Lee, S. S., et al. 2015. Cellular uptake of poly (dl-lactide-co-glycolide) nanoparticles: effects of drugs and surface characteristics of nanoparticles. *Journal of Pharmaceutical Investigation,* 45**,** 659-667.

Leibel, S. A. & Sheline, G. E. 1987. Radiation therapy for neoplasms of the brain. *Journal of neurosurgery,* 66**,** 1-22.

Lewis, D. H. 1990. Controlled release of bioactive agents from lactide/glycolide polymers. *Drugs and the pharmaceutical sciences,* 45**,** 1-41.

Li, J., et al. 2011. Targeting the brain with PEG–PLGA nanoparticles modified with phage-displayed peptides. *Biomaterials,* 32**,** 4943-4950.

Liebner, S., et al. 2000. Claudin-1 and claudin-5 expression and tight junction morphology are altered in blood vessels of human glioblastoma multiforme. *Acta neuropathologica,* 100**,** 323-331.

Lollo, G., et al. 2015. Development of multifunctional lipid nanocapsules for the co-delivery of paclitaxel and CpG-ODN in the treatment of glioblastoma. *International journal of pharmaceutics,* 495**,** 972-980.

Lombardo, S. M., et al. 2020. Key for crossing the BBB with nanoparticles: The rational design. *Beilstein journal of nanotechnology,* 11**,** 866-883.

Lonardi, S., et al. 2005. Adjuvant chemotherapy in the treatment of high grade gliomas. *Cancer treatment reviews,* 31**,** 79-89.

Louis, D. N. 2006. Molecular pathology of malignant gliomas. *Annu. Rev. Pathol. Mech. Dis.,* 1**,** 97-117.

Louis, D. N., et al. 2007. The 2007 WHO classification of tumours of the central nervous system. *Acta neuropathologica,* 114**,** 97-109.

Louis, D. N., et al. 2016. The 2016 World Health Organization classification of tumors of the central nervous system: a summary. *Acta neuropathologica,* 131**,** 803-820.

Loureiro, J. A., et al. 2014. Targeting nanoparticles across the blood–brain barrier with monoclonal antibodies. *Nanomedicine,* 9**,** 709-722.

Lovely, M. P., et al. 2014. Care of the adult patient with a brain tumor. *Journal of Neuroscience Nursing,* 46**,** 367-369.

Madani, F., et al. 2018. Investigation of effective parameters on size of paclitaxel loaded PLGA nanoparticles. *Advanced pharmaceutical bulletin,* 8**,** 77-84.

Maherally, Z., et al. 2018. Real-time acquisition of transendothelial electrical resistance in an all-human, in vitro, 3-dimensional, blood-brain barrier model exemplifies tight-junction integrity. *The FASEB Journal,* 32**,** 168-182.

Mahmoud, B. S., et al. 2020. Polymeric Nanoparticles for the Treatment of Malignant Gliomas. *Cancers,* 12**,** 175-203.

Malik, A., et al. 2019. Single-dose Ag85B-ESAT6–loaded poly (lactic-co-glycolic acid) nanoparticles confer protective immunity against tuberculosis. *International journal of nanomedicine,* 14**,** 3129-3143.

Malikmammadov, E., et al. 2018. PCL and PCL-based materials in biomedical applications. *Journal of Biomaterials science, Polymer edition,* 29**,** 863-893.

Malinovskaya, Y., et al. 2017. Delivery of doxorubicin-loaded PLGA nanoparticles into U87 human glioblastoma cells. *International journal of pharmaceutics,* 524**,** 77-90.

Mandl, E. S., et al. 2008. Repeated surgery for glioblastoma multiforme: only in combination with other salvage therapy. *Surgical neurology,* 69**,** 506-509.

Mansourizadeh, F., et al. 2020. Designing Salvigenin–loaded mPEG-b-PLGA@ Fe3O4 nanoparticles system for improvement of Salvigenin anti-cancer effects on the breast cancer cells, an in vitro study. *Journal of Drug Delivery Science and Technology,* 57**,** 101619-101632.

Mao, S., et al. 2008. Effects of process and formulation parameters on characteristics and internal morphology of poly (d, l-lactide-co-glycolide) microspheres formed by the solvent evaporation method. *European journal of pharmaceutics and biopharmaceutics,* 68**,** 214-223.

Markoutsa, E., et al. 2011. Uptake and permeability studies of BBB-targeting immunoliposomes using the hCMEC/D3 cell line. *European journal of pharmaceutics and biopharmaceutics,* 77**,** 265-274.

Masood, F. 2016. Polymeric nanoparticles for targeted drug delivery system for cancer therapy. *Materials Science and Engineering: C,* 60**,** 569-578.

Matsumura, Y., et al. 2004. Phase I clinical trial and pharmacokinetic evaluation of NK911, a micelle-encapsulated doxorubicin. *British journal of cancer,* 91**,** 1775-1781.

Matusewicz, L., et al. 2015. The effect of statins on cancer cells. *Tumor Biology,* 36**,** 4889-4904.

Mcgirt, M. J., et al. 2009. Gliadel (BCNU) wafer plus concomitant temozolomide therapy after primary resection of glioblastoma multiforme. *Journal of neurosurgery,* 110**,** 583-588.

Meyers, J. D., et al. 2013. Nanoparticles for imaging and treating brain cancer. *Nanomedicine,* 8**,** 123-143.

Millau, J. F., et al. 2010. p53 functions and cell lines: have we learned the lessons from the past? *BioEssays,* 32**,** 392-400.

Misra, A., et al. 2003. Drug delivery to the central nervous system: a review. *J Pharm Pharm Sci,* 6**,** 252-273.

Moghimi, S. M., et al. 2001. Long-circulating and target-specific nanoparticles: theory to practice. *Pharmacological reviews,* 53**,** 283-318.

Murakami, H., et al. 1997. Influence of the degrees of hydrolyzation and polymerization of poly (vinylalcohol) on the preparation and properties of poly (DL-lactide-co-glycolide) nanoparticle. *International journal of pharmaceutics,* 149**,** 43-49.

Nafee, N., et al. 2009. Relevance of the colloidal stability of chitosan/PLGA nanoparticles on their cytotoxicity profile. *International journal of pharmaceutics,* 381**,** 130-139.

Nakano, I. 2015. Stem cell signature in glioblastoma: therapeutic development for a moving target. *Journal of neurosurgery,* 122**,** 324-330.

Network, C. G. a. R. 2008. Comprehensive genomic characterization defines human glioblastoma genes and core pathways. *Nature,* 455**,** 1061-1068.

Newcomb, E. W., et al. 1998. Survival of patients with glioblastoma multiforme is not influenced by altered expression of p16, p53, EGFR, MDM2 or Bcl-2 genes. *Brain pathology,* 8**,** 655-667.

Nieder, C., et al. 2006. Combined modality treatment of glioblastoma multiforme: the role of temozolomide. *Reviews on recent clinical trials,* 1**,** 43-51.

Nielsen, S. F., et al. 2012. Statin use and reduced cancer-related mortality. *New England Journal of Medicine,* 367**,** 1792-1802.

Ohgaki, H., et al. 2004. Genetic pathways to glioblastoma: a population-based study. *Cancer research,* 64**,** 6892-6899.

Ohgaki, H. & Kleihues, P. 2007. Genetic pathways to primary and secondary glioblastoma. *The American journal of pathology,* 170**,** 1445-1453.

Ohgaki, H. & Kleihues, P. 2013. The definition of primary and secondary glioblastoma. *Clinical cancer research,* 19**,** 764-772.

Olar, A., et al. 2012. Absence of IDH1-R132H mutation predicts rapid progression of nonenhancing diffuse glioma in older adults. *Annals of diagnostic pathology,* 16**,** 161-170.

Omidi, Y., et al. 2003. Evaluation of the immortalised mouse brain capillary endothelial cell line, b. End3, as an in vitro blood–brain barrier model for drug uptake and transport studies. *Brain research,* 990**,** 95-112.

Ommaya, A. 1963. Subcutaneous reservoir and pump for sterile access to ventricular cerebrospinal fluid. *The Lancet,* 282**,** 983-984.

Ommaya, A. K. 1984. Implantable devices for chronic access and drug delivery to the central nervous system. *Cancer Drug Delivery,* 1**,** 169-179.

Omuro, A. & Deangelis, L. M. 2013. Glioblastoma and other malignant gliomas: a clinical review. *Jama,* 310**,** 1842-1850.

Ose, L. 2011. Pitavastatin: finding its place in therapy. *Therapeutic advances in chronic disease,* 2**,** 101-117.

Ostrom, Q. T., et al. 2014. The epidemiology of glioma in adults: a "state of the science" review. *Neuro-oncology,* 16**,** 896-913.

Ostrom, Q. T., et al. 2017. CBTRUS statistical report: primary brain and other central nervous system tumors diagnosed in the United States in 2010–2014. *Neuro-oncology,* 19**,** v1-v88.

Panigrahi, M., et al. 2011. Brain tumor and Gliadel wafer treatment. *Indian journal of cancer,* 48**,** 11-17.

Pardridge, W. M. 2003. Blood-brain barrier drug targeting: the future of brain drug development. *Molecular interventions,* 3**,** 90-105.

Paw, I., et al. 2015. Mechanisms regulating glioma invasion. *Cancer letters,* 362**,** 1-7.

Peters, K. B., et al. 2015. Phase II trial of upfront bevacizumab, irinotecan, and temozolomide for unresectable glioblastoma. *The oncologist,* 20**,** 727-728.

Phillips, H. S., et al. 2006. Molecular subclasses of high-grade glioma predict prognosis, delineate a pattern of disease progression, and resemble stages in neurogenesis. *Cancer cell,* 9**,** 157-173.

Poller, B., et al. 2008. The human brain endothelial cell line hCMEC/D3 as a human blood-brain barrier model for drug transport studies. *Journal of neurochemistry,* 107**,** 1358-1368.

Rajpoot, K. & Jain, S. K. 2019. Irinotecan hydrochloride trihydrate loaded folic acid-tailored solid lipid nanoparticles for targeting colorectal cancer: development,

characterization, and in vitro cytotoxicity study using HT-29 cells. *Journal of microencapsulation,* 36**,** 659-676.

Ramalho, M., et al. 2018. Receptor-mediated PLGA nanoparticles for glioblastoma multiforme treatment. *International journal of pharmaceutics,* 545**,** 84-92.

Ramchandani, M. & Robinson, D. 1998. In vitro and in vivo release of ciprofloxacin from PLGA 50: 50 implants. *Journal of controlled release,* 54**,** 167-175.

Raymond, E., et al. 2003. Multicentre phase II study and pharmacokinetic analysis of irinotecan in chemotherapy-naive patients with glioblastoma. *Annals of oncology,* 14**,** 603-614.

Re, F., et al. 2012. Nanotechnology for neurodegenerative disorders. *Maturitas,* 73**,** 45-51.

Reed, A. & Gilding, D. 1981. Biodegradable polymers for use in surgery—poly (glycolic)/poly (Iactic acid) homo and copolymers: 2. In vitro degradation. *Polymer,* 22**,** 494-498.

Régina, A., et al. 1999. Dexamethasone regulation of P-glycoprotein activity in an immortalized rat brain endothelial cell line, GPNT. *Journal of neurochemistry,* 73**,** 1954-1963.

Reifenberger, G., et al. 2017. Advances in the molecular genetics of gliomas—implications for classification and therapy. *Nature reviews Clinical oncology,* 14**,** 434-452.

Reis, C. P., et al. 2006. Nanoencapsulation I. Methods for preparation of drug-loaded polymeric nanoparticles. *Nanomedicine: Nanotechnology, Biology and Medicine,* 2**,** 8-21.

Remsen, L. G., et al. 2000. Enhanced delivery improves the efficacy of a tumor-specific doxorubicin immunoconjugate in a human brain tumor xenograft model. *Neurosurgery,* 46**,** 704-709.

Robert, J. & Rivory, L. 1998. Pharmacology of irinotecan. *Drugs of today,* 34**,** 777-804.

Rothenberg, M. L. Efficacy and toxicity of irinotecan in patients with colorectal cancer. Seminars in oncology, 1998. 39-46.

Rothenberg, M. L. 2001. Irinotecan (CPT-11): recent developments and future directions-colorectal cancer and beyond. *The oncologist,* 6**,** 66-80.

Roux, F., et al. 1994. Regulation of gamma-glutamyl transpeptidase and alkaline phosphatase activities in immortalized rat brain microvessel endothelial cells. *Journal of cellular physiology,* 159**,** 101-113.

Rowther, F. B., et al. 2016. Cyclic nucleotide phosphodiesterase-1C (PDE1C) drives cell proliferation, migration and invasion in glioblastoma multiforme cells in vitro. *Molecular carcinogenesis,* 55**,** 268-279.

Rubin, L., et al. 1991. A cell culture model of the blood-brain barrier. *The Journal of cell biology,* 115**,** 1725-1735.

Ruggiero, A., et al. 2010. Paradoxical glomerular filtration of carbon nanotubes. *Proceedings of the National Academy of Sciences,* 107**,** 12369-12374.

Ryken, T. C., et al. 2014. The role of cytoreductive surgery in the management of progressive glioblastoma. *Journal of neuro-oncology,* 118**,** 479-488.

Ryu, S., et al. 2014. The role of radiotherapy in the management of progressive glioblastoma. *Journal of neuro-oncology,* 118**,** 489-499.

Sai, Y., et al. 1998. Adsorptive-mediated endocytosis of a basic peptide in enterocyte-like Caco-2 cells. *American Journal of Physiology-Gastrointestinal and Liver Physiology,* 275**,** G514-G520.

Salvati, A., et al. 2013. Transferrin-functionalized nanoparticles lose their targeting capabilities when a biomolecule corona adsorbs on the surface. *Nature nanotechnology,* 8**,** 137-143.

Sampson, J. H., et al. 2008. Intracerebral infusion of an EGFR-targeted toxin in recurrent malignant brain tumors. *Neuro-oncology,* 10**,** 320-329.

Sant, M., et al. 2012. Survival of European patients with central nervous system tumors. *International journal of cancer,* 131**,** 173-185.

Saraiva, C., et al. 2016. Nanoparticle-mediated brain drug delivery: overcoming blood–brain barrier to treat neurodegenerative diseases. *Journal of Controlled Release,* 235**,** 34-47.

Sarkaria, J. N., et al. 2008. Mechanisms of chemoresistance to alkylating agents in malignant glioma. *Clinical cancer research,* 14**,** 2900-2908.

Sauer, I., et al. 2005. An apolipoprotein E-derived peptide mediates uptake of sterically stabilized liposomes into brain capillary endothelial cells. *Biochemistry,* 44**,** 2021-2029.

Saunders, M. & Iveson, T. 2006. Management of advanced colorectal cancer: state of the art. *British journal of cancer,* 95**,** 131-138.

Sawada, S., et al. 1995. Synthesis and antitumor activity of A-ring or E-lactone modified water-soluble prodrugs of 20 (S)-camptothecin, including development of irinotecan hydrochloride trihydrate (CPT-11). *Curr Pharm Design,* 1**,** 113-132.

Scaringi, C., et al. 2018. Technical advances in radiation therapy for brain tumors. *Anticancer research,* 38**,** 6041-6045.

Scholes, P., et al. 1993. The preparation of sub-200 nm poly (lactide-co-glycolide) microspheres for site-specific drug delivery. *Journal of controlled release,* 25**,** 145-153.

Schröder, U. & Sabel, B. A. 1996. Nanoparticles, a drug carrier system to pass the blood-brain barrier, permit central analgesic effects of iv dalargin injections. *Brain research,* 710**,** 121-124.

Schwartzbaum, J. A., et al. 2006. Epidemiology and molecular pathology of glioma. *Nature clinical practice Neurology,* 2**,** 494-503.

Seidel, S., et al. 2015. Isolation and culture of primary glioblastoma cells from human tumor specimens. Methods in molecular biology. 1235, 263-175.

Shah, A., et al. 2021. Nanocarriers for targeted drug delivery. *Journal of Drug Delivery Science and Technology***,** 62, 102426.

Shao, K., et al. 2010. Angiopep-2 modified PE-PEG based polymeric micelles for amphotericin B delivery targeted to the brain. *Journal of Controlled Release,* 147**,** 118-126.

Shapiro, W. R., et al. 1989. Randomized trial of three chemotherapy regimens and two radiotherapy regimens in postoperative treatment of malignant glioma: Brain Tumor Cooperative Group Trial 8001. *Journal of Neurosurgery,* 71**,** 1-9.

Sharma, N., et al. 2016. Effect of process and formulation variables on the preparation of parenteral paclitaxel-loaded biodegradable polymeric nanoparticles: A co-surfactant study. *Asian journal of pharmaceutical sciences,* 11**,** 404-416.

Shi, J., et al. 2011. Self-assembled targeted nanoparticles: evolution of technologies and bench to bedside translation. *Accounts of chemical research,* 44**,** 1123-1134.

Södergård, A. & Stolt, M. 2002. Properties of lactic acid based polymers and their correlation with composition. *Progress in polymer science,* 27**,** 1123-1163.

Song, X., et al. 2008. PLGA nanoparticles simultaneously loaded with vincristine sulfate and verapamil hydrochloride: systematic study of particle size and drug entrapment efficiency. *International journal of pharmaceutics,* 350**,** 320-329.

Soppimath, K. S., et al. 2001. Biodegradable polymeric nanoparticles as drug delivery devices. *Journal of controlled release,* 70**,** 1-20.

Spinelli, V., et al. 2010. Occupational and environmental risk factors for brain cancer: a pilot case-control study in France. *La Presse Medicale,* 39**,** e35-e44.

Srinivasan, B., et al. 2015. TEER measurement techniques for in vitro barrier model systems. *Journal of laboratory automation,* 20**,** 107-126.

Stark-Vance, V. 2005. Bevacizumab and CPT-11 in the treatment of relapsed malignant glioma. *Neuro-oncol,* 7**,** 369-369.

Stubbs, M., et al. 2000. Causes and consequences of tumour acidity and implications for treatment. *Molecular medicine today,* 6**,** 15-19.

Stupp, R., et al. 2009a. Effects of radiotherapy with concomitant and adjuvant temozolomide versus radiotherapy alone on survival in glioblastoma in a randomised phase III study: 5-year analysis of the EORTC-NCIC trial. *The lancet oncology,* 10**,** 459-466.

Stupp, R., et al. 2006. Changing Paradigms—An Update on the Multidisciplinary Management of Malignant Glioma. *The Oncologist,* 11**,** 165-180.

Stupp, R., et al. 2005. Radiotherapy plus concomitant and adjuvant temozolomide for glioblastoma. *New England journal of medicine,* 352**,** 987-996.

Stupp, R., et al. 2009b. Malignant glioma: ESMO clinical recommendations for diagnosis, treatment and follow-up. *Annals of Oncology,* 20**,** iv126-iv128.

Sugano, M., et al. 2000. Antibody targeting of doxorubicin-loaded liposomes suppresses the growth and metastatic spread of established human lung tumor xenografts in severe combined immunodeficient mice. *Cancer research,* 60**,** 6942-6949.

Suzuki, H., et al. 2007. Simple and easy method to evaluate uptake potential of nanoparticles in mammalian cells using a flow cytometric light scatter analysis. *Environmental science & technology,* 41**,** 3018-3024.

Tam, V. H., et al. 2016. Nanomedicine as a non-invasive strategy for drug delivery across the blood brain barrier. *International Journal of pharmaceutics,* 515**,** 331-342.

Tamimi, A. F. & Juweid, M. 2017. Epidemiology and outcome of glioblastoma. *Exon Publications***,** 143-153.

Tefas, L. R., et al. 2015. Development and optimization of quercetin-loaded PLGA nanoparticles by experimental design. *Clujul Medical,* 88**,** 214-223.

Tewes, F., et al. 2007. Comparative study of doxorubicin-loaded poly (lactide-co-glycolide) nanoparticles prepared by single and double emulsion methods. *European journal of pharmaceutics and biopharmaceutics,* 66**,** 488-492.

Thakkar, J. P., et al. 2014. Epidemiologic and molecular prognostic review of glioblastoma. *Cancer Epidemiology and Prevention Biomarkers,* 23**,** 1985-1996.

Thies, C. & Bissery, M. 1984. Biodegradable microspheres for parenteral administration. CRC Press, Boca Raton, FL.

Thurnher, M., et al. 2012. Novel aspects of mevalonate pathway inhibitors as antitumor agents. *Clinical Cancer Research,* 18**,** 3524-3531.

Tian, G., et al. 2014. Engineered design of theranostic upconversion nanoparticles for tri-modal upconversion luminescence/magnetic resonance/X-ray computed tomography imaging and targeted delivery of combined anticancer drugs. *Journal of Materials Chemistry B,* 2**,** 1379-1389.

Tomasetti, C., et al. 2017. Stem cell divisions, somatic mutations, cancer etiology, and cancer prevention. *Science,* 355**,** 1330-1334.

Török, M., et al. 2003. Modulation of transendothelial permeability and expression of ATP-binding cassette transporters in cultured brain capillary endothelial cells by astrocytic factors and cell-culture conditions. *Experimental brain research,* 153**,** 356-365.

Tousi, M. S., et al. 2021. Evaluation of apoptotic effects of mPEG-b-PLGA coated iron oxide nanoparticles as a eupatorin carrier on DU-145 and LNCaP human prostate cancer cell lines. *Journal of pharmaceutical analysis,* 11**,** 108-121.

Tracy, M., et al. 1999. Factors affecting the degradation rate of poly (lactide-co-glycolide) microspheres in vivo and in vitro. *Biomaterials,* 20**,** 1057-1062.

Tripathi, A., et al. 2010. PLGA nanoparticles of anti tubercular drug: drug loading and release studies of a water in-soluble drug. *Int J Pharm Tech Res,* 2**,** 2116-2123.

Truong, N. P., et al. 2015. The importance of nanoparticle shape in cancer drug delivery. *Expert opinion on drug delivery,* 12**,** 129-142.

Urbańska, K., et al. 2014. Glioblastoma multiforme–an overview. *Contemporary oncology,* 18**,** 307.

Valle, J. W., et al. 2011. A phase 2 study of SP1049C, doxorubicin in P-glycoprotein-targeting pluronics, in patients with advanced adenocarcinoma of the esophagus and gastroesophageal junction. *Investigational new drugs,* 29**,** 1029-1037.

Van Den Bent, M., et al. 2005. Long-term efficacy of early versus delayed radiotherapy for low-grade astrocytoma and oligodendroglioma in adults: the EORTC 22845 randomised trial. *The Lancet,* 366**,** 985-990.

Verhaak, R. G., et al. 2010. Integrated genomic analysis identifies clinically relevant subtypes of glioblastoma characterized by abnormalities in PDGFRA, IDH1, EGFR, and NF1. *Cancer cell,* 17**,** 98-110.

Verreault, M., et al. 2015. Determination of an optimal dosing schedule for combining Irinophore C™ and temozolomide in an orthotopic model of glioblastoma. *Journal of Controlled Release,* 220**,** 348-357.

Villano, J. L., et al. 2009. Temozolomide in malignant gliomas: current use and future targets. *Cancer chemotherapy and pharmacology,* 64**,** 647-655.

Vogelbaum, M. A. 2007. Convection enhanced delivery for treating brain tumors and selected neurological disorders: symposium review. *Journal of neuro-oncology,* 83**,** 97-109.

Von Roemeling, C., et al. 2017. Breaking down the barriers to precision cancer nanomedicine. *Trends in biotechnology,* 35**,** 159-171.

Vredenburgh, J. J., et al. 2007a. Phase II trial of bevacizumab and irinotecan in recurrent malignant glioma. *Clinical cancer research,* 13**,** 1253-1259.

Vredenburgh, J. J., et al. 2007b. Bevacizumab plus irinotecan in recurrent glioblastoma multiforme. *Journal of clinical oncology,* 25**,** 4722-4729.

Vredenburgh, J. J., et al. 2009. Experience with irinotecan for the treatment of malignant glioma. *Neuro-oncology,* 11**,** 80-91.

Vyas, S. & Sihorkar, V. 2000. Endogenous carriers and ligands in non-immunogenic site-specific drug delivery. *Advanced drug delivery reviews,* 43**,** 101-164.

Wada, R., et al. 1988a. Preparation of Lactic-Acid Oligomer Microspheres Containing Anti-Cancer Drugs. Bull. *Inst. Chem. Res., Kyoto Univ.,* 66, 241-250.

Walker, M. D., et al. 1978. Evaluation of BCNU and/or radiotherapy in the treatment of anaplastic gliomas: a cooperative clinical trial. *Journal of neurosurgery,* 49**,** 333-343.

Walker, M. D., et al. 1979. An analysis of dose-effect relationship in the radiotherapy of malignant gliomas. *International Journal of Radiation Oncology* Biology* Physics,* 5**,** 1725-1731.

Wang, H., et al. 2015. Hyaluronic acid-decorated dual responsive nanoparticles of Pluronic F127, PLGA, and chitosan for targeted co-delivery of doxorubicin and irinotecan to eliminate cancer stem-like cells. *Biomaterials,* 72**,** 74-89.

Wang, T., et al. 2019. Pore change during degradation of octreotide acetate-loaded PLGA microspheres: The effect of polymer blends. *European Journal of Pharmaceutical Sciences,* 138**,** 104990.

Wang, Z. H., et al. 2010. Trimethylated chitosan-conjugated PLGA nanoparticles for the delivery of drugs to the brain. *Biomaterials,* 31**,** 908-915.

Weber, E. L. & Goebel, E. A. 2005. Cerebral edema associated with Gliadel wafers: two case studies. *Neuro-oncology,* 7**,** 84-89.

Weksler, B., et al. 2013. The hCMEC/D3 cell line as a model of the human blood brain barrier. *Fluids and Barriers of the CNS,* 10**,** 1-10.

Weksler, B., et al. 2005. Blood-brain barrier-specific properties of a human adult brain endothelial cell line. *The FASEB journal,* 19**,** 1872-1874.

Weller, M., et al. 2013. Standards of care for treatment of recurrent glioblastoma—are we there yet? *Neuro-oncology,* 15**,** 4-27.

Westphal, M., et al. 2003. A phase 3 trial of local chemotherapy with biodegradable carmustine (BCNU) wafers (Gliadel wafers) in patients with primary malignant glioma. *Neuro-oncology,* 5**,** 79-88.

Wicki, A., et al. 2015. Nanomedicine in cancer therapy: challenges, opportunities, and clinical applications. *Journal of controlled release,* 200**,** 138-157.

Wilson, T. A., et al. 2014. Glioblastoma multiforme: State of the art and future therapeutics. *Surgical neurology international,* 5, 64-82.

Winer, J. L., et al. 2011. Visualizing the future: enhancing neuroimaging with nanotechnology. *World neurosurgery,* 75**,** 626-637.

Wohlfart, S., et al. 2011. Efficient chemotherapy of rat glioblastoma using doxorubicin-loaded PLGA nanoparticles with different stabilizers. *PloS one,* 6**,** e19121.

Wong, E. T., et al. 1999. Outcomes and prognostic factors in recurrent glioma patients enrolled onto phase II clinical trials. *Journal of Clinical Oncology,* 17**,** 2572-2572.

Wong, H. L., et al. 2012. Nanotechnological advances for the delivery of CNS therapeutics. *Advanced drug delivery reviews,* 64**,** 686-700.

Wu, X. S. 1995. Synthesis and properties of biodegradable lactic/glycolic acid polymers. *Encyclopedic handbook of biomaterials and bioengineering,* 2**,** 1015-1054.

Xin, H., et al. 2011. Angiopep-conjugated poly (ethylene glycol)-co-poly (ε-caprolactone) nanoparticles as dual-targeting drug delivery system for brain glioma. *Biomaterials,* 32**,** 4293-4305.

Xin, H., et al. 2012. Anti-glioblastoma efficacy and safety of paclitaxel-loading Angiopep-conjugated dual targeting PEG-PCL nanoparticles. *Biomaterials,* 33**,** 8167-8176.

Xiong, S., et al. 2011. Cellular uptake of Poly-(D, L-lactide-co-glycolide)(PLGA) nanoparticles synthesized through solvent emulsion evaporation and nanoprecipitation method. *Biotechnology journal,* 6**,** 501-508.

Xu, Y. & Villalona-Calero, M. 2002. Irinotecan: mechanisms of tumor resistance and novel strategies for modulating its activity. *Annals of oncology,* 13**,** 1841-1851.

Yanae, M., et al. 2011. Statin-induced apoptosis via the suppression of ERK1/2 and Akt activation by inhibition of the geranylgeranyl-pyrophosphate biosynthesis in glioblastoma. *Journal of Experimental & Clinical Cancer Research,* 30**,** 1-8.

Yung, W., et al. 2005. Combination of temozolomide (TMZ) and irinotecan (CPT-11) showed enhanced activity for recurrent malignant gliomas: a North American Brain Tumor Consortium (NABTC) phase II study. *Journal of Clinical Oncology,* 23**,** 1521-1521.

Zambaux, M., et al. 1998. Influence of experimental parameters on the characteristics of poly (lactic acid) nanoparticles prepared by a double emulsion method. *Journal of Controlled Release,* 50**,** 31-40.

Zhang, P., et al. 2008. Critical role of notch signaling in osteosarcoma invasion and metastasis. *Clinical Cancer Research,* 14**,** 2962-2969.

Zucker, R., et al. 2013. Detection of silver nanoparticles in cells by flow cytometry using light scatter and far-red fluorescence. *Cytometry Part A,* 83**,** 962-972.

Zucker, R., et al. 2010. Detection of TiO2 nanoparticles in cells by flow cytometry. *Cytometry Part A,* 77**,** 677-685.

Zweers, M. L., et al. 2003. The preparation of monodisperse biodegradable polyester nanoparticles with a controlled size. *Journal of Biomedical Materials Research Part B: Applied Biomaterials: An Official Journal of The Society for Biomaterials, The Japanese Society for Biomaterials, and The Australian Society for Biomaterials and the Korean Society for Biomaterials,* 66**,** 559-566.